DESIGN AND REALIZATION OF A HYBRID MEDICAL IMAGING SYSTEM: HARMONIC MOTION MICROWAVE DOPPLER IMAGING

A THESIS SUBMITTED TO
THE GRADUATE SCHOOL OF NATURAL AND APPLIED SCIENCES
OF
MIDDLE EAST TECHNICAL UNIVERSITY

BY

AZADEH KAMALI TAFRESHI

IN PARTIAL FULFILLMENT OF THE REQUIREMENTS
FOR
THE DEGREE OF DOCTOR OF PHILOSOPHY
IN
ELECTRICAL AND ELECTRONICS ENGINEERING

FEBRUARY 2016

Approval of the thesis:

DESIGN AND REALIZATION OF A HYBRID MEDICAL IMAGING SYSTEM: HARMONIC MOTION MICROWAVE DOPPLER IMAGING

submitted by **AZADEH KAMALI TAFRESHI** in partial fulfillment of the requirements for the degree of **Doctor of Philosophy in Electrical and Electronics Engineering Department, Middle East Technical University** by,

Prof. Dr. Gülbin Dural Ünver
Dean, Graduate School of **Natural and Applied Sciences** ______________

Prof. Dr. Gönül Turhan Sayan
Head of Department, **Electrical and Electronics Engineering** ______________

Prof. Dr. Nevzat Güneri Gençer
Supervisor, **Electrical and Electronics Eng. Dept., METU** ______________

Examining Committee Members:

Prof. Dr. Mustafa KUZUOĞLU
Electrical and Electronics Eng. Dep., METU ______________

Prof. Dr. Nevzat Güneri GENÇER
Electrical and Electronics Eng. Dep., METU ______________

Prof. Dr. Ergin ATALAR
Electrical and Electronics Eng. Dep., Bilkent Uni. ______________

Prof. Dr. Osman EROĞUL
Biomedical Engineering Dep., TOBB-ETU ______________

Assoc. Prof. Dr. Yeşim SERİNAĞAOĞLU DOĞRUSÖZ
Electrical and Electronics Eng. Dep., METU ______________

Date: 16.02.2016

I hereby declare that all information in this document has been obtained and presented in accordance with academic rules and ethical conduct. I also declare that, as required by these rules and conduct, I have fully cited and referenced all material and results that are not original to this work.

Name, Last Name: AZADEH KAMALI TAFRESHI

Signature :

ABSTRACT

DESIGN AND REALIZATION OF A HYBRID MEDICAL IMAGING SYSTEM: HARMONIC MOTION MICROWAVE DOPPLER IMAGING

Tafreshi, Azadeh Kamali
Ph.D., Department of Electrical and Electronics Engineering
Supervisor : Prof. Dr. Nevzat Güneri Gençer

February 2016, 177 pages

Harmonic Motion Microwave Doppler Imaging (HMMDI) is a novel imaging modality to image electrical and mechanical properties of body tissues. This modality is recently proposed by the researchers in the METU EEE department for early-stage diagnosis of cancerous tissues. The main goal of this thesis study is to contribute various stages of the HMMDI's development processes. Specifically, phantom development, dielectric and elastic characterization of the phantoms, experimental system realization, phantom experiments, and system performance evaluation, are in the scope of this thesis study.

In the earlier stages, different phantoms that mimic the mechanical and electrical properties of the body tissues are developed and characterized. In parallel to the phantom studies, experimental system design and realization studies are performed and the performance of the designed system is tested using phantom materials.

The developed phantoms are scanned using the HMMDI method and the extracted information is used to generate HMMDI data profiles of the phantoms. The potential of detecting different tissues phantoms from the generated data profiles is explored. Effect of different vibration frequencies in HMMDI is discussed. In the acquired 2-D HMMDI data profiles, the potential of this imaging method in detecting 1) 5 mm tumor inside the fat, 2) 14 mm tumor phantom inside 25 mm fibro-glandular phantom in the middle of the fat phantom, 14 mm fibro-glandular phantom inside the fat phantom, and 14 mm tumor inside the fat phantom, at the depth of 20 mm depths are observed. The experimental system limitations are clarified and the possible solutions to improve the system are presented.

Keywords: Harmonic Motion Microwave Doppler Imaging, Breast cancer detection, Microwave imaging, Acoustic radiation force, Doppler signal, Focused ultrasound transducer

ÖZ

HİBRİT BİR TIBBİ GÖRÜNTÜLEME SİSTEMİNİN TASARIMI VE GERÇEKLENMESİ: HARMONİK HAREKET MİKRODALGA DOPPLER GÖRÜNTÜLEME

Tafreshi, Azadeh Kamali
Doktora, Elektrik ve Elektronik Mühendisliği Bölümü
Tez Yöneticisi : Prof. Dr. Nevzat Güneri Gençer

Şubat 2016, 177 sayfa

Harmonik Hareket Mikrodalga Doppler Görüntüleme (HHMDG) vücut dokularının elektriksel ve mekanik özelliklerini görüntülemek için kullanılan yeni bir yöntemdir. Bu yöntem ODTÜ Elektrik-Elektronik mühendisliği bölümündeki araştırmacılar tarafından kanserli dokuların erken tanısı için yakın geçmişte önerilmiştir. Bu tez çalışmasının temel amacı HHMDG'nin geliştirme sürecinin farklı aşamalarına katkı sağlamaktır. Özellikle, doku benzeri malzeme (fantom) geliştirilmesi, fantomların elektriksel ve elastiklik karakterizasyonları, deneysel sistemin gerçekleşimi, fantom deneyleri ve sistemin performans değerlendirmesi bu tezin kapsamındadır.

Bu çalışmada ilk olarak, vücut dokusunun elektriksel ve mekanik özelliklerini taklit eden fantomlar geliştirilmiş ve karakterize edilmiştir. Bu fantom çalışmalarına paralel olarak, deneysel sistem tasarım ve gerçekleştirme çalışmaları yapılmış ve tasarlanan sistemin performansı farklı fantomlarla test edilmiştir.

Geliştirilen fantomların HHMDG yöntemiyle taraması yapıldıktan sonra toplanan bilgiler fantomların HHMDG veri profilini çıkarmak için kullanılmıştır. Oluşturulan görüntülerde farklı dokuların ayrıştırılabilme potansiyeli araştırılmıştır. Ayrıca HHMDG'de kullanılan titreşim frekansının etkisi tartışılmıştır. Elde edilen iki boyutlu HHMDG verileriyle, 1) yağ fantomunda 20 mm derinlikte 5 mm çapında tümor fantomu, 2) yağ fantomunda 25 mm bağ fantomu içinde 14 mm tümor fantomu, 3) yağ fantomunda 14 mm çapında bağ fantomu, ve 4) yağ fantomunda 14 mm tümor fantomu saptanmış, yöntemin görüntüleme potansiyeli gözlenmiştir. Deneysel sistemin kısıtlamaları belirginleştirilmiş ve sistemin iyileştirilmesi için olası çözümler sunulmuştur.

Anahtar Kelimeler: Harmonik Hareket Mikrodalga Doppler Görüntüleme, Meme kanseri tanısı, Mikrodalga görüntüleme, Akustik ışıma kuvveti, Doppler işareti, Odaklı ultrason dönüştürücü

To my beloved parents

ACKNOWLEDGMENTS

It is my great pleasure to take this opportunity to thank everyone who made this dissertation possible.

There are no proper words to convey my deepest gratitude and respect for my thesis and research advisor Professor Dr. Nevzat Güneri Gençer for his unfailing and invaluable guidance and support. I have benefited especially from his constructive comments and invaluable suggestions throughout this thesis. I would also like to thank him for endowing our team work at the laboratory with such a kind, devoted and trustworthy family environment.

My sincere thanks must also go to the members of my Thesis Monitoring Committee, Professor Dr. Mustafa Kuzuoğlu and Professor Dr. Ergin Atalar. They generously gave their time to offer me valuable suggestions and comments toward improving my work.

I would like to thank Prof. Dr. Şimşek Demir, METU Microwave and Antennas Group, Prof. Dr. Ergin Atalar, and National Magnetic Resonance Research Center (UMRAM) at Bilkent University for providing necessary equipment. I am also grateful to Prof. Dr. Nesrin Hasırcı, Necati Özkan, and Dr. Aysel Kızıltay for their help on the elasticity measurements of the phantom materials and Assoc. Prof. Dr. Barış Bayram for his help on the ultrasound field measurements.

A special gratitude goes to Dr. Can Bariş Top who in spite of living abroad I never felt his absence here. I sincerely appreciate his dedications and I am forever indebted to his inspiring discussions, suggestions, and unrelenting guidance, without which I would have not be able to finalize my thesis. His devotion of himself and his time has been beyond my expectations since I am aware of the burden of his own great responsibilities. Being deeply influenced and inspired by his successes in life, I would always look upon him as my role model throughout my future life.

Most importantly, I would like to show an extensive and inexpressible gratitude to my dear friend, Mürsel Karadaş who has warmly contributed his heartful supports during many days and nights. He believed in me more than anyone else. He fought with my worries, concerns, and anxieties throughout this long and difficult journey as if they were his own. He always tried compassionately to instill great confidence in both myself and my work. I am very blessed to have him as my close friend. This expedition was so unforgettable and enjoyable with him.

I would like to express my deep thanks to my dear friend Reyhan Zengin, who blessed me like a very kind sister with her priceless and unforgettable supports throughout all my PhD studies.

My thanks along with my sincerest love goes to my soul-mate Berna Akıncı for her unfailing support. I never forget how we laughed, cried and dreamed together and how she cheered me up through accomplishing my goals.

I have also shared many good and invaluable memories with my dear friend Burcu Kücük who had assisted in every way from the first day that I came to Ankara. I thank her for always being here for me during all my hard times.

I would also like to thank my friends and colleagues in Brain Research Laboratory at METU, Ümit İrgin and Hasan Balkar Erdoğan for lending me their invaluable experiences in technical studies.

I would like to dedicate my profound thanks to Associated Professor Dr. Ali Moti Nasrabadi. His kindness and support, that I already experience during my master studies in Iran, did not stop and continued to provide me with encouragements during my PhD program. He has been the one who had great influence over my decision to continue my studies, made me acquainted with the opportunities I could have had, and inspired me to begin my expedition.

I would like to acknowledge my gratitude to my friends Ali Razaghi, Samin Ronaghzadeh, Amin Ronaghzadeh, Saeedeh Nazirzadeh, Mahsa Keykhali, Alireza Mazlumi, Sona Khenehshenas, Furugh Gharbalchi, Mehdi Sadighi, Raha Shabani, Elmira Pourreza, Ufuk Suat Aydın, Didem menekşe, Selim Özgen, and Yusuf Bariş Güleç for their friendship and supports.

My thanks goes to METU Technical staff, Kemal Öncü at Machine Shop for assisting me in mounting the Focused ultrasound probe and the microwave antennas.

This research was generously supported by Scientific and Technical Research Council of Turkey (TÜBITAK) under the 114E036 (COST Action TD1301) and 112E031 projects. I would like to express my gratitude to all of the TÜBITAK officials who provided me with this opportunity.

Last but not the least, I would like to heartfully thank my family for their unconditional trust, patience, and love. I have always felt their generous love and encouragements despite the long distance between us. Without them, I would not have been able to achieve my present academic standing and moreover I owe all my lifetime achievements to them.

TABLE OF CONTENTS

LIST OF TABLES

TABLES

LIST OF FIGURES

FIGURES

LIST OF ABBREVIATIONS

HMMDI	Harmonic Motion Microwave Doppler Imaging
US	Ultrasound
USVA	Ultrasound-Stimulated Vibroacoustography
DCIS	Ductal Carcinoma In Situ
ARFI	Acoustic Radiation Force Impulse
FEM	Finite Element Method
MRI	Magnetic Resonant Elastography,
FDA	Food and Drug Administration
HMI	Harmonic Motion Imaging
FUS	Focused Ultrasound
AM	Amplitude- Modulated
HMIFU	Hrmonic Motion Imaging Utilizing Focused Ultrasound
I_{SPPA}	Spatial Peak-Pulse Average Intensity
I_{SPTA}	Spatial Peak-Temporal Average Intensity
DMA	Dynamic Measurement Analyzer
METU	Middle Eat Technical University
TX	Transmitter Antenna
RX	Receiver Antenna
SNR	Signal to Noise Ratio
A/D	Analog to Digital
PRI	Pulse Repetition Interval
BW	Bandwidth
MW	Microwave
RF	Radio Frequency
KZK	Khokhlov-Zabolotskaya-Kuznetsov

CHAPTER 1

INTRODUCTION

Breast cancer is known as one of the most common types of cancer among women [13]. Developing methods to assess the early-stage diagnosis and treatment of the breast cancer is the subject of many studies in the last decades. The primary imaging technique for breast cancer detection is Mammography. However, this technique suffers from false negative and false positive, difficulty in imaging of dense breasts, inconclusive results and patient discomfort [14]. In addition, in mamography ionizing radiation is used which increases the risk of cancer occurrence. Consequently, there is a need for an alternative, low-cost and safe diagnostic imaging method. Microwave imaging has been proposed as an alternative method in which the dielectric properties of the tissue is imaged [15–19]. This method provides means to image human body by utilizing nonionizing electromagnetic waves. The long wavelength of the microwaves, gives them the ability to penetrate into living tissues. In microwave imaging, the electromagnetic waves illuminate the breast tissue and scattered field provides information about the conductivity and permittivity distribution inside the tissues.

It has been reported that the electrical properties of the healthy and malignant breast tissues are different [4, 9, 20]. The contrast between dielectric properties of benign and malign breast tissues is demonstrated in Figure 1.1. In that sense, microwave imaging method focuses on the differentiating tissues based on their dielectric properties [20]. It must be noted that, the literature on the dielectric properties of normal and cancerous breast tissues at microwave

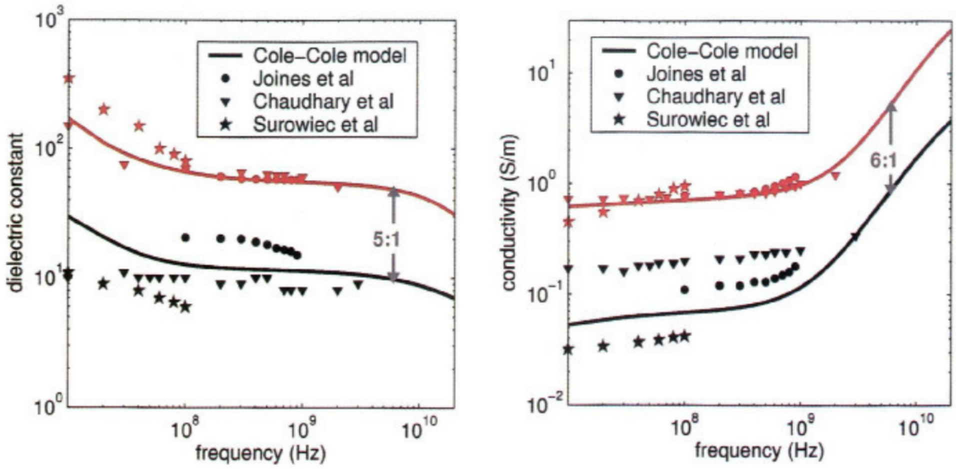

Figure 1.1: Measured dielectric constant data of normal (black) and malignant (red) breast tissue [4].

frequencies is limited. In a series of studies, dielectric properties of biological tissues were investigated for frequencies of 10 Hz up to 20 GHz were evaluated [21–23]. In an other study, a multiprobe radiometer working at 3 GHz was employed for breast tumor detection. In that study, some features were extracted for characterizing benign and malignant tissues [24]. A tomographic approach has been proposed to create 3D microwave images of a woman's breast [16]. In this method, the dielectric properties of tissues in the microwave range were used to develop a dielectrical model of the breast. In several other studies, the efficiency of ultra-wide band microwave imaging method in breast tumor detection was evaluated using simple homogeneous [17, 18] and inhomogeneous tissue mimicking phantoms [25].

In another study, the ultra-wideband microwave imaging method was investigated for detecting, localizing and focusing the microwave energy at the breast cancerous tissue for for both detection and treatment of the tumor [19]. The potential of ultra-wideband microwave imaging for breast cancer detection was evaluated utilizing phantoms which mimick the dielectric properties of the breast tissues [17, 18, 26, 27]. In one of these studies, the proper frequency range to discriminate the difference between normal and malignant breast tissues was reported to be between 600 MHz -1 GHz [20]. A new planar 2.45 GHz microwave camera was assessed for the breast cancer detection [28]. However, several studies show the limitation of distinguishing dielectric properties of the normal and the malign tissues [9]. Last but not least, the obtained resolution in the microwave imaging methods is high, about a few millimeters. The microwave frequency, is penetrable to biological tissues such as breast tissue. However, as the frequency increases the skin depth decreases. In microwave based methods, distinguishing the breast tumor inside the healthy fibro-glandular tissue still remains as a problem. Besides microwave imaging techniques, several studies have been proposed for cancer detection based on mechanical properties of normal and cancerous tissues [29–33]. In these methods, the possibility of detecting tumors from healthy breast tissues are explored similar to manual palpation test in which the physician tries to realize the hard lumps, possible to be tumors by the sense of touch. These methods are based on the difference between the Young's constant (Elastic constant) of the malign tissues and the normal breast tissues by a factor of 3 to 13 [34]. Therefore, these have been a subject of several studies in the recent years.

In [5], a review on imaging the soft tissue strain and elasticity is presented. In this study, the results of breast tissues Young Modulus measurement for two loading frequencies of 0.1 and 4 Hz with 5% static loading are summarized in Figure 1.2 (a). It has been shown that Young's modulus does not have a considerable change due to the loading frequency up to 4 Hz. In addition, they have reported the changes of Young Modulus value due to static pre-loading change from 5% to 20% percent (1.2 (b)). The measured values show that Young's modulus changes as the static loading changes and the contrast between the Young's moduli of different types of tissues becomes higher by increasing the static loading. They have concluded, the level of static pre-loading should be as small as practicable for obtaining reproducible Young's modulus measurements.

An ultrasound (US) method based on acoustic radiation force imaging was proposed to image the acoustic response of the tissues to mechanical stimuli [29–32]. Force which is exerted to the object in the propagation path of the acoustic waves as a result of momentum transfer from the acoustic wave to the object is called *acoustic radiation force*. This applied radiation force due to the ultra-

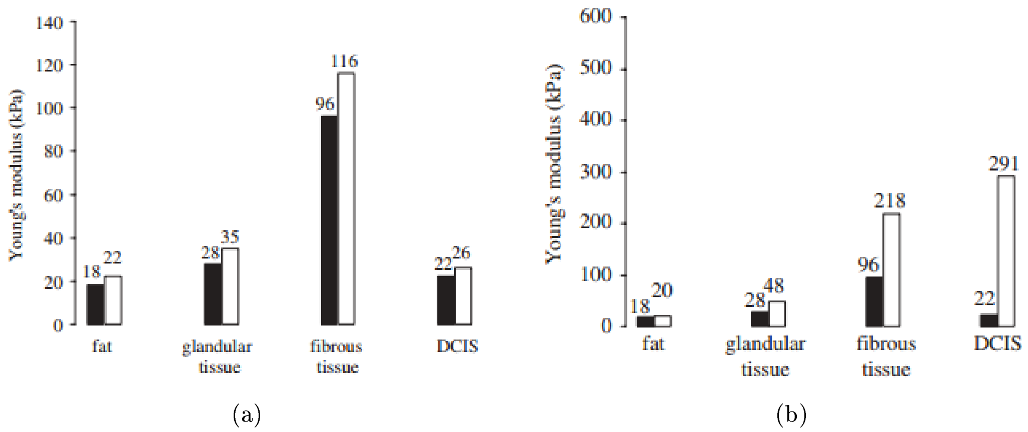

Figure 1.2: Young's moduli of different types of breast tissues, (a) measured for two loading frequencies of 0.1 Hz, (black bars) and 4 Hz (white bars) when static pre-loading was 5%. (b) Measured Young's moduli values for static preloading of 5% (black bars) and 20% (white bars) when when the (quasi-static) loading frequency was 0.1 Hz. Ductal carcinoma in situ (DCIS) is considered as the most common type of non-invasive breast cancer [5].

sound energy induces bulk displacement in the object, which can be measured to reconstruct elastic properties of tissues [33].

One of these methods is ultrasound-stimulated vibroacoustography (USVA) which utilize ultrasound to produce a low-frequency radiation force on the object (Figure 1.3) [6]. In this method, two beams with slightly different frequencies is used to induce the oscillatory radiation force. The resultant acoustic field due to the vibration of the object in response to the radiation force provides information about the mechanical properties of the object. In this technique, localized deformation is produced as a result of the applied radiation force. The average of ultrasound energy density over a short time period was used to obtain the amplitude of radiation force on the target. In addition, by means of ultrasound Doppler technique, the transient deformation as a result of this force can be measured as a function of time.

In Acoustic Radiation Force Impulse (ARFI) imaging method, the short duration acoustic radiation forces are applied to create localized displacements in the tissue [31]. The correlation based methods were applied to measure the displacements. Only one transducer was used for applying radiation force and

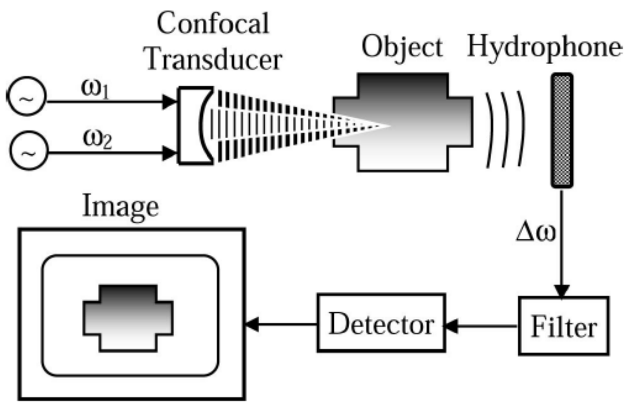

Figure 1.3: Ultrasound-stimulated vibroacoustography set up [6].

evaluating the displacement. In a latter study, the finite-element method (FEM) model was used to simulate the dynamic response of homogeneous tissues with different stiffness [35]. Another study was done to improve the data acquisition for real-time ARFI imaging and reducing the transducer heating due to the acoustic exposure [36]. A parallel receive beamforming method was proposed to evaluate displacements for several beam locations which are separated laterally. This is a common technique in B-mode imaging for increasing the frame rate without that much decrease in resolution.

In another method, the propagation speed of the shear waves has been used to measure the tissue elasticity [37]. In this method, calculated shear wave speed from the measured displacement using the Doppler ultrasound, was used to determine the tissue characteristics. In magnetic resonant elastography, MRI was used to measure the displacement in shear wave speed calculation [38]. A short pulse of ultrasound radiation force was used to create the broadband shear waves. The speed of the shear wave was estimated from the propagation of the wavefront [29].

In another study, narrow band, monochromatic shear waves were introduced inside the medium using an ultrasound radiation force [39]. The propagation speed of the shear waves are related to the frequency and elasticity and viscosity of the exposed tissue. For a known motion frequency and monochromatic wave, the shear wave, wave number can be calculated from the ratio of phase delay over distance traveled by shear wave. The propagation speed can be determined from the calculated wave number. In another study, Kalman filter was used to estimate the small harmonic motion resulted by ultrasonic radiation force [40]. In this method, amplitude and phase of the displacement was calculated by means of the least mean squared error by Kalman filter. The speed of the shear wave can be calculated from its phase. The measured speed can be used to find the viscoelastic properties of the tissues [40].

The harmonic motion imaging (HMI) technique was proposed as another tool for evaluating the mechanical properties of tissues based on the exerted localized radiation force. In this method, two transducers can be used to produce two ultrasonic beams with slightly different frequencies (Figure 1.4) [7] or one focused ultrasound (FUS) transducer may be used to generate Amplitude- Modulated (AM) focused beam (Figure 1.5) [8]. The resulted displacement in the tissue

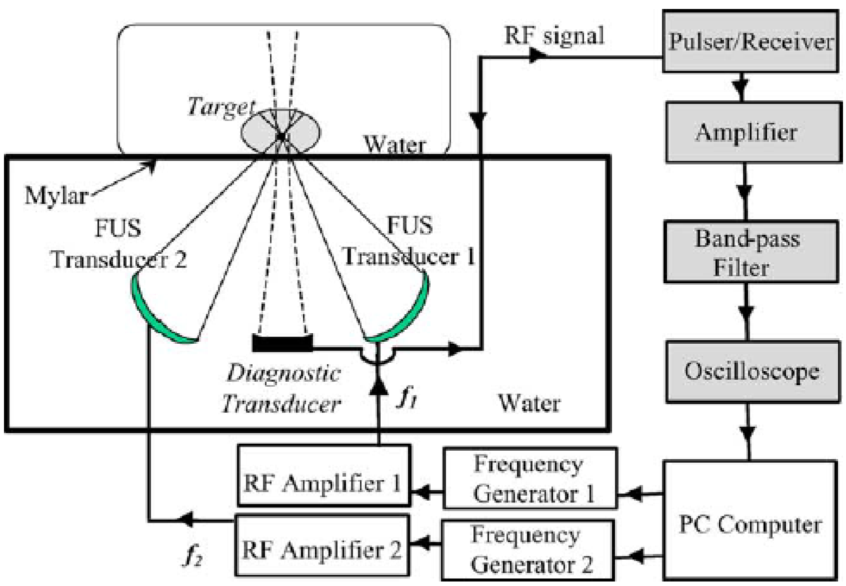

Figure 1.4: Harmonic motion imaging system set up [7].

was measured using a cross correlation method, from which mechanical proper-

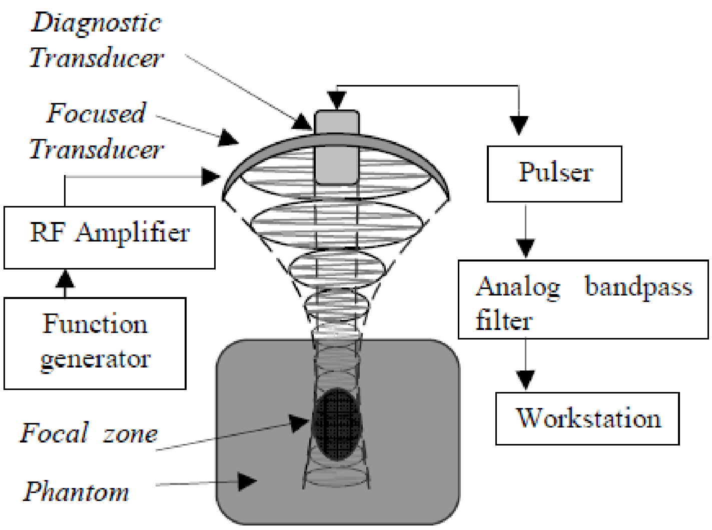

Figure 1.5: Harmonic motion imaging system set up [8].

ties of the target tissues were obtained. A mechanical model was developed to measure the displacement in amplitude modulated HMI [41]. In addition, the harmonic motion imaging utilizing focused ultrasound (HMIFU) which drives the focused ultrasound transducer at a higher energy acoustic beam for real time monitoring was investigated [42]. The 2D nonlinear wave propagation model and the finite-element method (FEM) were employed in HMIFU system for localization and size estimation of the lesions. The elastic contrast imaging methods are successful for distinguishing the malign and benign tissues but the studies are still continuing to develop an imaging device for clinical applications.

It is reported that the elastic contrast can be evaluated to gain the information from the elastic properties of different tissues in addition to their dielectric properties ([43–45]). In [44], and [45], the tissue was excited by up to a few kHz acoustic or mechanical compression/expansion and 2-D FDTD simulations were used to compute the scattered microwave signal due to boundary perturbation of the tumor. The use of elastic properties resulted in additional information about the malignancy of the tissue.

Recently, Harmonic Motion Microwave Doppler Imaging (HMMDI) has been proposed for the diagnosis of breast tumors [11, 46]. As it was mentioned and shown in Figures 1.2 and 1.1, the dielectric and elastic properties of malign and benign breast tissues are different. HMMDI method is a hybrid method that gives information about electrical and mechanical properties of the breast tissues. In this method, a local harmonic vibration is induced in the tissue using a focused ultrasound radiation force similar to the HMI system. The information about the vibration is measured by a microwave transceiver antenna. The microwave signal is transmitted to the vibrating tissue and the scattered signal is sensed by the receiver antenna. The induced vibration creates a Doppler shift which is changing in time since the speed of the vibrating tissue is changing sinusoidally. Therefore, the received data is frequency modulated due to this varying Doppler shift. In the frequency domain, this corresponds to infinite number of harmonics of the vibration frequency. In fact the first harmonic of the varying Doppler shift that contains the information of both electrical and elastic properties of the exposed tissue is detected. Therefore, the acquired data is induced by the Doppler effect, which is actually a frequency modulation due to the motion. The volume, maximum displacement, and dielectric properties of the vibrating region are the factors which determine the amplitude and phase of the received signal. Dimensions of the transducer(s) and ultrasound frequency define the focal volume of the transducer which determines the vibrating region volume. Frequency and intensity of the ultrasound in addition to elasticity determine the maximum displacement in vibrating region. In this method, 3-D images can be obtained. In addition, both mechanical and electrical properties of the tissue are explored which is superior to the usage of just mechanical properties in elastography, and electrical properties in microwave imaging technique. The localized radiation force is applied to the tissue by a single amplitude modulated focused ultrasound transducer, which increases the resolution of the obtained image.

1.1 Scope of the thesis

In this thesis study, for the first time the potential of such a hybrid method for breast cancer detection is investigated on tissue mimicking phantoms in the large-scale experimental studies. The method had been evaluated semi-analytically and numerically for breast tumor detection in [11]. In this thesis study, this method is implemented extensively on several phantoms, experimentally.

The goals in this thesis studies are listed as,

- To assess various stages of the HMMDI system development:

  The HMMDI system development consists of developing tissue mimicking phantoms, designing laboratory experimental set up, experimental studies on the developed phantoms, observing the practical problem related to this novel method, evaluating the performance of this method and finding its limitations.

- To design HMMDI experimental set up:

  Optimum transceiver microwave antenna location is investigated through several experiments. Coupling medium studies are done in simulation and practice. In this hybrid method, the coupling medium should have both appropriate acoustic and dielectric properties.

- To find the optimum operating microwave frequency and acoustic excitation frequency:

  The optimum microwave operating frequency that we can have the best coupling between the antennas and the phantom in addition to acoustic vibration frequency for receiving highest Doppler signal are investigated. In addition, the effect of different vibration frequencies on detecting different tissue phantoms are studied.

- To evaluate the performance of the designed HMMDI set up using spectrum analyzer as a receiver:

  In HMMDI method, a small induced vibration frequency (a few Hz) is so close to the microwave frequency (a few GHz). Therefore, the data is acquired with a high resolution spectrum analyzer. For the first time, a large scale experimental studies are done on the developed phantoms for evaluating the performance of the designed set up.

- To design the receiver system for real time data acquisition:

  for the first time a receiver system is designed for HMMDI system. In this method, the operating frequency is a few GHz while the applied acoustic ration force (vibration) has a frequency of a few Hz. Therefore, a receiver system is designed to bring the received signal to the base band and acquire the signal of interest at the vibration frequency.

- To evaluate the designed receiver system performance in experiments:

  The designed receiver system was evaluated on the developed tissue mimicking phantoms and the results were compared with the obtained results from the spectrum analyzer.

- To scan the phantoms in two dimensions (2-D)

  The developed inhomogeneous breast phantoms are scanned both in 1-D and 2-D. The obtained data is processed to evaluate the potential of this method in distinguishing malign from the benign breast tissues.

- To find the limitations of the HMMDI method

  It is the first time this method is implemented in practice for imaging different breast tissue phantoms. Therefore, by experimentally evaluating the HMMDI method, the problem and limitations of it was evaluated. Possible solutions to improve the performance of this novel imaging method are discussed.

1.2 Thesis organization

This thesis consists of 8 chapters as follows:

In chapter 2, HMMDI method and its basic principles are explained.

In chapter 3, different stages of tissue mimicking phantoms are given. In addition, the dielectric, elastic and acoustic properties measurement methods and measured results are presented.

In chapter 4, first generation of HMMDI in laboratory scale and the experimental results are given. The designed homodyne receiver system for the data acquisition through the designed system rather than spectrum analyzer is introduced. The obtained results of implementing the receiver system are discussed. It is shown that this method has a potential in discriminating tumor from fibroglandular and fat phantoms.

In chapter 5, the second generation of HMMDI is proposed to solve the observed problem of the first generation. The scan results of the phantoms using a new set up are presented. 2-D HMMDI data profiles are shown. The observed system limitations and possible solutions are discussed.

In chapter 6, a new HMMDI set up with new antenna configuration is proposed to overcome the limitations of introduced set up in chapter 5. The experimental results are presented. The effect of different vibration frequencies in ultrasound excitation is evaluated. 2-D data profiles of various inhomogeneous phantoms are given. The limitation and the possible solutions for the future studies are presented. The receiver system to acquire HMMDI data is introduced. The acquired data is processed using different processing tools. The results show the feasibility of this method for detecting breast tumors.

In chapter 7, the safety aspect of HMMDI as an imaging technique is presented. The temperature rise due to microwave and ultrasound exposure is dicussed. The temperature measurement results during HMMDI scan are given.

In chapter 8, conclusions and future work to realize this imaging technique are presented.

The block diagram of the outline of the thesis is shown in Figure 1.6.

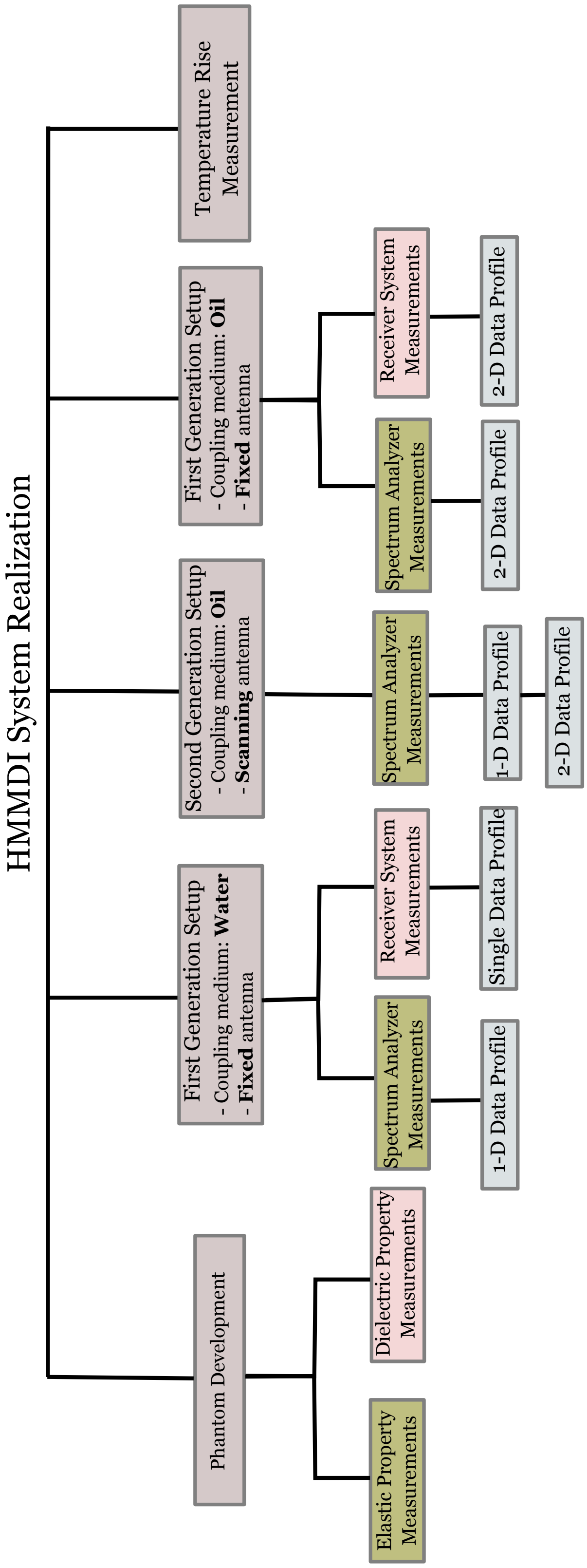

Figure 1.6: Thesis outline.

CHAPTER 2

HARMONIC MOTION MICROWAVE DOPPLER IMAGING (HMMDI)

2.1 Introduction

This thesis study is based on a recently proposed hybrid method, Harmonic Motion Microwave Doppler Imaging (HMMDI) [11]. This method provides information about electrical and mechanical properties of the breast tissues. In this chapter, the theoretical principles of this imaging method for breast cancer detection is presented.

A simplified HMMDI system set up is shown in Figure 2.1. In this method, a local vibration is induced in the tissue using a focused ultrasound radiation force similar to the Harmonic Motion Imaging (HMI) system. The microwave signal is transmitted to the vibrating tissue. The microwave signal scattered from the vibrating tissue is phase and amplitude modulated due to this vibration. The first spectral component of the received signal, is detected. Amplitude and phase of the detected signal depends on the maximum displacement, volume, and dielectric properties of the vibrating tissue. Focal volume of the transducer depends on the dimensions of the transducer and ultrasound frequency. Frequency and intensity of the ultrasound, in addition to elasticity of the vibrating tissue, determine the maximum displacement in the vibrating region.

In this method, both mechanical and electrical properties of the tissue are explored. This is the privilege of HMMDI over elastography which explores just the mechanical properties, and microwave imaging technique which is based on

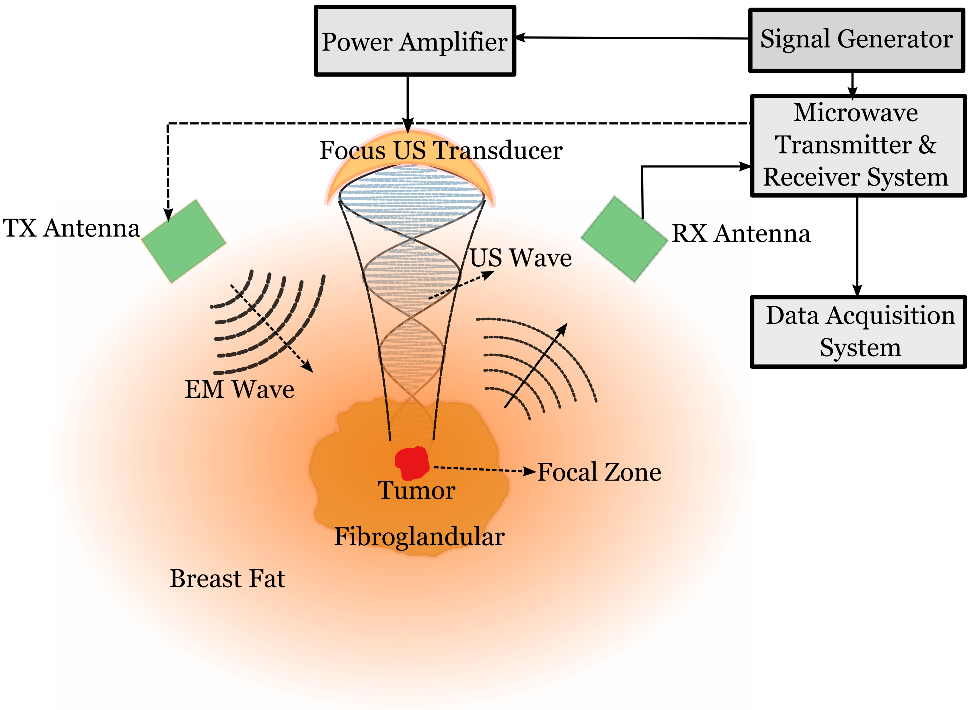

Figure 2.1: Simple HMMDI system set up.

the electrical properties of breast tissues.

2.2 Radiation force

In HMMDI, a localized radiation force is generated in the tissue by a single amplitude modulated ultrasound transducer [11]. The radiation force is a unidirectional force in the direction of propagation which is applied to the tissue due to transferring momentum from acoustic signal to the exposed tissue [6]. The amplitude of the radiation force is proportional to the acoustic beam intensity, and absorption [47]:

$$F = \frac{2\alpha I}{c_s} \tag{2.1}$$

where α $(1/m)$, I (W/cm^2) are the absorption constant and intensity of the acoustic beam, respectively. c_s $(\frac{m}{s})$ is the speed of the sound in the medium. F is the force per unit volume (kg/s^2cm^2) In HMMDI, an amplitude modulated (AM) waveform is used to drive the focused ultrasound (FUS) transducer [11].

Therefore, the acoustic pressure $P(t)$ of the AM waveform at the focus can be written as:

$$P(t) = P_0(1 + \cos(\Delta\omega t))cos(\omega_c t) \tag{2.2}$$

where P_0, $\Delta\omega$, and ω_c are the maximum instantaneous acoustic pressure, modulation frequency, and carrier frequency, respectively. The carrier frequency is the center frequency of the single element focused ultrasound transducer. In Figure 2.2 the resulting acoustic pressure $P(t)$ from the AM waveform is illustrated.

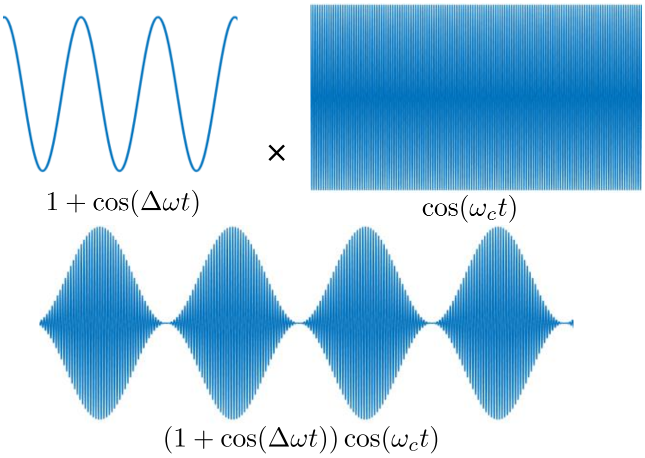

Figure 2.2: A sinusoidal waveform with a modulation frequency $\Delta\omega$ is multiplied by a sinusoidal waveform with a carrier frequency ω_c and yielding in an acoustic pressure $P(t)$.

The acoustic intensity is defined as the rate, at which the ultrasound energy is applied to a specific tissue location. The acoustic exposure is expressed by spatial-peak-temporal-average intensity (I_{spta}) and spatial peak-pulse-average intensity (I_{sppa}). I_{spta} defines the ability of the transmitted wave to heat the tissue and cause bio-effects. I_{sppa} describes the intensity of the transmitted acoustic waveform. In Figure 2.3 the acoustic pulses with duration t_{ON}, and pulse repetition time T are shown. The I_{spta} is calculated as:

$$I_{spta} = \frac{I_{sppa} \times t_{ON}}{T} \tag{2.3}$$

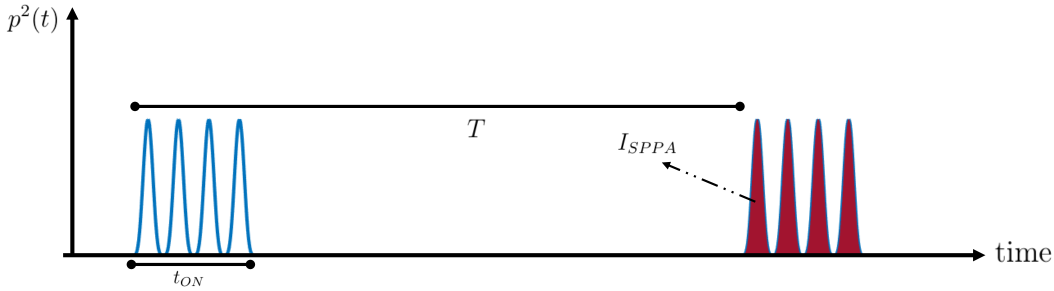

Figure 2.3: Illustration of acoustic intensity profile. The acoustic pulse duration, pulse repetition time, and spatial peak-pulse-average intensity are shown as t_{ON}, T, and I_{sppa}, respectively.

In the AM case, the average acoustic intensity $I(t)$, is characterized by the I_{sppa}. The average acoustic intensity I of the acoustic beam can be calculated as [48]:

$$I(t) = \int_0^t \frac{P^2(\tau)}{\rho c} d\tau \tag{2.4}$$

$$\begin{aligned} I(t) =& \frac{P_0^2}{\rho c} \int_0^t \{(1+\cos(\Delta\omega\tau))\cos(\omega_c\tau)\}^2 d\tau = \\ & \frac{P_0^2}{\rho c} \int_0^t \left\{\cos^2(\omega_c\tau) + 2\cos^2(\omega_c\tau)\cos(\Delta\omega\tau) + (\cos(\omega_c\tau)\cos(\Delta\omega\tau))^2\right\} d\tau \end{aligned} \tag{2.5}$$

where t is the exposure time, ρ is the density, and c is the sound speed.

By evaluating the integral one obtains,

$$\begin{aligned} I(t) = & \frac{P_0^2}{\rho c}\left[\frac{t}{2} + \frac{\sin(2\omega_c t)}{4\omega_c} + \frac{\sin(\Delta\omega t)}{\Delta\omega} + \frac{\sin((2\omega_c + \Delta\omega)t)}{2(2\omega_c + \Delta\omega)} + \frac{\sin((2\omega_c - \Delta\omega)t)}{2(2\omega_c - \Delta\omega)}\right] \\ & + \frac{P_0^2}{\rho c}\left[\frac{t}{4} + \frac{\sin(2\omega_c t)}{8\omega_c} + \frac{\sin(2\Delta\omega t)}{8\Delta\omega} + \frac{\sin(2(\omega_c + \Delta\omega)t)}{16(\omega_c + \Delta\omega)} + \frac{\sin(2(\omega_c - \Delta\omega)t)}{16(\omega_c - \Delta\omega)}\right] \end{aligned} \tag{2.6}$$

The sinusoidal function with a high carrier frequency component ω_c is assumed to be negligible. Therefore, the intensity can be approximated as:

$$I(t) = \frac{P_0^2}{\rho c \Delta\omega}\left[\sin(\Delta\omega t) + \frac{\sin(2\Delta\omega t)}{8}\right] \tag{2.7}$$

In a case where the pressure wave is in the form of double-sideband suppressed-carrier [48] as

$$P(t) = P_0 \cos(\Delta\omega t).cos(\omega_c t) \tag{2.8}$$

The the intensity is:

$$I(t) = \frac{P_0^2}{\rho c \Delta\omega} \frac{\sin(2\Delta\omega t)}{8} \tag{2.9}$$

The Young's Modulus as an elasticity parameter (E), Poisson's ratio of the tissue (ν), and displacement are related to each other according to [11]:

$$E = \frac{2(1-\nu)^2 F r_b}{X_0 A} \tag{2.10}$$

where F, r_b, A, X_0 are the acoustic radiation force, radius of the beam at the focus, cross sectional area of the beam at the focus, and the maximum displacement. When the excitation is sinusoidal ($F(t) = F_0 \sin(\Delta\omega t)$), it can be assumed that the vibrating tissue has a circular cross-section and vibrates like a piston, uniformly. So the displacement can be determined as [6]:

$$X(t) = \frac{F_0 \sin(\Delta\omega t)}{\Delta\omega Z} = X_0 \sin(\Delta\omega t + \phi) \tag{2.11}$$

where Z as the mechanical impedance of the tissue.

2.3 Effects of ultrasound radiation force on received microwave signal

In HMMDI, the tissue is exposed by an ultrasound radiation force. It is assumed that where there is an electrically small spherical tumor in the exposed tissue(Figure 2.4). Therefore, tissue has a local harmonic motion at the region of the focused ultrasound. From the other hand, a continuous-wave microwave signal is transmitted to this tissue with local harmonic motion. In such a case, the received signal due to the output of the transmitter antenna ($S_{TX}(t) = A\cos(\omega_m t)$) has the following form [11]:

$$\begin{aligned} S_{RX}(t) =& AC_{leak}\cos(\omega_m t + \phi_1) + AC_{Clut}cos(\omega_m t + \phi_2) + \\ & AC_t cos(\omega_m t + \frac{4\pi R}{\lambda} R + K\sin(\Delta\omega t) + \phi_2) \end{aligned} \tag{2.12}$$

where the first term in the argument of the right hand side is related to the received signal from the transmitter antenna (leakage C_{leak}), second term shows the received signal from the clutter (C_{Clut}), and the last term is the received signal due to the vibrating region (C_t). Here, R is the distance from antennas to locally vibrating tissue (it is assumed that the locally moving region is on the mid-plane of transmitting and receiving antennas), ω_m is the operating frequency of the antenna, $\Delta\omega$ is the vibration frequency of the tissue. ϕ is a constant phase which depends on the total path length. K is the phase change (in radians) of the signal, which depends on the elastic properties of the focal region. B is the magnitude of the received signal for the case that there is no vibration, which depends on the electrical properties of the focal region and the background tissue. The received signal due to vibrating dipole can be written as [11]:

$$S_{RX}(t) = Bcos(\omega_m t + \frac{4\pi R}{\lambda} + K\sin(\Delta\omega t) + \phi) \tag{2.13}$$

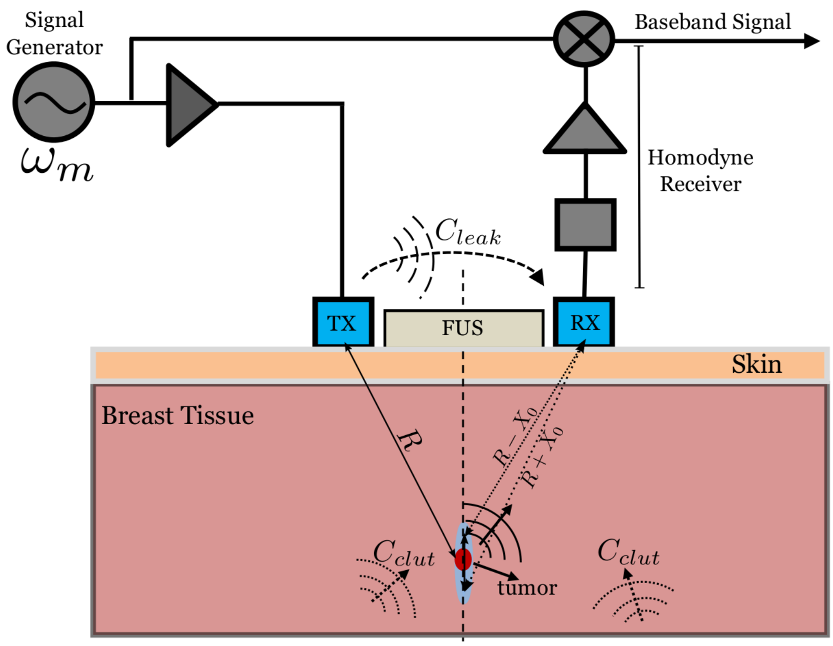

Figure 2.4: Simple geometry of the problem.

The cosine term in the right hand side of equation 2.12 can be expressed as [11]

$$\begin{aligned}
&\cos(\omega_m t + \frac{4\pi R}{\lambda} + K\sin(\Delta\omega t) + \phi) = \\
&\cos(\omega_m t + \phi + \frac{4\pi R}{\lambda})\cos(K\sin(\Delta\omega t)) - \\
&\sin(\omega_m t + \phi + \frac{4\pi R}{\lambda})\sin(K\sin(\Delta\omega t))
\end{aligned} \tag{2.14}$$

Since X_0 is very small compared to wavelength of electromagnetic wave, $K << 1$, cosine and sine terms can be simplified as:

$$\cos(K\sin(\Delta\omega t)) \approx 1 \tag{2.15}$$

$$\sin(K\sin(\Delta\omega t)) \approx K\sin(\Delta\omega t) \tag{2.16}$$

Equation 2.14 can be written as:

$$\begin{aligned}
&\cos(\omega_m t + \frac{4\pi R}{\lambda} + K\sin(\Delta\omega t) + \phi) = \\
&\cos(\omega_m t + \phi + \frac{4\pi R}{\lambda}) - \sin(\omega_m t + \phi + \frac{4\pi R}{\lambda}).K\sin(\Delta\omega t)
\end{aligned} \tag{2.17}$$

The received signal has a component at the operating frequency ω_m and also at the two different main frequency components at $\omega_m + \Delta\omega$ and $\omega_m - \Delta\omega$ (Figure 2.5). Since the vibration frequency $\Delta\omega$ is known, the received signal can be down converted to the baseband and through the proper receiver system the Doppler component of the received signal can be detected.

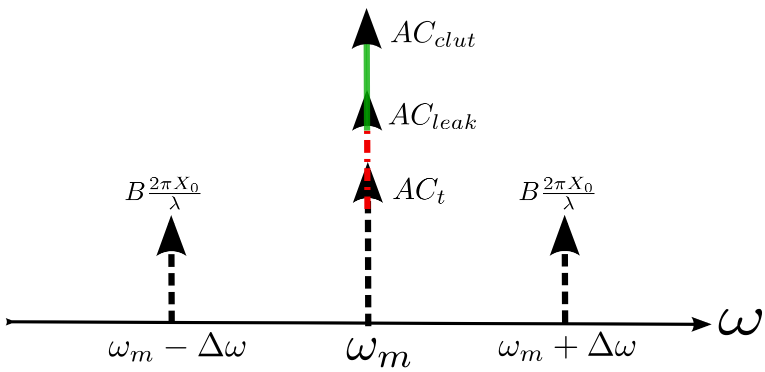

Figure 2.5: The frequency components of the received signal.

Consequently the received signal can be written as [11]:

$$S_{RX}(t) = Bcos(\omega_m t + \phi + \frac{4\pi R}{\lambda}) + B\frac{K}{2}[\sin(\omega_m t + \Delta\omega t + \phi_1) + \sin(\omega_m t - \Delta\omega t + \phi_2)] \tag{2.18}$$

By means of mixer, signal can be down converted to the base-band. The Doppler frequency component of the received signal is the DC component multiplied by K.

CHAPTER 3

TISSUE MIMICKING PHANTOMS

3.1 Introduction

To evaluate the performance of HMMDI as a breast imaging method, realistic breast phantoms are required. These phantoms should exhibit similar dielectrical and mechanical properties, as the living breast tissues. Several studies have been done on the development of tissue mimicking phantoms which show similar dielectric properties (permittivity, and conductivity) in the microwave frequency range [1, 2, 25, 49–51]. In addition, a number of investigations have been conducted for developing breast phantom suitable for radiation force imaging and elastography [3, 52–55]. Some phantoms were studied to mimic the ultrasonic properties [56]. Referring to a number of studies, oil-in-gelatin emulsion phantoms are proper for elastography [54, 55] and microwave imaging [1, 2, 49, 51]. These type of phantoms contain gelatin, kerosene, safflower oil, p-toluic acid, n-propanol, deionized water, formaldehyde, and surfactant. It was shown that their mechanical and electrical properties are stable over a time.

In this chapter, different instructions for developing breast tissue mimicking phantoms are implemented. Three different breast tissue phantoms, fibro-glandular, fat, and tumor phantoms which are produced for HMMDI experimental studies are shown. The dielectric and elastic measurement methods for testing these phantoms are presented. The results of elasticity and dielectric measurements for the developed phantoms are given. The developed phantoms are compared to find the optimum breast tissue phantom production instruction.

3.2 Development of Tissue Mimicking Phantoms

As mentioned above, oil in gelatin solutions are the proper choice for phantoms which mimick both elastic and dielectric properties of the breast tissues. By using p-toluic acid and n-propanol as preservatives, they can last long [9, 55]. Formaldehyde is used for cross-linking of the gelatin, and could be a proper choice for developing stable phantoms [9]. Variation of oil and gelatin percentages gives us the opportunity to change the electrical and mechanical properties. In addition, the amount of surfactant plays an important role for homogeneity and solidity of the phantom solution.

Fat tissue as a high-adipose content tissue could be made by adding high rates of oil [9]. From the other hand, since the dielectric and elastic constants of the tumor are high it is developed using low amount of oil. In addition, the amount of gelatin and water can be another factor for setting the dielectric and mechanical properties of the fibro-glandular tissue with high dielectric constant but low elastic constant. By decreasing the amount of gelatin mixed in water, the stiffness can be decreased without changing the dielectric constant. In addition, it has been proposed that the Young modulus of the phantom can be decreased if it is baked at 50 $°C$ [57].

In this study, three different type of phantoms (breast fat, fibro-glandular, and tumor) are produced. The composition of materials to prepare about 1 liter phantom volume is given in Table 3.1. Two methods are evaluated for making fibro-glandular phantoms. In one of them the fibro-glandular tissue phantoms are obtained by baking tumor phantom at 50 $°C$ for 4 days. In the other, the instruction given in [2] where 35% of phantom materials is oil, is implemented. phantom development steps are as follows (3.1) [1]:

i) The p-toluic acid is mixed with n-propanol in a small beaker. In order to dissolve the p-toluic acid, the mixture is heated and stirred.

ii) The deionized water is mixed with the obtained solution in a beaker.

iii) The gelatin is mixed with the solution. The mixture should be kept at the

Table3.1: Composition of 1 liter realistic phantoms [1]. Abbreviations: TM: Tumor, FG: Fibro-glandular, p-tol: p-toluic acid, n-prop: n-propanol, formald.: Formaldehyde, surf.: Surfactant.

Tissue type	Kerosene (ml)	Oil (ml)	p-tol (gr)	n-prop (ml)	water (ml)	gelatin (gr)	formald (ml)	surf (ml)
fat	330	330	167	8.3	158	28.6	1.67	140
TM/FG	49.5	49.5	800	39.6	753.5	135	7.9	10.1

room temperature.

iv) The beaker is covered and heated. In order to uniformly heat the solution, it is completely kept in water while heating.

v) The procedure is continued until obtaining a transparent mixture with no air bubbles at about 90 $°C$.

vi) The mixture is stirred to produce the uniform solution and then the air bubbles on the surface are removed.

vii) The solution is put inside a water bath and stirred until its temperature is $50°C$.

viii) The oil mixture containing the safflower oil and kerosene, is heated to reach 50 $°C$.

ix) The oil is added to the transparent uniform gelatin solution at $50°C$. If the oil percentage is above 50 % oil, some part of oil is added and the solution is stirred until the oil drops becomes so small. After that the rest of the oil mixture is added, partially and stirred continuously to minimize the oil drops. If the oil percentage is below 50% oil, whole oil mixture is added at the first time.

x) While mixing the surfactant is added by a syringe with a needle.

xi) The mixture is stirred when the baker is in cool water bath to reach 40 $°C$.

xii) The formaldehyde (37%) is added using needle and syringe.

xiii) The mixture is cooled to $34°C$ and poured into the mold to become cool and solid. The cross-linking of gelatin is completed in about 5 days.

Table3.2: Composition of 1 Liter realistic Phantoms [2]. Abbreviations: FG: Fibro-glandular, p-tol: p-toluic Acid, n-prop: n-propanol, formald.: Formaldehyde, surf: Surfactant.

Tissue type	Kerosene (ml)	Oil (ml)	p-tol (gr)	n-prop (ml)	water (ml)	gelatin (gr)	formald (ml)	surf (ml)
Tumor	44.6	44.6	787	39.7	753.5	134.8	2.93	8
FG	248.9	248.9	787	39.7	753.5	134.8	2.93	25.7

The produced phantoms is shown in Figure 3.2. The developed fat and tumor phantoms are homogeneous while gelatin is settled down in the fibro-glandular phantoms. The elastic and dielectric properties of the developed phantoms are measured. These measurement techniques are presented in the following sections.

The elasticity of the developed tumor phantoms is measured and found higher than the reference values [3]. As the tumor phantoms gets stiffer, more ultrasound radiation force is needed to introduce a detectable displacement. As a consequence, the induced heat increases, which is not desirable from the patient safety perspective.

Therefore, other phantom development instructions are investigated. It is observed that the formaldehyde amount has a critical role in the stiffness of the phantoms. So, less amount of formaldehyde [2] is used to produce the tumor and fibro-glandular phantoms. The amount of materials in these new phantoms are given in Table 3.2.

The phantoms are developed and poured into the falcon tubes (Figure 3.3). After 7 days when the cross linking of the gelatin is completed and the phantoms are solidified, the dielectric and elastic property measurements are done. The elastic property of the new developed tumor phantom [2] is decreased to 50 kPa which is close to the reference value given in Table 3.3. In order to develop the fibro-glandular phantom, the developed tumor phantom is baked for 5 days. During the baking period, the phantom is melted. After 2 days keeping the melted fibro-glandular phantom in the room temperature, it is again solidified.

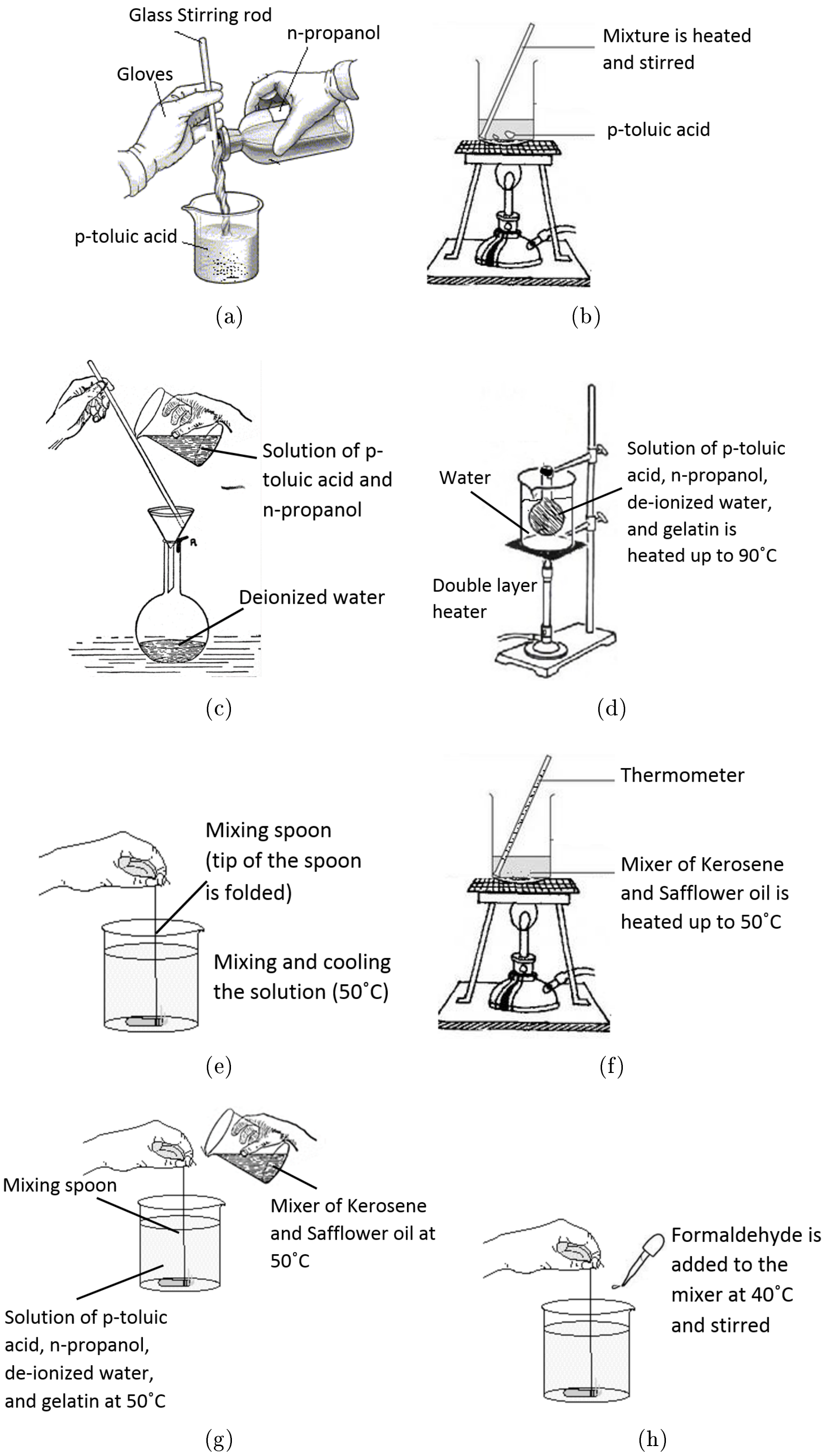

Figure 3.1: Gelatin in oil based tissue mimicking breast phantom development stages according to [1] given instruction.

Figure 3.2: The produced phantoms, from left to right: Breast Fat, Fibroglandular-1, Fibroglandular-2, Tumor-1, Tumor-2.

In addition, the fibro-glandular with the ingredient given in Table 3.2 [2] is produced. But, this phantom does not become homogeneous and the oil part comes on top of the phantom and the gelatin part is settled down (Figure 3.3-right). Therefore, the fibro-glandular phantoms which are made by baking the tumor phantoms (developed according to [1, 2]) are used in the HMMDI experimental studies. In the following sections, the measurement techniques for calculating the dielectric and elastic properties of the developed phantoms and results are provided.

3.3).

Figure 3.3: Developed fibroglandular (left) and the tumor (right) phantoms with the ingredients given in Table 3.2.

3.2.1 Measuring the dielectric and elastic properties of the tissue mimicking phantoms

Phantom development is essential for investigating the performance of HMMDI method. To obtain accurate experimental results, phantoms should mimic the electrical and elastic properties of biological breast tissue. Therefore, they should satisfy the following characteristics:

- They should be stable over a time.
- They should be made from nonpoisonous materials.
- They should be easy to develop.
- They should mimic dielectric and elastic properties of the biological tissues.

In the following sections, both dielectric and the elastic measurement methods which are selected for evaluating the properties of the developed phantoms are discussed.

3.2.2 Measurement of dielectric properties

The virtual line method is used to measure the dielectric properties of the phantoms [11, 58]. In this method, when the coaxial probe is inside the material, it is assumed that it is extended inside the material, virtually. It can be assumed that dielectric constant of the material under the test is the dielectric constant of this virtual section of the coaxial probe. The radiation loss of the probe is ignored, and the virtual line is terminated with open circuit. The probe model in the virtual line method is shown in Figure 3.4. The parameters in this method are as follow:

Y_d: Characteristic admittance of the virtual line.
ε_d: Complex dielectric constant of the sample material.
β_d: Propagation constant of the virtual line.
Y_t: Characteristic admittance of the coaxial probe.

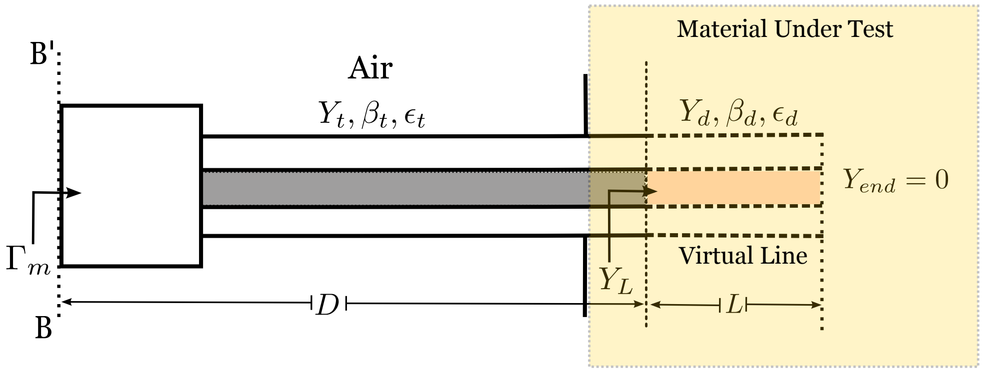

Figure 3.4: Virtual line method and the coaxial probe model for dielectric constant measurement. Y_d is the characteristic admittance of the virtual line, ε_d is the complex dielectric constant of the sample. β_d is the propagation constant of the virtual line and Y_t is the characteristic admittance of the coaxial probe. Complex dielectric constant of the dielectric material used in the probe is ε_t. β_t is propagation constant of the probe and Y_L is the admittance at the probe's open end. The reflection coefficient at B-B' section is shown by Γ_m. D and L are physical length of the probe and length of the virtual line, respectively

ε_t: Complex dielectric constant of the dielectric material used in the probe.

β_t: Propagation constant of the probe.

Y_L: The admittance at the probe's open end

Γ_m: The reflection coefficient at B-B' section.

D: Physical length of the probe.

L: Length of the virtual line.

The admittance at the probe's open end can be written as:

$$Y_L = jY_d \tan(\beta_d L) \tag{3.1}$$

The characteristic admittance of the virtual line is:

$$Y_d = \frac{\sqrt{\varepsilon_d}}{60 \ln \frac{b}{a}} \tag{3.2}$$

Relationship between Γ_m, Y_t and Y_L is given as:

$$Y_L = Y_t \frac{1 - \Gamma_m e^{2j\beta_t D}}{1 + \Gamma_m e^{2j\beta_t D}} \tag{3.3}$$

where

$$Y_t = \frac{\sqrt{\varepsilon_t}}{60 \ln \frac{b}{a}} \tag{3.4}$$

By using above relations, complex dielectric constant of the material is given by:

$$\varepsilon_d = \frac{-jc\sqrt{\varepsilon_t}}{2\pi f L} \frac{1-\Gamma_m e^{2j\beta_t D}}{1+\Gamma_m e^{2j\beta_t D}} \coth(\frac{(2\pi f L\sqrt{\varepsilon_d})}{c}) \tag{3.5}$$

D and L at each measuring frequency are unknown. D and L can be calculated using two standard dielectric mediums. Substituting 3.1 into 3.3, one can obtain

$$\Gamma_m e^{2j\beta_t D} = \frac{\rho + e^{-2j\beta_d L}}{1+\rho e^{-2j\beta_d L}} \tag{3.6}$$

where

$$\rho = \frac{\sqrt{\varepsilon_t}-\sqrt{\varepsilon_d}}{\sqrt{\varepsilon_t}+\sqrt{\varepsilon_d}} \tag{3.7}$$

Air ($\varepsilon_{air} = 1$) and deionized water are used as standard dielectric mediums for probe calibration procedure. The dielectric constant of pure water is defined by the Cole-Cole equation [58]:

$$\begin{aligned} \varepsilon(\omega) &= \varepsilon_\infty + \frac{\varepsilon_s - \varepsilon_\infty}{1+(j\omega\tau)^{1-\alpha}} \\ &= 4.6 + \frac{78.3-4.6}{1+(j\omega 8.08\times 10^{-12})^{1-0.014}} \end{aligned} \tag{3.8}$$

where ε_s and ε_∞ are the static and infinite frequency dielectric constants, ω is the angular frequency, and τ is a time constant. Therefore, the cost functions in our problem are defined as:

$$F_1(D,L) = \begin{bmatrix} \Gamma_{m,air} e^{2j\beta_t D} - \frac{\rho_{air}+e^{2j\beta_{air}L}}{1+\rho_{air}e^{2j\beta_{air}L}} \\ \Gamma_{m,water} e^{2j\beta_t D} - \frac{\rho_{water}+e^{2j\beta_{water}L}}{1+\rho_{water}e^{2j\beta_{water}L}} \end{bmatrix} \tag{3.9}$$

$$F_2(\varepsilon_d) = \varepsilon_d - \frac{-jc\sqrt{\varepsilon_t}}{2\pi f L} \frac{1-\Gamma_m e^{2j\beta_t D}}{1+\Gamma_m e^{2j\beta_t D}} \coth(\frac{2\pi f L\sqrt{\varepsilon_d}}{c}) \tag{3.10}$$

To find the three unknowns, D, L, and ε_d, optimization methods can be used. In this study, the system of nonlinear equations is solved by MATLAB built-in function, $fsolve$.

3.2.2.1 Solving systems of nonlinear equations

A system of nonlinear equations can be solved by MATLAB built-in function, $fsolve$. In this function, two algorithms of Trust-Region Reflective and Levenberg-Marquardt are used to solve the problem [59]. However, it is not accept any constraints, such as bound constraints. It solves a the following expression: $F(x) = 0$ for x, where $F(x)$ is a function that returns a vector value, and x is a vector or a matrix. Limitations of this method are: It handles continuous functions. $fsolve$ gives one root if the algorithm is successful. $fsolve$ may converge to a nonzero point. In this case, different initial values should be applied. $fsolve$ accept real variables. In a case where x has complex variables, the variables should be written as real and imaginary parts.

Assuming a set of n nonlinear functions $F_i(x)$, where n is the number of components of the vector x, the equation solver find a vector x that makes all $F_i(x) = 0$. By minimizing the sum of squares of the components, $fsolve$ algorithm solves a system of nonlinear equations. The system of equations is solved if the sum of the squares becomes zero [59].

$fsolve$ optimization algorithm is based on trust regions concept [59]. Assuming minimizing f(x), that function accept vector arguments and gives scalars. For going from an initial point x in n-space to a point with a lower function value, a simpler function q can be considered which behaves similar to f function in a neighborhood N around the point x. This neighborhood is called as trust region. The trust-region subproblem is a trial step s which is computed by minimizing around N.

$$min_s \{q(s), s \in N\} \tag{3.11}$$

If $f(x + s) < f(x)$, x is updated to $x + s$. Otherwise, the x is not changed and the region of trust N, is shrunk and the trial stage computation is repeated. The questions are how to choose q, how to choose and update the trust region N, and how to solve the trust-region subproblem. There are three algorithms in $fsolve$ to define the trust region [59]:

- Trust-region-reflective
- Trust-region dogleg
- Levenberg-Marquardt

The default algorithm of $fsolve$ for trust region definition is Levenberg-Marquardt

[59]. This algorithm, uses a search direction which is a solution of the following linear set of equations.

$$\left(J(x_k)^T J(x_k) + \lambda_k I\right) d_k = -J(x_k)^T F(x_k), \tag{3.12}$$

where the scalar λ_k controls both the magnitude and direction of d_k. When λ_k is zero, the direction d_k is the Gauss-Newton method. As λ_k increases to infinity, d_k tends towards the steepest descent direction, with magnitude tending to zero. Therefore, the term $F(x_k + d_k) < F(x_k)$ holds true for large λ_k. In Levenberg-Marquardt method, the search direction is first the Gauss-Newton direction and then the steepest descent direction.

3.2.2.2 Genetic Algorithms

The results of dielectric measurement using nonlinear optimization algorithms are highly dependent on the initial values of L and D. Therefore, the Genetic Algorithms (GAs) which do not require initial values, could be a proper method to find the initial value for system of nonlinear equation solver.

GAs are adaptive stochastic search algorithm based on the evolutionary natural selection and survival phenomenon [60]. Firstly, some candidates are generated, randomly. Then, these candidates are evolve and compete to reach the better solutions by using genetic operators. In each generation, the most successful individuals produce more offspring comparing the others. An evaluation function which has the environment role, is used to realize good from bad solutions.

The main differences between genetic algorithm and a classical, derivative-based, optimization algorithm are as follows:

- In the classical algorithm, a single point is generated at each iteration and a sequence of points evolves to an optimal solution.
- In GA, a number of points is generated at each iteration and the best of them reaches the best solution.
- In classical algorithm, the next point in the sequence is selected by a deterministic algorithms.

- In GA, the next population is selected through algorithms that uses random number generators.

3.2.2.3 Dielectric property measurement algorithm

The convergence of nonlinear optimization algorithms in dielectric property calculations based on virtual line method, depends on the initial values of L and D. Therefore, the genetic algorithm is used for finding initial values of D and L. Since the problem is 2-D, the complexity of the genetic algorithm is low. For calculating the dielectric constant of the tissue mimicking phantoms, MATLAB tool provided by [11] is modified as the following algorithm,

---

Dielectric Property Measurement Virtual Line Method

Measurement: Obtain reflection parameters $\Gamma_{m,air}$, $\Gamma_{m,water}$, Γ_m for air, deionized water and medium.

Reference material properties :

$\varepsilon_{water}(\omega) = 4.6 + \frac{78.3-4.6}{1+(j\omega 8.08\times 10^{-12})^{1-0.014}}$, $\varepsilon_{air} = 1$, and calculate ρ_{air}, ρ_{water} from 3.7

Finding Initial Value of D and L: Define $\vec{x} = [D\ L]^T$, and set lower and upper bound as:

$\vec{x}_{lb} = [0.1\ \ 0.0002]^T$, $\vec{x}_{ub} = [0.15\ \ 0.001]^T$

$$F_1(\vec{x}) = \begin{bmatrix} \Gamma_{m,air}e^{2j\beta_t x(1)} - \frac{\rho_{air}+e^{2j\beta_{air}x(2)}}{1+\rho_{air}e^{2j\beta_{air}x(2)}} \\ \Gamma_{m,water}e^{2j\beta_t x(1)} - \frac{\rho_{water}+e^{2j\beta_{water}x(2)}}{1+\rho_{water}e^{2j\beta_{water}x(2)}} \end{bmatrix}$$

$\vec{x}_1 = GeneticAlgorithm(F_1(\vec{x}),\ N_{dim} = 2,\ \vec{x}_{lb},\ \vec{x}_{ub})$

3.2.2.4 Experimental results

For calculating the dielectric constant of the tissue mimicking phantoms, the modified MATLAB tool provided by [11] is used. KEYSIGHT, FieldFox Microwave Analyzer N9915A is used for the measurements (Figure 3.5). A semi-

Finding Exact Value of D and L: Use Trust-Region Dogleg based *fsolve* function of MATLAB

$\vec{x} = fsolve(F_1(\vec{x}),$ Initial value $= \vec{x}_1)$ $D = x(1)$ and $L = x(2)$

Calculate ε_d:

$F_2(\varepsilon_d) = \varepsilon_d - \frac{-jc\sqrt{\varepsilon_t}}{2\pi fL}\frac{1-\Gamma_m e^{2j\beta_t D}}{1+\Gamma_m e^{2j\beta_t D}}\coth(\frac{2\pi fL\sqrt{\varepsilon_d}}{c})$

$\varepsilon_d = fsolve(F_2(\varepsilon_d),$ Initial value $= 3)$

rigid L-shaped coaxial cable with 130 mm length is used as the probe. In these measurements, air and de-ionized water are used for calibration references. The accuracy of the measurements is verified by measuring oil's dielectric constant. Frequency range of the measurements are considered as 1 - 9 GHz. Time domain gating is applied.

The fat and fibro-glandular phantoms inside the falcon tubes are cut into three pieces. The measurements are taken from top and bottom surfaces of each piece. The average of 6 measurements for each phantom is reported as the dielectric constant of the phantoms.

Finding proper initial value in the $fsolve$ optimization function in dielectric constant measurement is critical. This problem is solved by using the genetic algorithm with constrains to find the initial value of the D and L in the optimization problem solved by $fsolve$ function. In the implemented genetic algorithm, lower and upper bound are selected as $[0.1; 0.0002]$ and $[0.15; 0.001]$, respectively. The phantoms are developed according to the instructions given in [3] but since Young modulus of the developed fibro-glandular and tumor phantoms is high, more elastic phantoms are developed based on [2]. The fat phantom is developed just according to [3], because the elastic property of this phantom is consistent with the reference value [3]. The measured relative permittivity of the developed phantoms according to [3] are given in Figure 3.6. As it can be seen, the dielectric properties of these phantoms are in a good agreement with the reference values related to the biological breast tissues [9]. In Figure 3.7, the dielectric properties of the developed phantoms according to [2] is shown. As it can be seen, the dielectric properties of phantoms is consistent with the

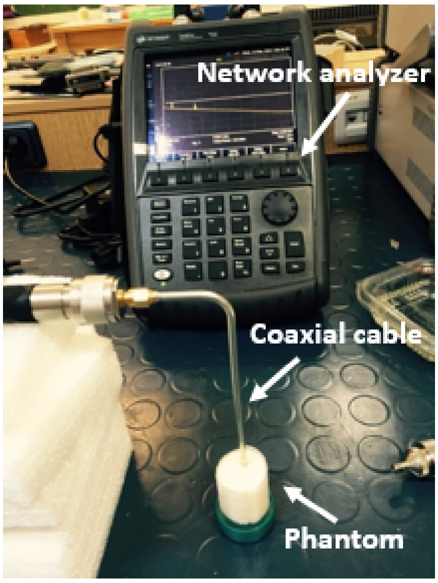

Figure 3.5: The system set up for the dielectric measurements.

dielectric properties of human breast tissues.

3.2.3 Measurement of elastic properties

The elastic properties of the phantoms are measured through dynamic and static measurements. Dynamic elastic tests are done using Perkin Elmer Pyris Diamond Dynamic Measurement Analyzer (DMA) in METU Central Laboratory (Figure 3.8). The fat and tumor phantoms are cut in a cylindrical shape with 5 mm diameter and height. Two samples from each type of the phantoms are sent for the tests. Fifteen measurements are done at $25°C$, for 0.1 Hz, 1 Hz, and 10 Hz frequencies. For more accuracy, 10 measurements are conducted in each frequency. The average of storage and loss moduli of the samples are presented in Table 3.3. Using the ingredients given in Table 3.1, the elasticity of the developed tumor phantoms are higher than the reference values [3]. To induce detectable displacement in these phantoms, stronger ultrasound radiation force is required. Therefore, the risk of induced heat and tissue damage becomes more. However, the measurements for the same type of phantoms are consistent.

Same measurements are done for the phantoms developed according to [2]. The

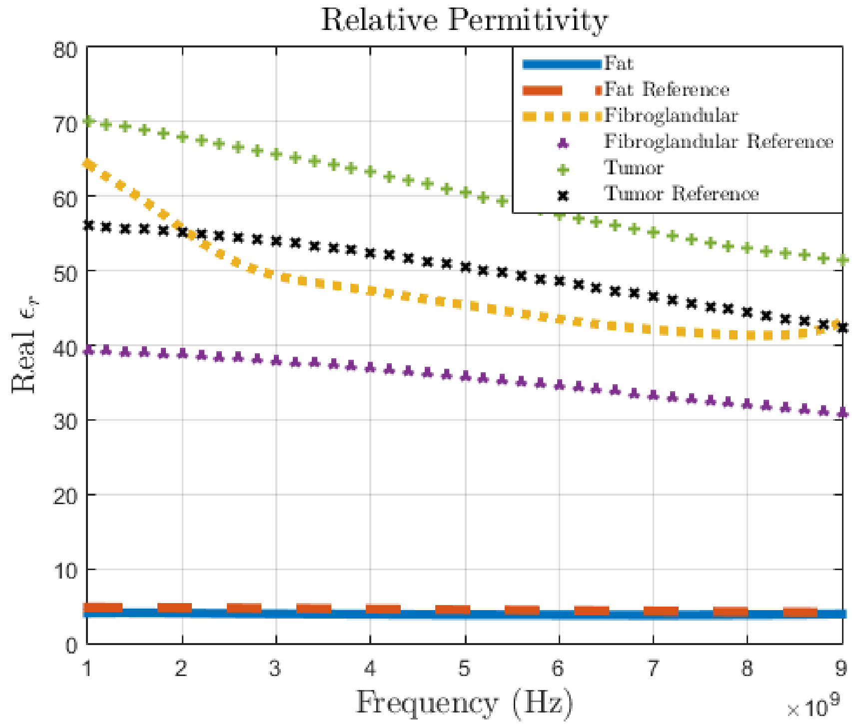

(a)

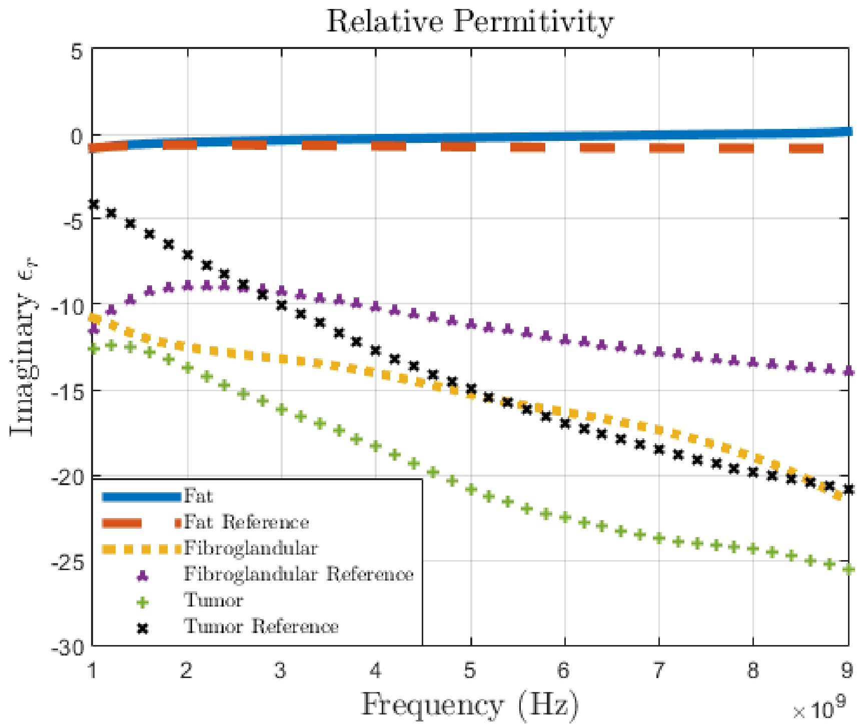

(b)

Figure 3.6: The measured relative permittivity of the developed phantoms [3] and the reference values related to the biological breast tissues [9] (a) real ϵ_r (b) imaginaryϵ_r.

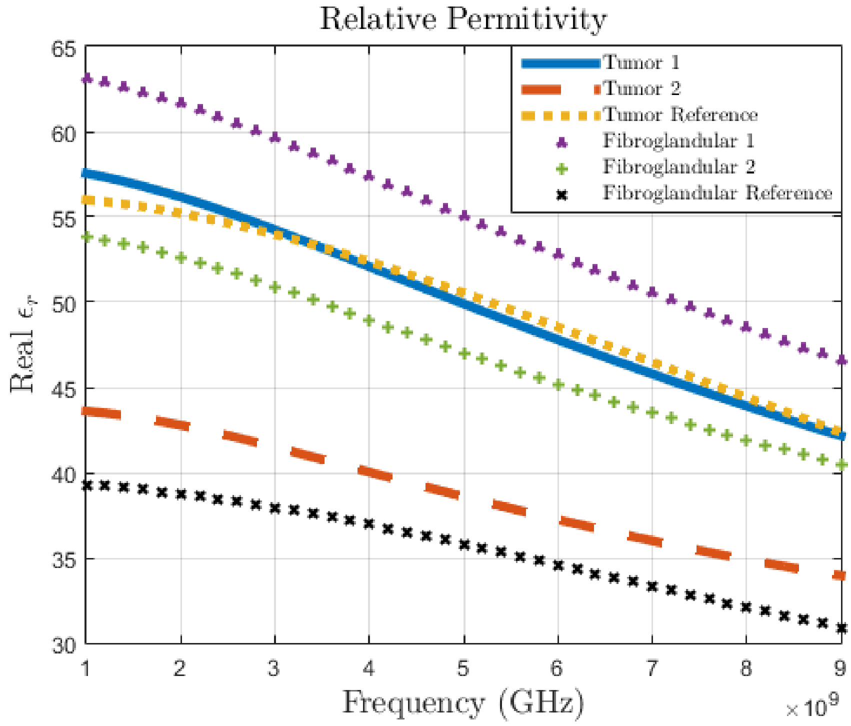

(a)

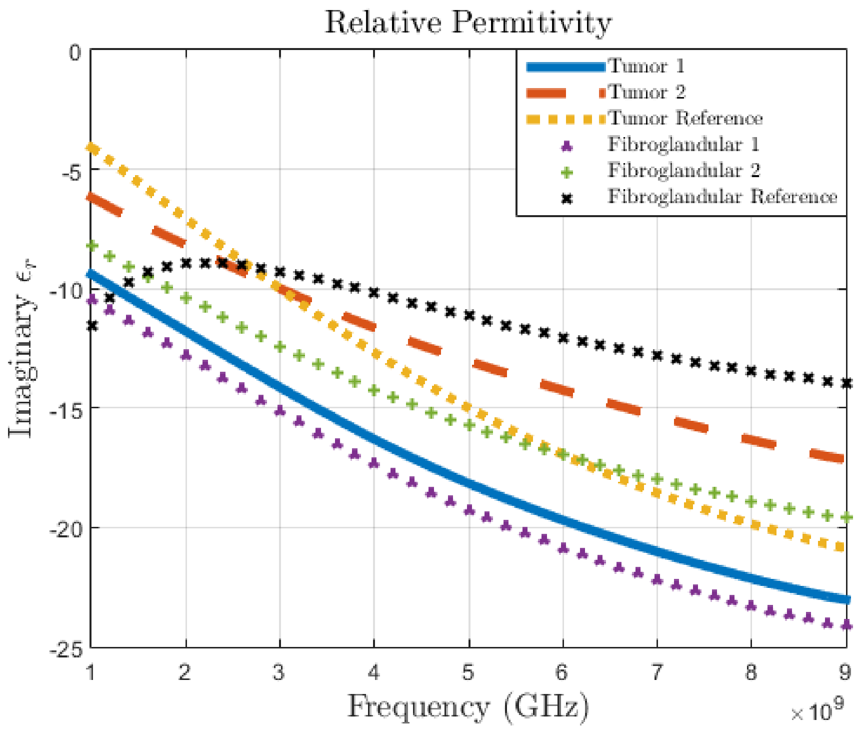

(b)

Figure 3.7: The measured relative permittivity of the developed phantoms as [2] called as tumor1 and fibroglandular1 and the one from [2] called as tumor2, fibroglandular2 [3] (a) real ϵ_r (b) imaginaryϵ_r.

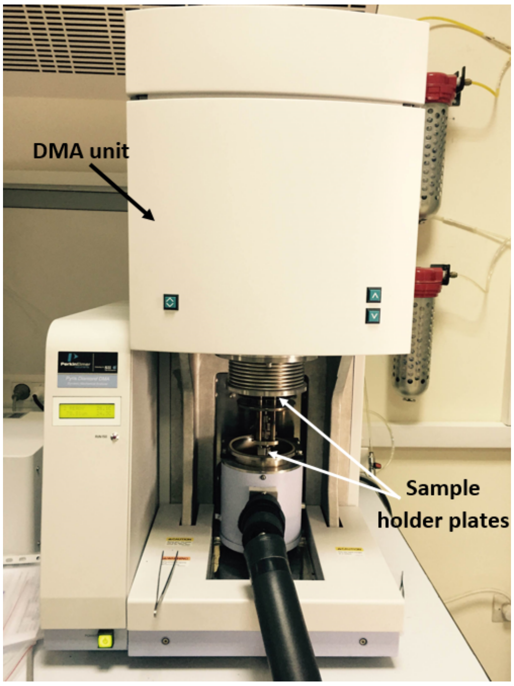

Figure 3.8: Perkin Elmer Pyris Diamond Dynamic Measurement Analyzer (DMA) in METU Central Laboratory. The phantom samples are placed between two sample holder plates and a sinusoidal mechanical force is introduced in the samples

measured storage modulus of these phantoms are given in Table 3.3. It can be seen that elastic constant of the tumor phantom is successfully decreased from 114.47 kPa to around 55 kPa in newly developed tumor phantoms. The results, are in good agreement with the values presented in [3]. So, it is expected that for the same amount of US excitation, higher Doppler signal can be received in these phantoms. Results also show that elastic modulus increases as the frequency increases. Due to the softness of the developed fibro-glandular phantoms, they are damaged by applying the dynamic force on them. So, the fibro-glandular phantoms elasticity are measured in static measurement tests.

In addition to dynamic elastic measurement test, the static elastic measurement is done. The static compression measurements are performed for the fat, tumor and fibro-glandular phantoms, as well. The stress versus strain curve of the phantom samples is obtained using Lloyd LRX 5K materials testing machine in METU BIOMATEN laboratory (Figure 3.9). The measurements are done in

Table3.3: Measured Storage (ϵ') modulus of the new phantom samples (DMA).

Measurement frequency (Hz)	ϵ' (kPa)		
	Fat	Tumor [3]	Tumor [2]
0.1	11.15	45.39	76.97
1	12.76	48.68	89.18
10	15.98	55.69	114.47
Reference	3.25	10.40-42.52	

room temperature. Samples for this test obtained from [3] are cylinders with diameter of 15 mm and height of 10 mm. The compression plate's diameter is 60 mm. In these measurement the stress-strain curve is obtained and the initial linear part of this curve is considered in Young's moduli calculation as:

$$\epsilon = kS \tag{3.13}$$

where ϵ is the Young's (elastic) modulus, k is a constant, and S is the slope of the stress-strain relation. The measured Young's modulus of the tumor phantom (at 0.1 Hz) is used as the reference for calculation of k value. The measured Young modulus values of the phantom samples and the reference values related to biological tissues are given in Table 3.4.

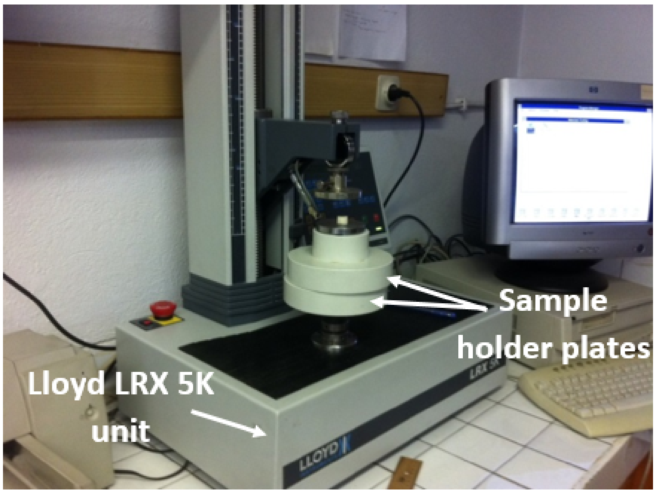

Figure 3.9: Lloyd LRX 5K materials testing machine in METU BIOMATEN laboratory used for static elastic property measurement of the developed tissue mimicking phantoms

Table3.4: Measured Young's modulus of the phantom samples developed as given in [3] (Static compression measurements).

Phantom Type	Measured ϵ' (kPa)	Reference ϵ' (kPa)
Fat	4.32	3.25
Tumor	76.96	10.40-42.52
Fibro-glandular	19.7	3.24

Table3.5: Measured Young's modulus of the phantom samples developed as given in [2] (Static compression measurements)

Phantom Type	Measured ϵ' (kPa)	Reference ϵ' (kPa)
Tumor	42	10.40-42.52
Fibro-glandular	10.15	3.24

The elasticity of the fat phantom is similar to the reference value. But, similar to the obtained results from the dynamic elastic measurement, the tumor and fibro-glandular phantoms are quite stiffer. This can be due to the amount of formaldehyde and also extra addition of surfactant for making the phantoms more homogeneous. As it is mentioned, this affects the experimental results, negatively. Comparing the real tissues, the produced displacement in these phantoms will be smaller for the same amount of mechanical force.

The instruction given in [2] is followed to develop softer tumor and fibro-glandular phantoms. The developed tumor phantom is baked for 3 days. During the baking period, the phantom is melted. The melted phantom was left for two days in the room temperature for solidification. Similar static elastic measurement is done for these phantoms. The measured young modulus of the developed tumor and fibro-glandular phantoms according to [2] are given in Table 3.5. The measurement results of static and dynamic tests are consistent.

From both measurement results, it can be seen that elasticity of the developed fibro-glandular and tumor phantoms are higher than the previously developed phantoms and closer to the ones related to biological breast tissue. It is expected to receive higher signal level using these developed phantoms in the experiments. In HMMDI laboratory experiments, both of these phantoms are used in making inhomogeneous phantoms and the results are compared.

Table3.6: Acoustic properties of the developed tissue mimicking phantoms.

	Speed of Sound	Attennuation at 1 MHz	Attennuation at 2 MHz
Fat Phantom	1625 m/s	0.36 dB/cm	0.46 dB/cm
Tumor Phantom	1655 m/s	0.49 dB/cm	0.88 dB/cm

3.2.4 Ultrasonic properties of the phantoms

The speed of the sound in the phantoms and the acoustic attenuation in the phantoms are measured in METU Non-Destructive Testing laboratory for 1 MHz and 2 MHz frequencies. The prepared samples from fat and tumor phantoms were 10 cm in height and 8 cm in diameter. The tone burst reflection tests are done to find the attenuation and speed of the sound in the phantoms. The calculated values are given in Table 3.6.

CHAPTER 4

FIRST GENERATION OF HMMDI EXPERIMENTAL SET UP

4.1 Introduction

In Harmonic Motion Microwave Doppler Imaging, microwave signal is transmitted to the tissue while the tissue is vibrated locally using a focused ultrasound transducer. The received signal at the vibration frequency (Doppler signal) contains information about both elastic and dielectric properties of the tissue. Using the Doppler signal information, fat, fibro-glandular and tumor tissues can be distinguished. In the following sections, the first generation HMMDI system set up (microwave transmitter/receiver set up and ultrasonic excitation system) is introduced. The system performance is assessed with experimental studies conducted using the custom made phantoms mimicking tissue properties.

4.2 First generation HMMDI system experimental setup

In this thesis study, the feasibility of the HMMDI method is evaluated experimentally using realistic breast phantoms. The block diagram of the setup is shown in Figure 4.1. Two waveform generators are used to produce an Amplitude Modulated (AM) RF signal. A burst signal waveform is used not to damage the transducer and the phantom due to the excessive exposure. The generated AM burst signal is given to the high power RF amplifier (Amplifier Research 150A100B). The gain of this amplifier is 52 dB gain. This signal feeds a single element focused ultrasound transducer (Sonic Concepts H-102). Developed ultrasonic waves, creates a vibration inside the phantom. The transmitting antenna is fed by a microwave signal generator (Agilent E8257C). In order to monitor the received signal, the frequency spectrum Analyzer (Agilent E4446a) is used. Waveform Generator 1 triggers the spectrum analyzer to start sweep with the burst signal.

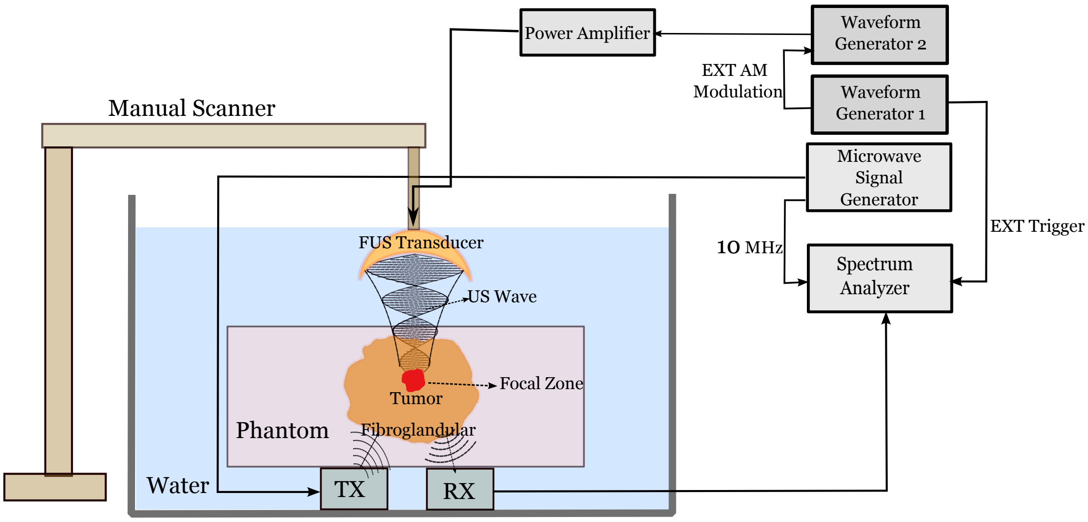

Figure 4.1: Block diagram of first generation HMMDI system.

4.2.1 Focused Ultrasound Transducer

To generate vibration inside the tissue, a single element focused ultrasound (FUS) transducer (Sonic Concepts H-102) is used. The properties of this transducer are given in Table 4.1. The pressure profile of this US transducer in its first and third harmonics in different XY and XZ planes are shown in Figure 4.2 [10].

The needle hydrophone (Onda Corporation, CA, USA) in the METU ULTRA-MEMS laboratory in Electrical and Electronics Engineering Department is used to investigate the pressure pattern of the FUS transducer. As a result of 1 V

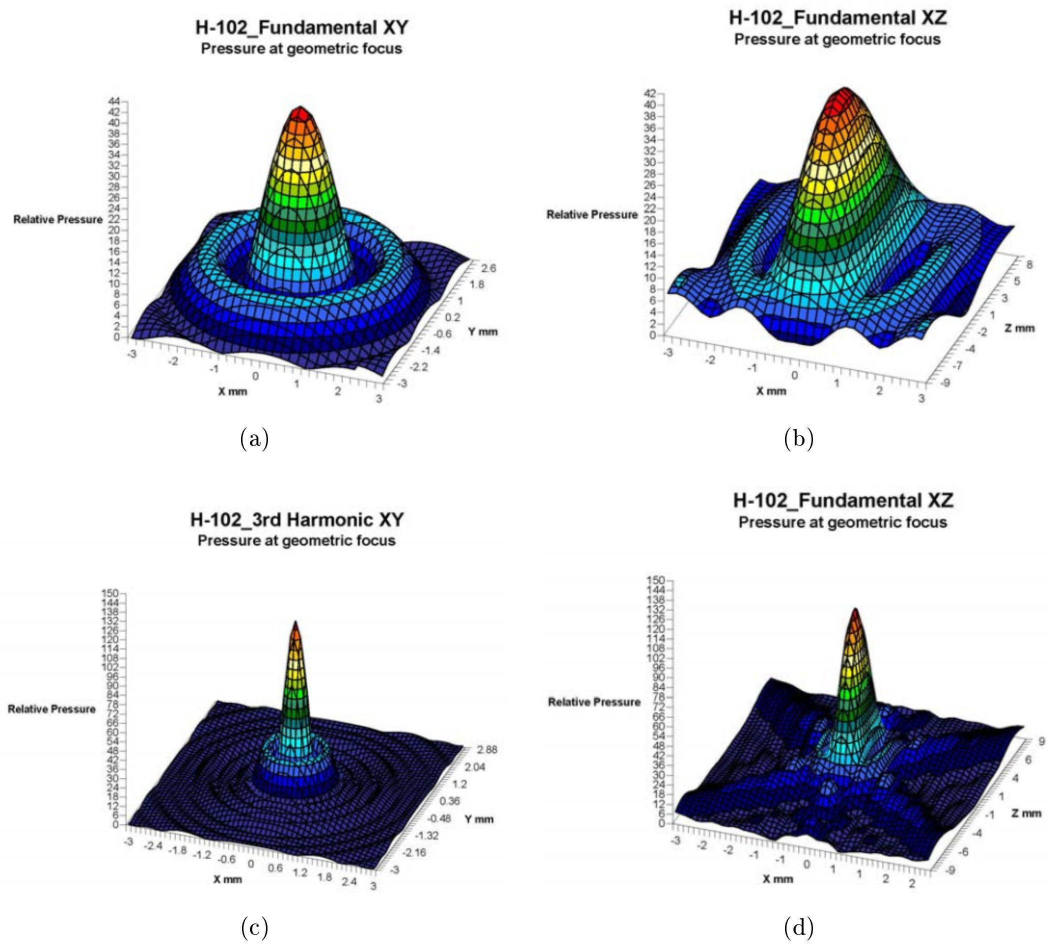

Figure 4.2: The pressure profile of the Sonic Concepts H-102, US transducer (a) in its first harmonic in XY plane, (b) in its first harmonic in XZ plane, (c) in its third harmonic in XY plane, and (d) in its third harmonic in XZ plane [10].

Table4.1: Properties of the FUS transducer Sonic Concepts H-102.

Frequency	1.1 MHz (Fundamental), 3.3 MHz (3^{rd} Harmonic)
Active Diameter	64 mm (Outer) $\times$ 22.6 mm (Inner)
Thru Opening	20 mm diameter central opening
Geometric Focus	63.2 mm
Focal Depth	53.5 mm (measured from transducer housing rim to geometric focus)
Power Handling	150 Watts (CW), 400 Watts (Pulsed)
Axial Half Intensity Beamwidth	15 mm (1.1 MHz), 5 mm (3.3 MHz)
Lateral Half Intensity Beamwidth	1.8 mm (1.1 MHz), 0.6 mm (3.3 MHz)

peak to peak excitation of the transducer the obtained axial and lateral pressure beams are plotted in figure 4.3 [11].

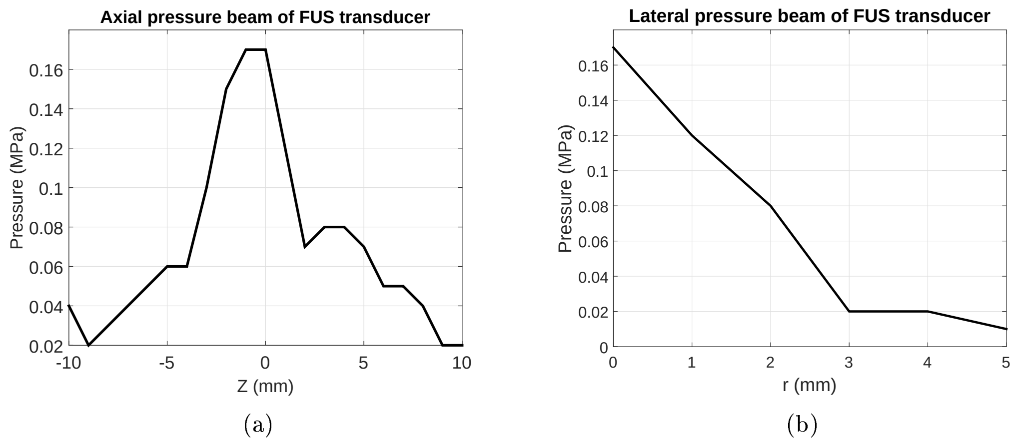

Figure 4.3: The measured (a) axial and (b) lateral beam patterns of the FUS transducer. In these measurements 1 V peak to peak excitation was used [11].

4.2.2 Antenna Design and configuration

Two different experimental setup are designed for the HMMDI system evaluation. In the first experimental setup, called as first generation set up, open-ended waveguide antennas are used for both transmitting and receiving microwave signals. These types of antennas are wide bandwidth, low loss and the design of them is simple [11]. The properties of these antennas are as follows:

- The antennas operation frequency band: 5 GHz to 8 GHz
- The dielectric material of the antenna: vegetable oil ($\varepsilon_r \approx 2.5, \sigma = 0.05$)
- Broad-wall dimension of the waveguide: 22.86 mm
- Narrow-wall dimension of the waveguide: 10.16 mm
- The cut-off frequency for TE_{10} mode: 4.07 GHz
- The next propagating mode: TE_{20} with cut-off frequency of 8.1 GHz

The antenna is fed using a coaxial probe having inner conductor radius of 0.69 mm, and outer conductor radius of 2.3 mm [11]. The dielectric material in the coaxial adapter is TeflonTM with relative permittivity 2.1, and dielectric loss tangent 0.001. Antenna has been modeled in Ansys HFSS (Ansys, Inc., PA, USA) [11]. The design parameters of p, d, and h are the length of the inner conductor inside the waveguide, the distance between the center point of coaxial probe to the short circuit, and the total length of the antenna, respectively. It has been reported that -10 dB bandwidth of 50% can be obtained when $d =$ 8 mm, $p = 5.6$ mm, and $h = 15$ mm [11]. The antennas are produced in the ASELSAN REWIS Machine Shop.

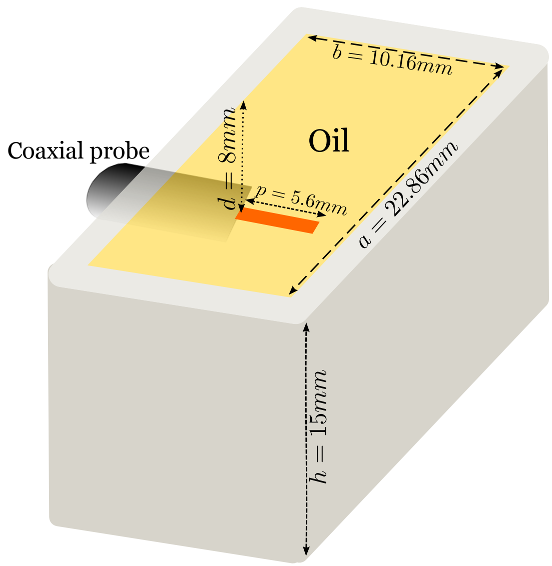

Figure 4.4: Waveguide antenna in the HMMDI system.

Vegetable oil is used inside the antenna and the waveguide antenna opening is closed using a plastic layer. This plastic layer is fixed to the antenna body using a waterproof adhesive glue. Bubbles appear when oil is poured inside the antenna. The resulting bubbles are extracted by injecting extra amount of oil with syringe into the antenna after closing the surface of it with the plastic layer.

In this setup (Figure 4.5), both transmitter (TX) and receiver (RX) antennas are fixed at the bottom of the phantom container and the ultrasound transducer is located on the phantom's upper surface. In this configuration, the phantom is scanned via transducer while the antennas are fixed at the bottom of the phantom container. The steps of preparing the antennas for the experiment are shown in Figure 4.6.

4.2.3 Phase Noise of the Transmitter

In HMMDI, the microwave frequency is in the order of a few GHz while the vibration frequency is in the order of Hz. Therefore, Doppler frequency is close to the carrier frequency. So, the phase noise of the transmitter is an important parameter which affect the Doppler signal detection. As the phase noise gets

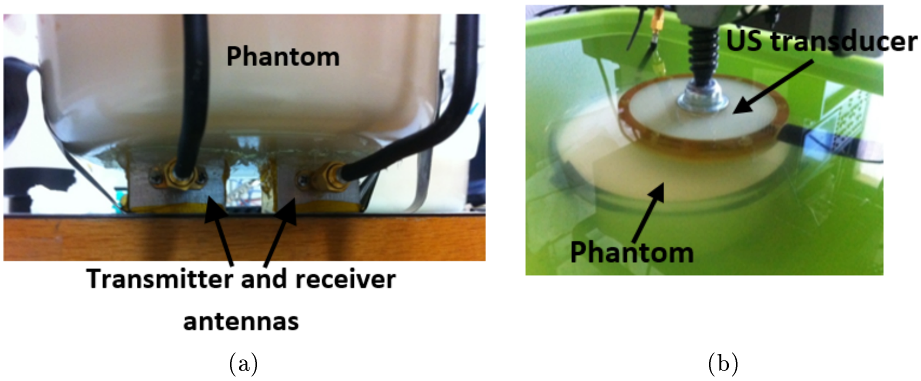

Figure 4.5: The antenna configuration in the first HMMDI experimental set up. (a) The location of the transmitter and receiver antennas at the bottom of the phantom container and (b) location of the US transducer on top of the phantom container.

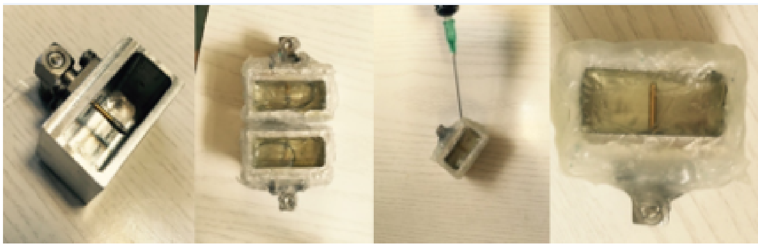

Figure 4.6: The transmitter/receiver waveguide antennas in the first generation of HMMDI set up. From left to right the antennas before pouring oil inside of them, antennas after filling and closing the open surface of them, injecting extra oil with syringe to remove the bubble from them and the last version of used antennas in the experiments.

higher, it will be more difficult to observe the small Doppler signal. In HMMDI experiments, the microwave signal generator Agilent E8257C was used. To measure the phase noise of this signal generator, its output is connected to the Spectrum Analyzer (Agilent E4446a) for 0 dBm output power. 10 MHz reference signal of the Spectrum Analyzer is used as 10 MHz reference for the Signal Generator. The spectrum analyzer resolution bandwidth, span, and the number of averaging are selected as 6.8 Hz, 500 Hz, and 20, respectively. Figure 4.7 shows the phase noise of the signal generator for various operation frequencies between 2 GHz to 8 GHz.

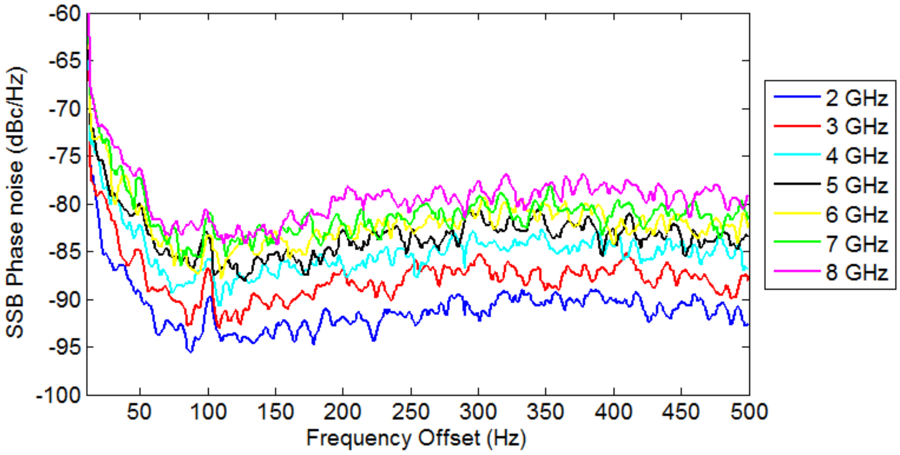

Figure 4.7: Measured phase noise of the microwave signal generator. In this measurement the signal generator is directly connected to the spectrum analyzer. The frequency span is 500 Hz.

4.3 Experimental studies on the first tissue mimicking phantom

In these experimental studies different inhomogeneous phantoms are tested for the HMMDI system evaluation. The first phantom contains fibro-glandular phantom with 25 mm diameter and 12 mm height inside the fat phantom. A tumor phantom with 5 mm diameter and 7 mm height is placed inside the fibro-glandular. This phantom is prepared inside a plastic bowl with 11 cm diameter and 5 cm height (Figure 4.8). The phantom development consists of two stages. Firstly, the fat phantom is prepared, and poured into the container up to a height of 2 cm from the bottom of the mold. The phantom is left for one day to solidify. As it can be seen in Figure 4.8, the prepared fibro-glandular phantom with the tumor phantom in the middle is located on top of the fat phantom. Another fat phantom material is prepared and poured in the same mold until the surface level reaches a height of 2.5 cm. The phantom is left for 7 days at room temperature for solidification.

The antennas are placed in H-plane format and the distance between their edges is set to 15 mm. The antennas are placed at the bottom of the phantom container (Figure 4.5). The area between the antennas and the glass is filled with a rubber layer. The transmitting antenna is fed by the signal generator with the output

Figure 4.8: Stages of in homogeneous phantom preparation including fibro-glandular and tumor phantoms inside the fat phantom. Tumor has 5 mm diameter, and 7 mm height, and Fibroglandular has 25 mm diameter, and 12 mm height.

power of 15 dBm. The Spectrum Analyzer is connected to the receiving antenna. Distilled water is used as a coupling medium. Phantom with the antennas at the bottom of the phantom container is placed at the bottom of the water tank.

The ultrasound transducer is inserted inside the water tank on top of the phantom. The FUS transducer is fed with 367 V_{pp} voltage, which produces 6.4 MPa peak pressure at the focus. Various vibration frequencies are tested, but the highest SNR is observed at 15 Hz. Above 30 Hz vibration frequency, the Doppler frequency component of the signal is masked by the coupled phase noise of the signal generator. In addition, for vibration frequencies below 10 Hz, the Doppler signal is not detectable from the fundamental frequency component. The focus of the US transducer is placed on the fibro-glandular phantom. The spatial peak pulse average intensity of the ultrasound beam is 630.2 $\frac{W}{cm^2}$. The US duration is set to 200 ms for 3 cycles of excitation.

In microwave measurements, the resolution bandwidth, span, sweep time, and averaging number are selected as 6.8 Hz, 200 Hz, 280 ms, and 20, respectively. The measured main component to Doppler component and the Doppler signal to noise level at Doppler frequency (SNR) are shown in Figure 4.9. In this experiment the SNR is more than 20 dB for 2 - 6 GHz applied frequencies. The Doppler component in comparison with the main frequency component has the highest value at 6 GHz due to the low direct coupling between the antennas in this frequency.

The phase noise level is dependent on the direct coupling level. Therefore, as the main component decreases, the phase noise decreases and the Doppler signal becomes more clear. It seems that coupled signal components from water/glass interface and glass/phantom interface cancels each other at this frequency. The interaction between surface waves and the scattered signal at 6 GHz may causes this results. The surface waves propagate along dielectric/dielectric or dielectric/metal interfaces such as water-rubber/glass and glass/phantom in our case. The interaction of the surface waves and the scattered signal affects the amplitude and phase of the received signal [61]. As a result, the received signal level at the center frequency is decreased but not the signal of interest at Doppler frequency. As it was observed in this experiment, the interaction or the out of phase addition of the surface waves and the scattered signal, is frequency dependent.

1-D scan results

In this experiment, microwave operating frequency is 6 GHz. The manual scanner is designed for 31 mm scan length. The scan steps are 1 mm. By changing the place of the scanner, 54 mm is scanned (Figure 4.10). In some areas the two scanned area overlapped each other. In order to keep the safety limit, the measurements are performed for 4.2 MPa maximum pressure at the focus point. In this experiment, I_{sppa} of the ultrasound beam is 271.4 $\frac{W}{cm^2}$. For lower values the SNR is poor. Although this intensity is higher than the safety limits, it is acceptable in these experimental studies because the elastic constants of the developed fibro-glandular and tumor phantoms are higher than the biological breast tissues. It is expected to receive higher signal with inducing lower radiation force in a real case. In addition, improving the transmitter and receiver will decrease the need for high ultrasound power. The microwave power could be increased using an amplifier, to decrease the requirement for ultrasound power and duration.

Another factor which can be the reason of receiving low Doppler signal level is the coupling medium. In these experimental studies, water is used as a coupling medium. Water is highly lossy in the microwave frequency range. Therefore,

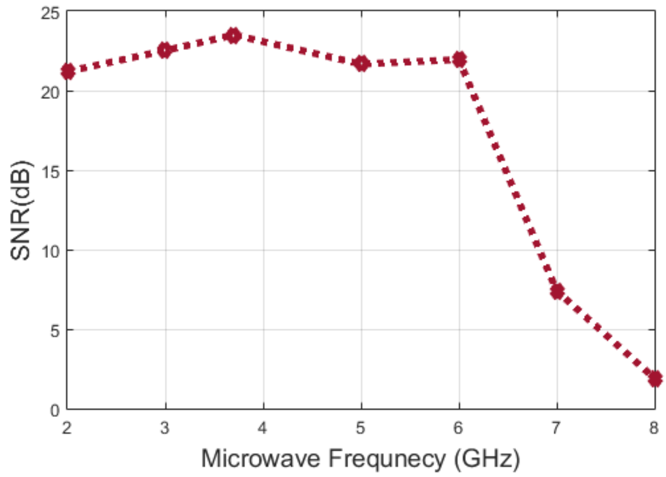

(a)

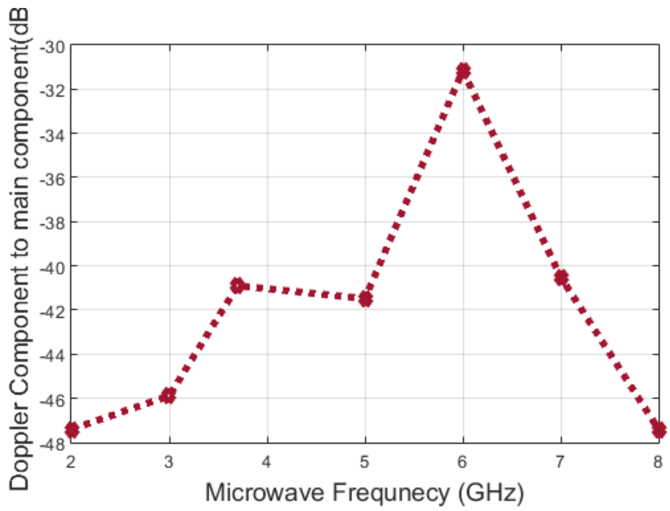

(b)

Figure 4.9: The measured (a) SNR and Doppler frequency component to fundamental frequency component. AM burst signal of 15 Hz is applied to induce vibration inside tissue.

an alternative coupling medium which has the proper acoustic and dielectric properties should be investigated to improve the received signal level at Doppler frequency.

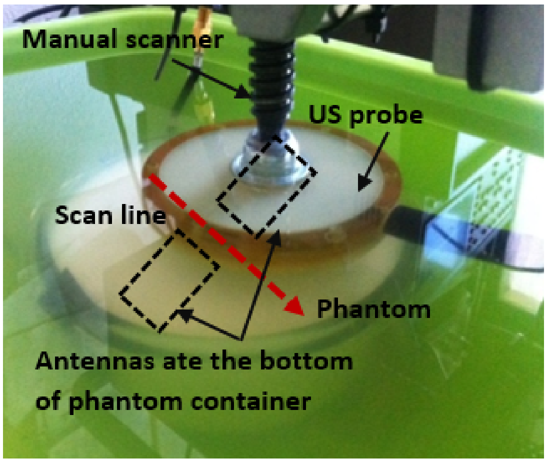

Figure 4.10: FUS probe scanning the breast phantom in a line passing between the antennas.

The measurement results are presented in Figure 4.11. As it can be seen, the signal level is about -127 to -125 dBm in fat phantom areas and whereas it is around -121 dBm when the focus is on the fibro-glandular phantom. The signal level on the tumor phantom is around -123 dBm. The results clarify that signal level on the tumor is about 3 dB less than the fibro-glandular and it is 2-3 dB higher than the fat. When the focus is on both fat and tumor phantoms, the Doppler signal is higher than the noise level. By using different vibration frequencies the difference between received signal level from fat and tumor can be distinguished.

Another 40 mm scan is done for the same phantom (Figure 4.12). It seems that in this scan the coupling to the phantom is better. This result is in agreement with the previous measurement results and shows the potential of HMMDI method for tumor detection in an inhomogeneous tissue phantom.

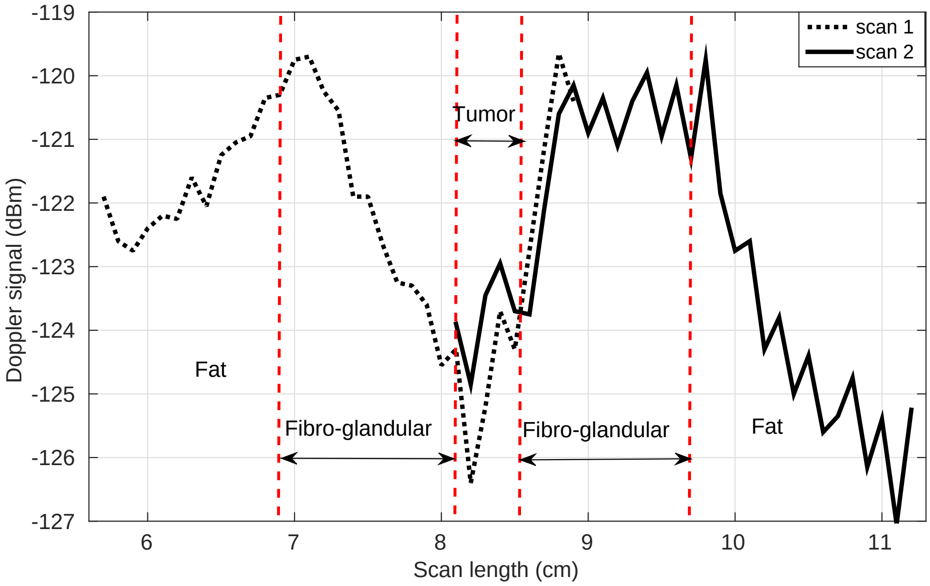

Figure 4.11: Measured signal level at the Doppler frequency for the linear scan which covers the fibro-glandular phantom, and the inside tumor.

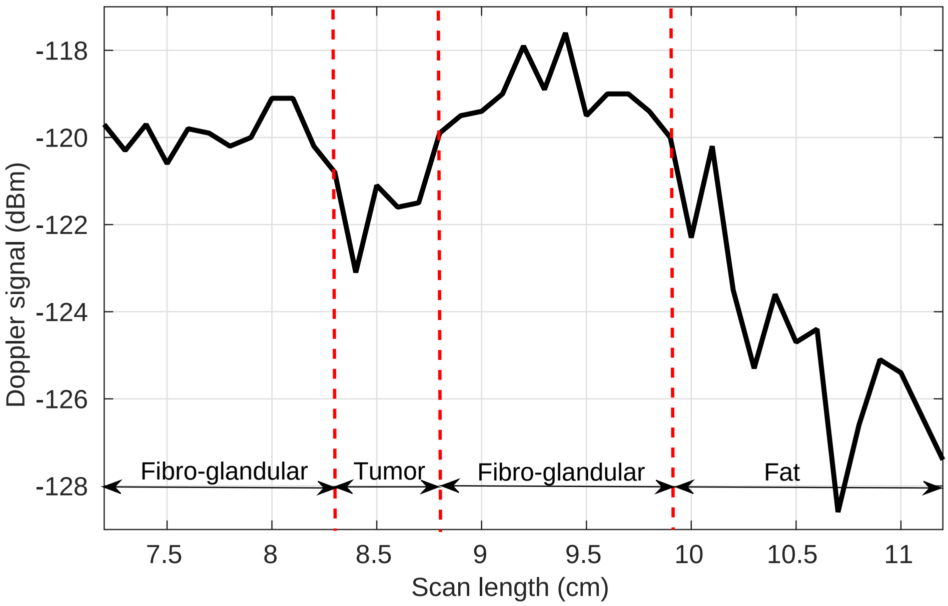

Figure 4.12: Measured signal level at the Doppler frequency for 40 mm scan which covers fibro-glandular phantom, and the inside tumor.

4.4 Experimental studies on the second tissue mimicking phantom

In this case, phantom is prepared inside a glass bowl with 11 cm diameter and 5 cm height (Figure 4.13). Three tumors with different sizes are located in 30 mm depth from the top surface on the pre-prepared fat phantom. Diameter and height of these three tumor phantoms are 3×2.5 mm, 10×5 mm, and 25×4.5 mm. The pre-prepared tumor phantoms are placed at the surface of the fat phantom in the center line of the container. Again, the fat phantom is poured on top of the tumor phantoms in a way that the surface level became 3 cm in height. In order to distinguish tumor phantom inside the fat phantom, the peak pressure is increased to 7.5 MPa. In this experiment, I_{sppa} of the ultrasound beam is 865.4 $\frac{W}{cm^2}$.

Since the scanning tool has a scan length limit, three scans are done to cover the whole tumors line. By means of these three scans, 78 mm is covered. Similar to the previous case, the scan step size is 1 mm. The microwave operating frequency is 3.7 GHz with +16 dBm output power. In this case, 30 Hz is considered as a the vibration frequency. In this case, the frequency sweep test for finding the best frequency according to the SNR is not done. In this experiment, the small and middle sized tumor phantoms are detectable 4.14, but the Doppler signal level on the big tumor region is weak. The results suggest that the induced displacement in the larger sized tumor is less comparing smaller sized tumor inclusion.

Figure 4.13: Stages of inhomogeneous phantom preparation including three different sizes of tumor phantom samples.

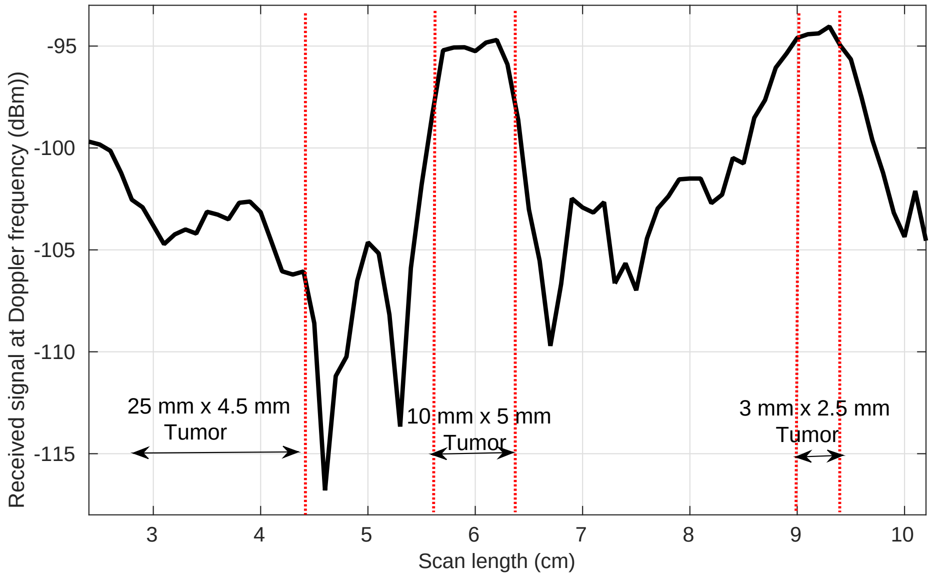

Figure 4.14: Measured signal level at the Doppler frequency for a line scan passing through 3 different tumors. The signal drops in the tumor regions

4.5 Data acquisition system in the first generation HMMDI set-up

Performance of the HMMDI method has been investigated with simulations in [62]. Also, phantom experiments using a spectrum analyzer as a receiver was mentioned in the previous sections. In this section, the designed homodyne receiver system for HMMDI system to receive the data without using the spectrum analyzer is presented. The experimental studies are performed on the breast phantom materials to test the performance of the designed system.

4.5.1 Tissue mimicking phantoms in experimental studies on designed HMMDI receiver system

For this experiment the phantom is prepared inside the same sized glass bowl. The fibro-glandular tissue phantom of 25 mm diameter and 16 mm height is placed at the center of the fat phantom. The tumor phantom of 13 mm diameter and 7 mm height is inserted in the fat phantom 30 mm away from the middle of the fat phantom container. Another fat phantom is prepared and poured in the same mold until the surface level reached a 3 cm in height. The phantom is left for 7 days at room temperature for solidification. Different stages of phantom development in addition to its MRI image are shown in Figure 4.15.

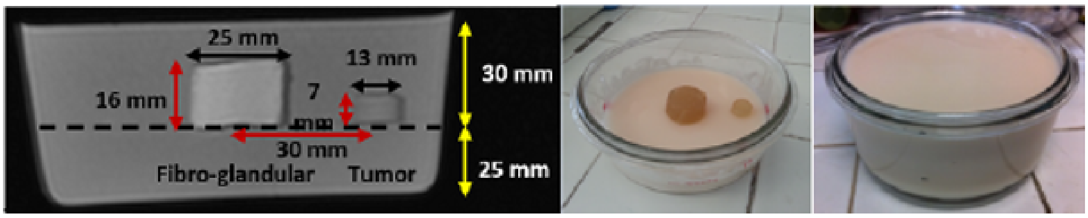

Figure 4.15: Inhomogeneous breast phantom including fibro-glandular and tumor phantoms. Left: MRI image of Phantom taken by 3 Tesla MRI System, UMRAM Research Institute in Bilkent University. Middle: Fibro-glandular and Tumor phantoms placed on the fat phantom at the first stage. Right: Final condition of the breast phantom after the second stage.

4.5.2 Experimental studies and results

A data acquisition system in the HMMDI method is designed and its efficiency is evaluated experimentally using the developed phantom materials. The block diagram of this receiver system is shown in Figure 4.16. Similar to the previous experiments, the focused US transducer is used in its third harmonic frequency (3.32 MHz). A 2-cycle 10 Hz sinusoidal burst signal (with 1 Hz pulse repetition frequency) is generated from waveform generator 1 and used to amplitude modulate the 3.32 MHz signal generated by the waveform generator 2. The AM signal is amplified with a high power RF amplifier (150A100B, Amplifier Research, WA, USA) of 52 dB gain. Spatial peak pulse average intensity (I_{sppa}) of the ultrasound beam is 271.4 $\frac{W}{cm^2}$. Since Youngs Modulus of the developed fibro-glandular and tumor phantoms are higher comparing the biological breast tissue, higher radiation force is required to induce detectable displacement inside phantoms.

Simulation studies showed that for biological tissues lower intensities below the safety limit would be sufficient to observe the Doppler signal [62]. Similar to

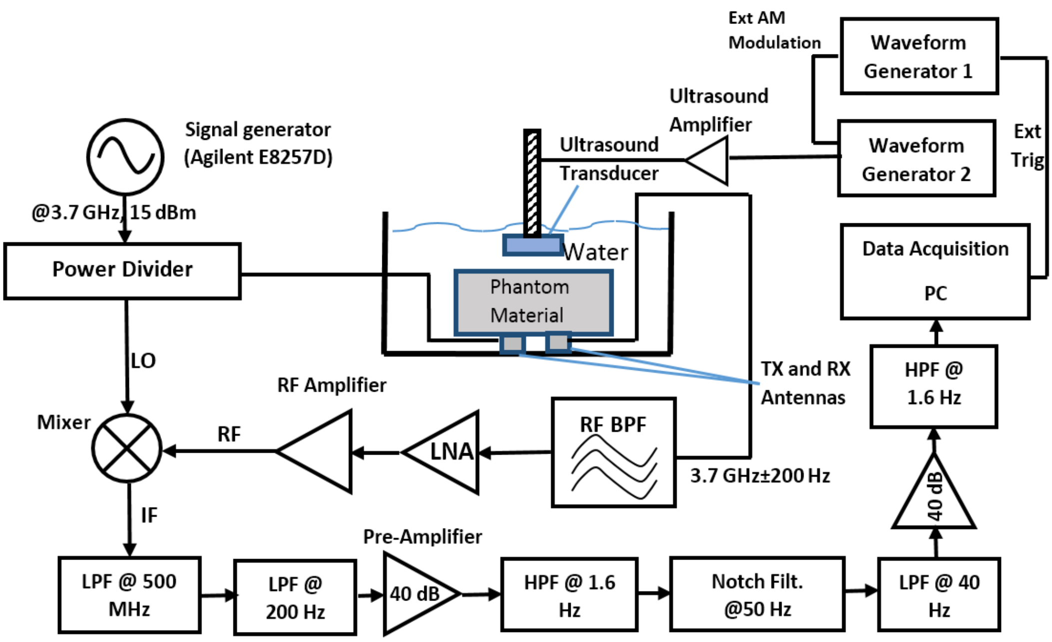

Figure 4.16: Block diagram of HMMDI data acquisition setup.

the previous case, open-ended waveguide antennas with the same configuration at the bottom of the phantom container are used. Glass is used as a mold for the breast phantoms. The focus of the FUS transducer is adjusted manually to point at 30 mm depth from the top surface of the phantom mold.

The transmitting microwave antenna is fed by the Agilent E8257C Signal Generator with an output power of +15 dBm at 3.7 GHz frequency. For data acquisition purpose, the signal should be down-converted to the baseband. As a consequence, the receiver antenna is filtered by a band pass filter (K&L Microwave 5C50-3700/U100-O/O), low noise amplifier (Mini Circuit ZX60-3800LN-S+), and wide-band amplifier (Mini Circuit ZX60-V83-S+), respectively (Figure 4.16). The output signal is given to the mixer (MITEQ DM0204 LA1). The output signal of signal generator is split using power divider (Mini Circuit ZFRSC-42-S+) and is fed to the mixer's other input as the local oscillator. The mixer output is given to a low-pass filter (Mini Circuit NLP-50).

Since the signal is small and noisy, further amplification and filtering sections are necessary. It is believe that the signal at the Doppler frequency (10 Hz) contains information about phantom elastic and dielectric characteristics. Consequently, the signal is filtered by the low-pass filter to eliminate the unwanted frequency components. The output of this filter is given to the commercial instrumentation amplifier (LT1167). To eliminate the DC offset, the amplified signal is fed to a high-pass filter. Furthermore, a notch filter is used to remove the 50 Hz line noise. The signal is filtered by a low-pass filter (cut-off frequency at 40 Hz). Additionally, the output is amplified more by an amplifier with 40 dB gain. The frequency response of the designed receiver system circuitry is shown in Figure 4.17.

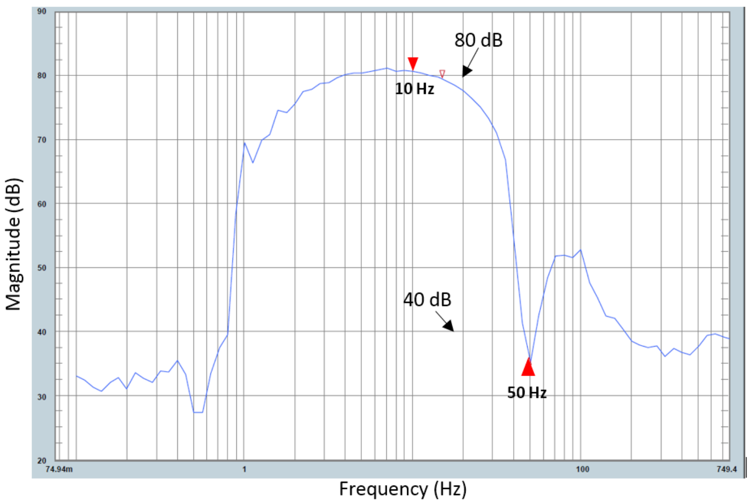

Figure 4.17: The designed receiver system frequency response.

The output signal of the RF receiver section, which is amplified by total 80 dB gain, is acquired by the data acquisition card. In this experiment, CM series 2004 model data acquisition card of ACQUITEK is utilized. This data acquisition card, supports up to 1 MS/s maximum sampling rate, and has 16 bit A/D resolution. The signal at each point is collected for 4 second. The sampling frequency is 15 kHz. In the data acquisition duration, there are at least three US excitation pulses (trigger pulses). The signal in the trigger duration contains information about coupled elastic and dielectric properties of the tissue in the focal region. Knowing the vibration frequency, the acquired data is filtered by band-pass IIR Butterworth digital filter ($f_{c_1} = 1$ Hz, $f_{c_2} = 25$ Hz) to obtain the signal in the interested frequency range. The received data in the absence of US excitation, during US excitation on the fat, fibro-glandular and tumor phantom regions, is illustrated in Figure 5.7. The US excitation duration or the so called trigger pulses are shown in red dashed lines. There is an unwanted noise even when there is no ultrasound excitation.

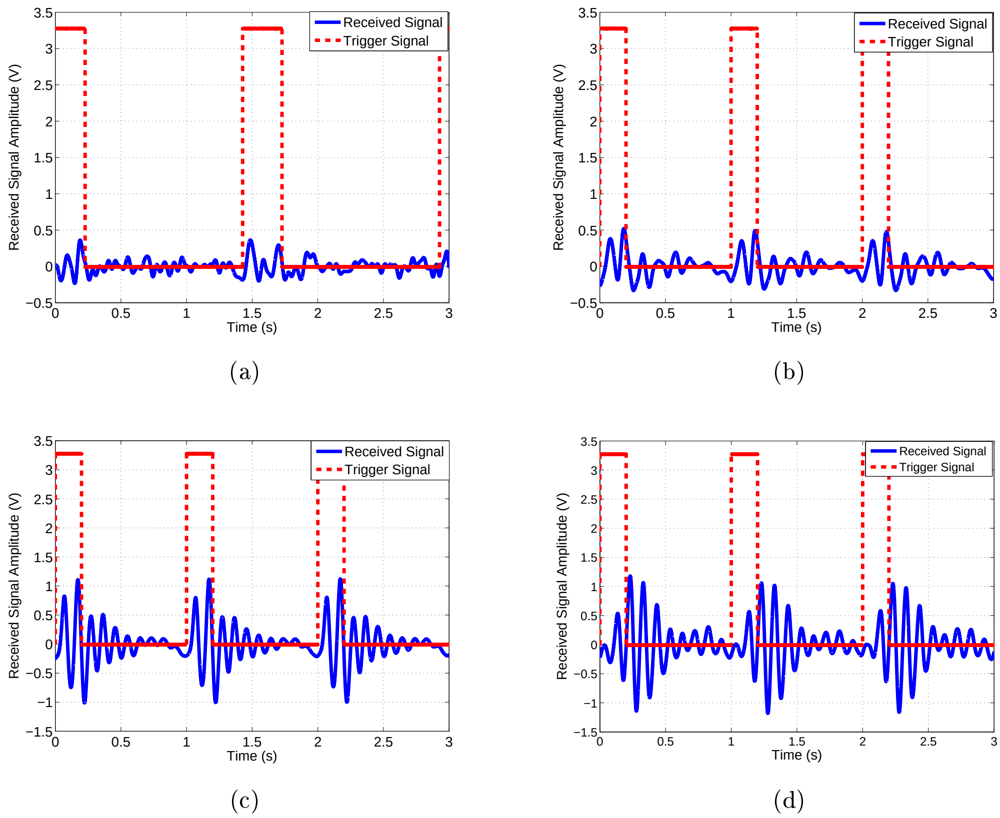

Figure 4.18: The received signal (a) without FUS transducer excitation, (b) with FUS transducer excitation from the fat region (c) from the fibro-glandular region, and (d) from the tumor area. The trigger signal from the waveform generator is shown in red dashed line.

However, the received signal due to the US excitation is observable in all cases. As it is very close to the glass phantom container edges, the signal from the tumor phantom region is distorted by the reflected signal from the glass. Consequently, just the first peak of the received signal from tumor is observed to be in the trigger pulse duration. A bigger phantom mold should be used for future studies to prevent the reflection. The average of the first peak values (ie. the received signal amplitude for the first excitation cycle) of the three received pulses are averaged to get the HMMDI data. The maximum signal is achieved when the focus is on the fibro-glandular phantom. The signal amplitude decreases about 3 dB in the tumor phantom. In the fat phantom, the signal level further decreases by an amount of 4 dB. These results are in a good agreement with the results obtained by directly connecting the receiver antenna to a spectrum analyzer given in the previous section. Even though the results are from specific points of the phantom, they prove the efficiency of the designed data acquisition system. It is shown that a low level displacement signal at Doppler frequency can be acquired for further processing steps. To detect the tumor inside the fibro-glandular in the fat phantom and to distinguish them from each other the phantom must be fully scanned.

4.6 Conclusion

In this part of the study, experimental studies show that it is possible to detect the tumor phantom inside the fibro-glandular phantom using the HMMDI method. But, the signal level in the tumor phantom was so close to the signal level in the fat region. Therefore, multiple vibration frequencies should be tested for solving this problem. Also, the data obtained from microwave imaging can be used in addition to the information given from HMMDI method to detect fat phantom from tumor phantom. The optimum microwave operating frequency range was detected as 2-6 GHz. The penetration depth inside the tissue is higher for lower frequencies but the phase modulation effect is better in higher frequencies with smaller wavelengths. The optimum vibration frequencies were measured as 10-30 Hz. Lower frequencies were masked by the main frequency component whereas the higher frequencies above 30 Hz were masked by the phase noise of the oscillator.

In addition, a receiver system was proposed for HMMDI method and its performance was investigated using the developed phantom materials. The local vibration was induced inside the phantom materials using a FUS probe. Microwave signals were transmitted to the vibrating tissue phantom. The amplitude of the received signal at the Doppler (vibration) frequency was down-converted to the base-band using the designed base-band circuit. Furthermore, the signal was amplified and filtered to receive the detectable Doppler signal. The results show that the received Doppler data from different phantom regions are detectable using the proposed receiver system.

Results obtained by using spectrum analyzer as a receiver and the ones obtained from the designed receiver system show that HMMDI method has a potential of detecting tumor inside the fibro-glandular tissue. More studies should be done for differentiating fat phantom from tumor phantom. The performance of the HMMDI set up should be investigated for a range of phantoms containing fat, fibro-glandular and tumor phantoms. In addition, better signal processing methods should be implemented for eliminating unwanted artifacts in the detected signals. Two dimensional scan of phantoms should be performed to obtain more information for imaging the dielectric and elastic characteristics of the tissue phantoms.

CHAPTER 5

SECOND GENERATION OF HMMDI EXPERIMENTAL SET UP WITH SCANNING ANTENNAS

5.1 Introduction

In the first generation of the HMMDI experimental set up, transducer, phantom, and the antennas were located in a container filled with distilled water. Since, water is lossy in the microwave frequency range, an alternative liquid which has proper acoustic and dielectric characteristic is required as a coupling medium. In the first generation set up, to inhibit the water leakage between the antennas and the phantom, the antennas were fixed to the phantom container. In this chapter the experimental set up is improved to address these problems. This configuration is referred as second generation set up. In the second generation set up, water is substituted by oil. By changing the coupling medium to oil, the antennas are separated from the phantom mold and they are placed on the top of the phantom together with the US transducer.

In the new configuration, the transmitter antenna is located in the middle hole of the US transducer and the receiver antenna is fixed on the outer edge of it (Figure 5.4). Therefore, it is possible to scan the phantoms with both ultrasound transducer and antennas, simultaneously. The performance of this set up configuration is examined on tissue mimicking phantoms. In this part of the study, different inhomogeneous phantoms (homogeneous tumor, homogeneous fat, fat including three different sized tumors, and fat phantom including fibro-glandular with the tumor inside) are developed using different types of phantoms given in Chapter 3. The phantoms are scanned mechanically and a data are acquired using spectrum analyzer. The effects of MW and vibration frequency, antenna coupling in the Doppler signal, and tumor and fibro-glandular inclusion on the HMMDI data profile are investigated, experimentally. The problem encountered in the experiments such as antenna movement, elasticity contrast of the phantoms, and size of them, are reported and possible solutions are discussed.

5.2 HMMDI experimental set up

A single element focused ultrasound transducer H-102 (Sonic Concepts, WA, USA) is used for generating vibrations inside the tissue. The transducer is used in its third harmonic frequency (3.32 MHz). As it can be seen from the block diagram of the HMMDI method in Figure 5.1, a sinusoidal burst signal (with 1 Hz pulse repetition frequency) is generated from the first waveform generator and used to amplitude modulate the 3.32 MHz signal generated by the second waveform generator. The AM signal is amplified with a high power RF amplifier (150A100B, Amplifier Research, WA, USA) of 52 dB gain.

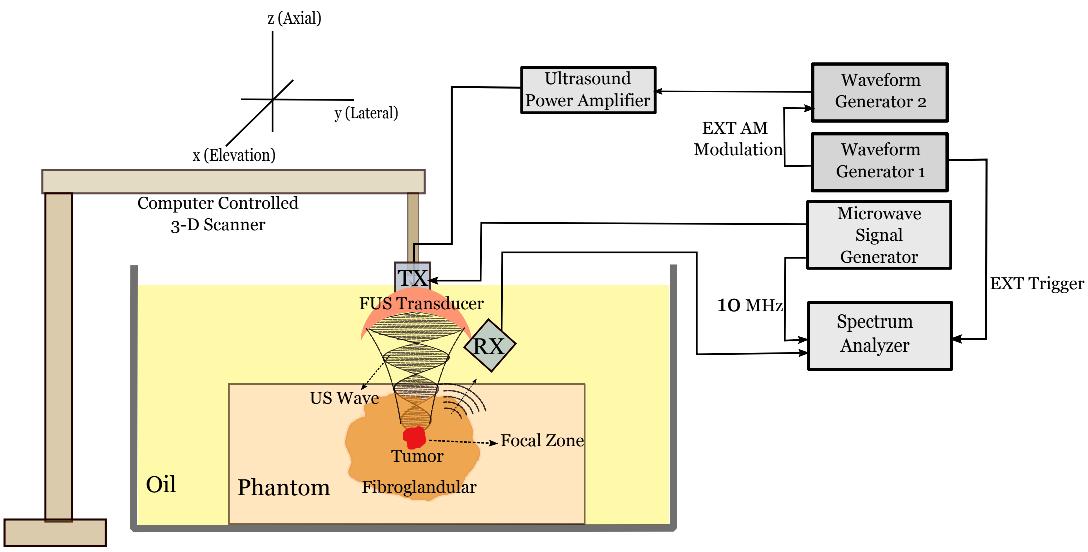

Figure 5.1: Second generation of HMMDI set up block diagram.

In this set up, oil is selected as the coupling medium. Both antennas and the US transducer are located on the top side of the phantom inside oil. the antennas and the US transducer are connected to the scanner. The transmitter antenna is placed inside the US transducer probe and the receiver antenna is fixed on its outer edge. The coupling medium selection and antenna configuration are discussed with more details in the following sections.

5.2.1 Coupling medium selection

The ultrasound probe used in the experiments is an immersion type that can operate in the water medium, properly. However, the microwave signal is attenuated considerably due to the dielectric loss of the water in microwave range. Considerable signal level reduction was observed as a result of water leakage between antennas and the phantom container. To prevent this problem, the antennas were fixed at the bottom of the phantom container with silicon adhesive glue. However, the same procedure should be done in each experiment and a number of phantoms and antenna pairs were required for the tests. This procedure is time consuming and might not be practical in a clinical setting. In addition, when the antennas were fixed, they were more sensitive to the middle area of the phantom and their sensitivity degraded toward the edges.

Substituting water with a different liquid gives the opportunity of having different scan configurations. The dielectric loss of this liquid in the microwave frequency range should be low to inhibit signal attenuation, and its acoustic properties should be similar to the water for ultrasound wave propagation purposes. Any oil type of liquids may satisfy the mentioned properties.

Dielectric and acoustic parameters of oil and water are given in Table 5.1). Note that, the speed of sound, mass density and acoustic impedance in these two mediums are close to each other while the microwave loss is nearly 10 times less in oil.

Due to its availability and low cost, sunflower oil is used in our experiments. To analyze the effect of sunflower oil on the acoustic field intensity, the intensity

Table5.1: Dielectric and acoustic properties of oil in compare with water.

Material	Water	Oil
Relative dielectric constant	77.15-j15.86	3-j0.16
Speed of sound ($\frac{m}{s}$)	1482	1470
Mass density ($\frac{kg}{m^3}$)	1000	920
Acoustic impedance (MegaRayls)	1.482	1.352

distribution inside the tissue, is calculated by the HIFU simulator tool developed by U.S Food and Drug Administration (FDA) [63]. This MATLAB tool solves axis-symmetric Khokhlov-Zabolotskaya-Kuznetsov (KZK) equation [64] in the frequency domain.

In this simulation, a transducer outer radius is 2.1 cm, its inner radius is 1 cm and the focal depth at 3.3 MHz is considered as 6 cm. In this simulation, 150 harmonics are considered. Oil layer (3.5 cm) is assumed between fat tissue (5.5 cm) and the transducer. It is assumed that the focus of the transducer is 2.5 cm inside the tissue. The simulation is repeated by replacing the oil layer with distilled water. The parameters that are considered in the simulations to calculate the acoustic intensity, pressure, and heat are given in Table 5.2.

Table5.2: Parameters used for pressure, intensity, and heat calculations with HIFU Simulator.

Material Parameter	Oil	Breast
Speed of sound ($\frac{m}{s}$)	1470	1479
Mass density ($\frac{kg}{m^3}$)	920	1000
Attenuation (dB/m/MHz)	7	34
Power of attenuation vs. frequency curve	2	1
Material transition distance (cm)	3.5	-
Transducer Parameter	**Value**	
Outer radius (cm)	2.1	
Inner radius (cm)	1	
Focusing Depth (cm)	6	
Frequency (MHz)	3.3	
Power (W) and	3.35	
No. of Harmonics	150	

From the simulations, the axial and lateral intensity resolutions are calculated as 6.75 mm and 0.48 mm, respectively (Figure 5.2 (a) and (b)). The maximum intensity at the focus is around 345 $\frac{W}{cm^2}$ in the water medium and it is around 192 $\frac{W}{cm^2}$ in the oil. The intensity maps for cases that oil or water layer is between the transducer and the tissue, are shown in Figure 5.3. The calculated intensity is used to calculate the mechanical force distribution inside the tissue. Resultant pressure waveform, heat, peak positive and negative pressure are plotted in Figure (Figure 5.2 for both cases of using water and oil as a coupling medium. Although the intensity of the acoustic wave in oil is a bit lower than water, their intensity, heat and pressure profiles are found to be similar to each other.

5.2.2 Phantom development

Similar to previous studies oil in gelatin emulsion type phantoms, which are suitable for elastography and microwave studies [1–3, 25, 49–55] are developed. Three different types of phantoms; normal breast fat, normal fibro-glandular, and tumor are produced. In the previous experiments, the tumor and fibro-glandular phantoms were developed according to the instructions given in [3]. The elastic constant of these phantoms comparing the biological breast tissues are high. As the phantoms get stiffer, more acoustic radiation force is necessary to introduce displacement yielding increased heat and damage inside the phantom.

In the following sections, the developed phantoms containing fibro-glandular/fat, tumor/fat, and tumor/fibro-glandular/fat are introduced. These phantoms are scanned and the 2-D scan results are presented to evaluated the performance of HMMDI method in distinguishing breast tissues.

5.2.3 Antenna Configuration

In the second experimental setup studies, a cylindrical waveguide transmitter antenna which is placed inside the central hole of the transducer probe, is used (Figure 5.4). This antenna is filled with the high permittivity material, Rogers 3210

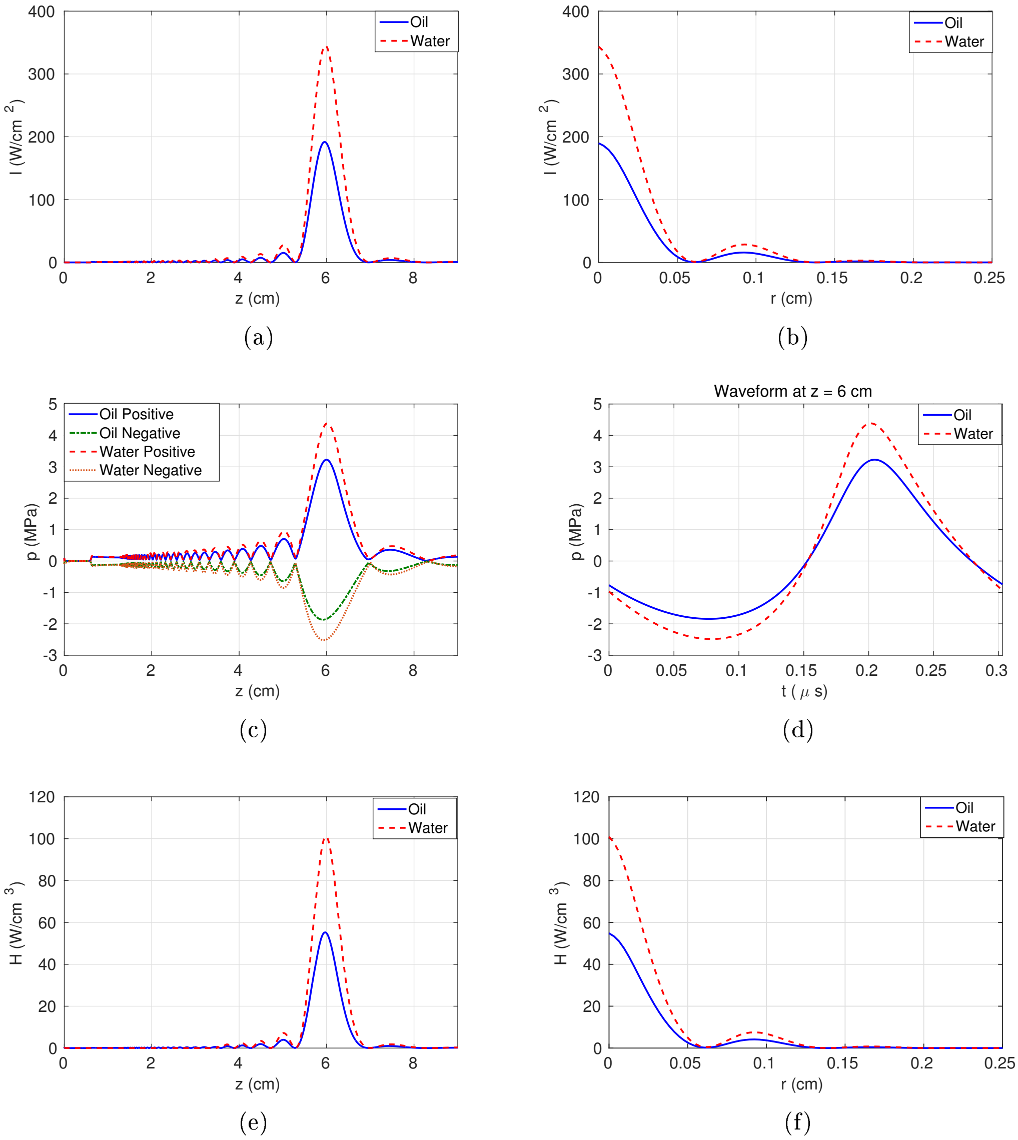

Figure 5.2: Ultrasound beam (a) axial and lateral intensity assuming 3.5 cm water (dashed red) or oil (blue) between antenna and the fat phantom. In this simulation, 150 harmonics are included. (c) lateral (a) peak positive and negative pressure, (b) pressure in time (e) axial heating (z = 6 cm), (f) lateral heating for water and oil medium.

(RO3210) ($\varepsilon_r = 10.2$). The geometry of antenna is shown in Figure 5.5. The measured resonance frequency of the transmitter antenna using the KEYSIGHT, FieldFox Microwave Analyzer N9915A is about 3.5 GHz. A rectangular open ended waveguide antenna is used as the receiver antenna. This antenna is fixed at the edge of the ultrasound transducer. The dielectric material used in the

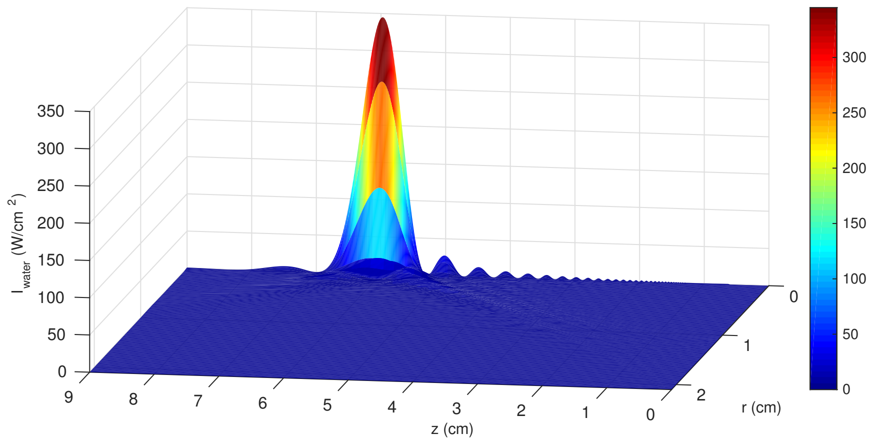

(a)

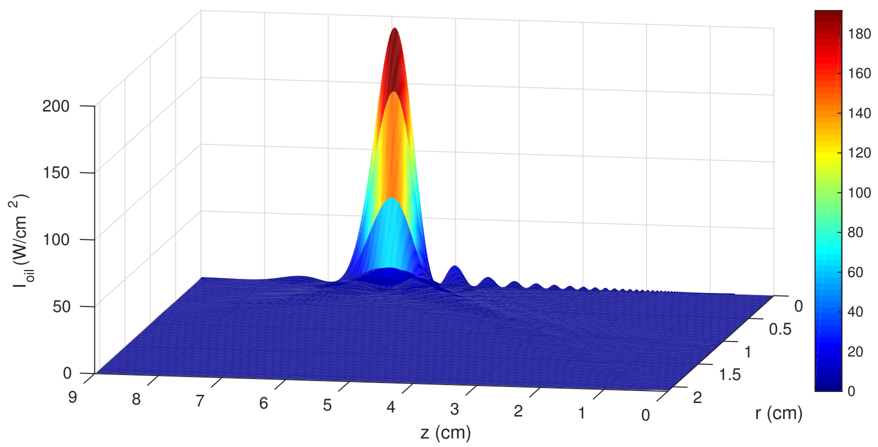

(b)

Figure 5.3: Axially symmetric ultrasound intensity map inside the tissue for (a) water and for (b) oil medium).

receiver antennas is sunflower oil ($\varepsilon_r = 2.5, \sigma = 0.05$ S/m [62, 65]). The steps of preparing the antennas for the experiment are shown in Figure 5.6.

In previous studies, since the antennas were fixed to the mold, it was not possible to scan the phantom with both ultrasound probe and the antennas. Therefore, the received signal was dependent on the position of the antenna. In addition, the glass mold could have caused ultrasound reflection which might have affected the Doppler signal. Also, the water leakage between the antennas and the phantom container caused too much microwave loss and as a result the received signal level was decreased. In the second generation set up, water is replaced by oil

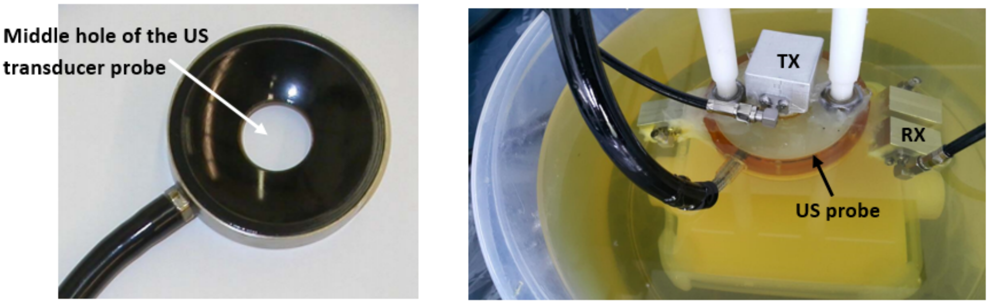

(a) (b)

Figure 5.4: The antenna and ultrasound transducer configuration in the second generation of HMMDI setup. (a) The US transducer probe with the open circular hole in the middle. (b) The location of the TX in the middle of the US transducer and the RX antenna on the outer edge of the transducer.

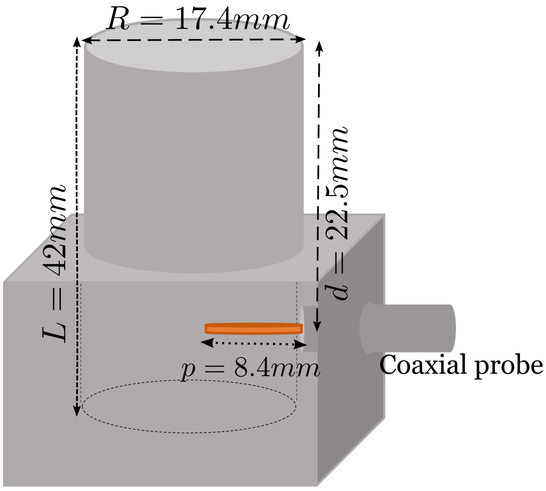

Figure 5.5: Cylindrical waveguide antenna in HMMDI.

as a coupling medium, glass phantom container is replaced by plastic mold to reduce ultrasound reflection, and antennas are attached to the transducer.

The optimum position of the receiver antenna that provides highest amount of scattered signal from the phantom is studied. For this purpose, a rectangular transmitting antenna is placed at the bottom of the oil container (where we will locate phantom) and the received microwave signal is measured from the other antenna on top side of the container. This measurement is done both in the presence and in the absence of the US transducer. The measurement is done using KEYSIGHT, FieldFox Microwave Analyzer N9915A. For the case that US

(a)

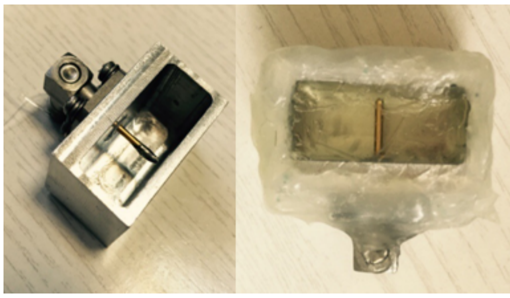

(b)

Figure 5.6: Steps of preparing the antennas for the HMMDI experiment. (a) The transmitter antenna in the second HMMDI set up studies before and after filling with the high permitivity material. (b) The rectangular waveguide antennas before and after filling with oil.

Table5.3: The measured S_{21} between two rectangular antennas in cases with and without the US transducer. When the transducer does not exist, the distance between the antennas is 4.5 cm.

Antenna 4.5 cm away from the center	θ	S_{21} (dB)
E-plane	0	-23.13
E-plane	180	-26
E-plane	30	-24.22
E-plane	45	-23.21
E-plane	60	-24.26
Antenna around the transducer		
H- plane	45	-26.70
E- plane	45	-30.37
H-plane	0	-31.34

transducer is not present, the distance between the top side antenna and the center of the container is kept at 45 mm (figure 5.7 (a)). The received signal for various antenna direction with respect to the transducer plane (Figure 5.8) is given in Table 5.3.

As it can be seen in the results, at 45 degree and H-plane configuration the signal level is highest. Although receiving a higher signal from the phantom is important, direct coupling between the transmitter (TX) and receiver antennas (RX) should be kept at minimum to increase the SNR level. To measure the TX-RX direct coupling signal, the rectangular antennas (at 45 degree with respect to US transducer) are fixed around the transducer using silicon adhesive glue,

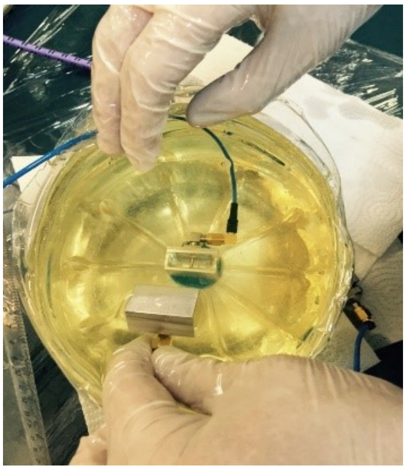

(a)

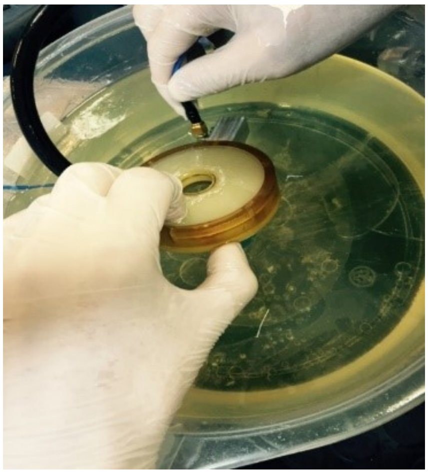

(b)

Figure 5.7: The set up for finding the optimum configuration to receive the highest scattered signal from the phantom (a) without US transducer and (b) with US transducer

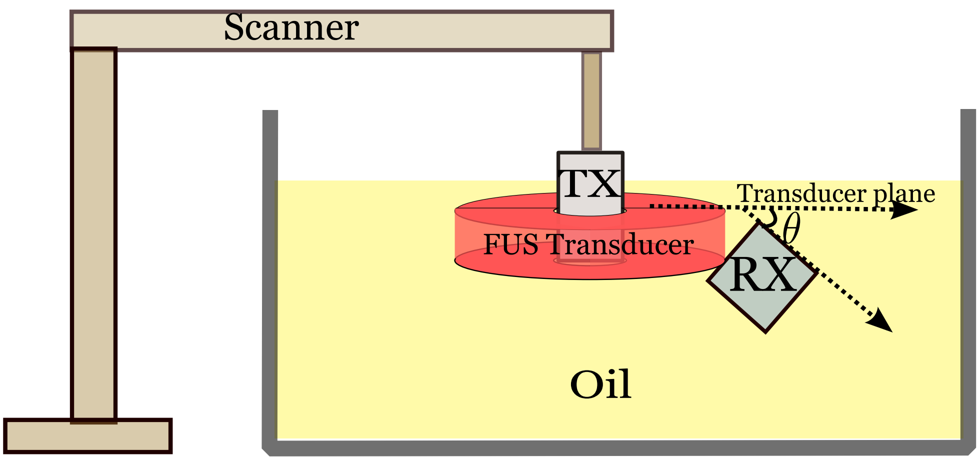

Figure 5.8: The transmitter (TX) and receiver (RX) antenna location with respect to the transducer plane for S_{21} measurement.

and the transmitter antenna is placed in the middle hole of the US transducer (Figure 5.9). The measured S_{21} from each pair of the antenna is given in Table 5.4. It is observed that S_{21} in H-plane in different configurations is lower in comparison with the E-plane which is more desirable for HMMDI analysis. As the direct coupling between the antennas gets higher, the phase noise level gets higher and the Doppler signal observation becomes more difficult.

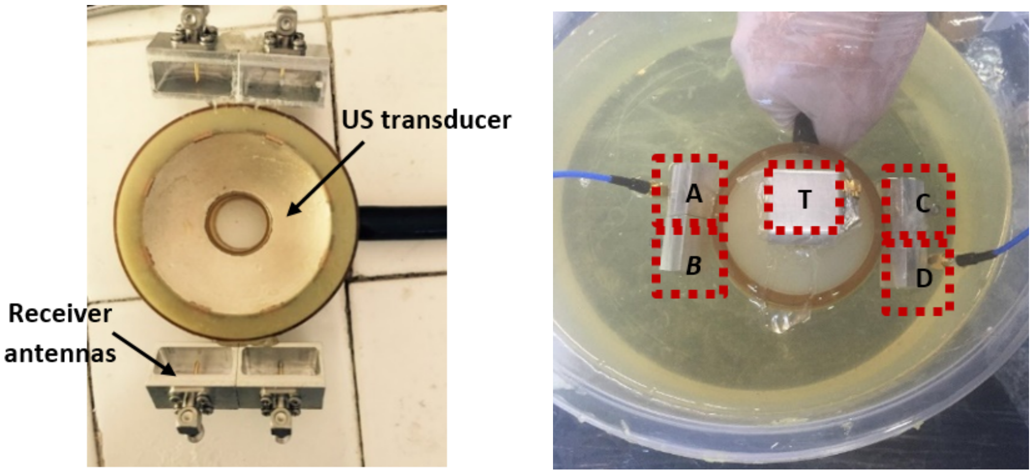

(a) (b)

Figure 5.9: From right to left, position of the receiver antennas around the US transducer, (b) different antenna pairs for S_{21}, and (c) experimental set up for measuring the S_{21}.

The S_{11} and the S_{21} of the transmitter and receiver antennas are measured inside the oil (Figure 5.10).

5.2.4 Phase Noise of the Transmitter

The Doppler frequency in the HMMDI is around few Hz which is very close to the carrier frequency. Therefore, as the phase noise of the transmitter gets higher the detection of the Doppler signal becomes more difficult. The microwave signal generator that is used in this studies is Agilent E8267D Signal Generator (250 kHz - 20 GHz). To measure its phase noise, its output is connected to Agilent N9010A EXTA Signal Analyzer for 0 dBm output power. 10 MHz

Table5.4: The measured S_{21} between each pair of the antennas.

Antenna Pair (E-plane)	S_{21} (dB)
A-TX (with and without 50 load on B	-29.60
B-TX	-30.4
C-TX	-30.04
D-TX	-30
A-B	-31.6
A-C	-33
A-D	-32
Antenna Pair (H-plane)	**S_{21} (dB)**
A-TX	-33.85
B-TX	-35.06

reference signal of the Signal Analyzer is used as 10 MHz reference for the Signal Generator. The Signal Analyzer resolution bandwidth, span, and the number of averages is selected as 6.8 Hz, 500 Hz, and 20, respectively. The phase noise plots of the signal generator for different operation frequencies from (2-8 GHz) is given in Figure 5.11. As the frequency is increased, the phase noise of the transmitter gets higher. The results suggest that, the Doppler signal may be better realized in lower MW operating frequencies.

5.3 Microwave and vibration frequency test using homogeneous tumor phantom

To test the effect of microwave and vibration frequency on the received signal, a homogeneous tumor phantom [2] was developed. This phantom is prepared in the plastic molds of 60 mm diameter and 45 mm height(Figure 5.12). A 3-cycle 15 Hz AM burst signal induce the localized vibration inside the phantom. Spatial peak pulse average intensity (I_{sppa}) of the ultrasound beam is 271.4 $\frac{W}{cm^2}$.

The focus of the US transducer is at the homogeneous tumor phantom (Figure 5.13). The transmitter microwave antenna is fed by the Agilent E8267D Microwave Signal Generator with an output power of 10 dBm. The received

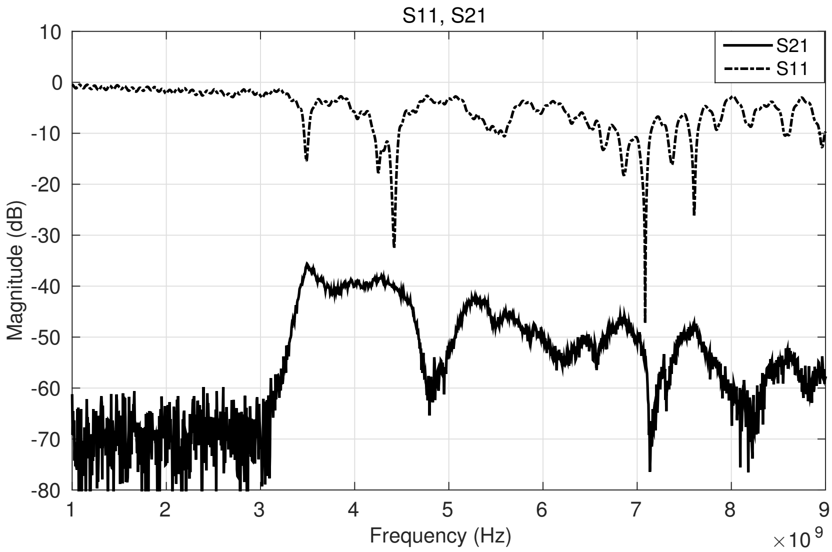

Figure 5.10: The measured S_{11} of the transmitter antenna (dashed line) and S_{21} in the inside the oil (solid line).

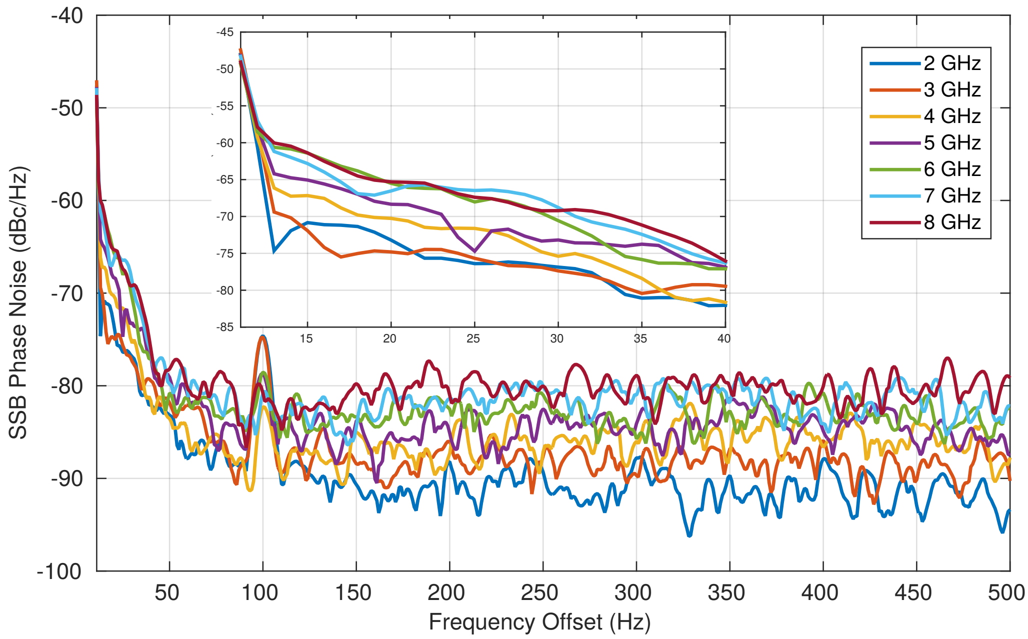

Figure 5.11: Measured phase noise of the microwave signal generator. In this measurement the signal generator is directly connected to the spectrum analyzer. The frequency span is 500 Hz.

Figure 5.12: Homogeneous fat and tumor phantom of 60 mm diameter and 45 mm height.

microwave signal is connected to the Agilent (N9010A) EXA Signal Analyzer. 10 MHz reference signal of the spectrum analyzer comes from the microwave signal generator. The spectrum analyzer parameters for the measurement are: resolution bandwidth = 6.8 Hz, span = 200 Hz, number of samples for averaging = 20.

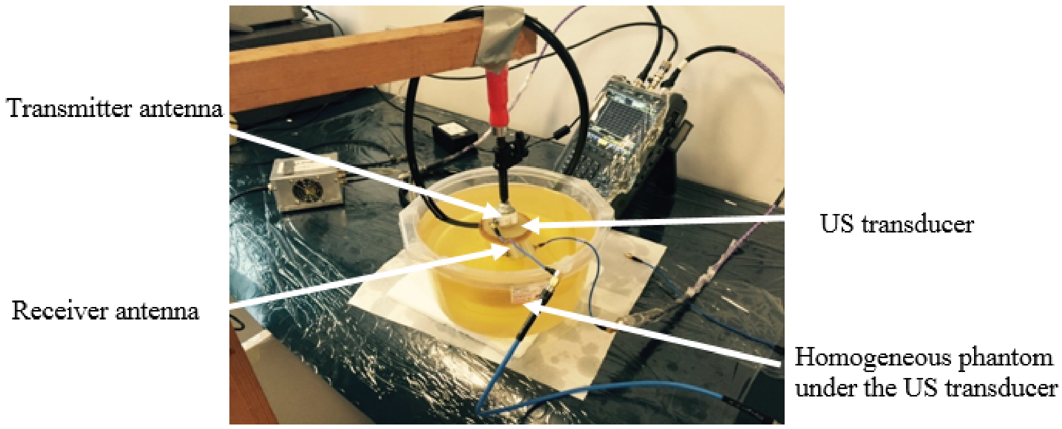

Figure 5.13: The HMMDI experimental set up. The transducer is fed with the amplified AM burst signal. The transmitter antenna is fed by the microwave signal generator. The receiver antenna is connected to the spectrum analyzer.

The measured signals from the homogeneous tumor phantom at center frequency, Doppler frequency and the noise level at Doppler frequency are measured for different microwave frequencies. The results for 3.5-6 GHz microwave signal for 10 dBm power is given in Figure 5.14. Considering the SNR and the ratio of the signal at Doppler signal to signal level at center frequency 5.15), 3.5 GHz and 6 GHz are selected as the optimum vibration frequencies.

Similar to previous experimental results reported in Chapter 4, the signal level reduction in the main frequency, 6 GHz, could be due to scattered wave interaction or its out of phase summation with the surface waves. This causes a decrease in the signal level at the center frequency but not the signal at Doppler frequency. Consequently, the Doppler signal can be better detected compared to the main component.

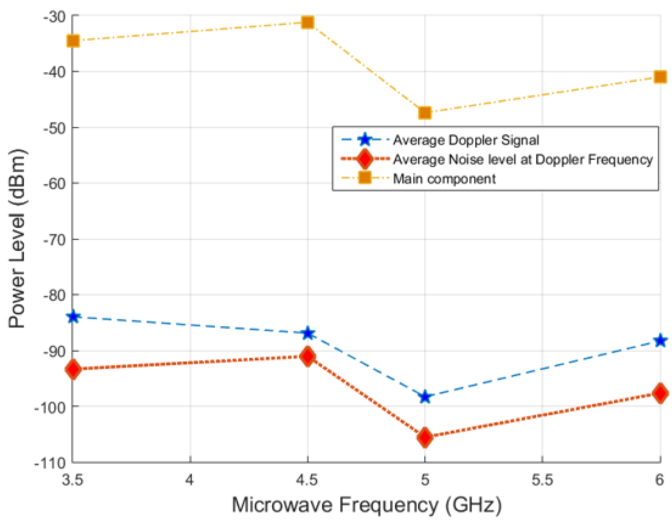

Figure 5.14: Received Doppler signal around the center frequency, noise level at Doppler frequency and the signal at center frequency when the focus is on the tumor phantom. 15 Hz vibration with 3 cycles is applied with 1 second PRI.

Since the SNR and the ratio of Doppler signal to the signal at main frequency (Doppler/main signal) are higher at 3.5 and 6 GHz, different mechanical vibration frequencies are tested at these microwave operating frequencies. 10, 15, 30,

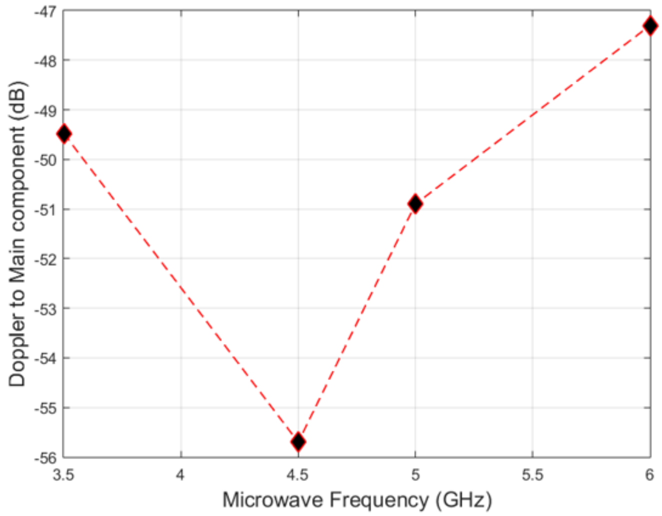

(a)

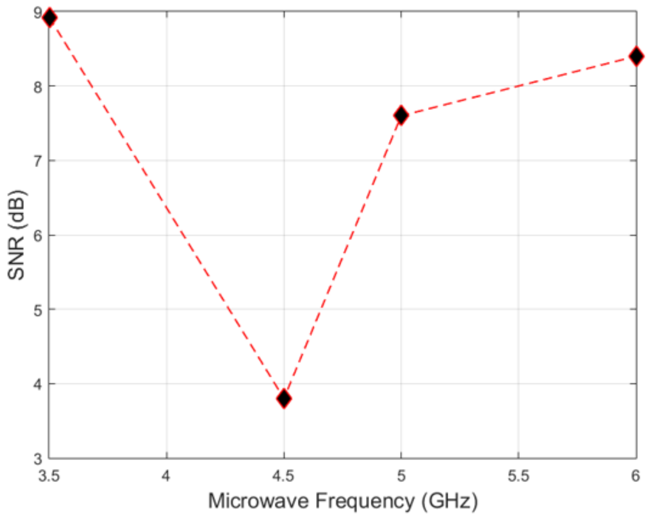

(b)

Figure 5.15: The measured (a) SNR and the ratio of the signal at Doppler frequency to the signal at center frequency when 15 Hz vibration with 3 cycles is applied with 1 second PRI.

and 70 Hz with 2, 3, 6 and 14 cycles are employed to produce the vibration. The duration of the US pulse is 200 ms in each case. The best result is obtained when 30 Hz vibration is applied to the phantom. Doppler signal at 10 Hz is not detectable from the main component.

The received signal spectrum at 30 Hz vibration frequency is given Figure 5.16 for 3.5 GHz and 6 GHz microwave frequency. The signal at vibration frequency on the right and left side of the center frequency, are not equal. This asymmetry could be due to the position of the US transducer or the reflection from the phantom container edges. This phenomenon is discussed further in section 5.4.4.6.

Realizing the Doppler signal is dependent on the coupled signal level. As the coupling at fundamental frequency decreases, the phase noise gets lower and the Doppler signal becomes more distinguishable. Since the microwave loss in water is high, blocking the path between the transmitter and receiver antenna with water can be helpful to decrease the direct coupling between the transmitter and receiver antennas. A 15 ml falcon tube of 15 mm diameter and 117 mm height filled with water is inserted between the US transducer and the receiver antenna (Figure 5.17). Since the transmitter antenna is in the middle of the transducer, this water container, blocks the TX-RX path. As it is can be seen in Figure 5.18, the direct coupling between the TX and RX, and the phase noise level are decreased about 15 dB. As a result, the SNR at Doppler frequency is increased about 8 dB.

5.4 Experimental studies on inhomogeneous phantoms

In order to automatize the scanning procedure, a FUS probe with the TX antenna in the middle and the RX antenna on the outer edge are mounted on the 3D scanner (Figure 5.19). A MATLAB program is written to control the scan procedure and set the parameters of the microwave signal generator, waveform generator, and the spectrum analyzer. The block diagram of this program is shown in Figure 5.20. The FUS starts to induce vibration inside the phantom.

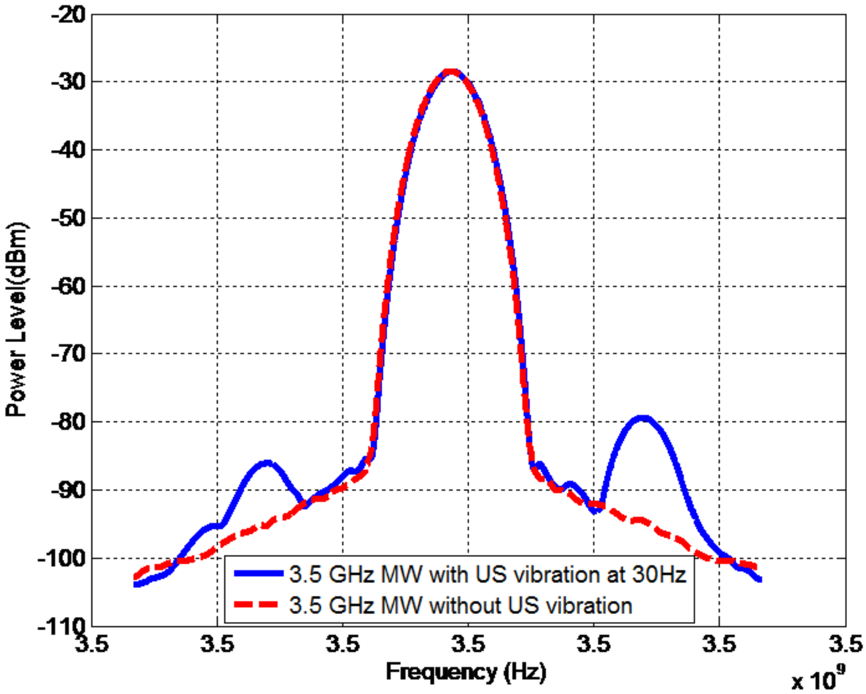

(a)

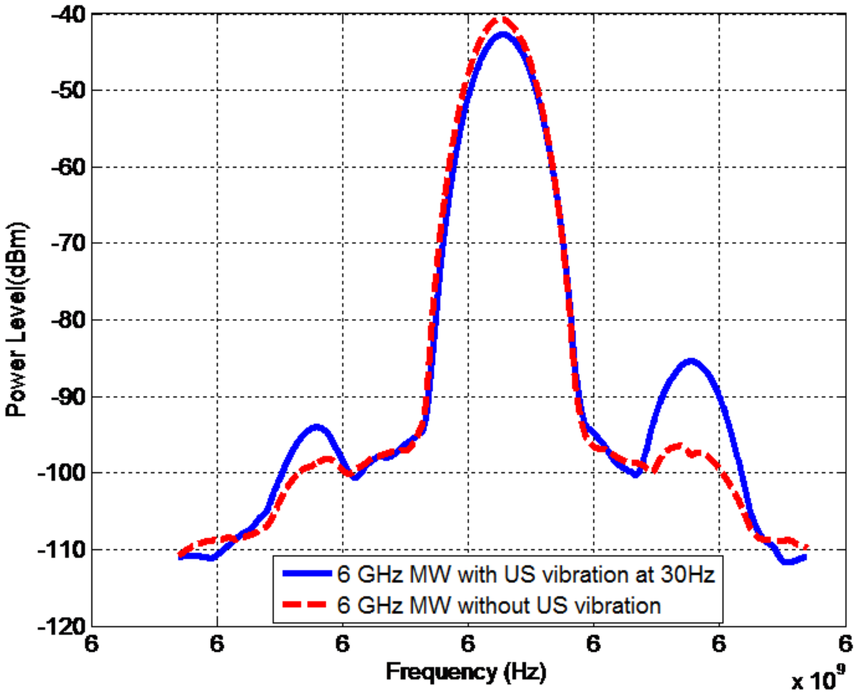

(b)

Figure 5.16: The measured signal at (a) 3.5 GHz and (b) 6 GHz microwave frequency in the homogeneous tumor phantom when the vibration frequency is 30 Hz.

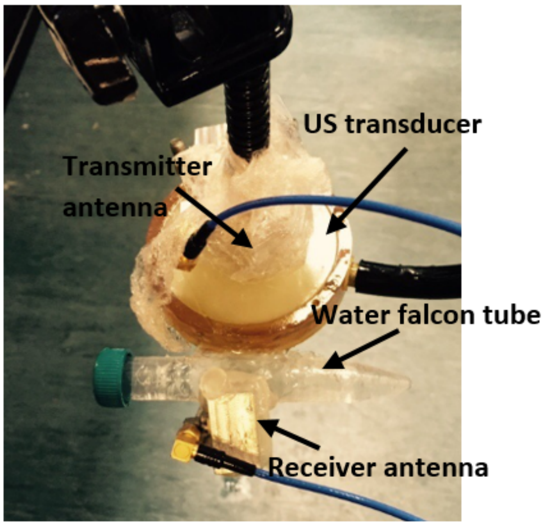

Figure 5.17: Blocking the path between the transmitter and receiver antenna with 15 ml falcon tube of 15 mm diameter and 117 mm height which is filled with water to decrease the direct coupling between transmitter and receiver antennas.

The data is recorded after averaging (with 8 samples) period of the spectrum analyzer. Then, the mechanical excitation is ceased and the scanner moves to the next step through the predefined scan path. At the new position, the US excitation is applied and the data is recorded, similarly. By this way, the data profiles of the developed inhomogeneous phantoms are acquired.

5.4.1 Experimental results on phantom-1 (fat phantom including three different sized tumors)

For this experiment, a layer of fat phantom is prepared an poured into the plastic container of 11 mm diameter and 50 mm height. Three different sized tumor phantoms with diameter and height of 9 mm $\times$ 5 mm, 5 mm $\times$ 4 mm, and 4.5 mm $\times$ 4 mm are placed on top of the solidified fat phantom in the middle line of the container. Another fat phantom is prepared and poured into the container. The developed phantom and its MRI image, are shown in Figure 5.21.

The experimental system set up is similar to the one shown in Figure 5.1. The focused US transducer is used in its third harmonic frequency (3.32 MHz). To create the US excitation, a 5-cycle 25 Hz sinusoidal burst signal (with 1 Hz pulse

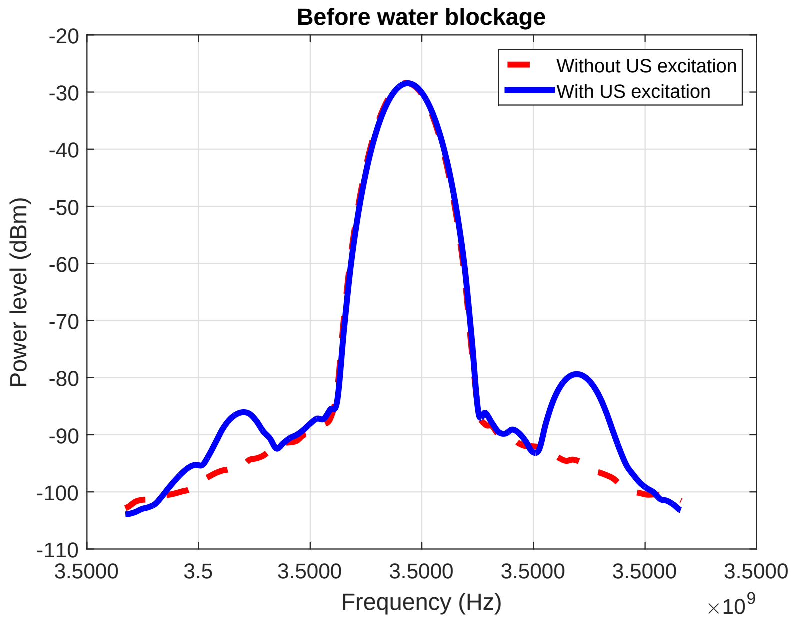

(a)

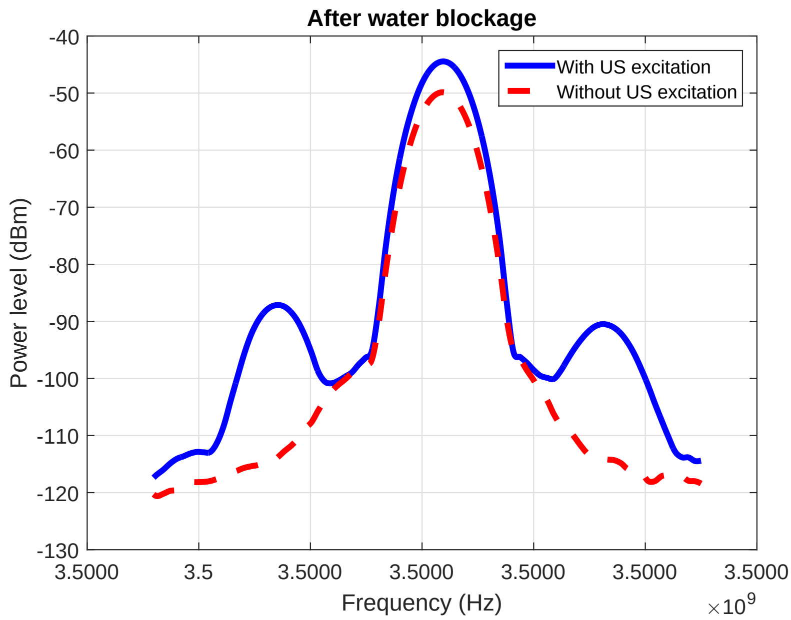

(b)

Figure 5.18: The measured signal while the transmitted microwave frequency is 3.5 GHz in the (a) presence of water blockage and (b) in the absence of water blockage. The signal is taken from the homogeneous tumor phantom when the vibration frequency is 30 Hz.

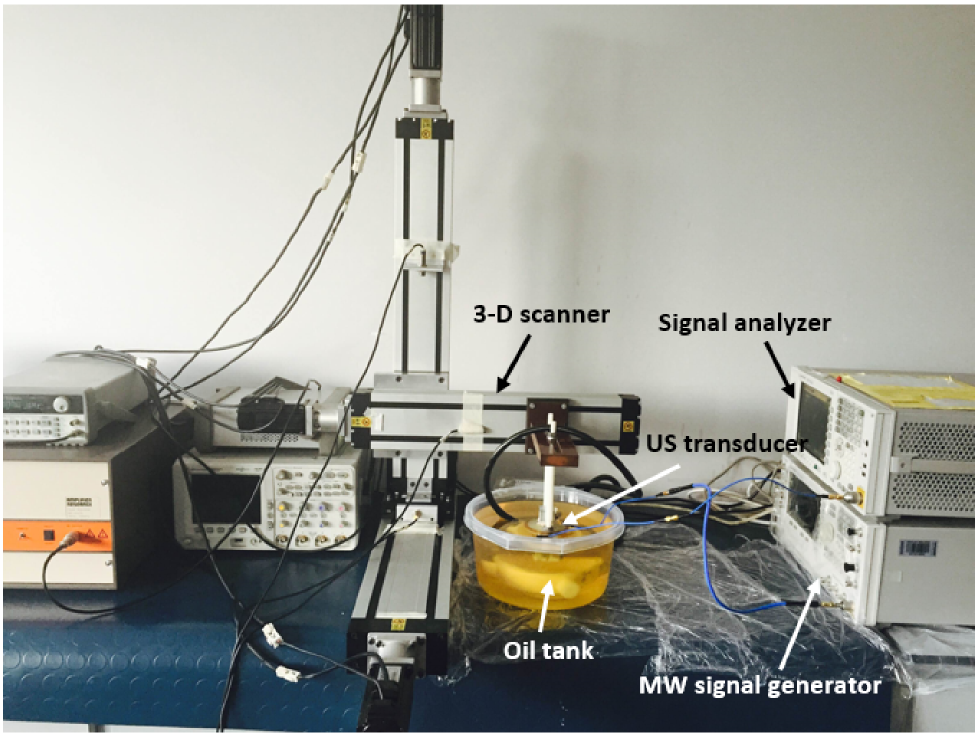

(a)

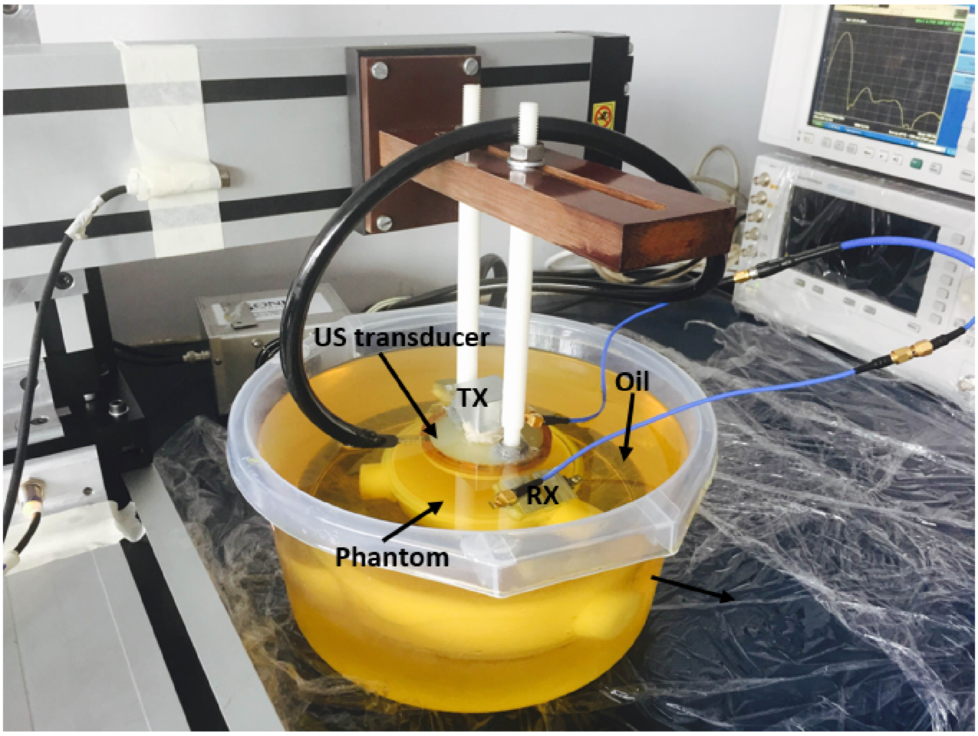

(b)

Figure 5.19: The experimental HMMDI scan set up with the (a) 3D scanner and mounted FUS probe and (b) mounted FUS and the TX-RX antennas.

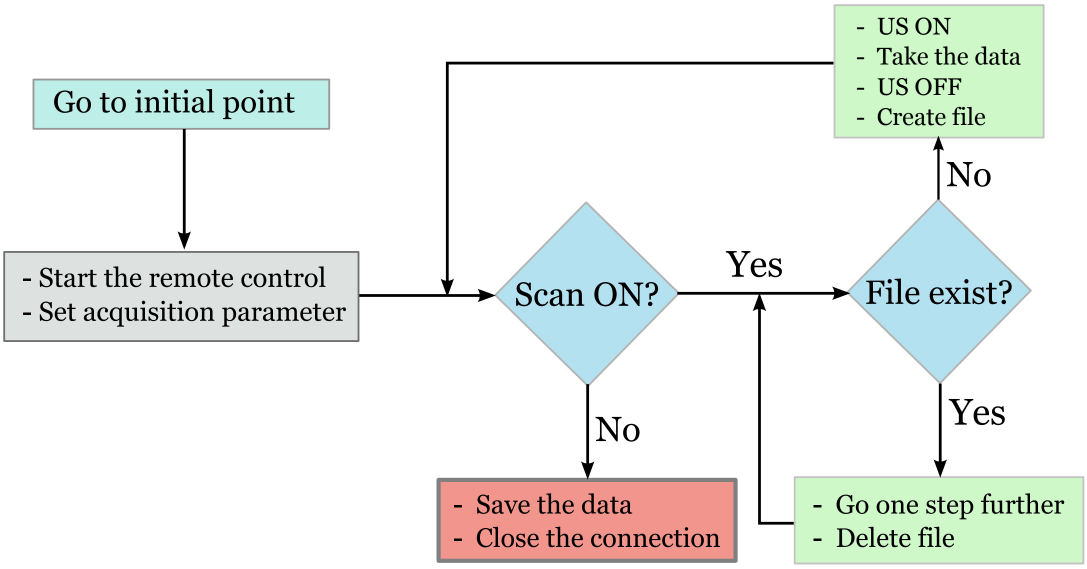

Figure 5.20: Block diagram of the automatized scan procedure for HMMDI data acquisition.

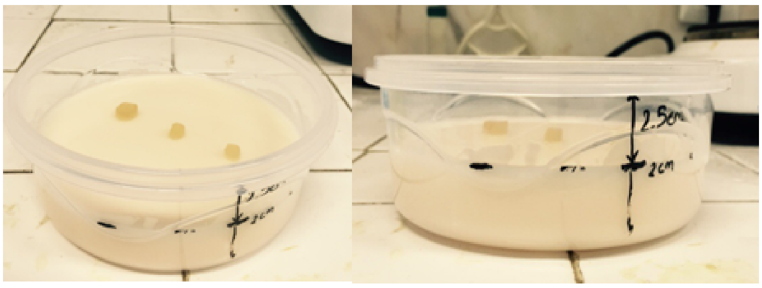

(a)

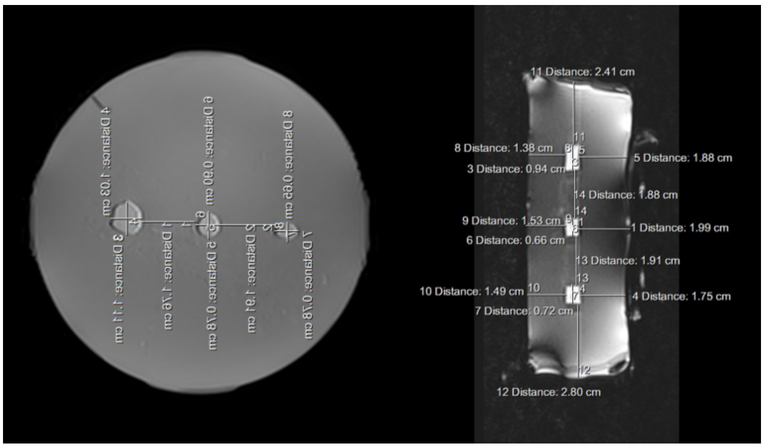

(b)

Figure 5.21: (a) Prepared inhomogeneous phantom containing three different sized tumors inside the fat phantom and (b) MRI image of it taken by 3 Tesla MRI System, UMRAM Research Institute in Bilkent University.

repetition frequency) is used to amplitude modulate the 3.32 MHz signal. The AM signal is amplified with gain of 52 dB gain. Spatial peak pulse average intensity (I_{sppa}) of the ultrasound beam is 271.4 $\frac{W}{cm^2}$. The transmitting microwave antenna in the middle of the transducer is fed by +10 dBm microwave signal. In order to find the optimum MW operating frequency, the MW frequency is applied in the frequency range 3.4-7 GHz. At 5.7 GHz, the ratio of the signal at the center frequency to the Doppler signal is low and SNR is high (Figure 5.22). Therefore, this frequency is selected as the optimum frequency.

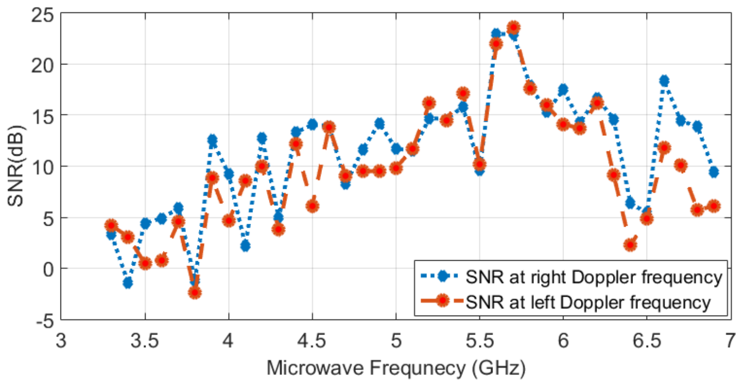

(a)

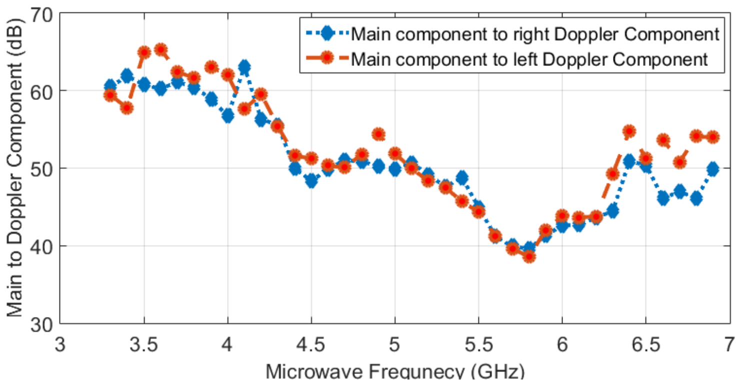

(b)

Figure 5.22: MW operating frequency test when a 5-cycle 25 Hz sinusoidal burst signal (with 1 Hz pulse repetition frequency) is used and the spatial peak pulse average intensity (I_{sppa}) of the ultrasound beam is 271.4 $\frac{W}{cm^2}$. The (a) SNR and (b) the ratio of the signal at center frequency to signal at Doppler frequency are presented.

5.4.1.1 1-D scan results

A linear scan (1-D) is applied to evaluate the system's performance in detecting the tumors. The scan lines and the results related to different paths in the phantom container is shown in Figure 5.23. The scan lines are selected with respect to the center line of the phantom container where three tumors are located. It is observed that, the Doppler component of the received signal level increases about 3 to 10 dB in the tumor area for different line scans. Three peaks in the received signal are related to the three tumor phantoms. As the distance to the center line is increased, the signal level is decreased. The signal level decreases about 7 dBm (specially in the first and last tumor region) when the scan line is 18 mm away from the central line.

5.4.1.2 2-D scan results

To obtain a data profile on a 2D area, the same antenna/transducer configuration is used to scan the phantom. The scan step size is 2 mm. The scan path and results (signal level at vibration frequency around the center frequency) are shown in Figure 5.24. It is observed that, the Doppler signal level nearby the tumors, is around -86 dBm to -82 dBm which is about 10 dB higher than the received Doppler signal from the fat phantom. Although there is a shift in the detected tumor location (red dashed circles), the tumors can be clearly distinguished from the fat phantom. The shift could be related to manually locating the phantom under the scanner. That is, the x and y scan paths may not be exactly vertical and parallel to the center line passing from the tumors.

It is observed that, the Doppler signal at right and left side of the center frequency are not equal. This may be due to position of the US transducer which is not completely parallel to the phantom, or it can be due to the microwave and acoustic reflections. Although the right and left Doppler signals are asymmetric, the place of three tumors can be seen in the obtained images. More studies are done to find the reason of this phenomenon.

The signal level at the center frequency to signal level at the Doppler frequency

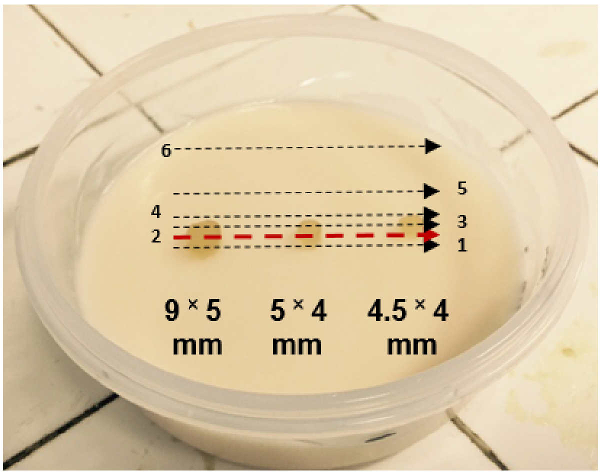

(a)

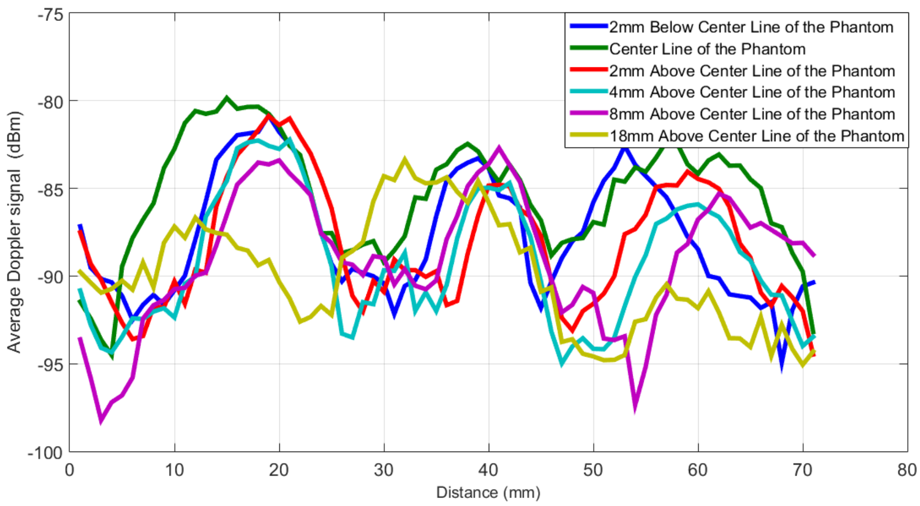

(b)

Figure 5.23: The 1-D scan (a) paths and (b) obtained results in each scan line. The signal rises in the tumor regions and decreases in the fat area.

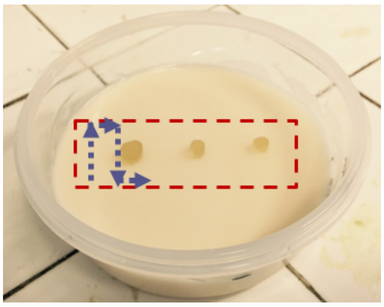

(a)

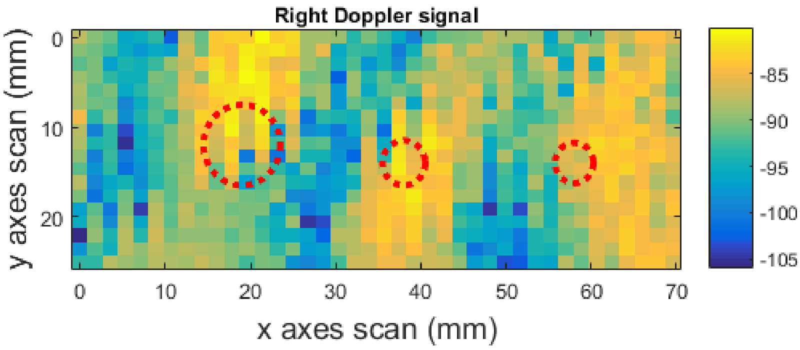

(b)

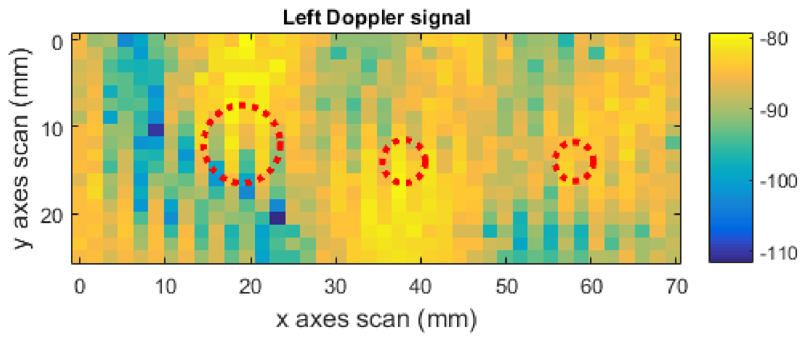

(c)

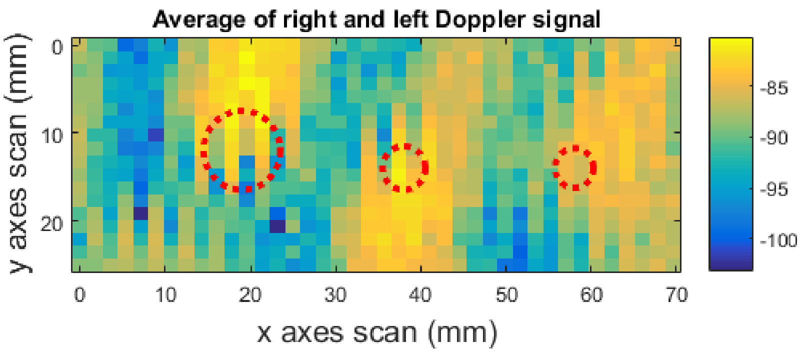

(d)

Figure 5.24: A 2-D (a) scan path and (b) obtained image of three tumors from right Doppler signal, (c) from left Doppler signal, and (d) average of right and left Doppler signal. Tumor phantoms are located at the depth of 2.5 cm inside the fat phantom. From left to right they are 9 mm × 5 mm, 5 mm × 4 mm, and 4.5 mm × 4 mm. The real place of the tumors are shown by red rash circles.

is calculated from the received data (Figure 5.25). The main component to Doppler component signal decrease around 10 dB in the tumor area comparing the fat region. From the obtained result, the existence of three tumor phantoms is realizable, but it does not provide information about the size of the tumors.

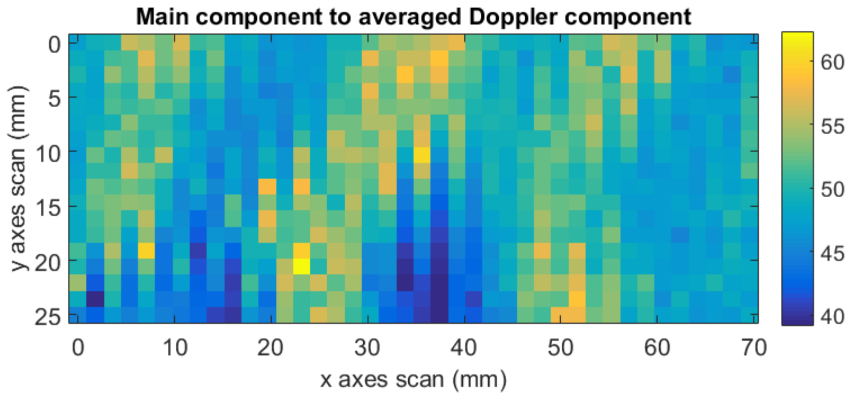

Figure 5.25: Main component to Doppler component Image of the phantom containing three tumors.

5.4.2 Experimental results on phantom-2 (homogeneous fat phantom)

In order to obtain HMMDI data profile without a tumor inclusion, a homogeneous fat phantom is developed. Doppler component of the received signal and the signal at center frequency to signal at Doppler frequency (main/Doppler signal) obtained from 30 mm $\times$ 30 mm scan area are shown in Figure 5.26. No specific pattern is observed that shows the existence of an inhomogeneity inside the phantom. In this case, the Doppler signal level is embedded in noise. Therefore, an increase in the Doppler component of the received signal level as in the previous experiment, is just due to the existence of tumors.

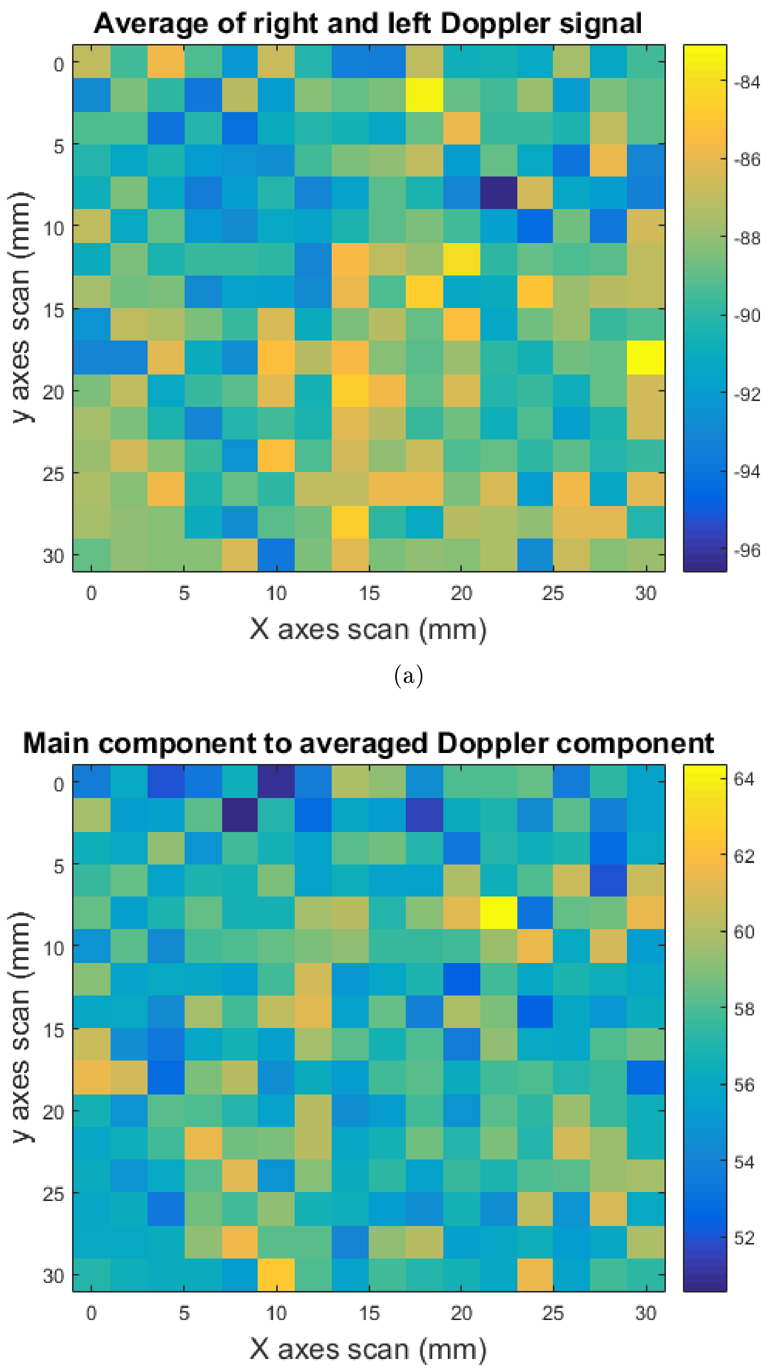

(a)

(b)

Figure 5.26: The 2-D image obtained from 30 mm × 30 mm scan of homogeneous fat phantom from both (a) signal at Doppler frequency and (b) the main/Doppler signal.

5.4.3 Experimental results on phantom-3 (fibro-glandular with tumor inside in the middle of fat)

Another experiment is conducted to detect tumor inside the fibro-glandular tissue which has high dielectric constant. Due to similar dielectric properties, these tissues cannot be distinguished in microwave imaging. However, the Young modulus of the tumor is about 3-13 times greater than the Young modulus of the fibro-glandular [34]. In this study, the possibility of distinguishing these tissues based on their elastic contrast and separating them from the fat tissue is evaluated.

A fat phantom containing 5.5 mm diameter and 7 mm height tumor inside the 25 mm diameter and 7 mm height fibro-glandular phantom is developed (Figure 5.27). These phantoms are located in a layer 25 mm below the surface level of the fat phantom and 20 mm above the bottom layer.

Figure 5.27: Fat phantom containing 5.5 mm $\times$ 7 mm height tumor (red dashed circle in the right figure) inside the 25 mm $\times$ 7 mm height fibro-glandular phantom (yellow dashed circle in the right figure). The fibro-glandular and tumor phantoms are 25 mm inside the fat phantom from the top surface. A yellow dashed circle in the middle figure shows a damage in the phantom while preparing it.

5.4.3.1 1-D scan results

Set up is prepared for a linear scan of the phantom. A 5-cycle 25 Hz sinusoidal burst signal (with 1 Hz pulse repetition frequency) is used for inducing the US excitation. Similar to the previous studies, spatial peak pulse average intensity

(I_{sppa}) of the ultrasound beam is 271.4 $\frac{W}{cm^2}$. The transmitting microwave antenna is fed by +10 dBm microwave signal. The optimum MW operating frequency is selected by sweeping the MW frequency from 3.4-7 GHz. At 7.5 GHz the SNR is higher and the signal level at the main/Doppler signal is low. The scan line is assumed as a line in the middle of the phantom container which passes through all three different phantoms; fat, fibro-glandular and tumor phantoms (Figure 5.28).

In the first experiment antennas and the transducer are immersed in a small oil tank (Figure 5.28 (a)), it is observed that the reflection from the edges, at the beginning and end of the scan path is high. Since at the beginning and at the end of the scan line, the transducer is so close to the border of the oil container. Sudden change in material properties from oil to the air, caused a considerable reflection. This reflection perturbs the received signal. Therefore, a larger oil tank is selected to solve this problem (Figure 5.28 (b)).

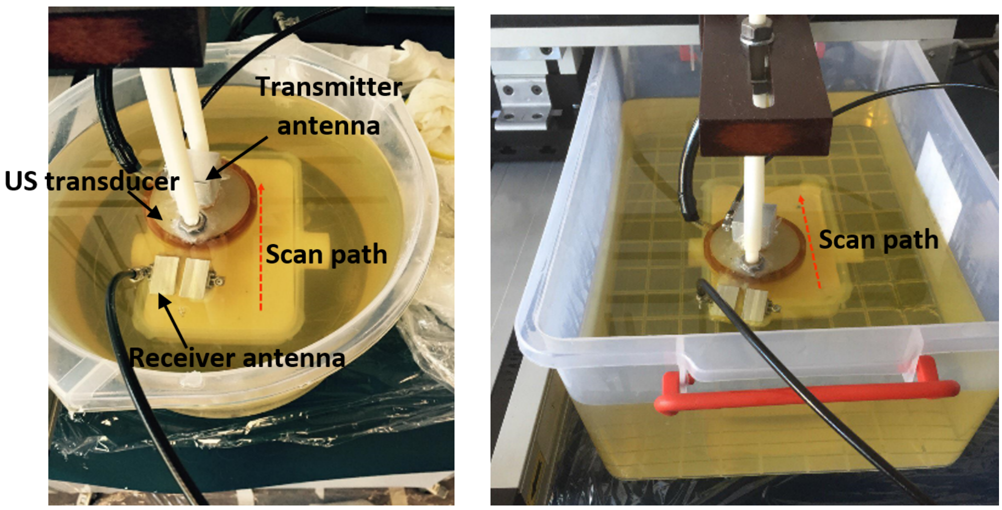

(a) (b)

Figure 5.28: US transducer and antenna configuration in the experimental studies. Ultrasound transducer, antennas, and the phantom are located in the (a) small or (b) larger oil tank.

The scan is done for both cases when the acoustic excitation is induced inside the phantom (Doppler signal evaluation) and when the traducer is off (noise level evaluation). The resulted data are plotted in Figure 5.29. It is expected to receive the maximum Doppler signal level in the fibro-glandular phantom region. The Doppler signal level in tumor should be above the one in the fat. This phenomenon is observable in the SNR and main/Doppler signal, as shown in Figure 5.29 (b) and (d). But, it is quite difficult to visualize it in the Doppler signal plot (Figure 5.29 (a)).

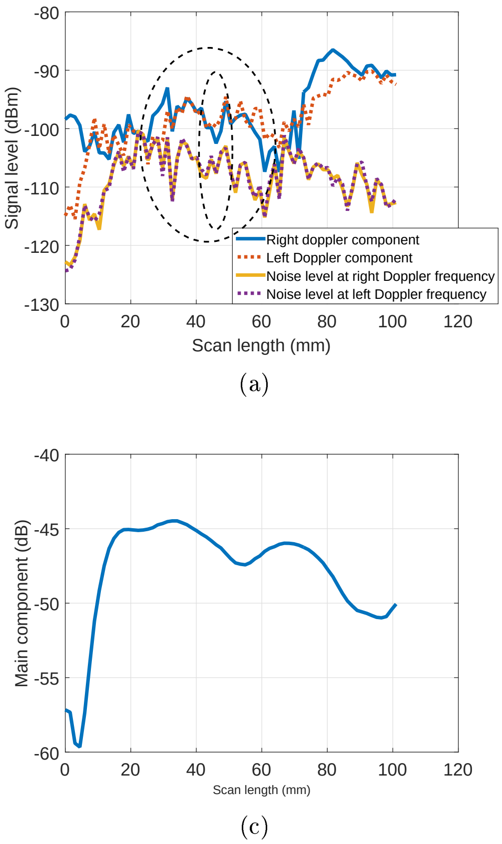

(a) (b) (c) (d)

Figure 5.29: Experimental results on the fat phantom containing fibro-glandular and tumor phantoms. (a) Doppler component of the received signal and noise level at Doppler frequency, (b) SNR, (c) signal at main frequency, and (d) main/Doppler signal. The region that the signal rises (larger circle) or falls (smaller circle) are shown with dashed circles

This can be due to the stiffness of the phantoms. Therefore, the elasticity and

Table5.5: Elastic properties of the tumor and fibro-glandular phantoms.

	Young Modulus (kPa)	
Measurements	44.5	19.7
Reference	10.40-42.52	3.32

dielectric properties of the phantoms are measured. The measured dielectric properties of the tumor and fibro-glandular phantoms (Figure 5.30) are consistent with the reference values [9]. The measured Young modulus of the utilized fibro-glandular phantom (Table 5.5), is higher than previously used phantom in the first generation of the HMMDI system evaluation given in chapter 4. Therefore, the received Doppler signal from the fibro-glandular region comparing the one on the fat and tumor, is not high.

In addition, the Doppler signal level at the beginning and at the end of the scan path increases sharply even higher than the Doppler signal level in the fibro-glandular area. This can be related to the location of the receiver antenna. At the beginning of the scan path, the receiver antenna is located completely out the phantom container (US transducer diameter is 64 mm). So the material under the antenna, is oil and plastic phantom container. During the scan procedure, the antenna passes the plastic mold and travels through the phantom. This change in the material under the antenna, may affect the direct coupling between the transmitter and receiver and as a result reflection occurs.

The signal is affected by the huge sized fibro-glandular tissue as the antennas move with the transducer. So, the 'B' component in the received signal (2.13) is affected by movement of the antennas and a combined response from vibration and microwave reflection. This effect of the antenna movement was much less for the phantom with 3 tumors since their sizes were relatively small. For the softer fibro-glandular phantom, the effect of antenna movement comparing the Doppler signal may be less. The reflection from the phantom container edges counts as another parameter which can cause the signal rise close to the edges.

As it can seen in the figure 5.29, after 70 mm, a rapid rise is observed in the signal

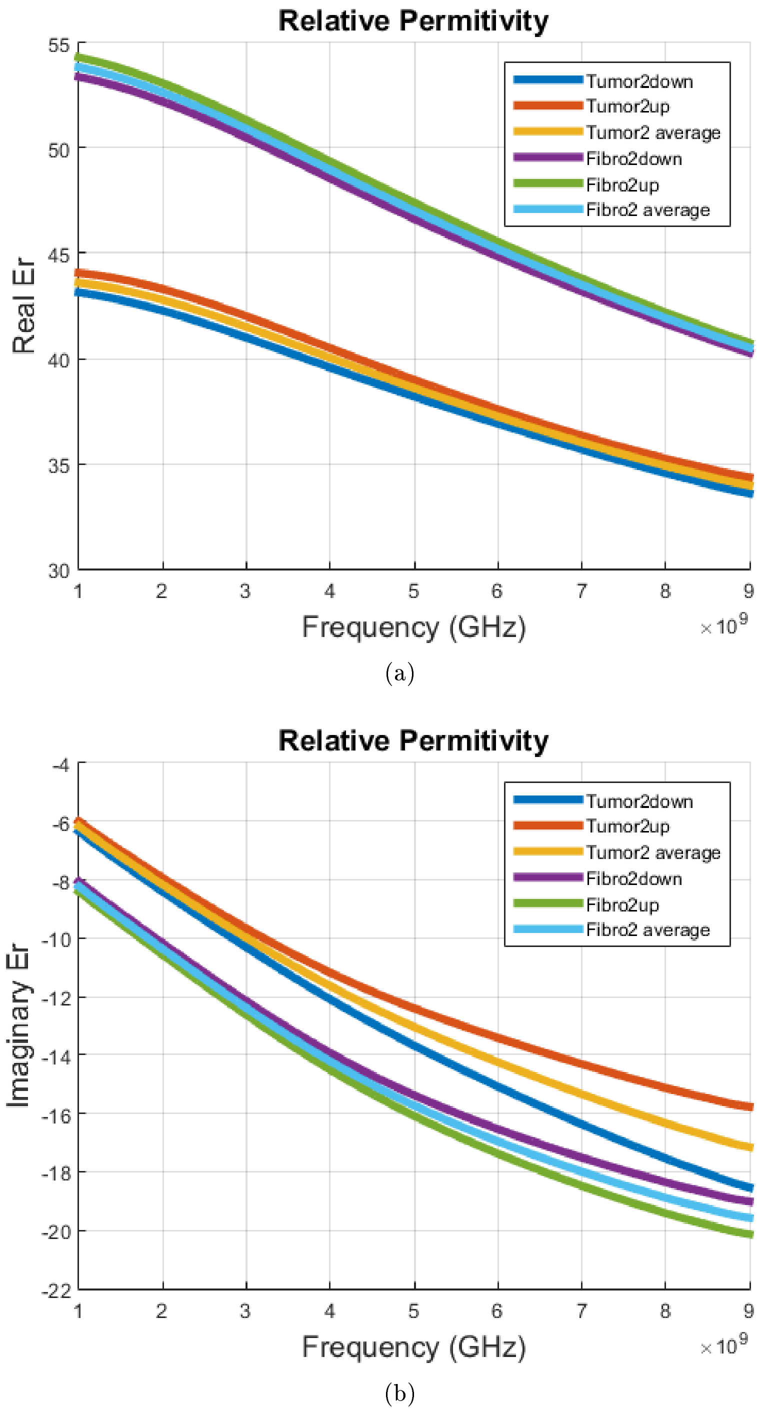

(a)

(b)

Figure 5.30: The relative permitivity of the utilized Fibro-glandular and tumor phantoms. (a) Real ϵ_r and (b) Imaginary ϵ_r.

at Doppler frequency. A damage in the phantom (Figure 5.27 (yellow dashed area in the middle figure)) may be the reason of this signal rise. In the first generation of HMMDI set up, antennas were fixed so that this problem was not observed. Fixing the antennas can eliminate the changes of the main component and microwave reflections. Therefore, the system should be evaluated for the case where the antennas are fixed at the bottom of the phantom baker.

5.4.3.2 2-D scan results

Since the microwave reflection occurs while antenna is traveling from oil to the phantom container and then through the phantom, 2-D scan (area of 40 mm $\times$ 10 mm) is done around the fibro-glandular phantom in the middle of the mold. Signal level at vibration frequency around the center frequency is recorded for each scan point. The obtained results are shown in Figure 5.31.

As it can be seen, the signal level at Doppler frequency is around -95 dBm to -90 dBm in the fibro-glandular region but it is around -100 dBm in the middle of it where we expect to see the tumor. But, the received signal from the fibro-glandular phantom is too much affected by the unwanted reflection rather than tissue characteristics. This can be understood by looking at the huge size of area that Doppler signal is increased. The fibro-glandular diameter is 25 mm while the high Doppler signal level (-95 dBm to -90 dBm) is seen in an area about 5 cm. Therefore, it is difficult to conclude the system is able to discriminate tumor from fibro-glandular with respect to these results. More experiments are necessary to evaluated the potential of HMMDI method in distinguishing these tissues. As it was mentioned above, the artifact may be a result of antenna movement. To evaluate this hypothesis, the antennas are fixed to the phantom. This set up configuration is discussed in the next chapter.

5.5 Conclusion

In this chapter, the water coupling medium in the first generation of HMMDI experimental set up was replaced by oil. The microwave loss in the oil is around

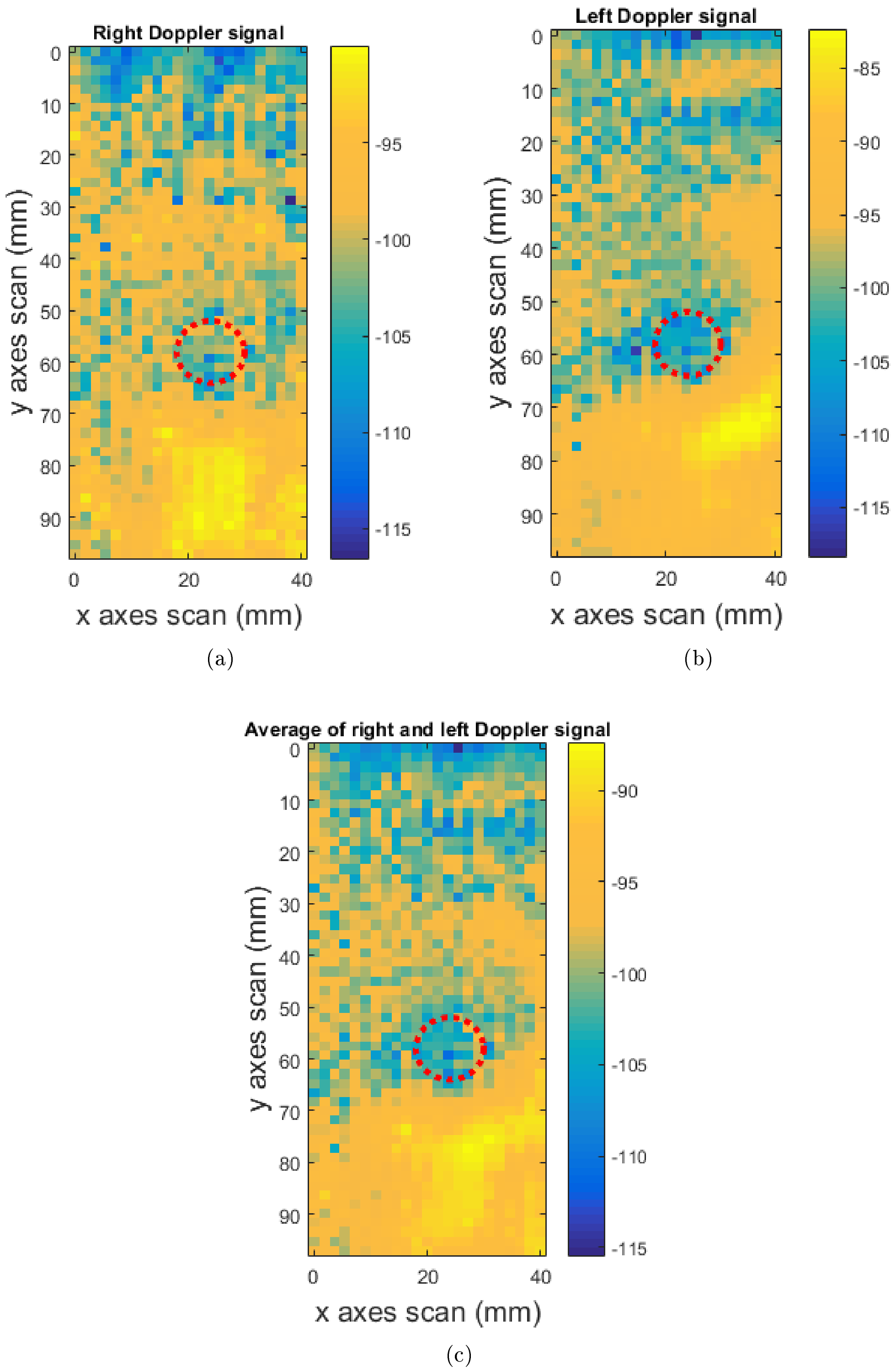

Figure 5.31: The received signal when the MW operating frequency was 7 GHz and 25 Hz, 5 cycle amplitude modulated burst signal is used to feed the transducer (a) Left Doppler signal (dBm) (b) right Doppler signal (dBm), and(c) average Doppler signal (dBm). The area that Doppler signal drops around -110 dBm to -105 dBm comparing the signal level at surrounding area is shown by red dashed circle.

10 times less in oil compared to water. It has been shown the pressure, intensity and heat profile of the acoustic wave inside tissue in the presence of these two coupling medium is similar.

The transmitter and antennas were moved to the top surface of the phantom, together with the transducer. In this configuration, it was possible to scan the phantom with US transducer and antennas. Three phantoms were developed and the performance of the second HMMDI experimental set up with scanning antennas was evaluated on the developed phantoms. The HMMDI scan procedure and the data acquisition was automatize to be controlled through MATLAB program. The received data from the phantoms were acquired by spectrum analyzer.

In the received 1-D and 2-D HMMDI data from phantom containing three different sized tumor inclusion, the Doppler signal on the tumor regions were about 10 dB higher than the one on the fat phantom. From the results, 4.5 mm tumor phantom was detectable inside the surrounding fat phantom. The 2-D HMMDI data acquired from homogeneous fat phantom suggested that the Doppler signal is embedded in noise when there is no tumor or fibro-glandular inclusions.

A phantom containing three types of breast tissue phantoms was developed. It was expected to receive Doppler signal rise in the fibro-glandular region. But, the artifact in the acquired data in the phantom edges was high. The high Doppler signal was recorded from an area, around 2 times bigger than the fibro-glandular inclusion. Therefore, the signal from different regions of phantom was not distinguishable. This artifact may be due to the antenna movement from outside of the phantom container to the inner regions. It was suggested to solve this problem by fixing the antenna at the bottom of the phantom container, similar to first generation of HMMDI experimental set up.

CHAPTER 6

SECOND GENERATION OF HMMDI EXPERIMENTAL SET UP WITH FIXED ANTENNAS

6.1 Introduction

In the second generation of HMMDI experimental set up with scanning antennas configuration, TX antenna was in the middle of the FUS transducer and the RX antenna was on its edge. Consequently, the antennas were traveling with the FUS transducer through the scan path. Since the RX antenna was on the side edge of the FUS transducer and the FUS transducer diameter is 64 mm, the material under the antenna changes from surrounding oil to phantom throughout the scan. As a consequence, the direct coupling between TX and RX, and as a result, the phase noise level was changed. Due to these changes, the received signal level at Doppler frequency changes at the phantom edges.

In this chapter, the TX-RX antennas are fixed at the bottom of the oil container to solve this problem. To evaluate the performance of this system set up, several phantoms are developed. A fat phantom, containing a fibro-glandular inclusion inside, is developed and scanned in lateral plane (xy) to evaluate the effect of multiple vibration frequency, the number of samples use in averaging, and repeatability of the measurements. Different vibration frequencies are tested on a the fat phantom including a tumor inside. The phantoms are scanned using HMMDI and 2-D data is acquired using a spectrum analyzer.

Later, the performance of the HMMDI system is analyzed using tumor, fibro-glandular and fat phantoms. In one of these phantoms, the tumor is placed inside the fibro-glandular, and in the other one, fibro-glandular and tumor are placed separately in the middle of fat phantom. The HMMDI scan results are compared with the simulation results in [12]. The observations on the Doppler signal component on the right and left side of the fundamental component, are discussed. The possible reasons of this behavior are shown with simulations.

A receiver system is designed for the HMMDI experimental set up and its performance is evaluated on the phantoms. The phantoms are scanned mechanically and the 2-D data is acquired using the receiver system. Three different features; peak to peak value of the signal, power of the signal at Doppler frequency and the correlation based feature are extracted from the received signal to distinguish different phantoms from each other. 2-D scan results of the phantoms using these features are illustrated. The results obtained using spectrum analyzer and the designed receiver system show the capability of this imaging technique in differentiating different breast tissue phantoms from each other.

6.2 HMMDI system set up

The block diagram of new set up is shown in Figure 6.1. The focused US transducer is used in its third harmonic frequency (3.32 MHz). An AM burst signal (generated using waveform generator 1 and 2) is used to induce vibration inside the phantom. The AM signal is amplified with a high power RF amplifier of 52 dB gain. In these experiments, spatial peak pulse average intensity (I_{sppa}) of the ultrasound beam is 271.4 $\frac{W}{cm^2}$.

6.2.1 Antenna configuration

To eliminate the effect of antenna position on the received signal level, the TX-RX antennas are fixed at the bottom of the oil container using the silicon adhesive glue (Figure 6.2). Similar to the antenna configuration in the first generation of the HMMDI system set up, open ended waveguide antennas are used as TX and RX. They are located along their H-Plane and the distance between their edges are 15 mm. The phantom container is located on top of the

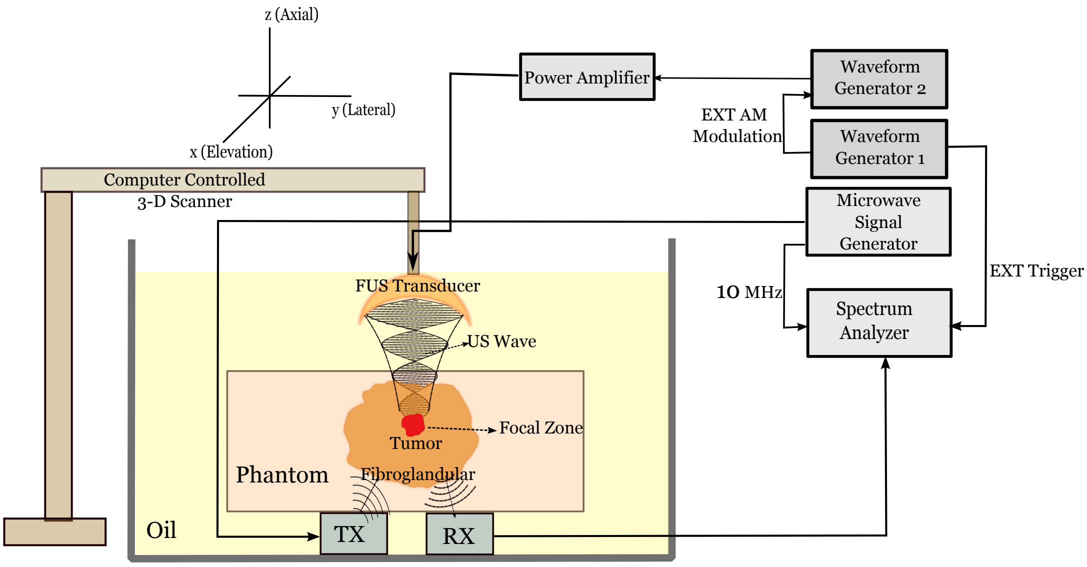

Figure 6.1: Second generation HMMDI set up with fixed antennas block diagram.

antennas as it is shown in Figure 6.2. The ultrasound transducer is located on top side of the phantom and it is connected to the 3-D scanner.

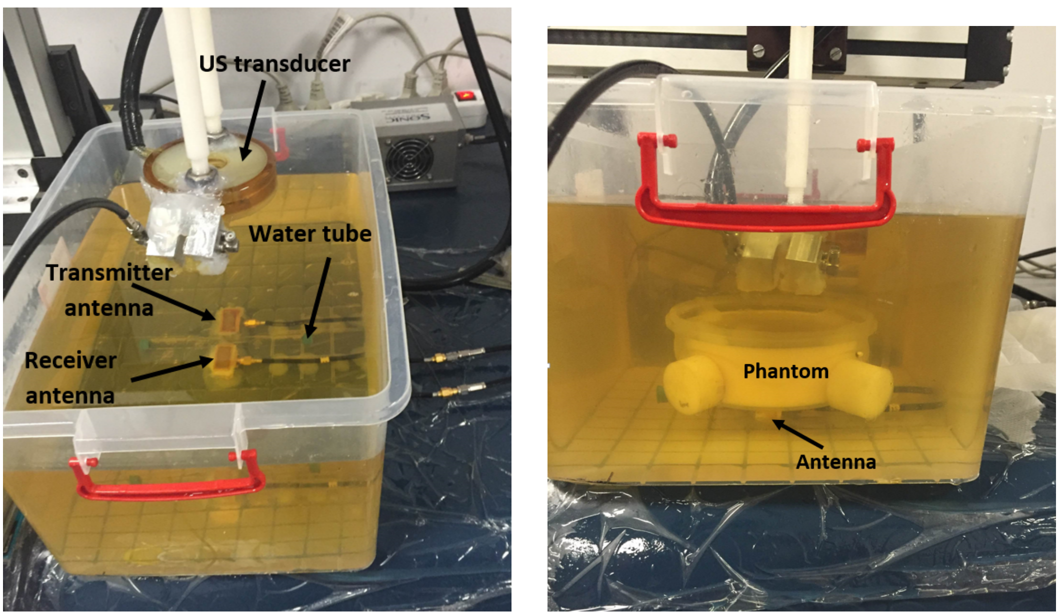

(a)

(b)

Figure 6.2: The new (a) antenna configuration and (b) the location of the phantom container for the scan procedure.

6.2.2 Experimental results on phantom-1 (fibro-glandular inclusion inside fat)

For experimental studies, an inhomogeneous phantom containing a fibro-glandular inclusion of 14 mm diameter and 9 mm height inside the fat phantom (Figure 6.3) is developed. The fibro-glandular is located inside the fat phantom 20 mm above the bottom of the phantom container and 20 mm below the top surface of it.

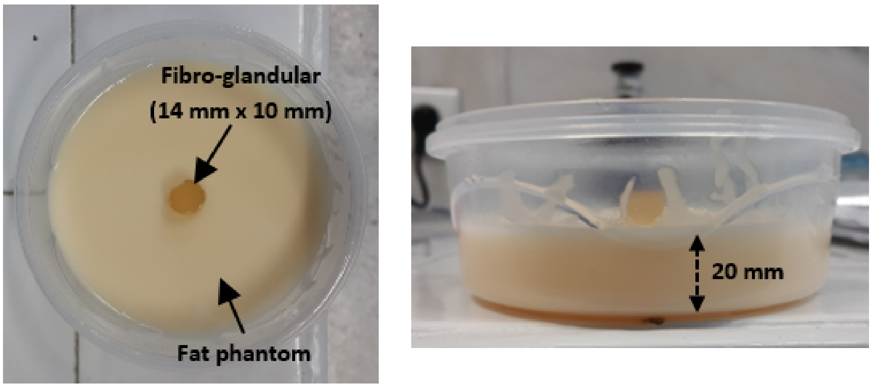

Figure 6.3: Inhomogeneous phantom. 14 mm $\times$ 9 mm height fibro-glandular phantom is placed inside the fat phantom 20 mm above the bottom surface of the container.

6.2.2.1 Optimum MW and vibration frequency selection

To find the optimum MW frequency, a 25 Hz, 5 cycles sinusoidal burst signal (with 1 Hz pulse repetition frequency) is used to amplitude modulate the 3.32 MHz signal. The transmitting microwave antenna is fed by +10 dBm microwave signal. Falcon tube of 11.5 mm diameter full of water is located between the antennas to decrease the direct coupling between the TX-RX antennas. In order to find the optimum MW operating frequency the SNR and the ratio of the signal at Doppler frequency to the signal at center frequency (Doppler/main signal) is measured for 3.4 - 7 GHz frequency range. In this measurement, the focus of the transducer is located in the middle of the fat phantom where the fibro-glandular is located. The highest SNR and Doppler/main signal is observed at 4.75 GHz (Figure 6.4).

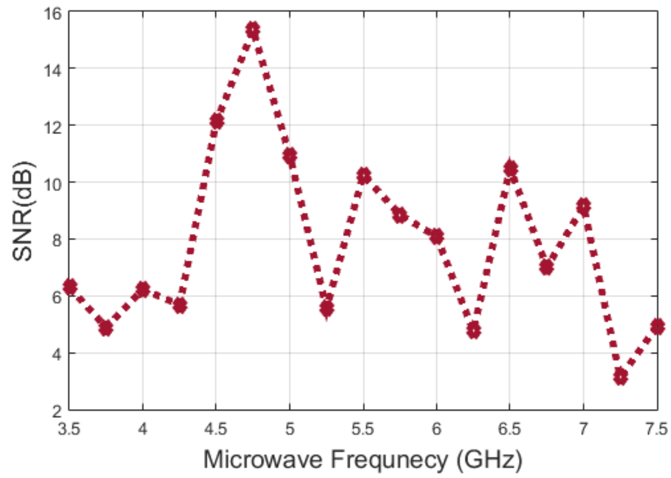

(a)

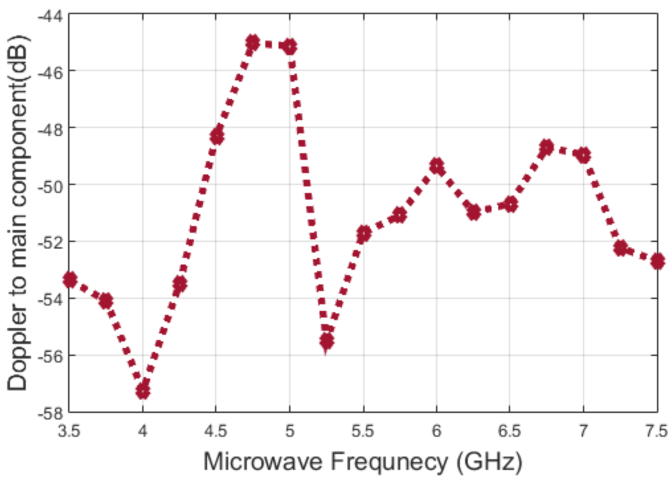

(b)

Figure 6.4: (a) SNR and (b) Doppler/main signal for the frequency sweep of 3.5-7 GHz. 25 Hz, 5 cycles burst signal is used for creating the vibration. Both TX and RX are located at the bottom of the oil tank.

After selecting the optimum microwave frequency, different vibration frequencies are tested. To find the optimum vibration frequency, an US transducer is used to induce 15 Hz, 20 Hz, 25 Hz, and 30 Hz with 3, 4, 5, and 6 cycles, respectively. The SNR and the Doppler/main signal are plotted in Figure 6.5. As it can be seen, the SNR is highest at 25 Hz. Therefore, the scan is done at this vibration frequency.

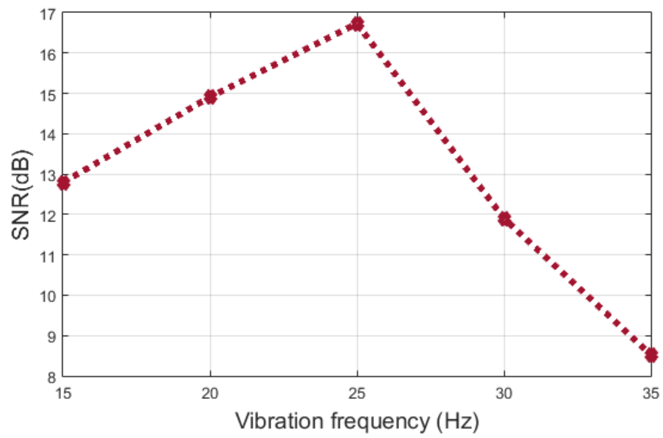

(a)

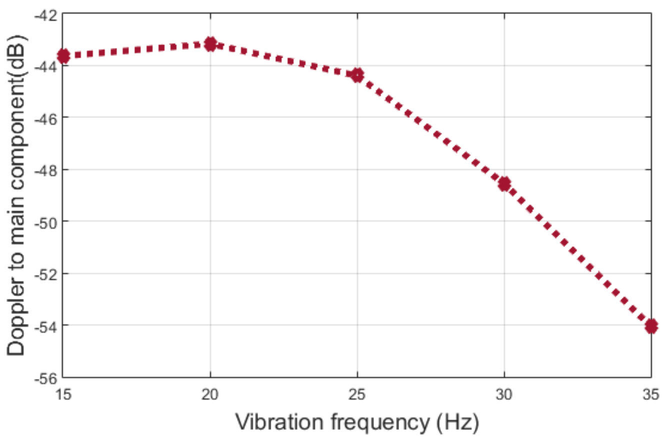

(b)

Figure 6.5: (a) SNR and (b) Doppler/main value for the RF frequency sweep of 15-30 Hz. The Microwave frequency is 4.75 GHz. Both TX and RX are located at the bottom of the oil container.

6.2.2.2 2-D scan results for a 25 Hz vibration frequency

An area of 42 mm to 35 mm around the fibro-glandular is scanned at 4.75 GHz MW operating frequency and 25 Hz, 5 cycles vibration pulse is applied to induce to the phantom with 1 s pulse repetition interval. A total of 11 pulses are applied at each position. The scan area size is selected to be as small as possible due to the long scan duration of about 3 hours. The transducer is located 5 cm above the plane that the fibro-glandular is located, z = 0 (Figure 6.6). The scan step size is 2 mm both in x and y directions. The received Doppler signal

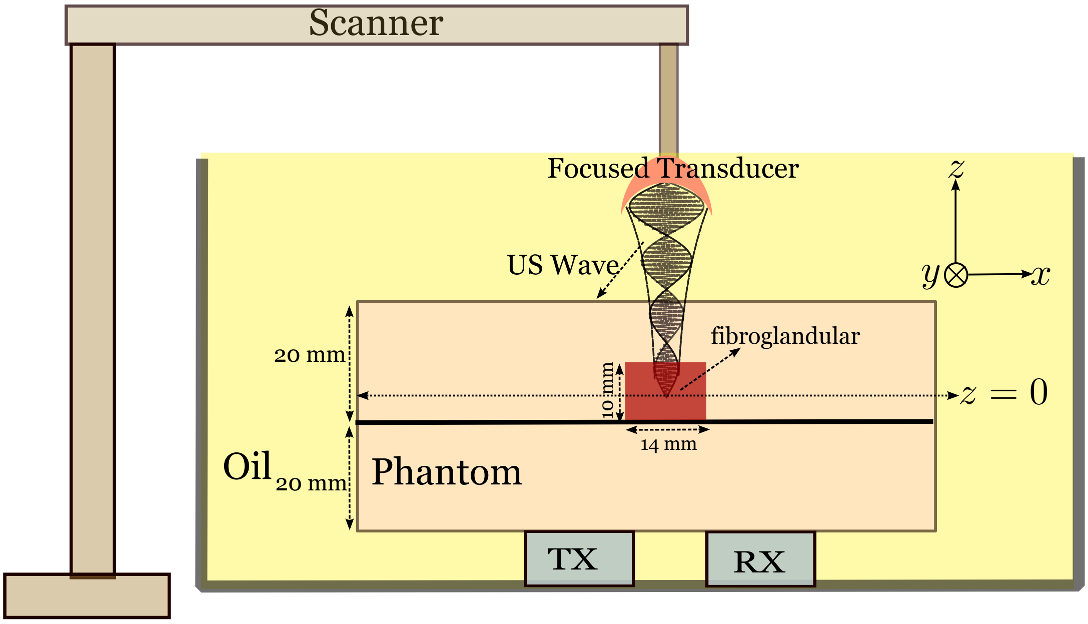

Figure 6.6: Inhomogeneous phantom. 14 mm × 9 mm height fibro-glandular phantom is placed inside the fat phantom 20 mm above the bottom surface of the container.

level at left Doppler frequency ($f_{MW frequency}$-25 Hz), right Doppler frequency ($f_{MW frequency}$+25 Hz), and their average, are shown in Figure 6.7. The location of the fibro-glandular phantom is shown inside the dashed red circle of 14 mm diameter. The fibro-glandular location is detectable in the resultant data profiles. The signal level rises up to -112 dBm in the fibro-glandular phantom and it drops up to -116 dBm in the fat region.

The Doppler signal level at right and left side of the center frequency are different. If mechanical alignment of the transducer is not flat, the induced vibrations are not perfectly vertical. It may be the reason for the difference in the left and right Doppler components. Microwave and acoustic reflections may also be the other reason of this asymmetry. A 4 dB (-112 dBm to -116 dBm) width may be used as a metric to compare the inclusion size in the data profile. similar results can be seen in the Doppler/main signal plots (Figure 6.8). These plots show that fibro-glandular inclusion (diameter of 14 mm) inside the fat phantom in 25 mm depth from the surface of the phantom is detectable using HMMDI method. The approximate size of the fibro-glandular inclusion in the left Doppler component, in the right Doppler component and in the average of right and left Doppler component plots is about 13 mm, 9 mm and 10 mm, respectively.

6.2.2.3 Repeatability of 2-D scan measurement

A 2-D scan is performed in 2 consequent experiments using same microwave operating frequency and vibration frequencies as 4.75 GHz and 25 Hz, respectively. The focus of the transducer is on the layer where the fibro-glandular is located. The results are given in Figure 6.9. The Doppler signal received from the fibro-glandular phantom is nearly same for two measurements. The only differences in the signal level in two consequent measurements is observed in the fat area where the signal level randomly changes.

6.2.2.4 2-D scan results in different depths in z direction

To investigate the performance of HMMDI in detecting the location of the fibro-glandular inclusion in the axial (z) direction, 2-D scans are repeated at different depths inside the phantom. 42 mm $\times$ 35 mm area around the fibro-glandular phantom is scanned when MW operating frequency is 4.75 GHz, and vibration frequency is 25 Hz. The scan steps are 2 mm. The received Doppler signal level from each point of the phantom is shown in Figure 6.10. As it can be seen, the detected Doppler signal level increases when the focus is on the plane where the fibro-glandular is located (6.10 (first row)). In these measurements,

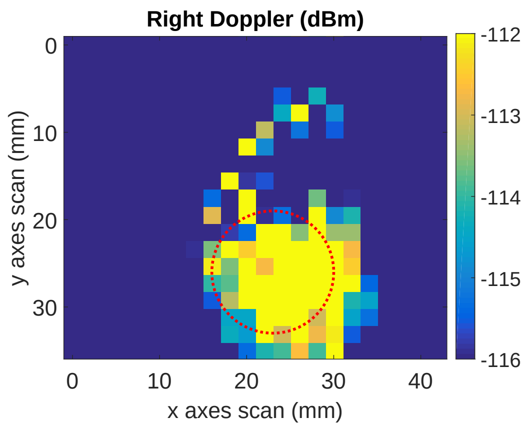

(a)

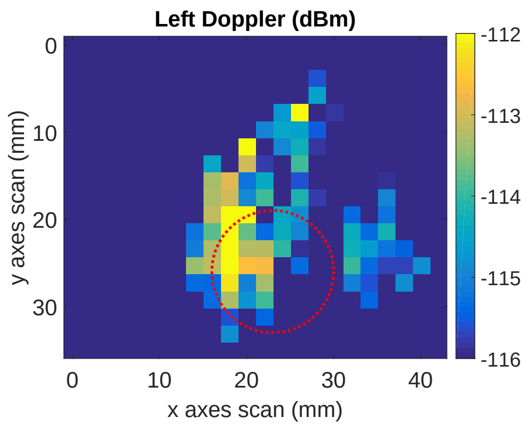

(b)

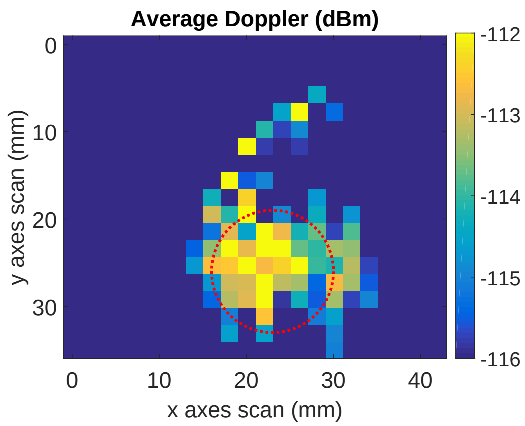

(c)

Figure 6.7: The constructed data profile from the Doppler signal (a) at right side of the main component, (b) at left side of the main component, and (c) the average of right and left Doppler signals. A 25 Hz, 5 cycles is applied for ultrasound excitation and the microwave operating frequency is 4.75 GHz. Yellow color shows the higher Doppler signal which we expect to receive from fibro-glandular phantom. Location of the fibro-glandular phantom is shown in red dashed circle

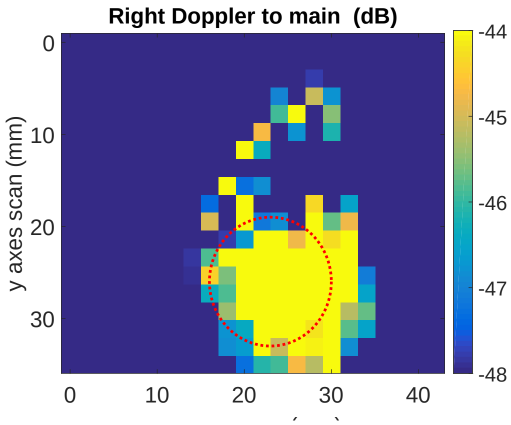

(a)

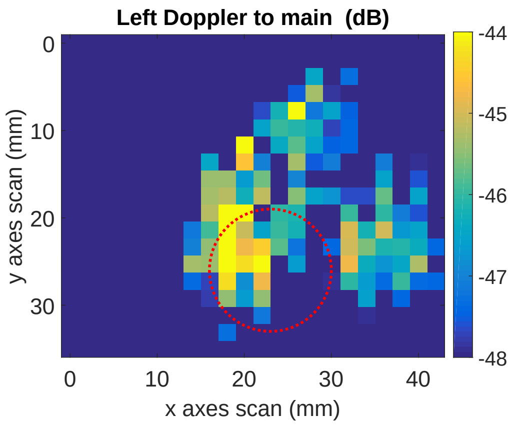

(b)

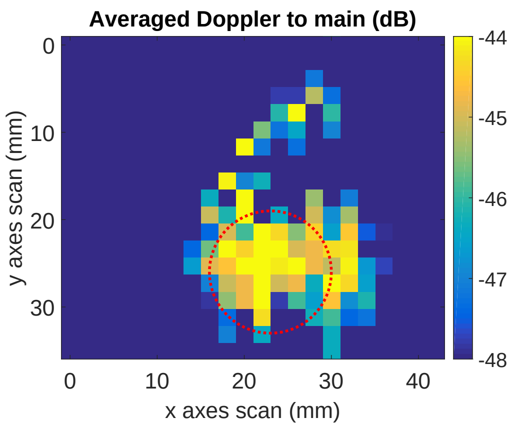

(c)

Figure 6.8: The obtained data profiles from the ratio of the Doppler signal to signal at main frequency. (a) Right Doppler signal to signal at main frequency, (b) left Doppler signal to main component of the signal, and (c) the average of both right and left Doppler signal to main component of the received signal. A 25 Hz, 5 cycles is applied for ultrasound excitation and the microwave operating frequency is 4.75 GHz. Yellow color shows the higher Doppler signal which we expect to receive from fibro-glandular phantom. Location of the fibro-glandular phantom is shown in red dashed circle.

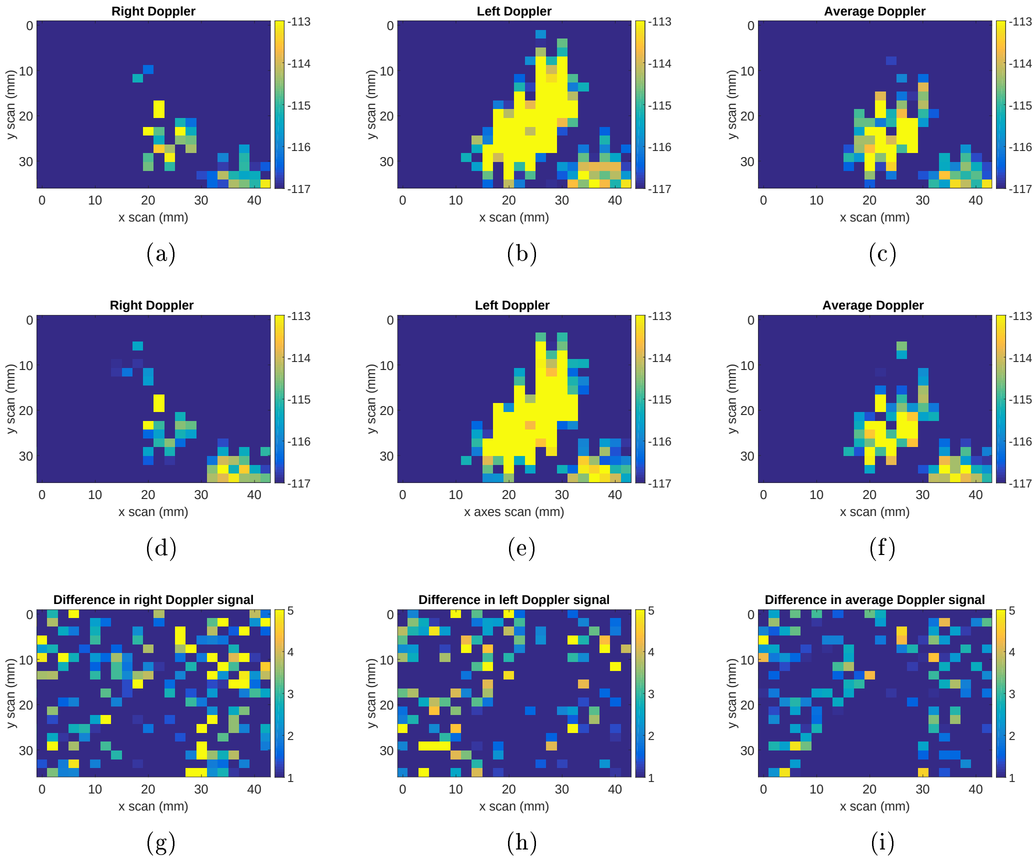

Figure 6.9: The obtained data profiles from the Doppler signal. (a) Doppler signal at right side of the main component, (b) at left side of the main component, and (c) the average of both right and left Doppler signal in the first measurement. (d)-(f) The measured right and left Doppler signals and the average of them for the second measurement. (g)-(i) the difference between the data in two measurements. A 25 Hz, 5 cycles is applied for ultrasound excitation and the microwave operating frequency is 4.75 GHz. Yellow color shows the higher Doppler signal which we expect to receive from fibro-glandular phantom.

the reference scan plane (z=0) is the plane that the focus of the transducer is on the fibro-glandular phantom (Figure 6.6). In this plane, the signal level in the fibro-glandular phantom is around -112 dBm while it is around -116 dBm in the fat area. Even the error in the detected fibro-glandular size is around 2 mm compared to its real size.

When the transducer focus distance to the fibro-glandular layer increases from 5 to 15 mm, the received signal level at Doppler frequency decreases. But, even in the layers where the fibro-glandular does not exist, the signal from the vibration of this inhomogeneity is sensible.

6.2.2.5 2D scan results for different vibration frequencies

In this section, 2-D scans are performed for different vibration frequencies to investigate the effect of vibration frequency on the HMMDI data profile. In the simulation studies [12], it has been shown that response from fibro-glandular and tumor region might be different in different vibration frequencies. This can be used as a feature to differentiate these tissues from each other. To test this hypothesis, 15-35 Hz (5-7 cycles) amplitude modulated burst signals are applied to the transducer to create vibrations with related frequencies. The scan plane is the plane which the fibro-glandular is located, i.e, 5 cm below the transducer rim. The spectrum analyzer averaging number is 11.

The Doppler component of the received signal at different vibration frequencies for each scan point is shown in Figure 6.11. The larger area is detected as fibro-glandular in lower frequencies. The inserted fibro-glandular diameter is 14 mm while it is estimated around 25 mm in the 15 Hz vibration frequency HMMDI data profile. By increasing the vibration frequency, the detected place of the inclusion become more localized. When the vibration frequency is smaller, the wavelength is larger. Therefore, Doppler component is coming from a larger area. By increasing the frequency, the resolution is increased.

In 25 Hz, the estimated fibro-glandular diameter is around 14-15 mm and in 30 Hz it is estimated smaller (11 mm) than its real size. For the vibration

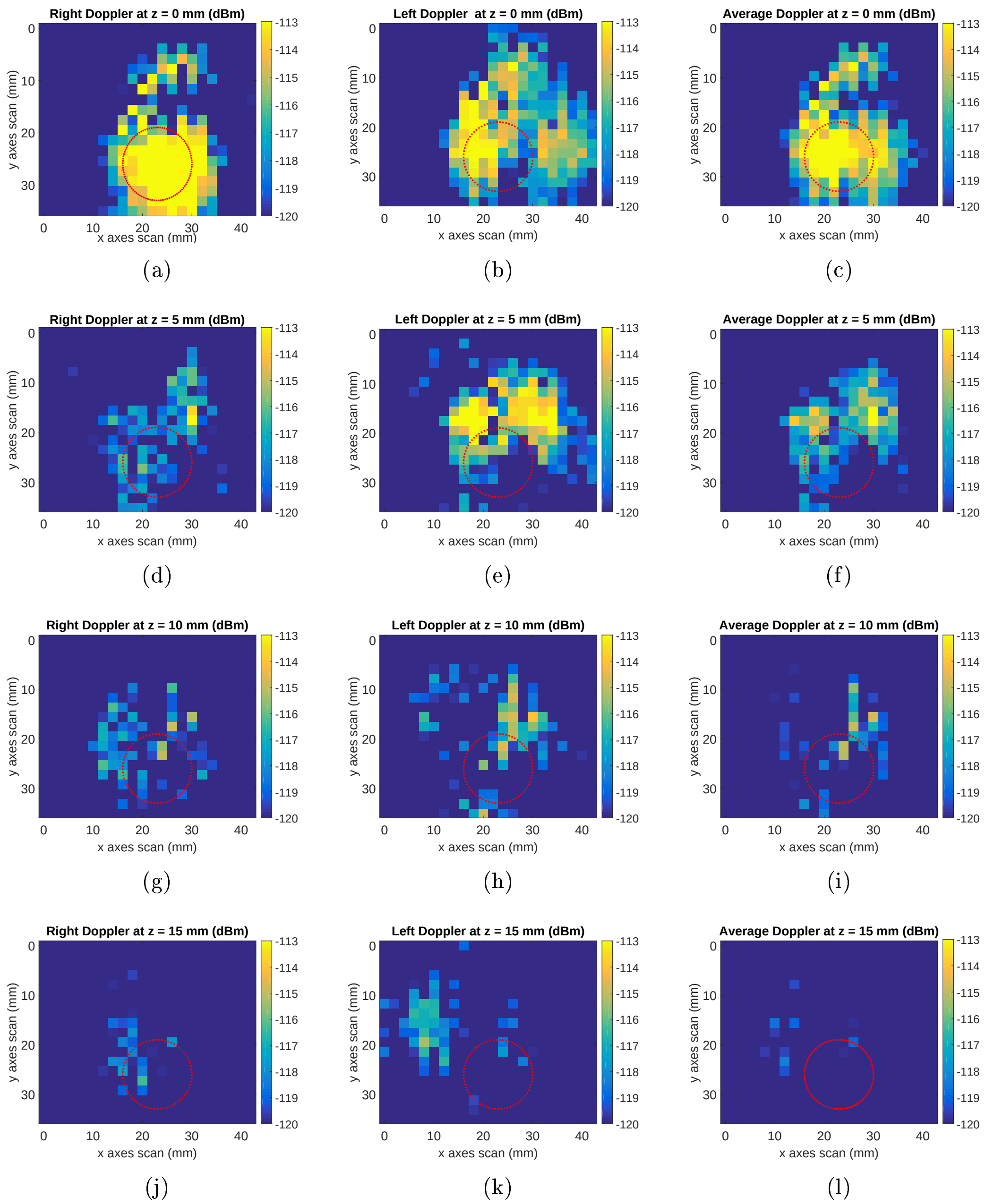

Figure 6.10: The obtained data profiles from the Doppler signal in different depths. From top to bottom each row is related to the received signal when the focus of the transducer is on the plane where the fibro-glandular is located as a reference plane (z=0), 5 mm above that plane (z=5), 10 mm above the reference plane (z=10), and 15 mm above the reference plane (z=15), respectively. A 25 Hz, 5 cycles is applied for ultrasound excitation and the microwave operating frequency is 4.75 GHz. The received signal from fibro-glandular region is shown in yellow and the one received from fat is dark blue. Yellow color shows the higher Doppler signal which we expect to receive from fibro-glandular phantom. Location of the fibro-glandular phantom is shown in red dashed circles.

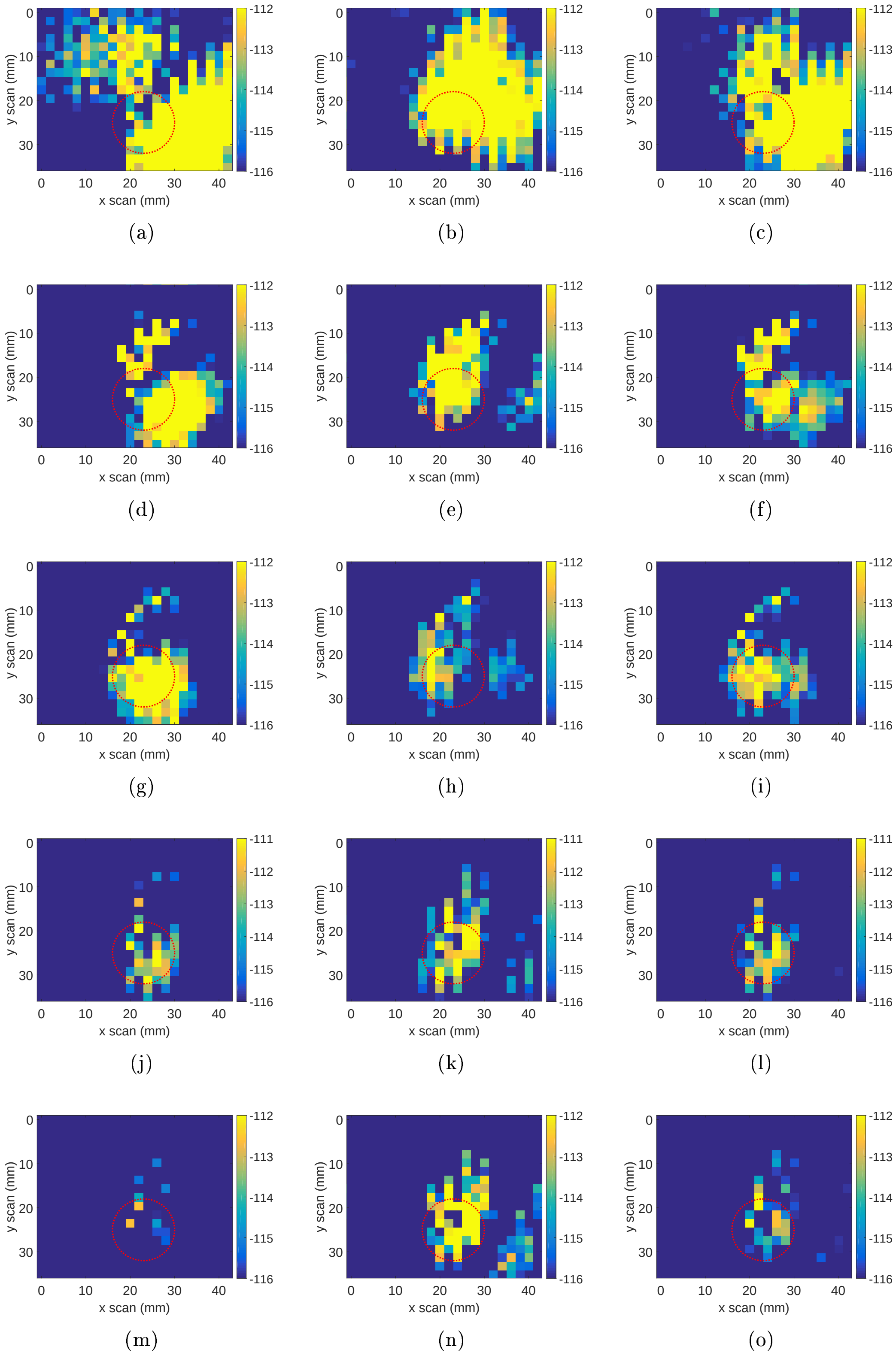

(a) (b) (c) (d) (e) (f) (g) (h) (i) (j) (k) (l) (m) (n) (o)

Figure 6.11: The obtained data profiles from the Doppler signal. From top to bottom, each row is related to the received signal at 15 Hz to 35 Hz vibration frequencies, respectively. Microwave operating frequency is 4.75 GHz. Location of the fibro-glandular phantom is shown in red dashed circles.

frequencies below 15 Hz, the Doppler component of the received signal is not realizable from the fundamental frequency component. The circular shape of the inclusion is lost at 15 Hz vibration frequency. On the other hand, in higher frequencies above 35 Hz, the signal is masked by phase noise. At 35 Hz vibration frequency, the signal level at right side of the center frequency, received from the fibro-glandular area is weak comparing the other vibration frequencies.

As the vibration frequency increases, the induced displacement and as a result Doppler signal level, decreases. Therefore, the vibration frequency should be increased to increase the resolution but it should be kept as low as possible to induce detectable displacement in the tissue.

6.2.2.6 Evaluating the effect of averaging number on the HMMDI data profile

The effect of averaging number N set for the spectrum analyzer is evaluated by changing it from 11 to 7, in two consequent measurements. By decreasing the averaging number, the scan time decreases. As scan duration increase, the heat and the induced damage due to the acoustic exposure increase. Figure 6.12 (a-c) shows the data profile when N = 11 and Figure 6.12 (d-f) shows the results when N = 7.

The results show that 7 times averaging the data in each scan point is enough to detect the fibro-glandular inside fat phantom. In the homogeneous fat region, Doppler signal level changes randomly as it was seen in Figure 5.26. So, the difference of the two data profiles are high mostly in the fat area. In the fibro-glandular region the received Doppler signal level in two measurements are consistent.

6.2.3 Experimental results on phantom-2 (tumor inclusion inside fat)

In this experiment, the inhomogeneous phantom containing a tumor phantom of 14 mm diameter and 9 mm height inside the fat phantom is used (Figure 6.13). Tumor phantom is located at a depth 20 mm above the bottom surface

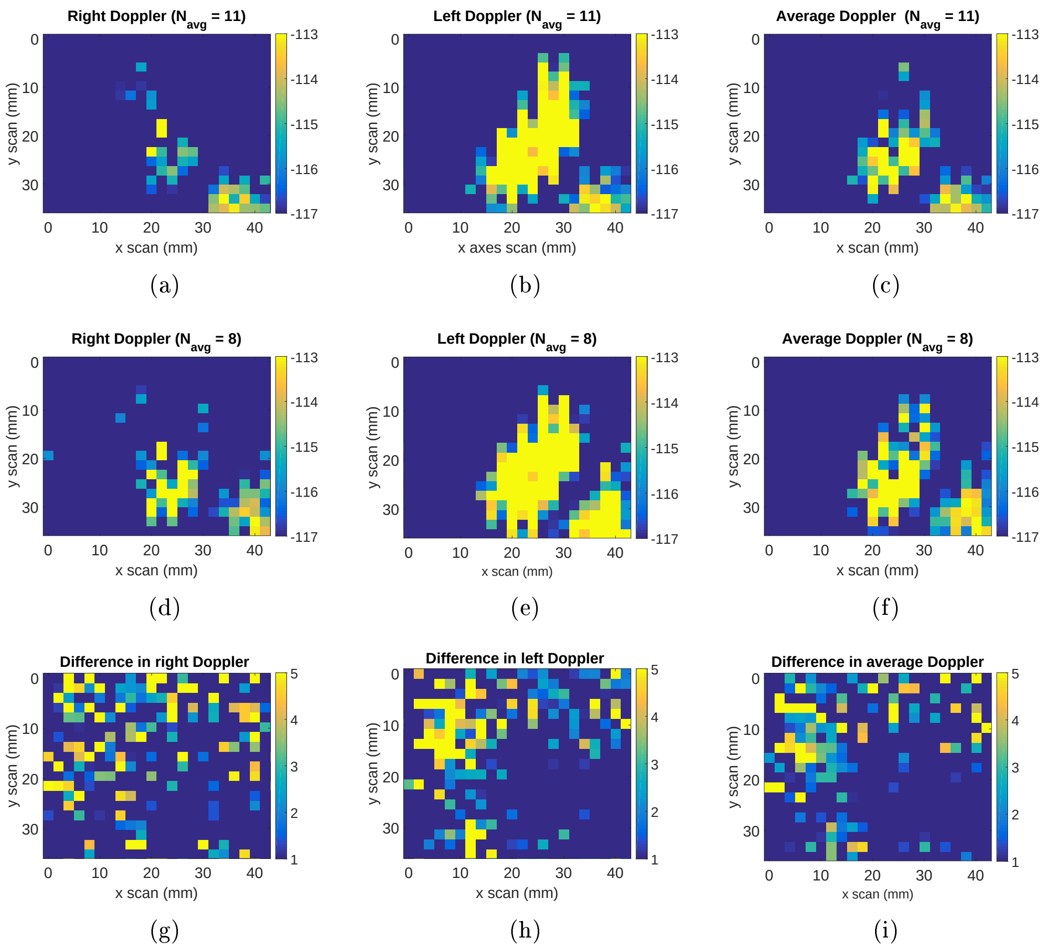

Figure 6.12: The obtained data profiles from the Doppler signal. (a)-(c) Doppler signal at right side of the main component, left side of it and the average of both right and left Doppler signal for averaging number of 11. (d)-(f) Doppler signal at right side of the main component, left side of it and the average of both right and left Doppler signal for averaging number of 8. (g)-(i) The difference between the data obtained from Doppler signals and their averages in two measurements. A 25 Hz, 5 cycles is applied for ultrasound excitation and the microwave operating frequency is 4.75 GHz. Yellow color shows the higher Doppler signal which we expect to receive from fibro-glandular phantom.

of the fat phantom. After locating this phantom, another layer of fat phantom is poured on it.

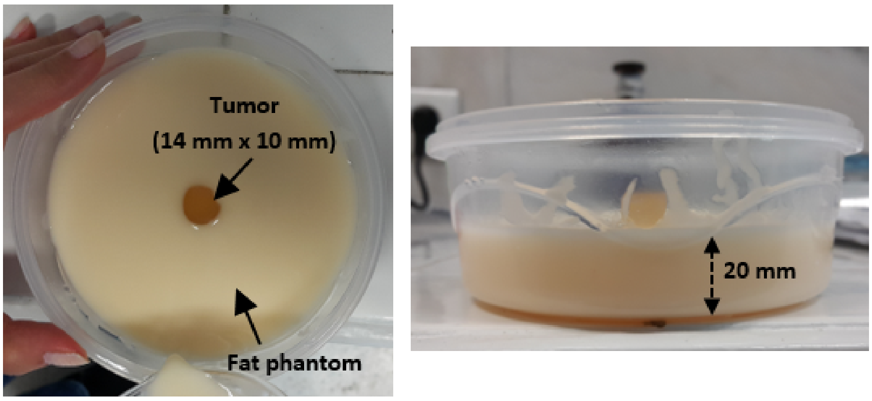

Figure 6.13: Inhomogeneous phantom containing 14 mm × 10 mm height tumor phantom inside the fat phantom 2 mm above the bottom surface of the container.

6.2.3.1 2-D scan results for 25 Hz vibration frequency

An area of 42 mm to 35 mm sized around the tumor phantom is scanned while the MW operating frequency is 4.75 GHz and the 25 Hz, 5 cycles is used to apply the vibration. The transducer is located 5 cm (focal depth) above the plane that the tumor is located. Scan steps are 2 mm in x and y directions. The obtained results are shown in Figure 6.14. The actual place of the tumor is shown in dashed red circle of 14 mm diameter. The existence of the tumor is detectable using HMMDI method. Although the tumor inclusion shape is not circular in the plots, the signal level at Doppler frequency is around -90 dBm in the tumor area while it is around -98 dBm in the fat phantom. Similar to the previous experimental results, the Doppler signal level at right and left side of the center frequency are different.

Same results can be seen in the obtained plots from Doppler signal to main component signal plots (Figure 6.15). In this experiment, the coupling between the antennas is around -52 dBm, but in the previous experiment (fibro-glandular

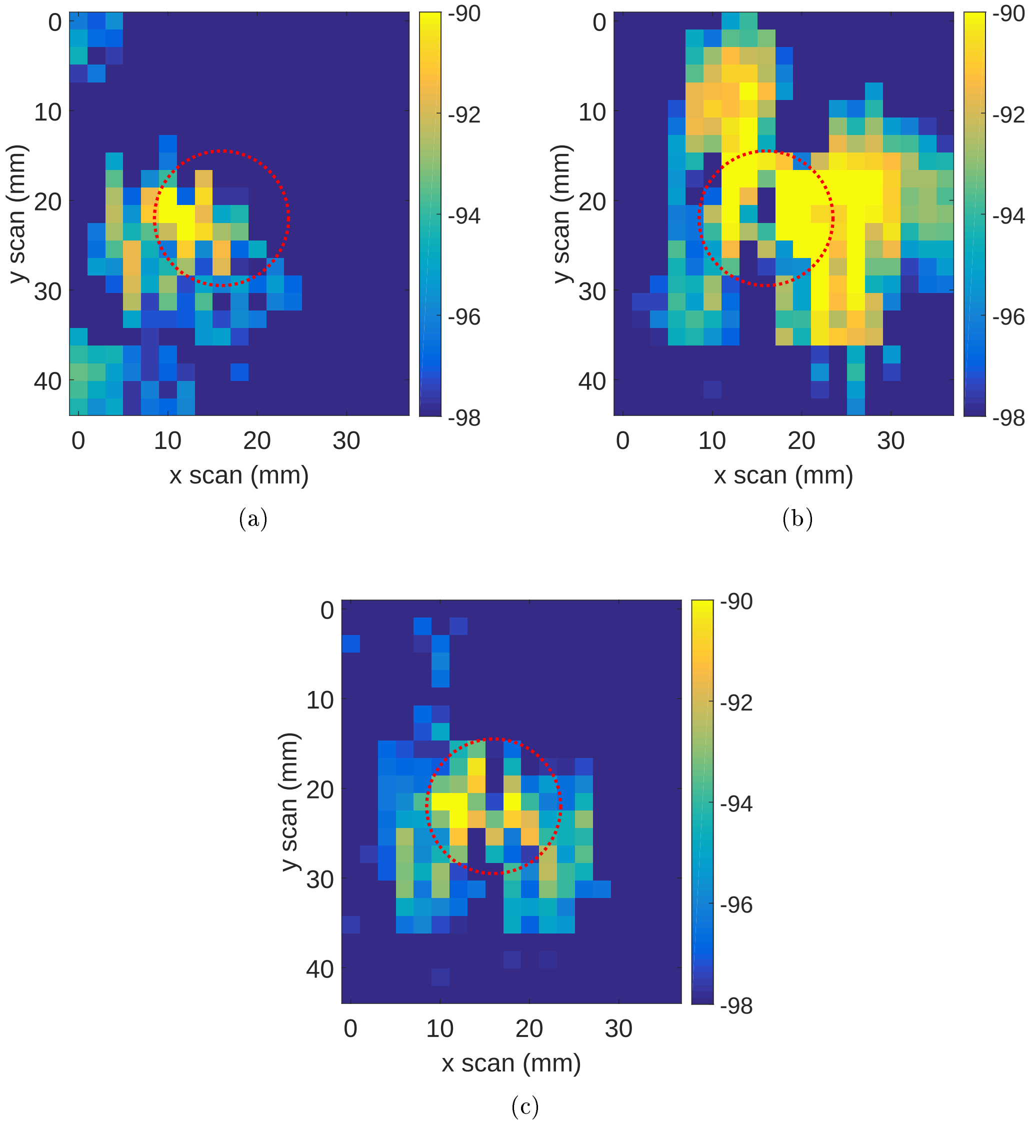

Figure 6.14: The obtained data profiles from the Doppler signal (a) at right side of the main component, (b) at left side of the main component, and (c) the average of both right and left Doppler signal. A 25 Hz, 5 cycles is applied for ultrasound excitation and the microwave operating frequency is 4.75 GHz. Yellow color shows the higher Doppler signal which we expect to receive from tumor phantom. Location of the tumor phantom is shown in red dashed circle.

inside the fat phantom) it was about -68 dBm . Consequently, the signal level at Doppler frequency is also higher. In order to compare the received signal from fibro-glandular and tumor phantoms, these inhomogeneities should be inserted inside a single phantom. In the following section, the results of scanning a phantom containing these breast tissue phantoms are presented.

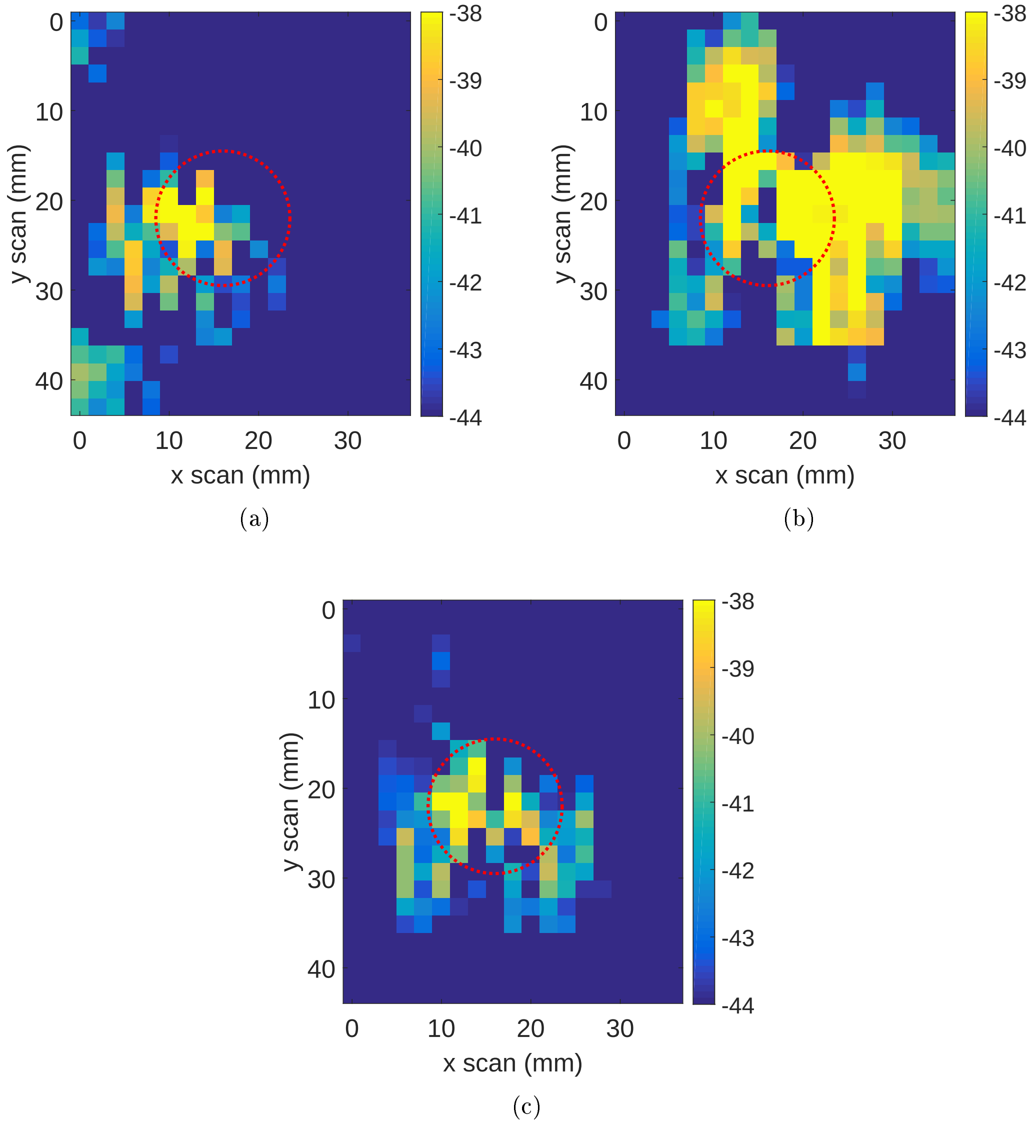

Figure 6.15: The obtained data profiles from the ratio of the Doppler signal to main frequency. (a) Doppler signal at right side of the main component, (b) at left side of the main component, and (c) the average of both right and left Doppler signal to main component of the received signal. A 25 Hz, 5 cycles is applied for ultrasound excitation and the microwave operating frequency is 4.75 GHz. Yellow color shows the higher Doppler signal which we expect to receive from tumor phantom. Location of the tumor phantom is shown in red dashed circle.

6.2.3.2 2-D scan results for different vibration frequencies

2-D scans are performed for different vibration frequencies and HMMDI data profiles are obtained for vibration frequencies between 15 Hz to 35 Hz in 5 Hz steps. vibrations are introduced inside the phantom. The scan plane is the transducer focal plane, i.e, 5 cm below the transducer rim where the tumor is placed. Similarly, the spectrum analyzer averaging is 11. The results are shown in Figures 6.16 and 6.17. At 15 Hz, the Doppler signal level is increased in the boundary of tumor up to -90 dBm but it decreases inside the tumor zone up to -98 dBm. By applying the low vibration frequency such as 20 Hz, high Doppler signal around -90 dBm is received from an area 2 times bigger than the real size of the tumor. As the vibration frequency is increased, the detected tumor region size is decreased. At 25 Hz and 30 Hz, the estimated tumor diameter is around 14-15 mm in the obtained plots of right Doppler and average Doppler signals. But, the left Doppler signal level is high in an area two times larger that tumor's size. At 35 Hz, the right Doppler and as a result the average of the right and left Doppler signals are low. At 15 Hz, tumor is not detected. In the previous experiment (fibro-glandular inside the fat), the fibro-glandular was detected at 15 Hz vibration frequency. Different behavior of tumor and fibro-glandular in different vibration frequencies has been reported in [12] simulation studies. These results suggest that changing the vibration frequency may be a tool to distinguish these phantoms from each other.

6.2.4 Experimental results on phantom-3 (fibro-glandular with tumor inclusion inside in the middle of the fat)

In the previous experiments, the performance of the HMMDI system set up was evaluated on the phantoms with fibro-glandular or tumor. In this section, 14 mm $\times$ 8 mm tumor tumor inside the 25 mm $\times$ 8 mm fibro-glandular that is placed inside in the fat phantom (Figure 6.18) is scanned. After pouring the first layer of fat phantom and its solidification, these phantoms are located in the middle of the phantom and another layer of fat is poured on the top side.

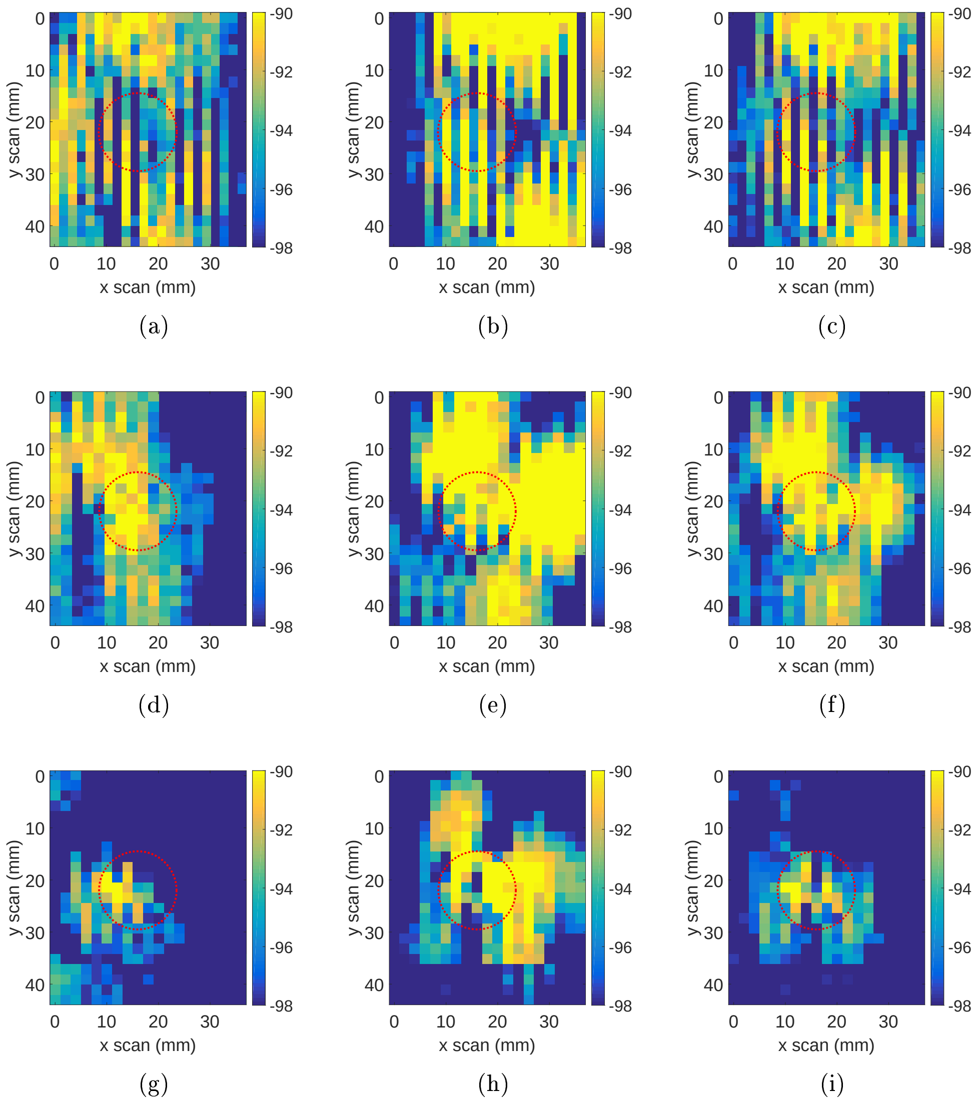

Figure 6.16: The obtained data profiles from the Doppler signal at right side of the main component, (first columns) at left side of the main component (second columns), and (c) the average of both right and left Doppler signal (third columns). From top to bottom, each row is related to the received signal at 15 Hz, 20 Hz, and 25 Hz vibration frequencies, respectively. Microwave operating frequency is 4.75 GHz. Location of the tumor phantom is shown in red dashed circle.

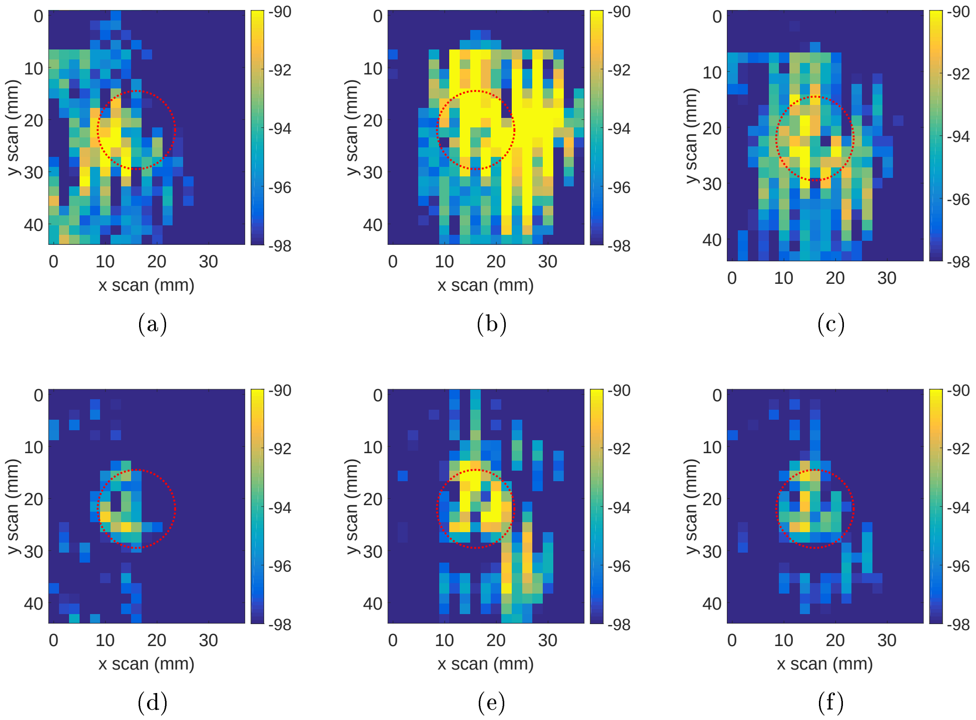

Figure 6.17: The obtained data profiles from the Doppler signal at right side of the main component, (first columns) at left side of the main component (second columns), and (c) the average of both right and left Doppler signal (third columns). From top to bottom, first row is related to the received signal at 30 Hz and the second row is related to 35 Hz vibration frequencies, respectively. Microwave operating frequency is 4.75 GHz. Location of the tumor phantom is shown in red dashed circle.

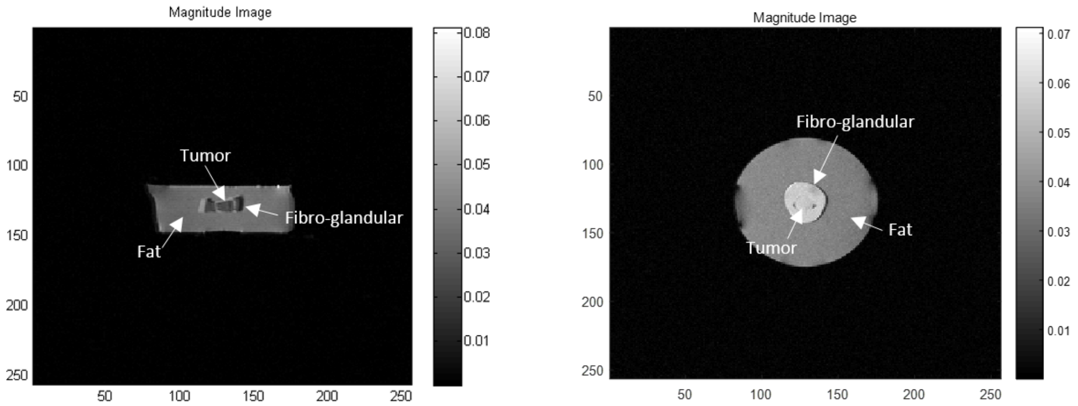

Figure 6.18: Inhomogeneous phantom containing tumor of 14 mm diameter inside the fibro-glandular of 24 mm diameter in the middle of fat phantom. These phantoms are located 25 mm below the surface of the fat phantom. MRI images are taken by 3 Tesla MRI System, UMRAM Research Institute in Bilkent University.

6.2.4.1 Operation frequency optimization

The US transducer is driven by 25 Hz and 5 cycle amplitude modulated burst signal and the microwave frequency is increased from 3.5-7.5 GHz to find the optimum microwave operating frequency. SNR and the Doppler/main signal is higher at 4.75 GHz (Figure 6.19). So, this frequency is used for feeding TX antenna during the scan.

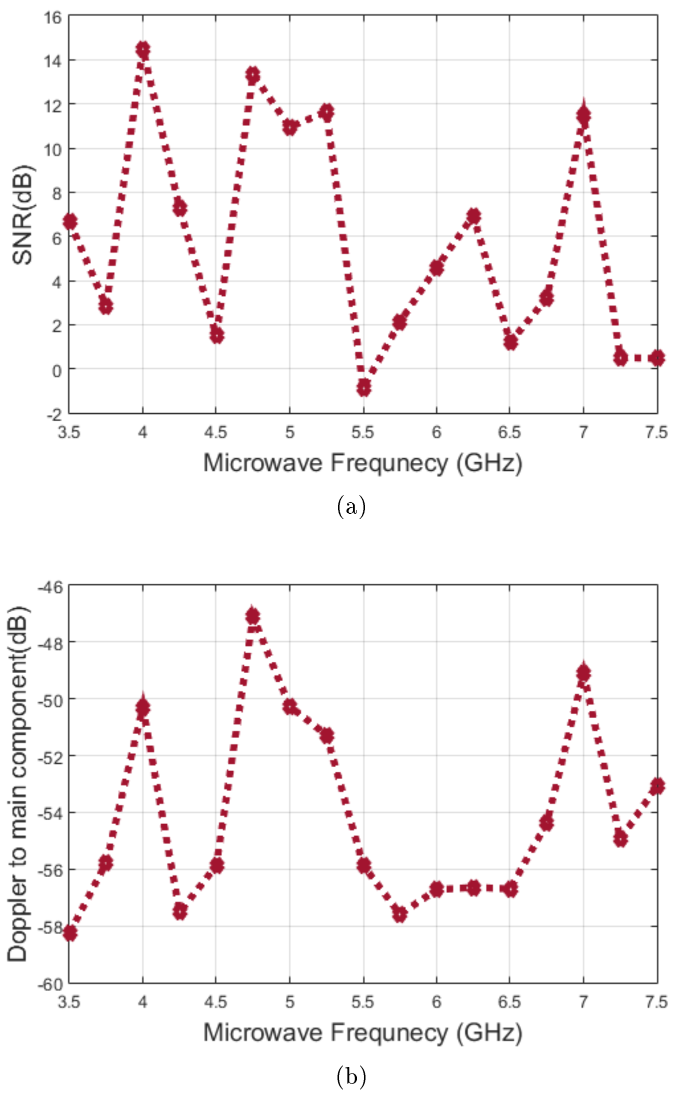

Figure 6.19: (a) SNR and (b) received signal level at Doppler frequency to signal at center frequency for the frequency sweep of 3.5-7 GHz. A 25 Hz, 5 cycles burst signal is used for creating the vibration. Both TX and RX are located at the bottom of the oil container.

6.2.4.2 2-D scan results for 25 Hz vibration frequency

The scan results for different depths are shown in Figure 6.20. The first top row plots are related to the received signal at Doppler frequency around the center frequency, when the focus of the transducer is on the layer that fibro-glandular and tumor phantoms are located (z=0). The second row plots were obtained when the focus of the transducer is 5 mm above the z=0 line. Since the height of the fibro-glandular and tumor phantoms are about 8 mm, still the existence of them is detectable in this layer. The last row shows the result when the US transducer is 10 mm above z=0 line. The smaller size of the detected fibro-glandular and tumor inclusion in the last row plots, implies that the scan plane is away from the inclusions. Since the axial resolution of the transducer is low comparing its lateral resolution, the HMMDI data profile resolution is also low in axial direction. On the other hand, the transducer focus is manually placed on the phantom, so there may be an error in setting the reference plane (z=0).

Same problem in the preceding sections about the left and right Doppler signal level is observed in the measurements. This can be due to the shear wave reflection and shear waves propagation inside the phantom. In the following section, this effect is discussed in more details.

However, the existence of the fibro-glandular and tumor phantoms is observable in the data profiles constructed from the left Doppler signal. It is observed that left Doppler signal is increased up to -117 dBm in tumor phantoms while it is around -121 dBm to -119 dBm in fibro-glandular, and below -123 dBm in the fat region. Because of the lower stiffness of the fibro-glandular phantom comparing the tumor phantom, a higher signal level is expected in the fibro-glandular region, but this results is not observed in this experiment. It is hypothesized that huge size of the fibro-glandular (25 mm $\times$ 8 mm) can cause this results.

The effect of the size the fibro-glandular on the Doppler signal level was analyzed with numerical simulations (Figure 6.21(a)) [12]. Simulations were done when the vibration frequency was 15 Hz. The fibro-glandular phantom diameter was changed in a range between 10 mm to 30 mm in 5 mm steps. When the size

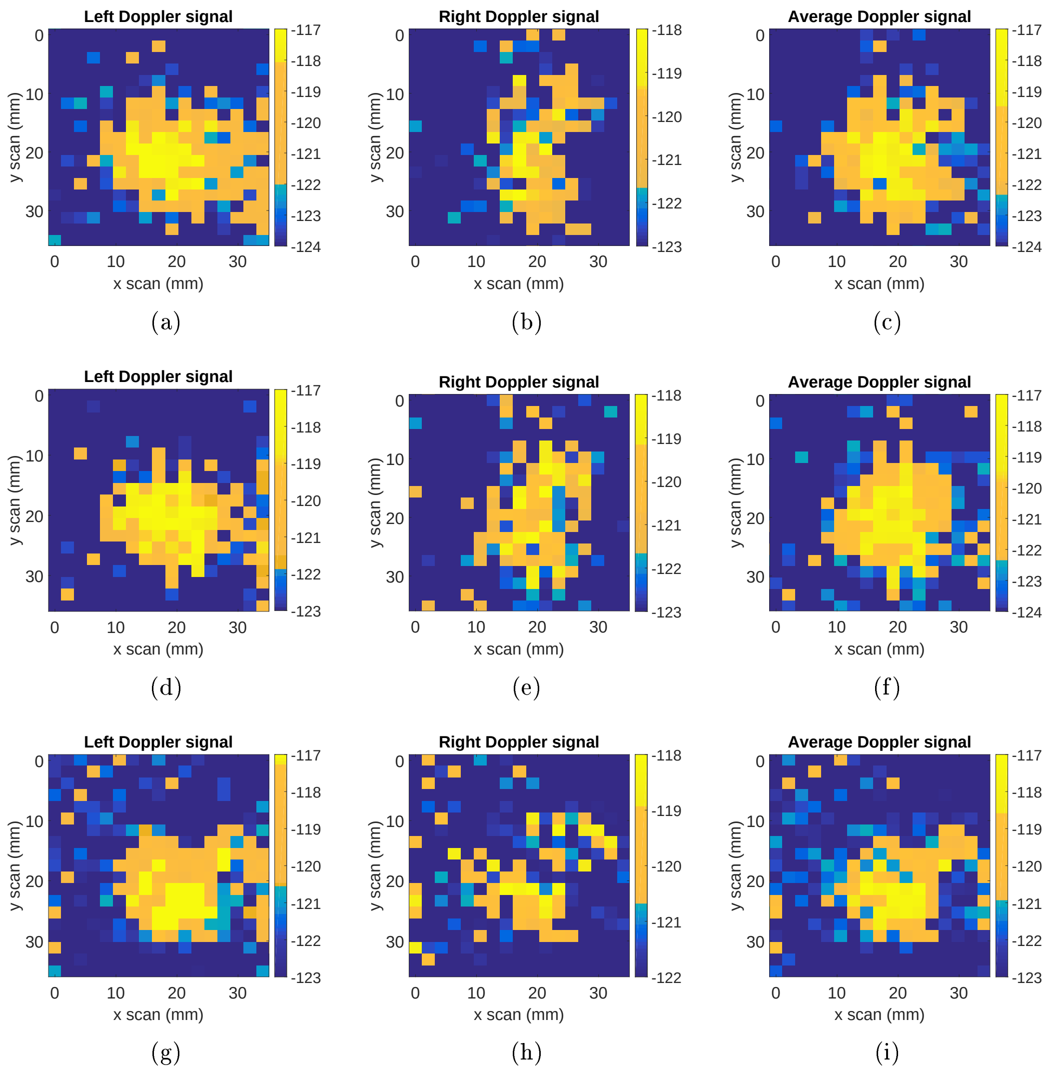

Figure 6.20: The obtained data profile from the Doppler signal in different depths. From top to bottom each row is related to the received signal when the focus of the transducer was on the layer that fibro-glandular was located as a reference level(z=0), 5 mm above that layer (z=5), and 10 mm above the reference layer (z=10), respectively. A 25 Hz, 5 is applied for ultrasound excitation and the microwave operating frequency is 4.75 GHz. In left Doppler and average Doppler data profiles, yellow color shows the signal level at tumor phantoms and orange color is related to the fibro-glandular region. In right Doppler data profile, it is not possible to see the place of them specially tumor phantom. Low signal level in fat region is shown by blue color.

of the fibro-glandular was less than 25 mm, the Doppler signal level on the tumor region was lower than the signal level in fibro-glandular region. But, the signal level increased at the tumor center. However, as the fibro-glandular size was increased above 25 mm, abrupt signal level change in the tumor region was disappeared.

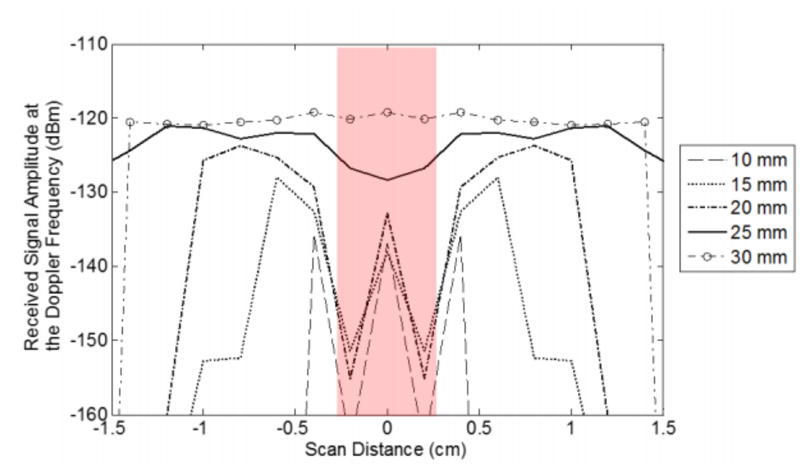

(a)

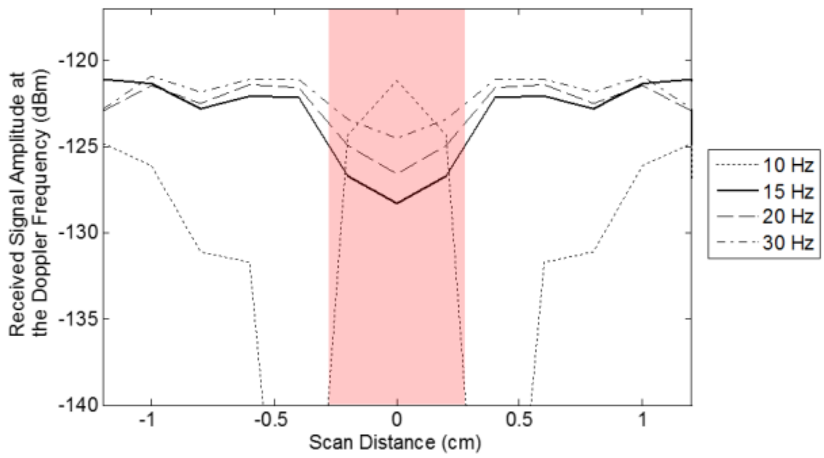

(b)

Figure 6.21: Simulation results for the received signal level at the Doppler frequency as a function of scan distance for (a) for various fibro-glandular sizes and (b) for different vibration frequencies. The tumor region is shown in red color [12].

In these simulation studies [12] the effect of vibration frequency was also evaluated. It was observed that, signal level on the tumor region increases with increasing vibration frequency from 15 Hz to 30 Hz while the changes in the signal level on fibro-glandular phantom was not significant (Figure 6.21 (b)). But, the signal characteristic was different for 10 Hz vibration. In this frequency, the Doppler signal level in the middle of the tumor was even higher than fibro-glandular.

These simulation results suggest that size of the fibro-glandular and the vibration frequency may be the reason why higher signal level was received from 14 mm tumor comparing 25 mm fibro-glandular phantom.

6.2.5 Experimental results on phantom-4 (same sized fibro-glandular and tumor inclusions inside the fat)

As it was mentioned in the previous section, the size of the fibro-glandular may be effective in the received signal level at Doppler frequency. For example, in the experiment with phantom-3, the signal level in tumor was 2 dB higher than the one received from the fibro-glandular phantom region. Therefore, a phantom including nearly same sized fibro-glandular and tumor phantom inclusions is developed (Figure 6.22). 13 mm $\times$ 9 mm fibro-glandular and 15 mm $\times$ 9 mm tumor phantoms are located 25 mm separate from each other inside the fat phantom. Since the fibro-glandular is softer than tumor phantom, it is difficult to cut it in the cylindrical shape exactly as tumor phantom. First one layer of fat phantom is poured in the phantom container up to 20 mm. One day later when it is solidified, fibro-glandular and tumor phantoms are located on top of it. Another layer of fat phantom is prepared and poured on them.

Similar to previous experiments, the microwave operating frequency sweep test is done to find the optimum microwave frequency according to the coupling between antennas and the phantom. In these experimental set up configurations, antennas are not fixed to the phantom container with adhesive glue. So, the coupling between antennas and phantom container may change from phantom to phantom and we have to check the optimum microwave frequency. A 25 Hz, 5 cycles AM burst signal (with 1 Hz pulse repetition frequency) is given

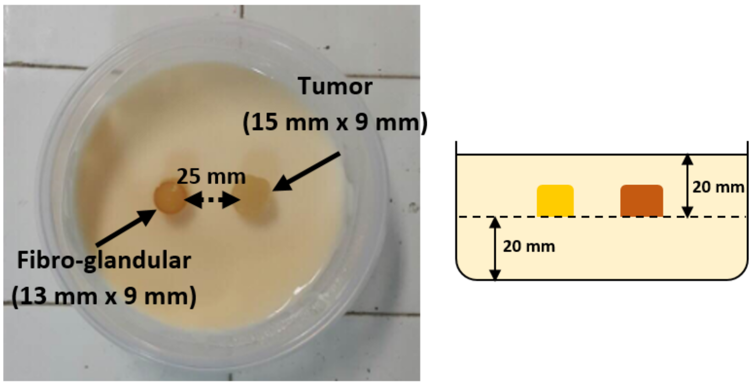

Figure 6.22: Fat phantom contains fibro-glandular (13 mm $\times$ 9 mm) and tumor (15 mm $\times$ 9 mm) phantoms 25 mm distant from each other. They are located at depth of 20 mm inside the fat phantom from the top surface and 20 mm above the bottom surface.

to US transducer after amplification. The SNR and received signal at Doppler frequency to the signal at center frequency are measured when the focus of the transducer is at fibro-glandular phantom (Figure 6.23).

Because of the coupling between antennas and antenna phantom, SNR was highest at 4.25 GHz microwave frequency. In addition, the ratio of the signal at Doppler frequency to signal at center frequency found to be highest at in this frequency. An area of 60 mm $\times$ 30 mm is scanned. The fibro-glandular and tumor phantoms are on the line passing between the antennas as shown in Figure 6.24. The focus of the transducer is placed on the layer that these phantoms are located. The scan step size is 2 mm. The results are demonstrated in Figure 6.25. Doppler signal level in fibro-glandular and tumor region is increased up to -112 dBm while it is below -115 dBm in the fat region.

Similar to previous experiments, the measured signal level at Doppler frequency in the right and left side of the center frequency is different. The difference between right and left Doppler signals is higher compared to the previous experiments in which fibro-glandular and tumor phantoms were in the middle of the two antennas. This is presumably cause by the location of the phantoms with respect to the antennas (Figure 6.24)). Existence of the tumor is not detectable from the right Doppler signal (Figure 6.25 (a)). However, the signal at right side

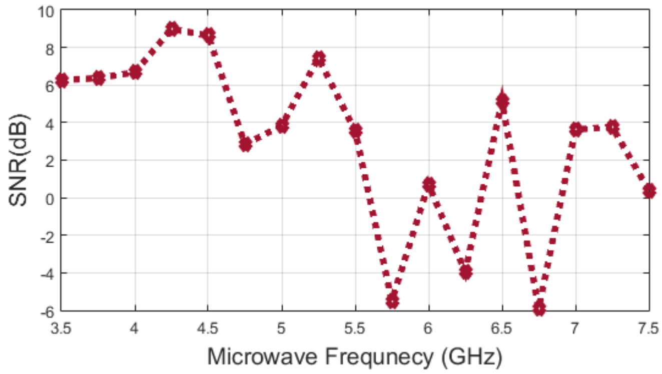

(a)

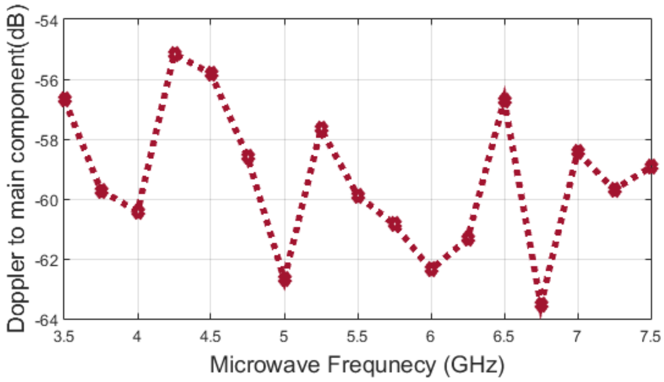

(b)

Figure 6.23: (a) SNR and (b) Doppler to main component of the received signal for the frequency sweep of 3.5-7 GHz. A 25 Hz, 5 cycles burst signal is used for creating the vibration. Both TX and RX are located at the bottom of the oil container.

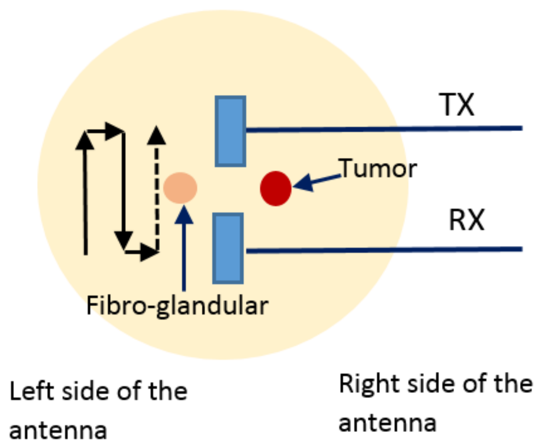

Figure 6.24: Position of fibro-glandular and tumor phantoms with respect to the antennas which are located at the bottom of the phantom container. The Ultrasound transducer is located on top surface of the phantom.

of the center frequency in the fibro-glandular region is about 3 dB higher than the one in the fat area (below -115 dBm). The real place of the fibro-glandular is shown by red dashed circle. A real fibro-glandular inclusion is about 13 mm in diameter but the approximate size in the data profile is around 10 mm in x direction and 18 mm in y direction.

In the information received from the left Doppler signal, the fibro-glandular inclusion is not resolved (Figure 6.25 (b)), but the tumor is detectable. The signal level is increased up to around -112 dBm in the tumor while it is lower than -114 dBm in fat region. The detected area of the tumor inclusion is 12 mm in x direction and 20 mm in y direction in the data profile, while the real diameter of it is around 15 mm.

The fibro-glandular is not distinguishable from tumor phantom in the obtained results, which can be due to the low contrast between the elastic constant of the developed phantoms. In biological tissues, the Young modulus of tumor is between 20-40 kPa while it is around 3 kPa in fibro-glandular. But the measured Young modulus of our developed fibro-glandular phantom is about 10 kPa. Even during the long experimental studies over a week, the phantom may get stiffer [54].

As it is observed in all experiments with all antenna configurations, the Doppler signal level at right and left side of the center frequency are different. This phenomenon can be due to the mechanical problem, such as location of the transducer on top of the phantom, antenna location, coupling between antenna and the phantoms, location of inhomogeneities with respect to antennas, microwave and ultrasound reflections. In the following section, the effect of the reflection on the signal level at Doppler frequency around the center frequency is discussed.

6.3 Doppler signal level at right and left side of the center frequency

Due to the shear wave propagation or shear wave reflection from the edges, the received signal from scatterers as a result of vibration can have different

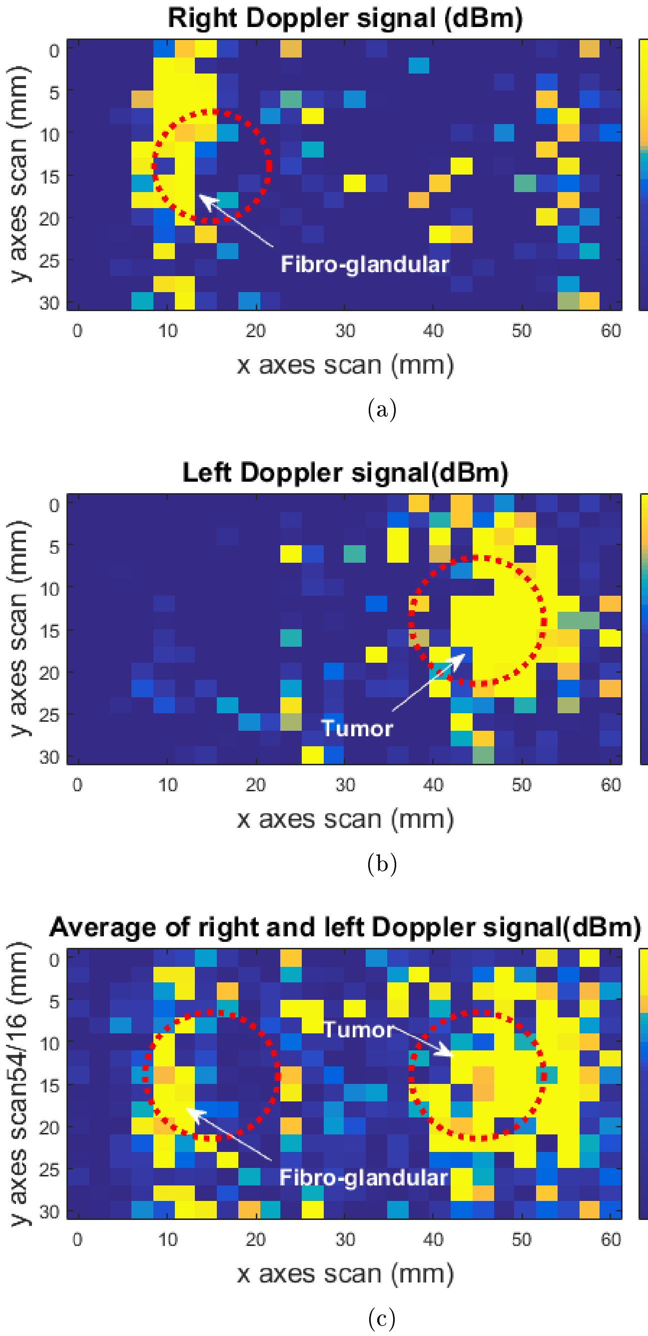

Figure 6.25: The obtained data profiles from the Doppler signal (a) at right side of the main component, (b) at left side of the main component, and (c) the average of both right and left Doppler signal. The phantom includes nearly same sized tumor and fibro-glandular phantoms inside the fat phantom. A 25 Hz, 5 cycles is applied for ultrasound excitation and the microwave operating frequency is 4.75 GHz. Yellow color shows the higher Doppler signal which we expect to receive from tumor phantom. Location of the tumor phantom is shown in red dashed circle.

amplitude and phase. In the following section, the effect of two scatterers on the received Doppler signal is analyzed.

6.3.1 Interference of two signals vibrating at the same frequency but with different phase and amplitude

The received microwave signals from two vibrating scatters can be written as:

$$\begin{aligned} S_{RX_1}(t) &= B_1[1 + M1\sin(\Delta\omega t)]\cos(\omega_m t + K1Sin(\Delta\omega t + \varphi_1) + \phi_1) \\ S_{RX_2}(t) &= B_2[1 + M2\sin(\Delta\omega t)]\cos(\omega_m t + K2Sin(\Delta\omega t + \varphi_2) + \phi_2) \end{aligned} \tag{6.1}$$

where B_1 and B_2 are scattered signal from the undisplaced scatterers. K_1 and K_2, φ_1 and φ_2 are the vibration amplitude and phase of the scatterers, respectively. ϕ_1 and ϕ_2 are the phases of the scattered EM signal for the undisplaced scatterers. Neglecting the amplitude modulation term and using trigonometric identities:

$$\begin{aligned} S_{RX_1}(t) =& B_1(\cos\left(\omega_m t + \phi_1\right) + \frac{K_1}{2}\cos\left(\left(\omega_m - \Delta\omega\right)t - \varphi_1 + \phi_1\right) \\ &- \frac{K_1}{2}cos\left(\left(\omega_m + \Delta\omega\right)t + \varphi_1 + \phi_1\right)) \\ S_{RX_2}(t) =& B_2\cos\left(\omega_m t + \phi_2\right) + \frac{K_2}{2}\cos\left(\left(\omega_m - \Delta\omega\right)t - \varphi_2 + \phi_2\right) \\ &- \frac{K_2}{2}cos\left(\left(\omega_m + \Delta\omega\right)t + \varphi_2 + \phi_2\right) \end{aligned} \tag{6.2}$$

Total signal at $(\omega_m - \Delta\omega)$ frequency is:

$$\begin{aligned} (S_{RX_1} + S_{RX_2})_{\omega_m - \Delta\omega} =& B_1\frac{K_1}{2}\cos\left(\left(\omega_m - \Delta\omega\right)t - \varphi_1 + \phi_1\right) \\ &+ B_2(\frac{K_2}{2}\cos\left(\left(\omega_m - \Delta\omega\right)t - \varphi_2 + \phi_2\right)) \end{aligned} \tag{6.3}$$

Total signal at $(\omega_m + \Delta\omega)$ frequency is:

$$\begin{aligned} (S_{RX_1} + S_{RX_2})_{\omega_m + \Delta\omega} =& B_1\frac{K_1}{2}\cos\left(\left(\omega_m + \Delta\omega\right)t + \varphi_1 - \pi + \phi_1\right) \\ &+ B_2\frac{K_2}{2}\cos\left(\left(\omega_m + \Delta\omega\right)t + \varphi_2 - \pi + \phi_2\right) \end{aligned} \tag{6.4}$$

Minus sign is replaced by adding $-\pi$ to the phase here.

There is a phase difference between the right and left Doppler components for each scatterer: $2\varphi_1 - \pi$ for the first scatterer, and $2\varphi_2 - \pi$ for the second scatterer. There is also a phase difference of $\phi_2 - \phi_1 = \Delta\phi$ between the received signals from two scatterer.

It can be shown that depending on the phases $\varphi_1, \varphi_2, \phi_1, \phi_2$, left and right Doppler component amplitudes can be different (See the example below). It can also be shown that if the phase difference $\Delta\phi = 0$, the right and left Doppler component magnitudes will be the same. Therefore, there must be phase difference in the received electromagnetic signal for the two undisplaced scatterers to have different left and right Doppler component amplitudes. This means that the scattering points should be at separate points.

Example: In phasor notation left $e^{j(\omega_m - \Delta\omega)t}$ and right $e^{j(\omega_m + \Delta\omega)t}$ Doppler components are:

$$\begin{aligned} (S_{RX_1} + S_{RX_2})_{(\omega_m - \Delta\omega)} =& B_1 \frac{K_1}{2} e^{j(-\varphi_1 + \phi_1)} + B_2 \frac{K_2}{2} e^{j(-\varphi_2 + \phi_2)} \\ (S_{RX_1} + S_{RX_2})_{(\omega_m + \Delta\omega)} =& B_1 \frac{K_1}{2} e^{j(\varphi_1 - \pi + \phi_1)} + B_2 \frac{K_2}{2} e^{j(\varphi_2 - \pi + \phi_2)} \end{aligned} \tag{6.5}$$

Let $A_1 = B_1 \frac{K_1}{2}$, $A2 = B_2 \frac{K_2}{2}$, $\phi_1 = 0$, $\varphi_1 = 0$, $\varphi_2 = \frac{\pi}{2}$, and $\phi_2 = \frac{-\pi}{2}$

In phasor representation, left and right Doppler components are given in Figure 6.26. The asymmetry in left and right Doppler signal is recognizable even in this simple example.

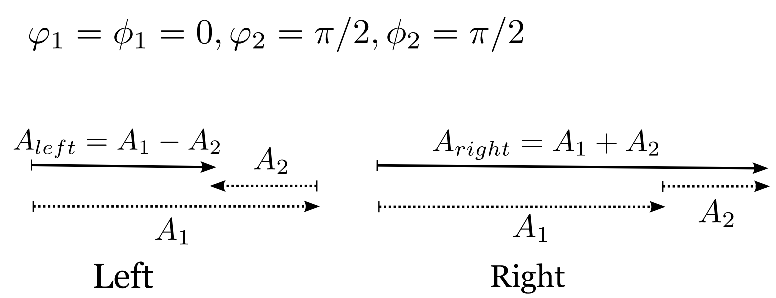

Figure 6.26: Left and right Doppler components of the received signal from two scatterers vibrating at the same frequency but different phase and amplitude.

For better visualization, left and right Doppler component difference are calculated from equation 6.5 for different A_1 and A_2 amplitudes (Figure 6.27. For a case when A_1=1 and A_2=0.5, the peak difference is huge (about 9 dB). These simulations shows that if there is no vibration phase or electromagnetic phase difference, the left and right Doppler component levels are equal. This is also the case the when the reflection has 180 degrees phase difference.

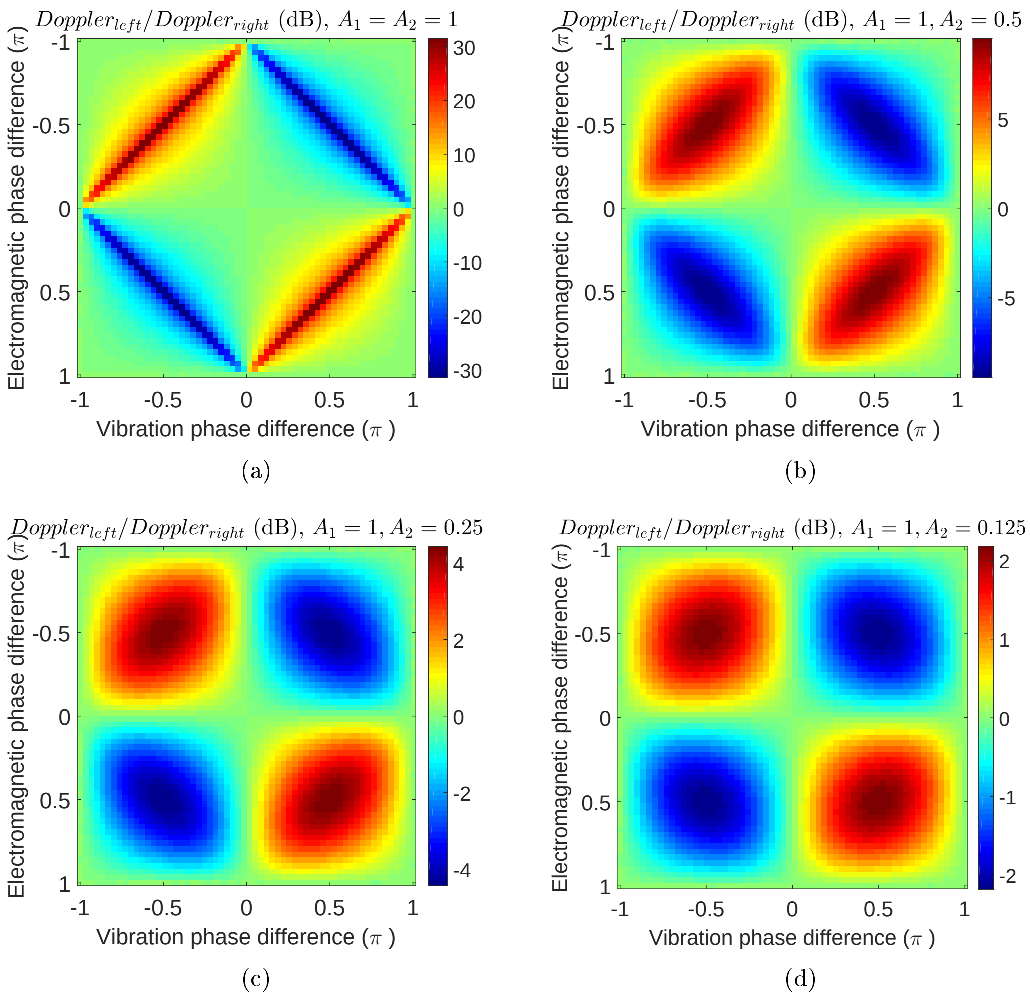

Figure 6.27: Ratio of the left Doppler signal to right Doppler signal for different reflection amplitudes.

In the studies with phantom-4, it is possible that there is a reflection from the mold boundary causing a vibration phase difference on fibro-glandular (or tumor phantom). Even in the last experiment, if the tumor and fibro-glandular are symmetric with respect to phantom container boundaries, they may not be symmetric with respect to antennas, which may cause a phase difference in the electromagnetic signal resulting in a difference in the right and left Doppler signals. The wavelength of electromagnetic wave at 4 GHz in fat is about 20 mm, and in tumor or fibro-glandular it is about 10 mm. Therefore, only spatial distance of about 2.5 mm in fat is sufficient to have 90 degree phase difference (using $\frac{4\pi R}{\lambda} = \frac{\pi}{2}$).

6.4 Data acquisition system for the second generation HMMDI set up

HMMDI method was evaluated using the spectrum analyzer as a receiver in the previous sections. In chapter 4, the data acquisition system in the first generation HMMDI set-up was discussed. In this section, the modified version of the previously designed homodyne receiver system is presented. In addition, the experimental results of using this receiver system on different tissue mimicking phantoms are provided.

6.4.1 Tissue mimicking phantoms in experimental studies on designed HMMDI receiver system

In order to test the performance of the receiver system, the phantom containing fibro-glandular inclusion of 14 diameter and 9 mm height (phantom-1 in section 5.3.1) is used. After evaluating the performance of the receiver system using the simple phantom, different signal processing methods are used to compare the data received from fibro-glandular and the one obtained from the fat phantom. Then, the receiver system and the processing tools are evaluated on the phantom consisting separately located fibro-glandular and tumor phantoms inside fat phantom (phantom-4 in section 5.3.4). The experimental results show the efficiency of the designed receiver system in acquiring the low level signal at Doppler frequency (around a few μV). The experimental studies and the results are presented in the following section.

6.4.2 Experimental studies and results

The block diagram of the designed receiver system is shown in Figure 6.28. Similar to the previous experiments, the focused US transducer is used in its third harmonic frequency (3.32 MHz). An AM burst signal at multiple frequencies is used to induce vibration inside the phantom. The AM signal is amplified with a high power RF amplifier of 52 dB gain. In these experiments, spatial peak pulse average intensity (I_{sppa}) of the ultrasound beam is 271.4 $\frac{W}{cm^2}$.

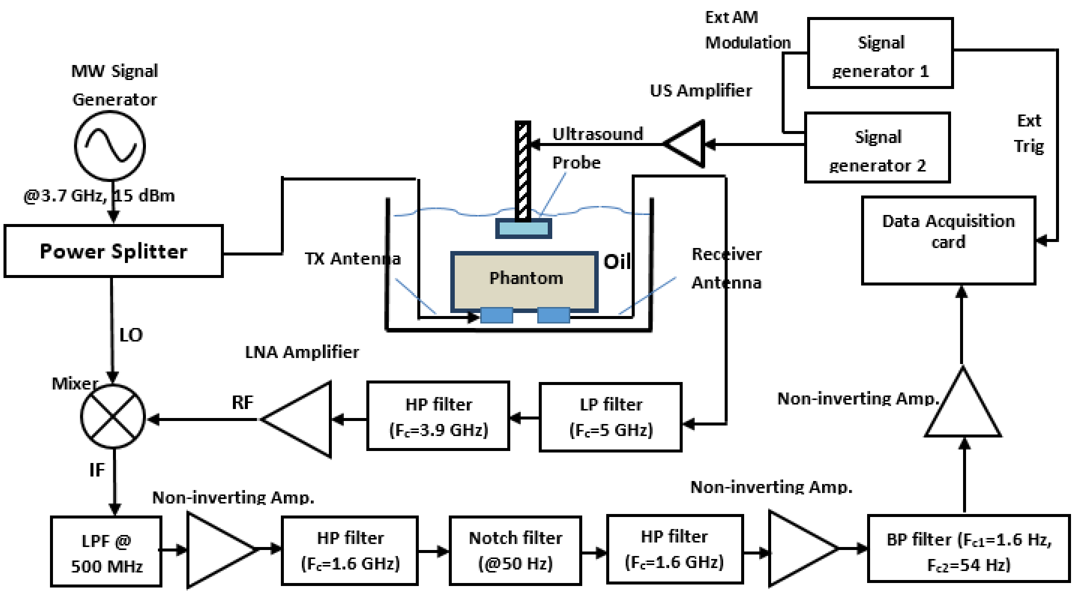

Figure 6.28: Block diagram of HMMDI data acquisition setup.

Open-ended waveguide transmitter and receiver antennas are placed in H-plane configuration and 15 mm away from each other. The transmitting microwave antenna is fed by the Agilent E8267D Vector Signal Generator (250 kHz - 20 GHz) with an output power of +15 dBm at 4.75 GHz frequency. For data acquisition in time domain, the signal is down-converted to baseband. For this purpose, the receiver antenna is connected to a low pass filter (minicircuit VLF-5000+, $f_c = 5$ GHz), a high pass filter (minicircuit VHF-3500+, $f_c = 4$ GHz), and a low noise amplifier (AML0120L3401 Microsemi), respectively. The filtered and amplified signal is fed to the mixer (Mini Circuit ZMX-7GLHR). The signal from signal generator is divided by two using power divider (Mini Circuit ZX10-2-71-S+) and one of the branches is used as the local oscillator for down-conversion. The output from the mixer is filtered using a low-pass filter (Mini Circuit NLP-50). Further amplification and filtering sections are used on the base-band signal to amplify the received low level noisy signal. The signal is amplified and passed through a high-pass filter (f_c=1.6 Hz) to eliminate DC offset. Furthermore, the notch filter is used to eliminate the 50 Hz line noise. After passing the signal through a high pass filter (f_c=1.6 Hz), the signal is amplified further. The output is fed to the band-pass filter (f_{c1}=1.6 Hz, f_{c2}=54 Hz) and the filtered signal is amplified using another non-inverting amplifier. The total gain of this system after the RF receiver section is around 73 dB. The frequency response of the presented circuitry is given in Figure 6.29. The amplified data is collected

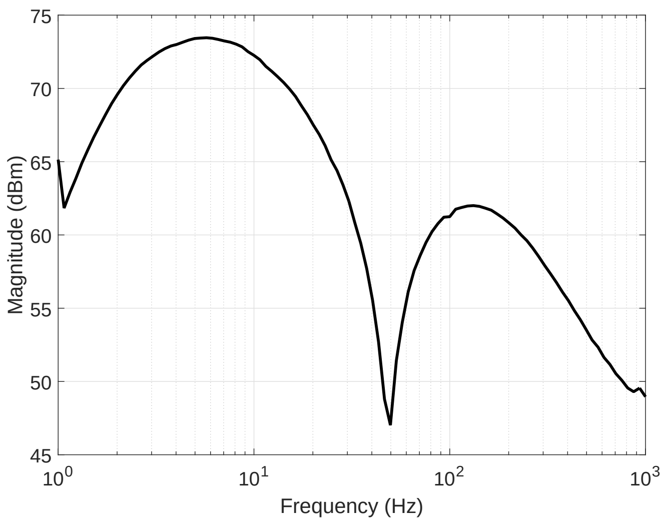

Figure 6.29: The designed receiver system frequency response.

using data acquisition card (National Instruments PCI-6281, M Series with 16 analog inputs at 18 bits, and 625 kS/s sampling rate).

6.4.2.1 Experimental results on the phantom-1 (fibro-glandular inclusion in fat)

In the first experiment, the phantom with fibro-glandular inclusion (14 mm $\times$ 9 mm) in the fat phantom is scanned. The scan step size is 2 mm. The signal at each point is recorded for 7 second with 10 kHz sampling frequency. In this duration, there are at least 6 trigger pulses which induce vibration. The signal received during the existence of the ultrasound pulse contains information about coupled elastic and dielectric properties of the focal region.

The acquired data is further processed by passing through digital band-pass IIR Elliptic filters with cut off frequencies around the applied vibration frequencies (15 - 35 Hz) to obtain the signal in the interested frequency range. The magnitude and phase of the applied digital filters for two different vibration frequencies, 15 Hz and 35 Hz, are illustrated in Figure 6.30. The filtered data in the trigger duration for these two vibration frequencies are given in Figure 6.30 (c) and (d). The duration of the burst signal is 200 ms and pulse repetition interval is 1 s. The received signals have the frequency as the applied vibration frequency.

i) 2-D HMMDI data profile generation using the peak to peak value of the received signal

In this section, HMMDI data profiles are generated using the digitally filtered data in the trigger duration. At each scan point, there are 7 trigger pulses (7 s). Therefore, the average of the peak to peak value of the filtered data during seven trigger pulses is obtained. The calculated values at each scan point (in dBm) are plotted in Figure 6.31. The real place of the fibro-glandular where the signal level is expected to be high is shown in red dashed circle in the figures. In all frequencies, the peak to peak value of the received signal at the fibro-glandular region is about 5 dB higher than the one at the fat region. In low frequencies (15 Hz and 20 Hz), in the right side of the phantom (fat) a high signal level was received. This increase is not observed in higher than 20 Hz frequencies. The signal rise in low frequencies can be due to the reflections from

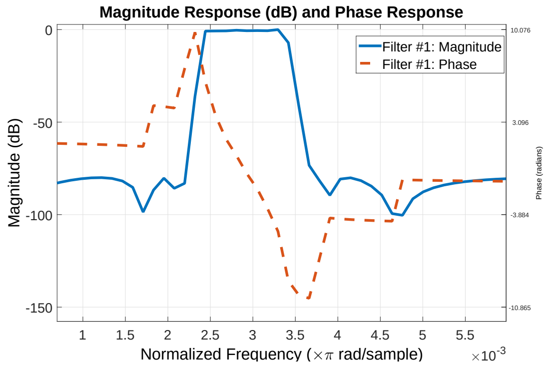

(a)

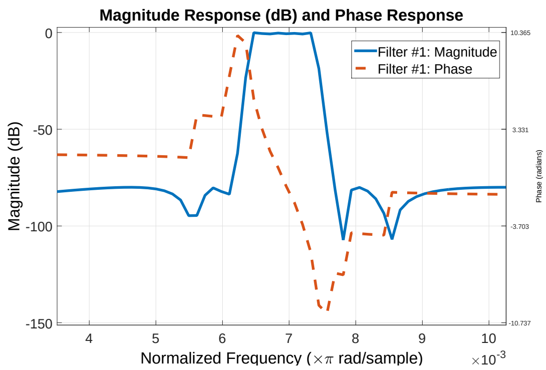

(b)

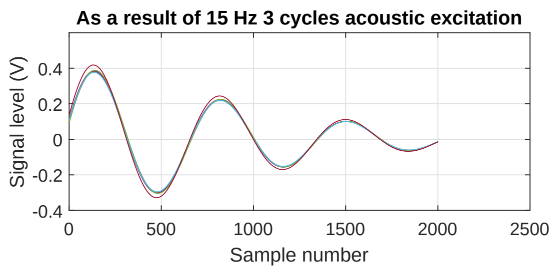

(c)

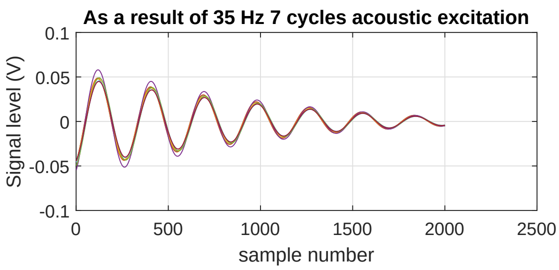

(d)

Figure 6.30: Implemented bandpass IIR Elliptic filters around (a) 15 Hz and (b) 35 Hz vibration frequencies. Digitally filtered received signal during the excitation for the case when (c) 15 Hz 3 cycles AM burst signal is used to create the vibration and when(d) 35 Hz 7 cycles AM burst signal is used. The burst signal duration is 200 ms and the pulse repetition interval is 1 s. Sampling frequency in these experiments is 10000.

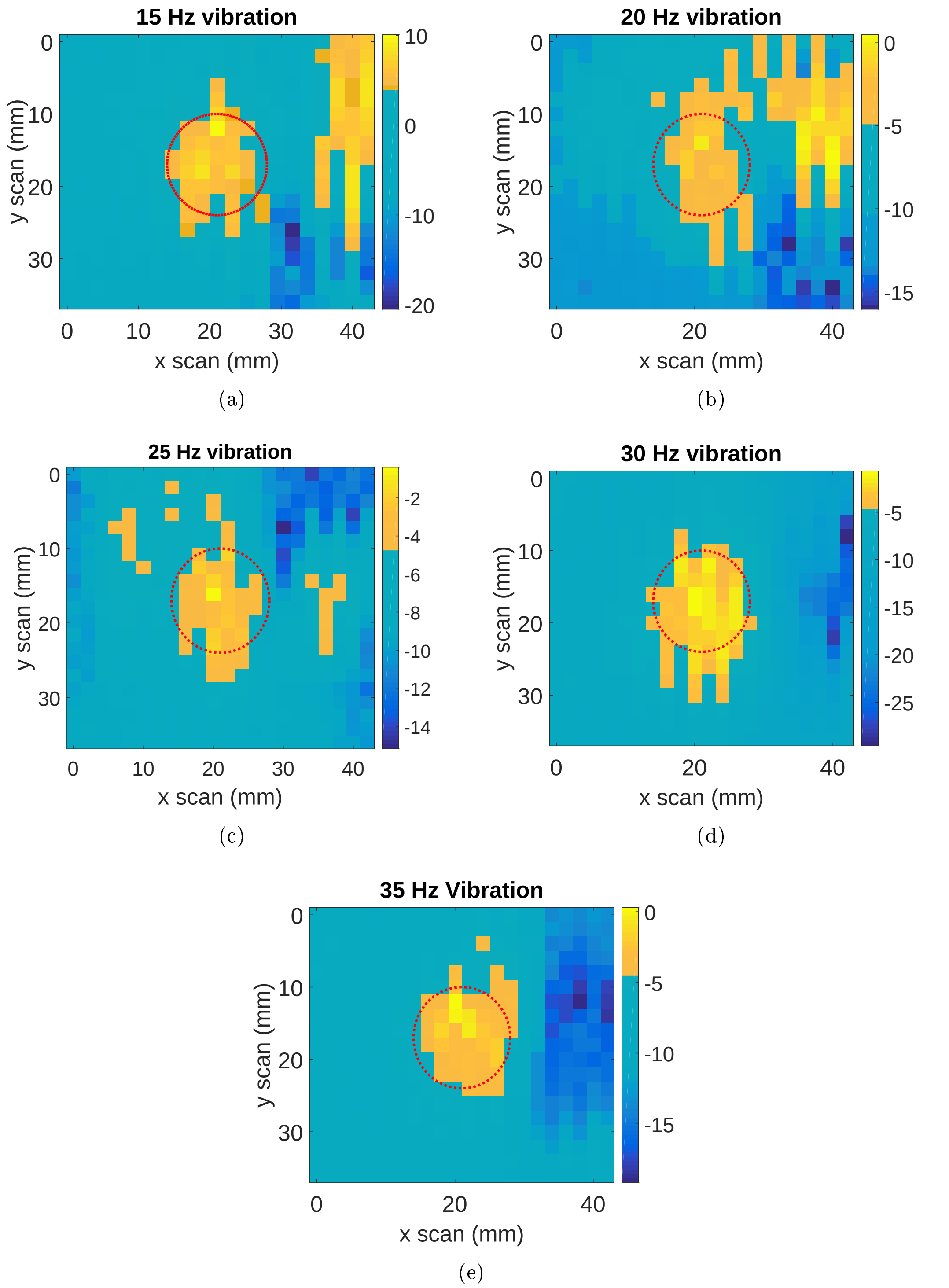

Figure 6.31: The peak to peak value of the received and filtered data during the phantom scan. The phantom contains 14 mm × 9 mm fibro-glandular inside fat background phantom. The obtained data profiles are plotted in (a) to (e) figures for vibration frequencies of 15 Hz to 35 Hz, respectively. The color bar values are in dBm. The burst signal duration is 200 ms and the pulse repetition interval is 1 s. Sampling frequency in these experiments is 10000.

the phantom container edge. The artifacts in the data profiles decreased with increasing vibration frequency.

In order evaluate the repeatability of the measurements, the standard deviation of the seven peak to peak value in 7 trigger pulses is calculated. The obtained standard deviations (in dBm) in each scan point are plotted in Figure 6.32. The highest standard deviation of the 7 samples (around -20 to -15 dBm) is seen in the fat region. As it was observed in the previous experiments, the data in the fat region randomly changes. Therefore, we expect to have the higher standard deviation in those regions. The standard deviation in the fibro-glandular region is between -30 dBm to -20 dBm.

ii) 2-D HMMDI data profile generation using the signal power at the vibration frequency

Another type of metric that can be extracted from the received signal to create data profile of the phantom is the power of the received signal. This is what the spectrum analyzer does. Therefore, the power of the received signal from the analog receiver system is calculated (using Fourier transform of the data) and the Doppler component of the power is used as a feature to construct the 2-D data profile of the scanned phantom. The obtained results are shown in Figure 6.33. The real place of the fibro-glandular is shown in red dashed circle in the figures. The power of the signal at Doppler frequency is about 4 dB higher in fibro-glandular comparing the fat phantom. However, the obtained results are not good for the cases that 15 Hz and 25 Hz acoustic excitation frequencies are applied. Looking at the related plots, one can realize that power of the signal is distributed around the fibro-glandular at 25 Hz vibration.

In order to check the repeatability of the measurements, the standard deviation of the power of the signal at Doppler frequency in 7 trigger pulses is calculated. The obtained standard deviations (in dBm) in each scan point are plotted in Figure 6.34. The standard deviation of the received signal samples at 15 Hz to 35 Hz is around -15 dBm to -25 dBm, respectively. This value is about 25 dB lower than the average signal value.

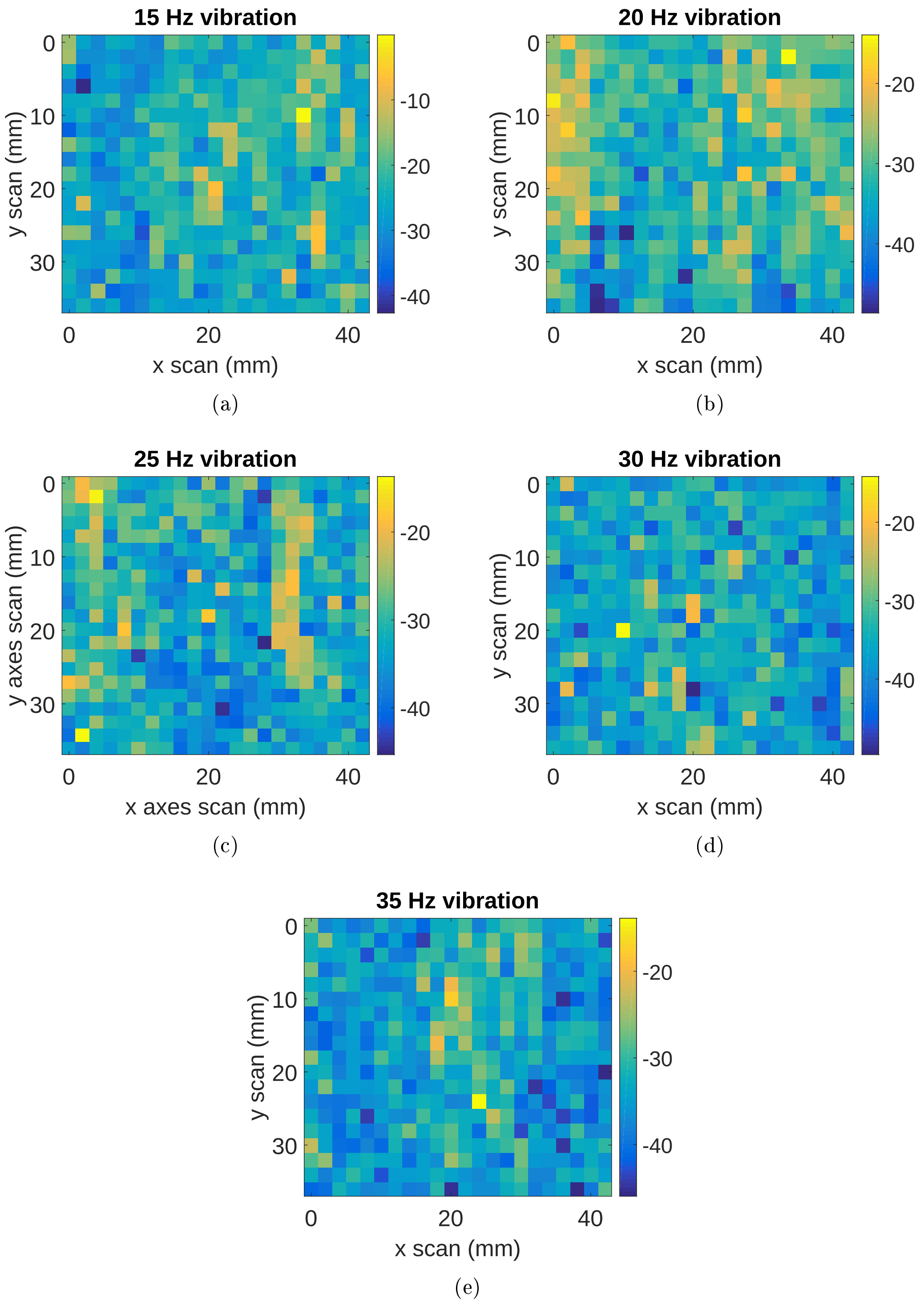

Figure 6.32: The standard deviation of the seven peak to peak value of the data (during seven trigger pulses) in each scan point. The obtained data profiles are plotted in (a) to (e) figures for vibration frequencies of 15 Hz to 35 Hz, respectively. The color bar values are in dBm.

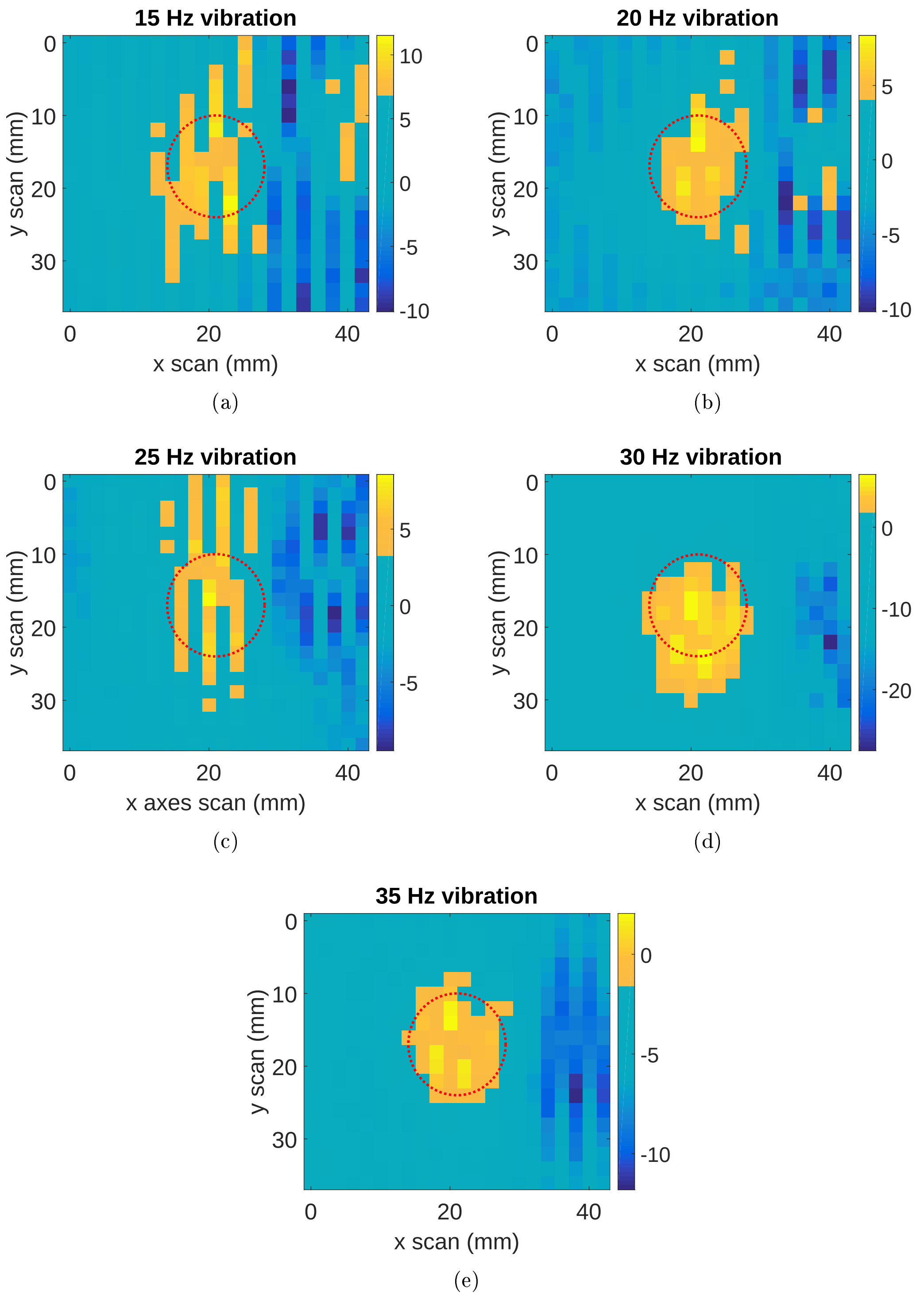

Figure 6.33: The obtained data profiles of the phantom from the power of the received signal at Doppler frequency (vibration frequency). The phantom contains 14 mm × 9 mm fibro-glandular inside fat background phantom. The constructed data profiles are plotted in (a) to (e) figures for vibration frequencies of 15 Hz to 35 Hz, respectively. The color bar values are in dBm. The burst signal duration was 200 ms and the pulse repetition interval is 1 s. Sampling frequency in these experiments is 10000 Hz.

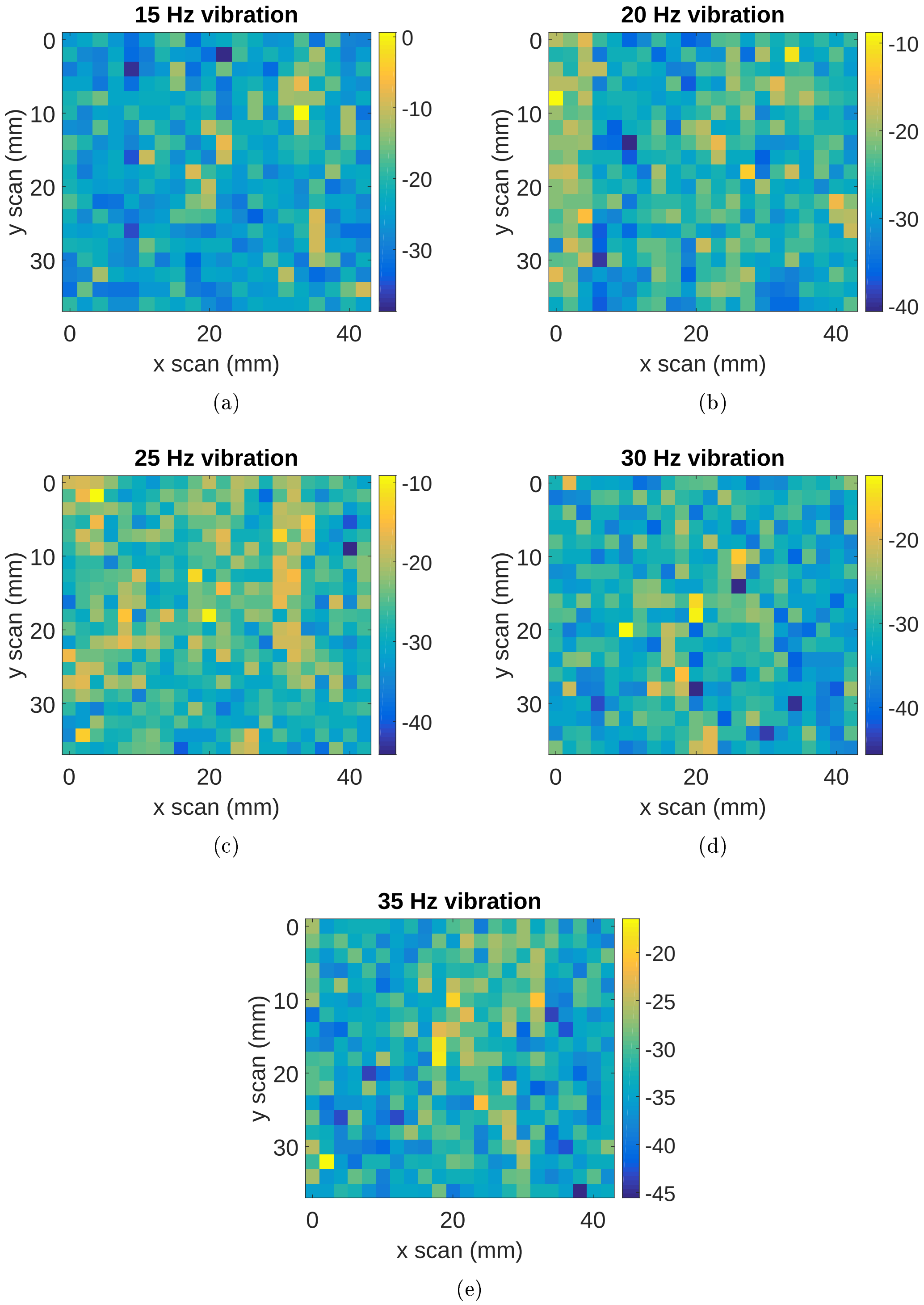

Figure 6.34: The standard deviation of the power of the signal at Doppler frequency (during seven trigger pulses) in each scan point. The constructed data profiles are plotted in (a) to (e) figures for vibration frequencies of 15 Hz to 35 Hz, respectively. The color bar values are in dBm.

iii) 2-D HMMDI data profile generation using correlation based method

It is observed that frequency of the received signal after digital filtering is same as the acoustic excitation frequency (Figure 6.30). It is expected to receive a sinusoidal signal at the vibration frequency. So, a correlation based method is proposed to extract a feature from the received signal that can be used for characterizing the data obtained from each point in the phantom. In this method, a pure sinusoidal at applied Doppler frequencies is used as a reference signal. A correlation of this signal with the received filtered data is calculated. This value at each scan point is normalized by the maximum of the correlation. The results are plotted in Figure 6.35. The results can be interpreted as the image of the scanned phantom. The information that can be extracted in these plots and the results obtained from the peak to peak value of the received signal are quite similar. The fibro-glandular region is not localized when the induced vibration frequency is 25 Hz. Similar problem was observed in the obtained results from power measurement method.

Same as other measurements, the standard deviation of the seven sample data is calculated. In this method, the correlation values at each point are normalized by the maximum of the correlation. Therefore, the standard deviation of the correlation is also divided by this value to be able to compare the results. The obtained standard deviations of 7 sample data in each scan point are plotted in Figure 6.36. As it can be seen, the standard deviation of the measurement is below 0.1.

From the standard deviation values in all cases, we can conclude that number of averaging can be decreased without considerable change in the constructed data profile. Therefore, the scan time and as a result induced heat in the phantom or tissue will be less. Therefore, the risk of possible damages as a result of temperature rise in the tissue will be decreased.

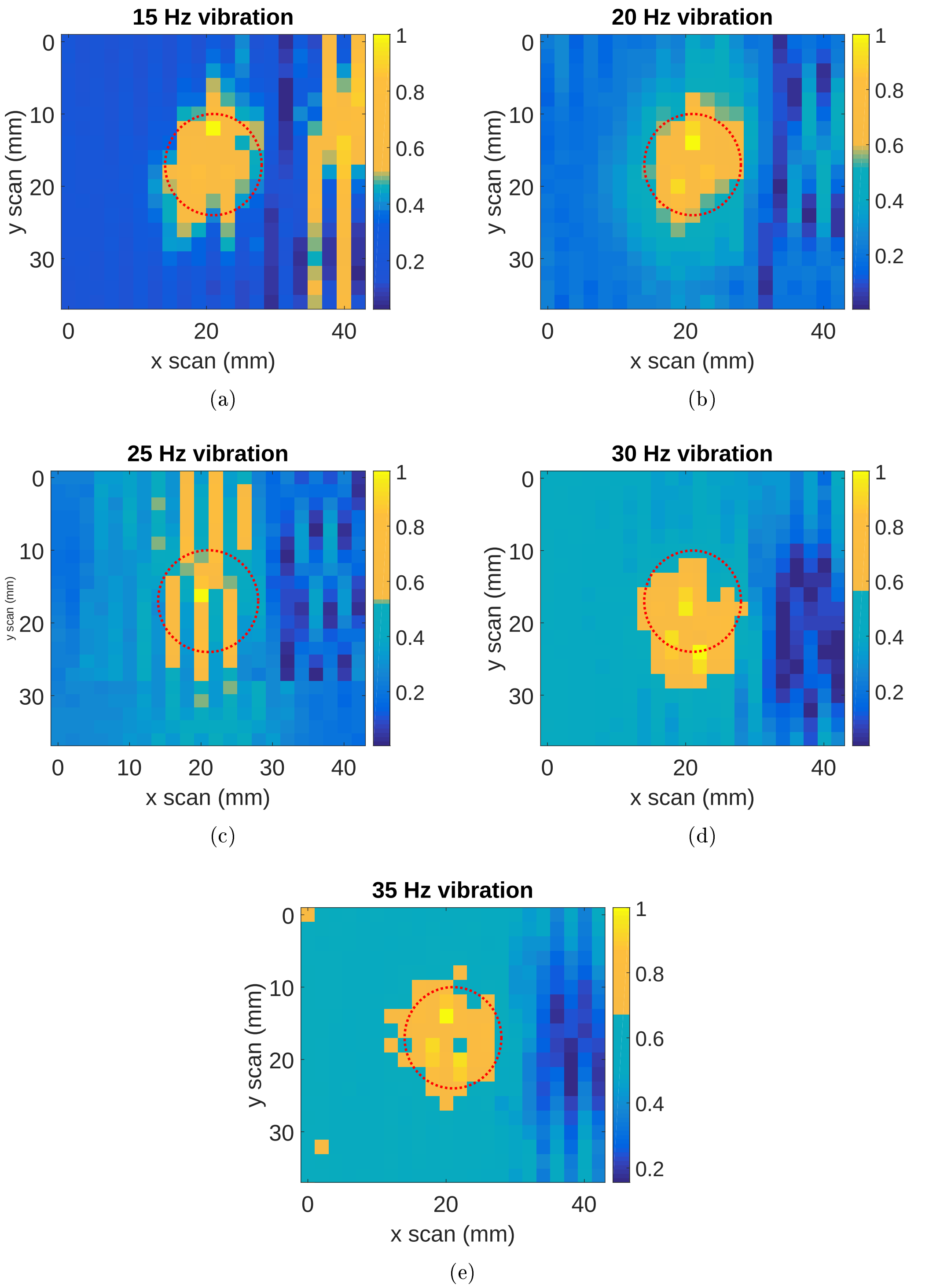

Figure 6.35: The obtained data profiles of the phantom from the correlation based feature. The phantom contains 14 mm × 9 mm fibro-glandular inside fat background phantom. The constructed data profiles are plotted in (a) to (e) figures for vibration frequencies of 15 Hz to 35 Hz, respectively. The burst signal duration is 200 ms and the pulse repetition interval is 1 s. Sampling frequency in these experiments is 10000 Hz.

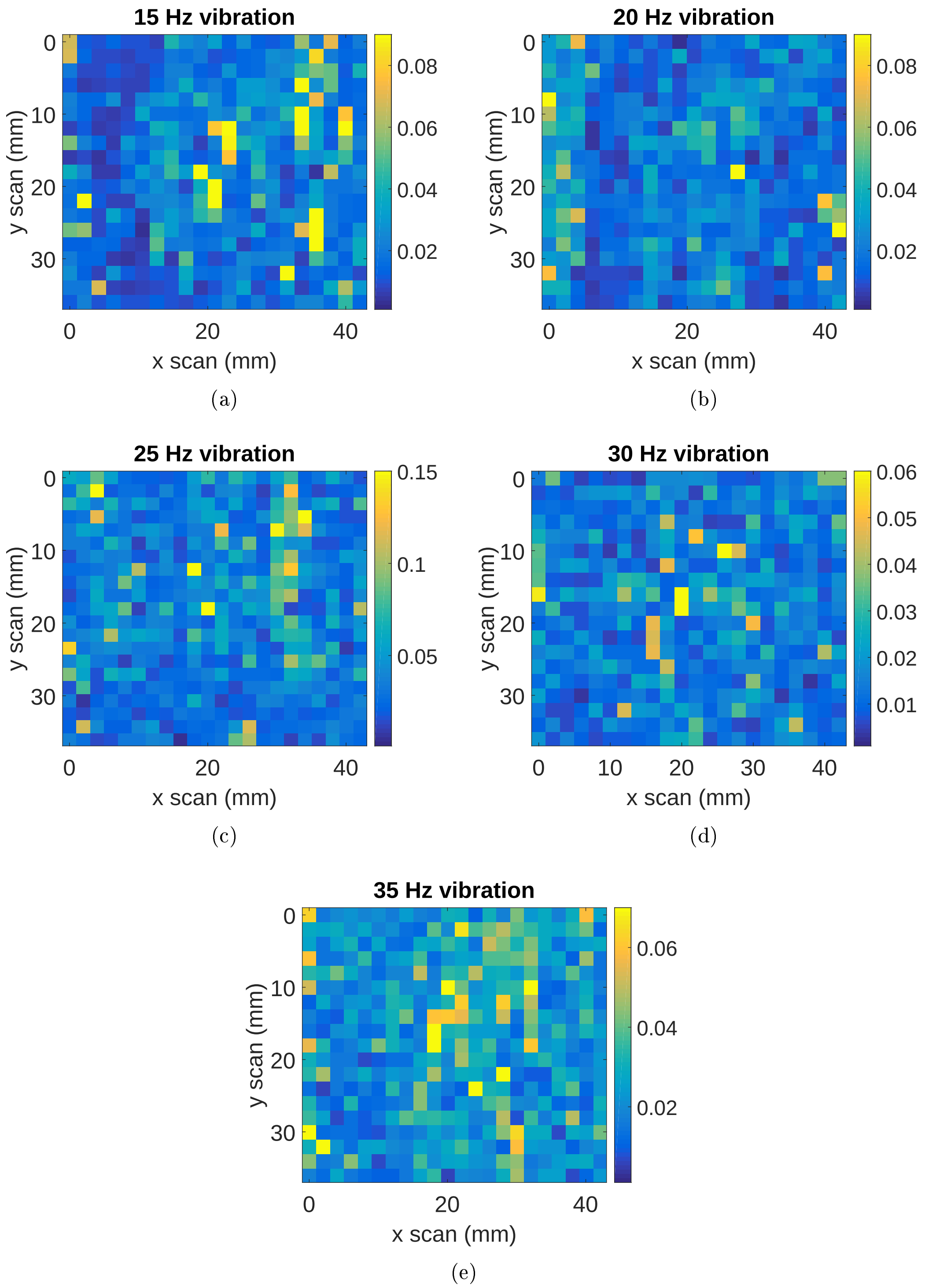

Figure 6.36: The standard deviation of the power of the signal at Doppler frequency (during seven trigger pulses) in each scan point. The obtained data profiles are plotted in (a) to (e) figures for vibration frequencies of 15 Hz to 35 Hz, respectively. The color bar values are in dBm.

6.4.2.2 Experimental results on phantom-4 separate (fibro-glandular and tumor inclusions in fat)

The phantom containing nearly same sized fibro-glandular (13 mm $\times$ 9 mm)and tumor (15 mm $\times$ 9 mm) phantoms, is scanned. The scan results of this phantom using the spectrum analyzer as the receiver is given in section 5.4.4.4. The three mentioned methods are used for processing the data.

i) 2-D HMMDI data profile generation using peak to peak value of the received signal

In order to generate an HMMDI data profile, the peak to peak value of the digitally filtered data is calculated. The obtained results are illustrated in Figure 6.37. The real place of the fibro-glandular that we expect to receive a high signal is shown in red dashed circle. In all frequencies, the peak to peak value of the received signals from the fibro-glandular and tumor is about 2-4 dB higher than the one received from fat region. At 15 Hz vibration frequency, we see a larger inclusion area, this may be caused by larger shear wave wavelength. By increasing the frequency to 35 Hz, the inclusion detected size becomes less.

Since the elasticity contrast between fibro-glandular and tumor phantoms is low in the developed phantoms, the Doppler signal level in these two phantoms is close to each other. However, comparing all five cases, one can see that the signal level in tumor becomes 0.5-1 dB lower than fibro-glandular in all cases except 15 Hz. In simulation studies on the fibro-glandular containing tumor phantom [12], it has been observed that signal level received from the tumor increases as frequency increases from 15 hz to 30 Hz while it was relatively unchanged in the surrounding fibro-glandular phantom (Figure 6.21 (b)). However, the signal characteristic was different for 10 Hz vibration frequency. In this frequency, the signal amplitude in the middle of the tumor was even relatively higher than fibro-glandular region. Similarly, in this experiment we observed higher signal level in the tumor comparing the signal level at fibro-glandular.

On the other hand, in the simulation study [12], the Doppler signal level in the fibro-glandular and in the middle of the tumor regions were close to each other

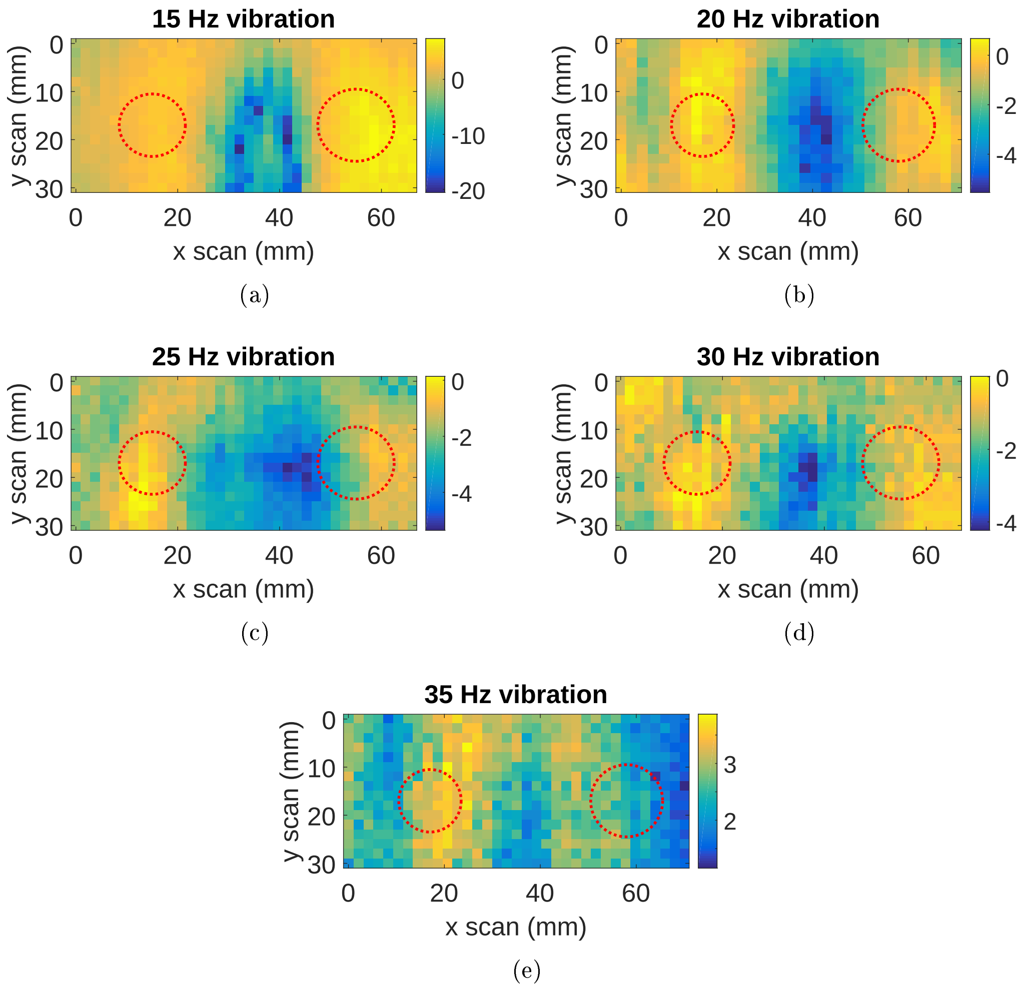

Figure 6.37: The peak to peak value of the received and filtered data during the phantom scan. The phantom contains 13 mm $\times$ 9 mm fibro-glandular and 15 mm $\times$ 9 mm tumor phantoms inside fat phantom. The obtained data profiles are plotted in (a) to (e) figures for vibration frequencies of 15 Hz to 35 Hz, respectively. The color bar values are in dBm. The burst signal duration is 200 ms and the pulse repetition interval is 1 s. Sampling frequency in these experiments is 10000 Hz.

for the fibro-glandular sizes of 10 mm to 20 mm (Figure 6.21 (a)). In these cases, the signal just at the boundaries of the tumor drops up to 15 dB comparing the signal level at the fibro-glandular region. In our experimental studies, since these two tissue phantoms are separately located in the fat phantom, it is not possible to see the signal level changes at the boundaries.

The measurements suggest that, although the signal level in tumor and fibro-glandular are close to each other due to their similar dielectric properties, they do not show same behavior in different vibration frequencies presumably due to the difference in their elastic characteristics. Therefore, differentiation of tumor and fibro-glandular may be be possible by acquiring multi-vibration frequency data. It was observed that size of the fibro-glandular tissue is effective on the received Doppler signal level. More experimental studies should be done for evaluating different sizes of the fibro-glandular phantom on the received Doppler signal.

To check the repeatabilty of the measurement, the standard deviation of peak to peak value for seven data samples (7 trigger pulses) is calculated. The obtained standard deviations of 7 sample data (in dBm) in each scan point are plotted in Figure 6.38. The standard deviation of the measurement is approximately between -15 dBm to -25 dBm. So, we are able to decrease the data acquisition (less number of excitation) time and as a result the induced heat in the phantom or tissue. This consideration, decreases the risk of possible harm or tissue damage in HMMDI method as a result of ultrasound radiation.

ii) 2-D HMMDI data profile generation using the signal power at Doppler frequency

Another feature that can be used to create the data profile of the phantom from is the power of the received signal. In this section, the power of the received signal is calculated and the Doppler component of the power is used to construct 2-D data profile of the phantom. The obtained results are shown in Figure 6.39. The power of the signal in tumor and fibro-glandular is about 2-4 dB higher than fat region. The tumor and fibro-glandular inclusions are not distinguishable from the results. Larger inclusion areas is seen at 15 Hz vibration frequency. The size of the inclusions in the plots are decreased by increasing the vibration frequency

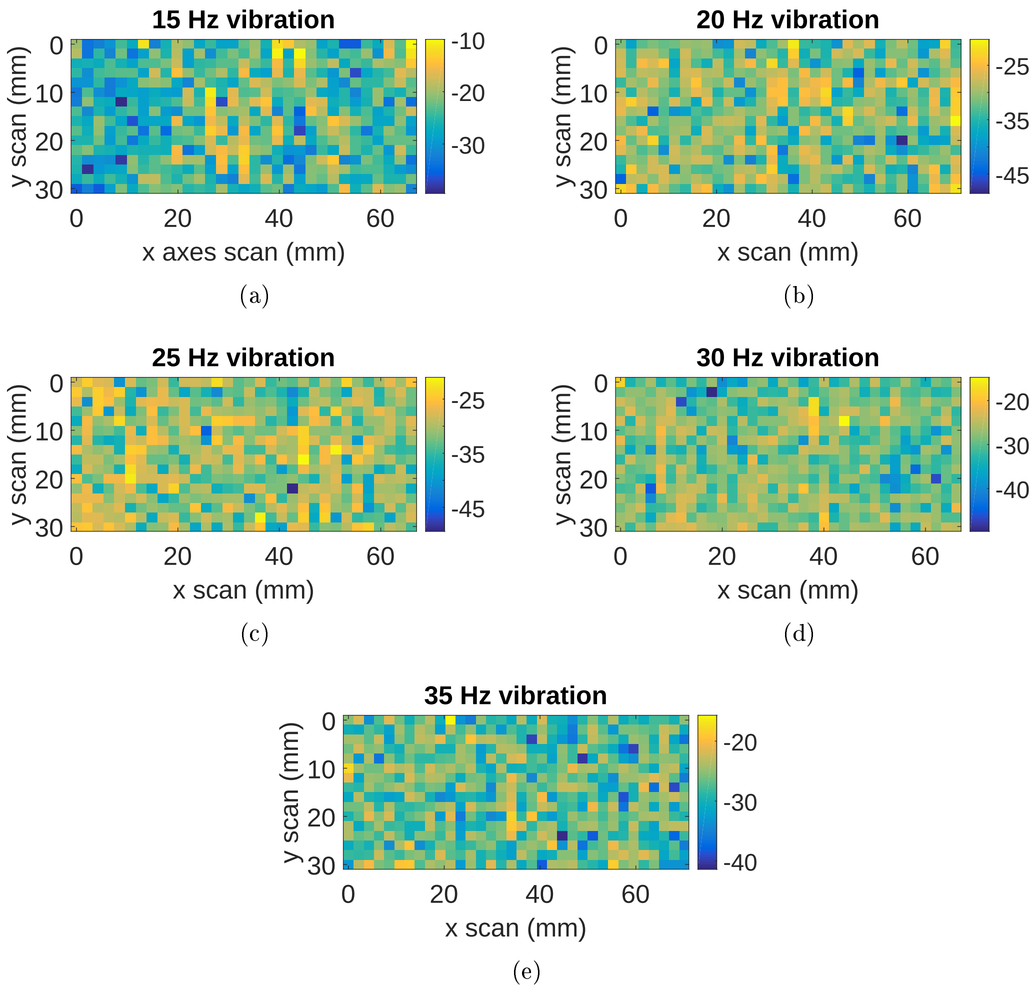

Figure 6.38: The standard deviation of the power of the signal at Doppler frequency (during seven trigger pulses) in each scan point. The obtained data profiles are plotted in (a) to (e) figures for vibration frequencies of 15 Hz to 35 Hz, respectively. The color bar values are in dBm.

to 35 Hz. These results are consistent with the generated data profiles using the peak to peak value.

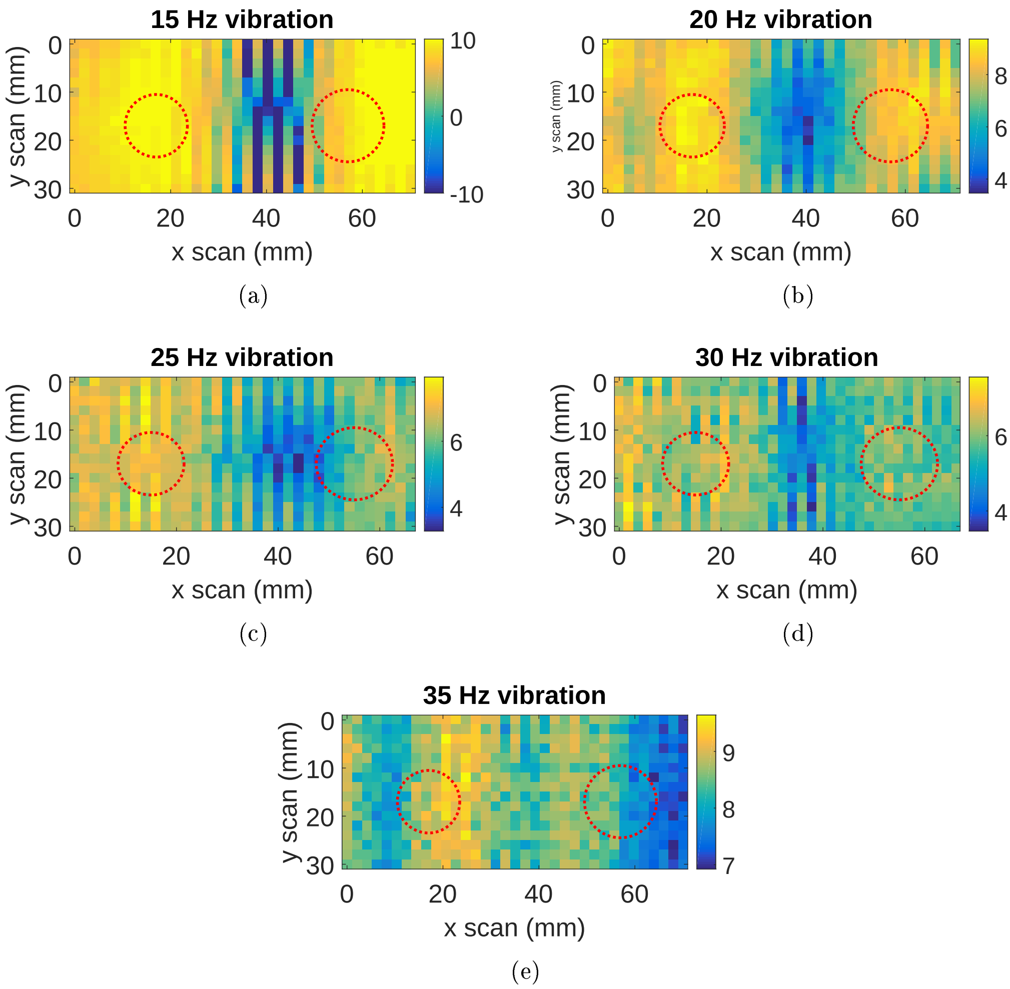

Figure 6.39: The obtained data profiles of the phantom from the power of the received signal at Doppler frequency (vibration frequency). The phantom contains 13 mm × 9 mm fibro-glandular and 15 mm × 9 mm tumor phantoms inside fat phantom. The obtained data profiles are plotted in (a) to (e) figures for vibration frequencies of 15 Hz to 35 Hz, respectively. The color bar values are in dBm. The burst signal duration is 200 ms and the pulse repetition interval is 1 s. Sampling frequency in these experiments is 10000 Hz.

iii) 2-D HMMDI data profile generation using correlation based method

The introduced correlation based method in the phantom-1 studies, is used to analyze the scan data. The correlation between the received signal from the phantom at US pulse duration and the reference signals for each vibration frequency (Figure 6.35) is calculated. The normalized correlation values for whole scan area are plotted in Figure 5.15. Different behaviors of fibro-glandular and tumor phantoms are more detectable in these data profiles comparing the one obtained from peak to peak value of the signal. At 15 Hz, the correlation value at tumor is around 0.9-1 in tumor while it is around 0.6-0.7 in the fibro-glandular and it is below 0.4 in fat region.

On the other hand, the correlation value in fibro-glandular is around 0.9-1 but it is around 0.8-0.85 in tumor region at 25 Hz vibration. The correlation values in these two inclusion regions are similar when 30 Hz vibration is applied. Such signal characteristics was also observed in [12] simulation studies. The results suggest that by sweeping the vibration frequency, the HMMDI has the potential of differentiating these tissues from each other. This observation should be further investigated in more phantoms.

6.5 Conclusion

In this chapter, the HMMDI set up with fixed transmitter and receiver antennas was evaluated. Several phantoms were developed and HMMDI data were acquired using spectrum analyzer. 14 mm fibro-glandular and tumor inclusions in fat phantom were detectable. At 25 Hz vibration, the marked area as a fibro-glandular in HMMDI data profiles, was around 11 mm. The Doppler signal in the detected region was 4 dB higher than the Doppler signal level on the surrounding fat phantom. The Doppler signal at detected region as tumor was 3 dB to 8 dB higher than the one on the fat region. It was difficult to obtain information about the size and shape of the tumor phantom from obtained HMMDI data profiles.

The possibility of distinguishing tumor from fibro-glandular tissue in HMMDI method, was evaluated on phantoms containing tumor, fibro-glandular, and fat phantoms. In the phantom with fibro-glandular containing tumor inside in the middle of fat, the Doppler signal on the tumor region was 2 to 4 dB higher

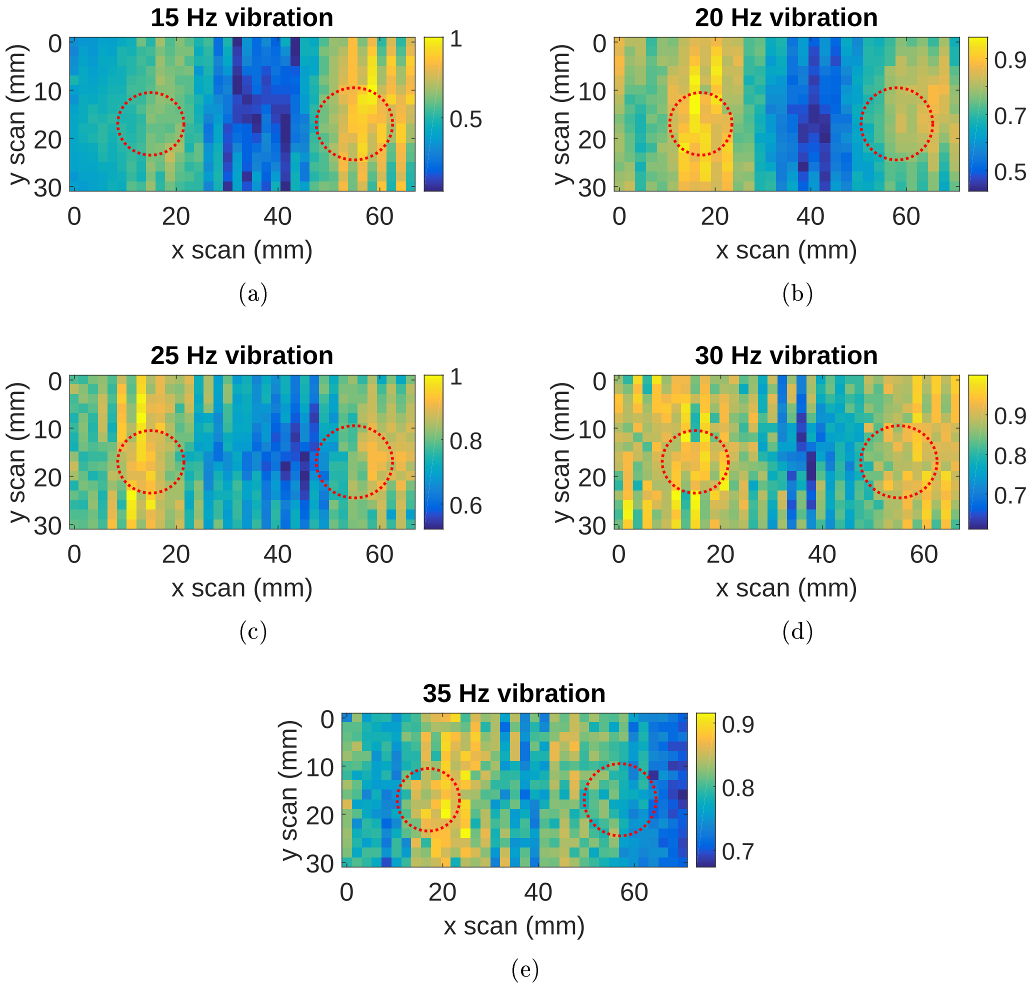

Figure 6.40: The obtained data profiles of the phantom from the correlation based feature. The phantom contains 13 mm × 9 mm fibro-glandular and 15 mm × 9 mm tumor phantoms inside fat phantom. The obtained data profiles are plotted in (a) to (e) figures for vibration frequencies of 15 Hz to 35 Hz, respectively. The burst signal duration is 200 ms and the pulse repetition interval is 1 s. Sampling frequency in these experiments is 10000 Hz.

than the one obtained from the fibro-glandular and 6 dB higher than the one in the fat region. This results was expected to be a result of the fibro-glandular phantom size (25 mm). This hypothesis was evaluated by comparing the results with the simulation studies in [12]. In the phantom containing separate fibro-glandular and tumor inclusions, the Doppler signal level on these phantoms were not separable. However, they could be distinguished from the surrounding fat phantom.

The designed receiver system and the acquired HMMDI data were presented. The acquired data was processed and three different features; peak to peak value of the signal during US excitation duration, power of the signal at Doppler frequency, and correlation base method were extracted from the obtained data. The HMMDI data profiles were generated using these features. Using 4 dB width as a metric, the fibro-glandular of 14 mm diameter was detectable from the HMMDI data profiles.

The phantom containing separate fibro-glandular and tumor phantoms inside fat, was scanned using the designed receiver system. Applying multiple vibration frequencies between 15 Hz to 35 Hz, different behaviors were observed from fibro-glandular and tumor phantoms. In low frequencies such az 15 Hz, the correlation value on the fibro-glandular was around 0.6-0.7 while it was 0.9 to 1 in the tumor region. In higher vibration frequency as 35 Hz, the correlation value in the tumor was 0.5 lower than this value in the fibro-glandular region. In all cases, these phantoms were distinguishable from the fat region.

The provided results using the data acquired by spectrum analyzer and designed receiver system, showed the potential of HMMDI method in distinguishing these tissues in different vibration frequencies. In order to have better contrast between fibro-glandular and tumor phantoms, the contrast between the elasticity of these tissue phantoms should be increased. In addition, more studies are required to evaluate the effect of the size of the inclusions in Doppler signal level.

CHAPTER 7

TISSUE TEMPERATURE RISE IN HMMDI SCAN

7.1 Introduction

As all other biomedical systems, the patient safety is also important beside the system performance. Therefore, all possible harms of medical devices that are in contact with the human body should be taken into account. In HMMDI, the patient body is exposed by both microwave waves and acoustic waves. Although the amount of the exposure power should be high enough to receive the proper data, it should be under the safety limits. The temperature rises as a result of US and microwave illumination. If the temperature rises over the safety limits, the exposed tissue may be damaged.

In the following sections, the temperature rise due to the microwave and US excitation is discussed. The temperature measurement measurement procedure is presented. The results are discussed and the temperature rise profile is compared with similar observed profiles in the literature. The results suggest that more studies are necessary for assessing the HMMDI safe insonation threshold.

7.2 Temperature rise in HMMDI due to microwave exposure

In microwave applications, the specific absorption rate (SAR) is used to define the microwave safety limit in healthy tissues. In 30 minutes microwave exposure inside the tissue, when SAR range 1-4 $\frac{W}{kg}$, the temperature rise is lower than 1 $°C$ [11]. Since, in the HMMDI experiments applied microwave power is less than 0.04 Watt, the microwave exposure may not harm the tissue.

7.3 Temperature rise due to ultrasound exposure

In ultrasound exposure, the temperature rise in the tissue is a critical issue for patient safety. Ultrasound radiation results in both predictable temperature increase and unpredictable temperature rise due to acoustic cavitation phenomenon. The U.S Food and Drug Administration (FDA) defined the limit for ultrasound field intensity as 190 $\frac{W}{cm^2}$ spatial peak pulse-average intensity (I_{sppa}) [63]. The ultrasound intensity that is used in the experimental studies of this thesis is 271 $\frac{W}{cm^2}$ which is higher than the FDA limit. As it was mentioned, due to the high elastic constant of the developed phantoms, stronger ultrasound excitation is applied to receive the detectable signal level. In biological tissue which are softer than the phantoms, it is expected to receive adequate signal level with less amount of ultrasonic exposure intensity.

Another safety issue for the clinical ultrasound applications, is the cavitation phenomenon. In the existence of high rarefactional ultrasound pressure bubbles can be formed [66]. Due to the acoustic pressure, these bubbles may grow and collapse volently that produces high amount of energy on the order of ionizing radiation in a short time. This phenomenon is called inertial cavitation [66]. Several precautions can be taken to minimize this risk of cavitation in ultrasound applications [67–70]. Due to the highly nonlinear behavior of the bubbles in converting the acoustic energy to mechanical motion, the mechanical index (MI) has been introduced which is the ratio of the peak negative pressure of the ultrasound beam in MPa to frequency of the ultrasound beam in MHz's. The FDA limit for MI is 1.9 [63]

7.3.1 Experimental studies on temperature rise

In order to measure the temperature rise during the HMMDI scan procedure using single element focused ultrasound transducer (Sonic Concept, H-102), an Omega Engineering HH82A digital thermometer is used. The thermometer probe is inserted into the middle of the fat phantom where the fibro-glandular is located. The focus of the US transducer is placed on the phantom (Figure 7.1).

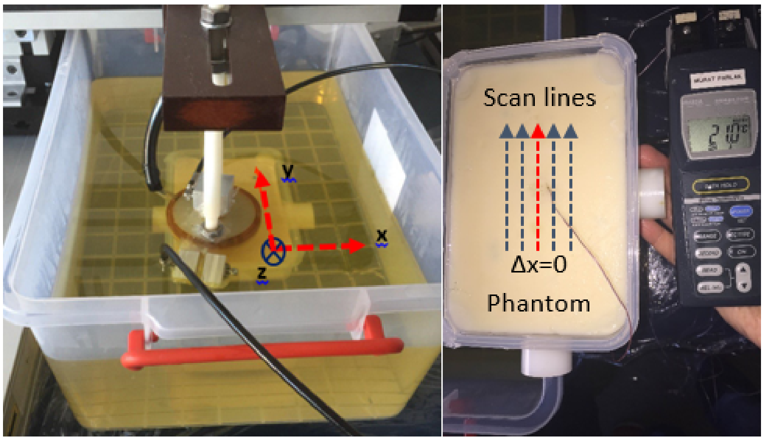

Figure 7.1: The temperature measurement set up using the Omega Engineering HH82A digital thermometer. The line scans are 2 cm in y direction. Several line scan are done in different x and z values while the US is introducing the mechanical vibration inside the phantom

Similar to the experimental studies, 25 Hz, 5 cycles AM burst signal is used to introduce mechanical vibration in the phantom. This causes 4.2 MPa and I_{SPPA} of about 271 $\frac{W}{cm^2}$ at the focal zone. A line scan of 2 cm (one cm below the center up to 1 cm above the center) length is done. In each point for 8 s, the US excitation is applied to the phantom. After 4 s keeping the US off, the scanner is moved to the next point in the scan line. The scan steps size is 1.5 mm. Several 1-D scan in the y direction, in different depths (Δz: distance between US transducer and thermometer probe head) is done. When the thermometer is exactly in the focus point ($\Delta z = 64$ mm), the temperature rise is about 24-26°C (Figure 7.2). Temperature was increased dramatically only after the first excitation pulse. For the remaining 7 pulses, this increase is not observed. The temperature rise is too high and it happens in a short time which shows that it is a result of cavitation in the focal zone.

The cavitation and sudden increase in the temperature has been reported in

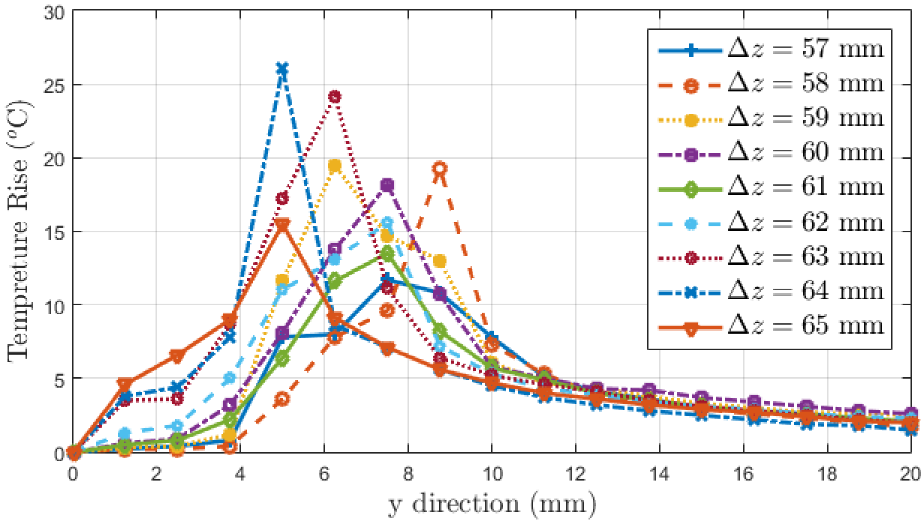

Figure 7.2: The temperature rise during in different depths ultrasound excitation for the scan length of 20 mm. The 25 Hz, 5 cycles AM burst signal is used to create the vibration in the phantom. The thermometer is in the middle of the phantom inside the fibro-glandular phantom

several studies during insonation [71–73]. In an study using 0.75-5 MHz ultrasound, a pressure threshold for sudden increase in the temperature measured via termocouple due to cavitation at 1 MHz was obtained as 5.3 MPa [72]. In another study, bubbles were introduced in a gel artificially to test their effect on the temperature while using 0.75 MHz transducer with I_{spta} of $10^4 \frac{W}{m^2}$ [74]. The maximum temperature in the existence of the bubbles was 6 times higher comparing a case when there was no bubble. In [75], during insonation of beef after contrast agent injection using 1.5 MHz and $9 \times 10^3 \frac{W}{m^2}$ continuous ultrasound wave for 3 minutes, double temperature elevation has been reported. In the absence of the contrast agent, they observed similar temperature at $1.8 \times 10^4 \frac{W}{m^2}$.

In [66], several experiments were conducted on insonation of the tissue mimicking phantoms with 1 MHz single element focused pulsed ultrasound transducer. They used a few MPa pressures. In their studies, the temperature and the pressure of the ultrasound were measured using an array of thermocouples and hydrophone. They used deionized and degassed water as a coupling medium. The agar based phantoms were developed as tissue mimicking phantoms. At 1.36 MPa pressure and 1.2 s exposure, they observed just about 3 °C. By increasing the pressure to 1.62 MPa for the same exposure duration, the temperature was increased to 15 °C. They repeated the experiments for different exposure periods. For a 10 s insonation, a sudden onset of enhanced heating was observed when pressure was increased from 1.39 MPa (just below the threshold pressure) to 1.42 MPa (just above the threshold pressure). A dramatic temperature rise was consistently observed above some insonation pressure, called cavitaion threshold. In these experiments, although the degassed water was used the cavitation was observed in different laboratory experiments.

Similar localized temperature rise profile is seen in our measurements, during HMMDI scan procedure. In HMMDI studies, the deionized water is used. Also, the oil that is used as a coupling medium is not degassed. On the hand, the bubbles may be created during the HMMDI scan procedure. In addition, while locating the thermometer inside the phantom, an air bubble may be produced inside the probe hole. Another immersion ultrasound transducer can be located inside the oil tank to detect the acoustic signal created from the bubble collapse while the US wave pressure is changing. More studies should be done for finding the cavitation threshold in HMMDI method application on tissue mimicking phantoms. In the experiment, the temperature increases above 10 degrees even up to some mm far from the focus. This can be due to large beamwidth of the FUS in the axial direction. So, the heat elevated in a larger area.

In continue, the line scan is shifted laterally when the depth is fixed. So, the scan line is shifted 2 mm to the right and left side of the first scan line (middle line). Therefore, five line scans are run by changing the scanner position in the x direction. Figure 7.3 shows that, a high temperature rise can be seen just in one line. This is due to the fact that the bandwidth of the transducer is much smaller in the lateral direction (lateral resolution higher than axial resolution). So, the temperature is increased just in the focal zone where the thermometer is located and around 1 mm far from the focus, the temperature does not elevated, considerably.

More studies are required to measure the cavitation pressure threshold in HM-MDI method. However the measured cavitation pressure threshold for 1.7 MHz

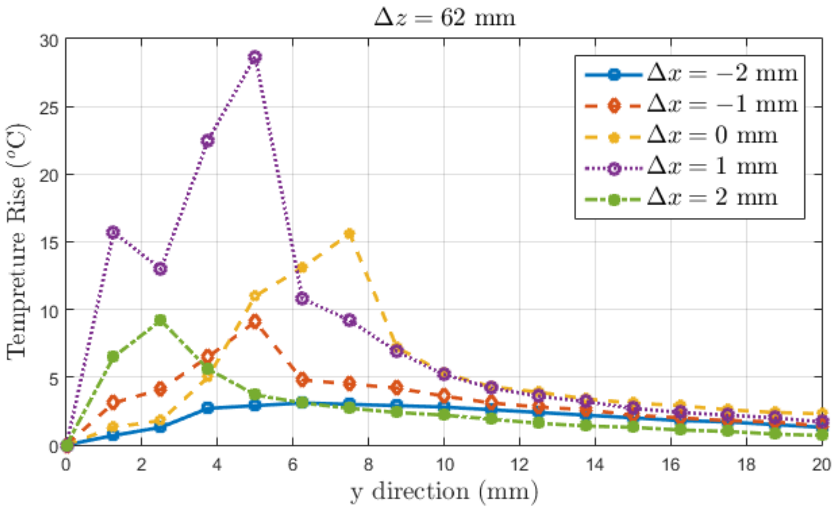

Figure 7.3: The temperature rise during ultrasound excitation for the scan paths in the y direction around the center line. A 25 Hz, 5 cycles AM burst signal is used to create the vibration in the phantom. The thermometer is in the middle of the phantom inside the fibro-glandular phantom.

insonation was 10 MPa [72], which is higher than the applied pressure in these measurements.

7.4 Conclusion

In this chapter, the temperature rise in HMMDI scan, due to microwave and acoustic excitation was discussed. In the HMMDI experimental studies, the applied microwave power was about 0.04 Watt which does not induce considerable heat (below 1 °C) inside the tissue. The phantom temperature was measured during HMMDI scan using a thermometer. Around the focus of the US transducer, a sudden heat rise (around 25 °C to 30 °C) was observed. The sudden, short duration temperature rise behavior, suggest that there exist a cavitation phenomenon. A literature survey was done and it was realized that similar temperature profiles have been observed in ultrasound applications. More studies are required to find the cavitation threshold in HMMDI for preventing unpredictable temperature rise.

CHAPTER 8

CONCLUSIONS AND FUTURE WORK

In this thesis, the potential of Harmonic Motion Microwave Doppler Imaging (HMMDI), was evaluated in large scale experimental studies. The method is based on distinguishing different tissues using their elastic and dielectric properties. In this method, a local harmonic vibration is induced inside the tissue while the microwave signals are illuminating the locally vibrating tissue. As a result of induced motion, the back scattered microwave signal is phase modulated. The first spectral frequency component of this signal (Doppler signal) contains information about the elastic and dielectric properties of the exposed tissue. HMMDI method,

- Expose the tissue to non-ionizing microwave and ultrasound waves, while in the conventional mammography the ionizing x-rays illuminate the tissue.
- Provides a patient friendly imaging method without a need for tissue compression as conventional mammography.
- Provides information on elastic and dielectric properties of the tissues. Conventional elasticity measurements methods for breast cancer detection, use only the elasticity information of the tissues. On the other hand, the conventional microwave imaging methods, give information on dielectric properties of the tissues.
- Has a potential of detecting high dielectric characteristics breast tissues, fibro-glandular and tumor. Although they have high dielectric properties, the fibro-glandular is softer than cancerous tissue. The hybrid HMMDI

method can be used to differentiate these tissues by adding the elasticity information.

- Provide high resolution by inducing the localized harmonic motion inside the tissue.
- HMMDI imaging can be used as a complementary imaging method beside microwave imaging. So, the dielectric and elastic properties can be both reconstructed for having better sensitivity and specificity.

The main goal of this thesis study was to contribute various stages of the HMMDI's development processes that can be listed as follows:

- Phantom development,
- Experimental system realization,
- Phantom experiments (obtaining 2-D GHMMDI data profile of the phantoms),
- Experimental problem observation,
- Finding the possible solutions,
- Designing a receiver system for HMMDI experimental set up,
- Analyzing the received HMMDI data.

In this thesis, fat, fibro-glandular, and tumor phantoms that mimic dielectric and elastic properties of the biological breast tissues were developed according to [3] and [2]. The measured dielectric properties of the developed phantoms were consistent with the reference values [20]. The developed tumor (around 77 KPa) and fibro-glandular (around 20 KPa) phantom material from [3] were stiffer than the tumor (around 43 KPa) and fibro-glandular (around 10 KPa) phantom material from [2]. Both phantom materials were used to produce experimental inhomogeneous phantoms.

The HMMDI experimental studies were classified in three different categories, experimental studies on the first generation of the HMMDI set up, on the second generation with scanning antennas and on the second generation with fixed antennas. In the first generation of HMMDI experimental set up, transmitter and receiver antennas were fixed at the bottom side of the glass phantom container, and the coupling medium was distilled water. In these studies, two different phantoms, fat including fibro-glandular with tumor inside, and fat including three different sized tumors were scanned. Through a linear scan (1-D) the potential of HMMDI for detecting the tumor inside the fibro-glandular phantom was observed.

A proposed data acquisition setup for HMMDI method that down-convert the received signal to the base-band and amplified and filtered it, was evaluated using the developed phantoms. Using this receiver system, the Doppler signal was observed in time-domain. The received Doppler signal in the tumor was about 4 dB higher than the one in fibro-glandular region and it was about 4 dB higher than the signal from the surrounding fat.

After evaluating the acoustic characteristics of the sunflower oil in simulation studies using HIFU simulator tool, the distilled water was replaced by this oil in the second generation of HMMDI set up. Considering oil as a coupling medium, two different antennas configuration was proposed for HMMDI set up. In the first configuration, second generation of HMMDI with scanning antennas, the transmitter and receiver antennas were placed on the top side of the phantom together with the US transducer. The antennas and the US transducer were connected to the scanner to scan the phantoms. 1-D and 2-D scan results were obtained. Three different sized tumors for which the smallest one had 4.5 mm $\times$ 4 mm size, were detected inside the fat phantom in the 2-D HMMDI results. In the experiment using the phantom including the fibro-glandular with the tumor inside, in the middle of the fat phantom, a huge artifact due to the antenna movement was observed. This artifact was dominant on the Doppler signal, so that it was not possible to interpret the data received from different regions. It is possible that the Doppler signal in the experiment with three different size tumors in the fat phantom was resolvable without a considerable artifact because the size of tumors were much smaller compared to the fibro-glandular phantom size (25 mm) in the second phantom.

The second generation of HMMDI with fixed antennas was suggested to solve the above mentioned problems of the set up with scanning antennas. 14 mm diameter fibro-glandular and 14 mm diameter tumor phantoms, in two different fat phantoms, were detected in HMMDI scan results. Using these phantoms, dependency of the Doppler signal on vibration frequencies, and averaging number was evaluated. As the scan time decreases, it is expected that the induced heat and tissue damages is decreased. The results suggested that, the number of ultrasonic excitation pulses can be decreased from 11 to 7. Since the PRI was 1 s, the scan time at each position can be decreased from at least 11 seconds to 7 seconds. In scanning the large area, this parameter is critical.

In the 2-D scan results, acquired from a 14 mm tumor inside 25 mm fibro-glandular phantom, the received Doppler signal from the tumor was about 0.5 dB to 1 dB higher than the signal level on the fibro-glandular. This unexpected behavior was discussed comparing the results with the simulation results in [12]. The results suggested that Doppler signal level is dependent on the size of the inclusion in addition to their elastic characteristics. This hypothesis should be evaluated with more phantom studies. However both fibro-glandular and tumor phantoms were detectable from the surrounding fat phantom.

A receiver system was designed to acquire the HMMDI data. Applying different vibration frequencies, the data was recorded. Three different features; peak to peak value, power of the signal at Doppler frequency, and correlation based feature were extracted from the data. HMMDI data profiles of 14 mm diameter fibro-glandular phantom inside the fat phantom, and nearly same sized fibro-glandular and tumor phantoms (around 14 mm diameter) inside the fat phantom was constructed using the extracted features. Considering 5 dB (in constructed data profiles from peak to peak and Doppler component of power features) and 0.4 width (in constructed data profiles from correlation based feature) as a metric, the fibro-glandular (nearly same as original size) was detectable inside the fat phantom. In the fat phantom with tumor and fibro-glandular phantom inclusions, different behavior of these phantoms were observed in different frequencies. At 15 Hz, the correlation value in the fibro-glandular region was 0.2-0.4 lower than the one in the tumor region. At 35 Hz, this value in the tumor was 0.5

lower than the one in the fibro-glandular region. In all cases, these phantoms were distinguishable from the fat region.

In the fat phantom including two same sized tumor and fibro-glandular, and in all other experiments, the Doppler signal component on the right and left side of the fundamental frequency, were different. This observation was evaluated using simulations. It was realized that if the back scattered signal comes from two vibrating scatteres that are vibrating with different amplitude and phase, the right and left Doppler signals may not be equal. The possible factors that could cause this phase difference, are shear wave propagation, shear wave reflection, and location of phantom with respect to antenna location.

The temperature rise in the HMMDI scan procedure was measured using the phantom materials. An unpredictable temperature rise up to around 30 °C was observed around the US transducer focus. This phenomenon was assessed comparing similar behaviors in other insonation applications in literature. The cavitation was noted to be the source of this results. More studies are necessary to verify this hypothesis and find the cavitation pressure threshold in HMMDI method.

This thesis is an initial experimental studies on realizing the potential of HMMDI method in detecting breast tumor using tissue mimicking phantom materials. As a consequence, there are a number of concerns that should be made in the future studies, as:

- Finding methods to increase the elasticity contrast in the experimental phantoms,
- Measuring the dielectric and elastic properties of the phantoms over a time,
- Eliminating the sensitivity to antenna position by using an array of receiver antennas,
- Receiving the information from the phase of the received signal in addition to the amplitude information by using a quadrature receiver system,
- Evaluating the effect of antenna position and movement in the electromag-

netic simulations,

- Evaluating the effect of size of the inclusion in the received Doppler signal through various phantom experiments,
- 3-D scan of the phantoms to obtain information on the location of the tumor,
- Decreasing the coupling between the transmitter and receiver antennas to increase the SNR,
- Scanning while multi-frequency vibrations are induced inside the phantoms for better tissue discrimination,
- Using the HMMDI information together with the microwave imaging information to increase the sensitivity and specifity in differentiating tissue,
- Evaluating a HMMDI data profile using a single excitation pulse to decrease the scan time,
- Evaluating the possibility of using this method for cancer detection in other soft tissues,
- Developing a clinical prototype of HMMDI system,
- Implementing better signal processing methods for de-noising and removing unwanted artifacts in the detected signals,
- Developing reconstruction algorithms for obtaining the elasticity and dielectric properties of the tissues from the HMMDI data,

REFERENCES

[1] M. Lazebnik, E. L. Madsen, G. R. Frank, and S. C. Hagness, "Tissue-mimicking phantom materials for narrowband and ultrawideband microwave applications," *Physics in Medicine and Biology*, vol. 50, no. 18, pp. 4245–4258, 2005. Times Cited: 40 44.

[2] J. Croteau, J. Sill, T. Williams, E. Fear, and Ieee, "Phantoms for testing radar-based microwave breast imaging," *2009 13th International Symposium on Antenna Technology and Applied Electromagnetics and the Canadian Radio Sciences Meeting (Antem/Ursi 2009)*, pp. 78–81, 2009. Times Cited: 0 13th International Symposium on Antenna Technology and Applied Electromagnetics/Canadian Radio Science Meeting Feb 15-18, 2009 Univ Calgary, Banff, CANADA Ieee 0 978-1-4244-2979-0.

[3] E. L. Madsen, G. R. Frank, T. A. Krouskop, T. Varghese, F. Kallel, and J. Ophir, "Tissue-mimicking oil-in-gelatin dispersions for use in heterogeneous elastography phantoms," *Ultrasonic Imaging*, vol. 25, no. 1, pp. 17–38, 2003. Times Cited: 42 CHEN, Jiangang/A-1549-2011 42.

[4] X. Li, E. J. Bond, B. Van Veen, and S. Hagness, "An overview of ultra-wideband microwave imaging via space-time beamforming for early-stage breast-cancer detection," *Antennas and Propagation Magazine, IEEE*, vol. 47, pp. 19–34, Feb 2005.

[5] P. N. T. Wells and H.-D. Liang, "Medical ultrasound: imaging of soft tissue strain and elasticity.," *Journal of the Royal Society, Interface / the Royal Society*, vol. 8, pp. 1521–49, nov 2011.

[6] M. Fatemi and J. F. Greenleaf, "Vibro-acoustography: An imaging modality based on ultrasound-stimulated acoustic emission," *Proceedings of the National Academy of Sciences of the United States of America*, vol. 96, no. 12, pp. 6603–6608, 1999. Times Cited: 209.

[7] E. E. Konofagou, M. Ottensmeyer, S. Agabian, S. L. Dawson, and K. Hynynen, "Estimating localized oscillatory tissue motion for assessment of the underlying mechanical modulus," *Ultrasonics*, vol. 42, no. 1-9, pp. 951–956, 2004. Times Cited: 20 Ultrasonics International 2003 Meetng JUN 30-JUL 03, 2003 Granada, SPAIN.

[8] C. Maleke, N. Pernot, E. E. Konofagou, and Ieee, "A single-element focused transducer methodfor harmonic motion imaging," *2005 IEEE Ultrasonics Symposium, Vols 1-4*, pp. 17–20, 2005. Times Cited: 0 IEEE International Ultrasonics Symposium SEP 18-21, 2005 Rotterdam, NETHERLANDS IEEE 0-7803-9382-1.

[9] M. Lazebnik, M. Okoniewski, J. Booske, and S. Hagness, "Highly accurate debye models for normal and malignant breast tissue dielectric properties at microwave frequencies," *Microwave and Wireless Components Letters, IEEE*, vol. 17, pp. 822–824, Dec 2007.

[10] S. Concept, "Ultrasound Engineering and Manufacturing." `http://www.sonicconcepts.com/images/pdf/h-102_datasheet.pdf/`, 2016. [Online; accessed 17 Feb. 2016].

[11] C. B. Top, *HARMONIC MOTION MICROWAVE DOPPLER IMAGING METHOD*. Thesis, 2013.

[12] C. Top, A. Tafreshi, and N. Gencer, "Medical ultrasound: imaging of soft tissue strain and elasticity.," *Transactions on Microwave Theory and Techniques*, Submitted, 2015.

[13] G. . World Health Organization, "Breast cancer Fact Sheet." `http://globocan.iarc.fr/Pages/fact_sheets_cancer.aspx`, 2012. [Online; accessed 02 Jan. 2016].

[14] G. A. Ybarra, Q. H. Liu, J. P. Stang, and W. T. Joines, *Microwave Breast Imaging*, book section 12. American Scientific Publishers, 2007.

[15] E. Fear and M. Stuchly, "Microwave detection of breast cancer," *Microwave Theory and Techniques, IEEE Transactions on*, vol. 48, pp. 1854–1863, Nov 2000.

[16] A. E. Bulyshev, S. Y. Semenov, A. E. Souvorov, R. H. Svenson, A. G. Nazarov, Y. E. Sizov, and G. P. Tatsis, "Computational modeling of three-dimensional microwave tomography of breast cancer," *Ieee Transactions on Biomedical Engineering*, vol. 48, no. 9, pp. 1053–1056, 2001. Times Cited: 56 56.

[17] X. Li, S. Davis, S. Hagness, D. Van Der Weide, and B. Van Veen, "Microwave imaging via space-time beamforming: experimental investigation of tumor detection in multilayer breast phantoms," *Microwave Theory and Techniques, IEEE Transactions on*, vol. 52, pp. 1856–1865, Aug 2004.

[18] J. Sill and E. Fear, "Tissue sensing adaptive radar for breast cancer detection - experimental investigation of simple tumor models," *Microwave Theory and Techniques, IEEE Transactions on*, vol. 53, pp. 3312–3319, Nov 2005.

[19] M. Converse, E. J. Bond, S. C. Hagness, and B. D. Van Veen, "Ultrawideband microwave space-time beamforming for hyperthermia treatment of breast cancer: A computational feasibility study," *Ieee Transactions on Microwave Theory and Techniques*, vol. 52, no. 8, pp. 1876–1889, 2004. Times Cited: 42 2.

[20] E. C. Fear, S. C. Hagness, P. M. Meaney, M. Okoniewski, and M. A. Stuchly, "Enhancing breast tumor detection with near-field imaging," *IEEE Microwave Magazine*, 2002.

[21] S. Gabriel, R. Lau, and C. Gabriel, "The dielectric properties of biological tissues: Ii. measurements on the frequency range 10 hz to 20 ghz," 1996.

[22] C. Gabriel, S. Gabriel, and E. Corthout, "The dielectric propertiesof biological tissues: I. literature survey," 1996.

[23] S. G. Lau and C. Gabriel., "The dielectric properties of biological tissues: Iii. parametric models for the dielectric spectrum of tissues," 1996.

[24] B. Bocquet, J. C. Vandevelde, A. Mamouni, Y. Leroy, G. Giaux, J. Delannoy, and D. Delvalee, "Microwave radiometric imaging at 3-ghz for the exploration of breast-tumors," *Ieee Transactions on Microwave Theory and Techniques*, vol. 38, no. 6, pp. 791–793, 1990. Times Cited: 35 36.

[25] J. C. Y. Lai, C. B. Soh, E. Gumawan, and K. S. Low, "Uwb microwave imaging for breast cancer detection-experiments with heterogeneous breast phantoms," vol. 16, pp. 19–29, 2011.

[26] S. M. Salvador and G. Vecchi, "Experimental tests of microwave breast cancer detection on phantoms," *Ieee Transactions on Antennas and Propagation*, vol. 57, no. 6, pp. 1705–1712, 2009. Times Cited: 9 9.

[27] M. Klemm, J. A. Leendertz, D. Gibbins, I. J. Craddock, A. Preece, and R. Benjamin, "Microwave radar-based breast cancer detection: Imaging in inhomogeneous breast phantoms," *Ieee Antennas and Wireless Propagation Letters*, vol. 8, pp. 1349–1352, 2009. Times Cited: 11 11.

[28] T. Henriksson, N. Joachimowicz, C. Conessa, and J.-C. Bolomey, "Quantitative microwave imaging for breast cancer detection using a planar 2.45 ghz system," *Ieee Transactions on Instrumentation and Measurement*, vol. 59, no. 10, pp. 2691–2699, 2010. Times Cited: 11 IEEE International Workshop on Medical Measurements and Applications May 29-30, 2009 Cetraro, ITALY IEEE; IEEE Instrumentat Soc, TC25 Med and Biol Measurements; Univ Calabria, Dept Elect, Comp and Syst; Univ Sannio 11.

[29] A. P. Sarvazyan, O. V. Rudenko, S. D. Swanson, J.Brian, and S. Y. E. Fowlkes, "Shear wave elasticity imaging: a new ultrasonic technology of medical diagnostics," *Ultrasound in Medicine and Biology*, vol. 24, no. 9, pp. 1419 – 1435, 1998.

[30] M. Fatemi and J. F. Greenleaf, "Ultrasound-stimulated vibro-acoustic spectrography," *Science*, vol. 280, no. 5360, pp. 82–85, 1998.

[31] K. Nightingale, M. S. Soo, R. Nightingale, and G. Trahey, "Acoustic radiation force impulse imaging: In vivo demonstration of clinical feasibility," *Ultrasound in Medicine and Biology*, vol. 28, no. 2, pp. 227–235, 2002. Times Cited: 341.

[32] F. Viola and W. Walker, "Radiation force imaging of viscoelastic properties with reduced artifacts," *Ultrasonics, Ferroelectrics, and Frequency Control, IEEE Transactions on*, vol. 50, pp. 736–742, June 2003.

[33] T. Sugimoto, S. Ueha, and K. Itoh, "Tissue hardness measurement using the radiation force of focused ultrasound," *Ieee 1990 Ultrasonics Symposium : Proceedings, Vols 1-3*, pp. 1377–1380, 1990. Times Cited: 9 MCAVOY, BR IEEE 1990 ULTRASONICS SYMP DEC 04-07, 1990 HONOLULU, HI IEEE, ULTRASON FERROELECT and FREQUENCY CONTROL SOC.

[34] A. Samani, J. Zubovits, and D. Plewes, "Elastic moduli of normal and pathological human breast tissues: an inversion-technique-based investigation of 169 samples," *Physics in Medicine and Biology*, vol. 52, no. 6, pp. 1565–1576, 2007. Times Cited: 114.

[35] M. L. Palmeri, A. C. Sharma, R. R. Bouchard, R. W. Nightingale, and K. R. Nightingale, "A finite-element method model of soft tissue response to impulsive acoustic radiation force," *Ieee Transactions on Ultrasonics Ferroelectrics and Frequency Control*, vol. 52, no. 10, pp. 1699–1712, 2005. Times Cited: 71.

[36] J. J. Dahl, G. F. Pinton, M. L. Palmeri, V. Agrawal, K. R. Nightingale, and G. E. Trahey, "A parallel tracking method for acoustic radiation force impulse imaging," *Ieee Transactions on Ultrasonics Ferroelectrics and Frequency Control*, vol. 54, no. 2, pp. 301–312, 2007. Times Cited: 44.

[37] Y. Yamakoshi, J. Sato, and T. Sato, "Ultrasonic-imaging of internal vibration of soft-tissue under forced vibration," *Ieee Transactions on Ultrasonics Ferroelectrics and Frequency Control*, vol. 37, no. 2, pp. 45–53, 1990. Times Cited: 227.

[38] R. Muthupillai, D. Lomas, P. Rossman, J. Greenleaf, A. Manduca, and R. Ehman, "Magnetic resonance elastography by direct visualization of propagating acoustic strain waves," *Science*, vol. 269, no. 5232, pp. 1854–1857, 1995.

[39] S. G. Chen, M. Fatemi, and J. F. Greenleaf, "Quantifying elasticity and viscosity from measurement of shear wave speed dispersion," *Journal of the Acoustical Society of America*, vol. 115, no. 6, pp. 2781–2785, 2004. Times Cited: 95.

[40] Y. Zheng, S. Chen, W. Tan, R. Kinnick, and J. F. Greenleaf, "Detection of tissue harmonic motion induced by ultrasonic radiation force using pulse-echo ultrasoundand kalman filter," *Ieee Transactions on Ultrasonics Ferroelectrics and Frequency Control*, vol. 54, no. 2, pp. 290–300, 2007. Times Cited: 24.

[41] B. Shan, A. A. Pelegri, C. Maleke, and E. E. Konofagou, "A mechanical model to compute elastic modulus of tissues for harmonic motion imaging," *Journal of Biomechanics*, vol. 41, no. 10, pp. 2150–2158, 2008. Times Cited: 8.

[42] G. Y. Hou, J. Luo, C. Maleke, E. E. Konofagou, and Ieee, "Simulation of hmifu (harmonic motion imaging for focused ultrasound) with in-vitro validation," in *2010 IEEE 36th Annual Northeast Bioengineering Conference.* Times Cited: 0.

[43] A. Abbosh and Ieee, "Early breast cancer detection using hybrid imaging modality," *2009 Ieee Antennas and Propagation Society International Symposium and Usnc/Ursi National Radio Science Meeting, Vols 1-6*, pp. 1456–1459, 2009. Times Cited: 0 IEEE Antennas and Propagation International Symposium /USNC/URSI National Radio Science Meeting JUN 01-05, 2009 N Charleston, SC IEEE; USNC; URSI 978-1-4244-3646-0.

[44] M. Zhao, J. Shea, S. Hagness, D. Van Der Weide, B. Van Veen, and T. Varghese, "Numerical study of microwave scattering in breast tissue via coupled dielectric and elastic contrasts," *Antennas and Wireless Propagation Letters, IEEE*, vol. 7, pp. 247–250, 2008.

[45] M. Zhao, *Contributions to Cost Reduction and Sensitivity Improvement of Microwave Breast Cancer Detection.* University of Wisconsin–Madison, 2009.

[46] C. Top and N. G. Gencer, "Harmonic motion microwave doppler imaging: A simulation study using simple breast model," 2013.

[47] K. R. Nightingale, M. L. Palmeri, R. W. Nightingale, and G. E. Trahey, "On the feasibility of remote palpation using acoustic radiation force," *Journal of the Acoustical Society of America*, vol. 110, no. 1, pp. 625–634, 2001. Times Cited: 281.

[48] C. Maleke, *In vivo detection and thermal treatment monitoring of breast tumors using Harmonic Motion Imaging (HMI).* PhD thesis, Columbia University, New York, NY, USA, 2010.

[49] M. Ostadrahimi, R. Reopelle, S. Noghanian, S. Pistorius, A. Vahedi, F. Safari, and Ieee, "A heterogeneous breast phantom for microwave breast imaging," in *Annual International Conference of the IEEE-Engineering-in-Medicine-and-Biology-Society*, IEEE Engineering in Medicine and Biology Society Conference Proceedings, pp. 2727–2730, 2009. Times Cited: 0.

[50] J. C. Y. Lai, C. B. Soh, E. Gunawan, and K. S. Low, "Homogeneous and heterogeneous breast phantoms for ultra-wideband microwave imaging applications," *Progress in Electromagnetics Research-Pier*, vol. 100, pp. 397–415, 2010. Times Cited: 7 Lai, Joshua Chong Yue/F-7313-2010; Low , Kay Soon/A-5028-2011 7.

[51] E. Porter, J. Fakhoury, R. Oprisor, M. Coates, M. Popovic, and Ieee, "Improved tissue phantoms for experimental validation of microwave breast cancer detection," *Proceedings of the Fourth European Conference on Antennas and Propagation*, 2010. Times Cited: 0 4th European Conference on Antennas and Propagation (EuCAP) Apr 12-16, 2010 Barcelona, SPAIN esa; CST; FEKO; TICRA; ANSOFT; ANSYS; speag; fractus; IET; WILEY-BLACKWELL; EPFL; EUREL; UPC 0 978-84-7653-472-4.

[52] L. A. Negron, F. Viola, E. P. Black, C. A. Toth, and W. F. Walker, "Development and characterization of a vitreous mimicking material for radiation force imaging," *Ieee Transactions on Ultrasonics Ferroelectrics and Frequency Control*, vol. 49, no. 11, pp. 1543–1551, 2002. Times Cited: 22 toth, cynthia/F-5614-2011 22.

[53] J. Oudry, C. Bastard, V. Miette, R. Willinger, and L. Sandrin, "Copolymer-in-oil phantom materials for elastography," *Ultrasound in Medicine and Biology*, vol. 35, no. 7, pp. 1185–1197, 2009. Times Cited: 14 15.

[54] T. J. Hall, M. Bilgen, M. F. Insana, and T. A. Krouskop, "Phantom materials for elastography," *Ieee Transactions on Ultrasonics Ferroelectrics and Frequency Control*, vol. 44, no. 6, pp. 1355–1365, 1997. Times Cited: 209.

[55] M. E. L., H. M. A., F. G. R., S. H., J. J., H. T. J., V. T., D. M. M., and W. J. B., "Anthropomorphic breast phantoms for testing e lastography systems," 2006.

[56] E. Madsen, J. Zagzebski, R. Banjavie, and J. RE., "Tissue mimicking materials for ultrasound phantoms," *Med. Phys.*, vol. 5, pp. 391–394, 1978.

[57] E. L. Madsen, M. A. Hobson, H. R. Shi, T. Varghese, and G. R. Frank, "Stability of heterogeneous elastography phantoms made from oil dispersions in aqueous gels," *Ultrasound in Medicine and Biology*, vol. 32, no. 2, pp. 261–270, 2006. Times Cited: 22 22.

[58] F. M. Ghannouchi and R. G. Bosisio, "Measurement of microwave permittivity using a 6-port reflectometer with an open-ended coaxial line," *Ieee Transactions on Instrumentation and Measurement*, vol. 38, no. 2, pp. 505–508, 1989. Times Cited: 22 23.

[59] MATLAB, "Equation Solving Algorithms." `http://www.mathworks.com/help/optim/ug/equation-solving-algorithms.html#brnpdsm/`, 2016. [Online; accessed 17 Feb. 2016].

[60] D. E. Goldberg, "Genetic Algorithms in Search, Optimization and Machine Learning," oct 1989.

[61] P. M. Meaney, F. Shubitidze, M. W. Fanning, M. Kmiec, N. R. Epstein, and K. D. Paulsen, "Surface wave multipath signals in near-field microwave imaging," *Journal of Biomedical Imaging*, vol. 2012, pp. 8:8–8:8, Jan. 2012.

[62] C. Top, A. Tafreshi, and N. Gencer, "Harmonic motion microwave doppler imaging method for breast tumor detection," in *Engineering in Medicine and Biology Society (EMBC), 2014 36th Annual International Conference of the IEEE*, pp. 6072–6075, Aug 2014.

[63] Food and D. Administration, "HIFU Simulator." `http://www.fda.gov/aboutfda/centersoffices/officeofmedicalproductsandtobacco/cdrh/cdrhoffices/ucm301529.htm/`, 2012. [Online; accessed 03 Sep. 2013].

[64] N. Bakhvalov and E. Zhileikin, Ya. M.and Zabolostskaya, *Nonlinear theory of sound beams.*

[65] A. Tafreshi, M. Karadag, C. Top, and N. Gencer, "Data acquisition system for harmonic motion microwave doppler imaging," in *Engineering in Medicine and Biology Society (EMBC), 2014 36th Annual International Conference of the IEEE*, pp. 2873–2876, Aug 2014.

[66] R. G. Holt and R. A. Roy, "Measurements of bubble-enhanced heating from focused, MHz-frequency ultrasound in a tissue-mimicking material.," *Ultrasound in medicine & biology*, vol. 27, pp. 1399–412, oct 2001.

[67] "The effects of the microbubble suspension SH U 454 (Echovist) on ultrasound-induced cell lysis in a rotating tube exposure system. - PubMed - NCBI."

[68] E. L. Carstensen, P. Kelly, C. C. Church, A. A. Brayman, S. Z. Child, C. H. Raeman, and L. Schery, "Lysis of erythrocytes by exposure to CW ultrasound.," *Ultrasound in medicine & biology*, vol. 19, pp. 147–65, jan 1993.

[69] D. P. Penney, E. A. Schenk, K. Maltby, C. Hartman-Raeman, S. Z. Child, and E. L. Carstensen, "Morphological effects of pulsed ultrasound in the lung.," *Ultrasound in medicine & biology*, vol. 19, pp. 127–35, jan 1993.

[70] E. C. Everbach, I. R. Makin, M. Azadniv, and R. S. Meltzer, "Correlation of ultrasound-induced hemolysis with cavitation detector output in vitro.," *Ultrasound in medicine & biology*, vol. 23, pp. 619–24, jan 1997.

[71] P. Lele, "Effects of ultrasound on "solid" mammalian tissues and tumors in vivo," in *Ultrasound* (M. Repacholi, M. Grandolfo, and A. Rindi, eds.), pp. 275–306, Springer US, 1987.

[72] K. Hynynen, "The threshold for thermally significant cavitation in dog's thigh muscle in vivo.," *Ultrasound in medicine & biology*, vol. 17, pp. 157–69, jan 1991.

[73] R. L. Clarke and G. R. ter Haar, "Temperature rise recorded during lesion formation by high-intensity focused ultrasound.," *Ultrasound in medicine & biology*, vol. 23, pp. 299–306, jan 1997.

[74] D. J. Watmough, R. Lakshmi, F. Ghezzi, K. M. Quan, J. A. Watmough, E. Khizhnyak, T. N. Pashovkin, and A. P. Sarvazyan, "The effect of gas bubbles on the production of ultrasound hyperthermia at 0.75 MHz: a phantom study.," *Ultrasound in medicine & biology*, vol. 19, pp. 231–41, jan 1993.

[75] S. Fujishiro, M. Mitsumori, Y. Nishimura, Y. Okuno, Y. Nagata, M. Hiraoka, T. Sano, T. Marume, and N. Takayama, "Increased heating efficiency of hyperthermia using an ultrasound contrast agent: A phantom study," *International Journal of Hyperthermia*, vol. 14, pp. 495–502, jan 1998.

CURRICULUM VITAE

PERSONAL INFORMATION

Surname, Name: Kamali Tafreshi, Azadeh
Nationality: Iranian
Date and Place of Birth: 21.09.1981, Tehran, Iran
Marital Status: Single
Phone: 0312 210 4407
Fax: 0312 210 2304
E-mail: azadehkt@gmail.com

EDUCATION

Degree	Institution	Year
M.S.	Science and Research Branch, Islamic Azad Uni., Iran	2008
B.S.	Science and Research Branch, Islamic Azad Uni., Iran	2005
High School	Abou Ali Sina High School, Tehran, Iran	1999

PROFESSIONAL EXPERIENCE

Year	Place	Enrollment
2012 - 2016	Middle East Technical University	Project assistant
2004 - 2006	Medical Engineer in AMS Company	Sales manager
2001 - 2003	Engineering Department of Milad Hospital	Engineer

PUBLICATIONS

C. B. Top, Tafreshi, A. K., Gencer, N., "Microwave Sensing of Acoustically Induced Local Harmonic Motion: Experimental and Simulation Studies on Breast Tumor Detection," Submitted to the Transactions on Microwave Theory and Techniques (TMTT), 2016.

Conference Publications

1. Tafreshi, Top, C. B., Gencer, N., "Multiple vibration frequencies in Harmonic Motion Microwave Doppler Imaging," Submitted to Engineering in Medicine and Biology Society (EMBC), 38^{th} Annual International Conference of the IEEE, 2016.
2. Tafreshi, A. K., Karadas, M., Top, C. B., Gencer, N., "Data acquisition system for Harmonic Motion Microwave Doppler Imaging," Engineering in Medicine and Biology Society (EMBC), 36^{th} Annual International Conference of the IEEE, p. 6072 - 6075, 2014.
3. Top, C. B., Tafreshi, A. K., Gencer, N., "Harmonic Motion Microwave Doppler Imaging Method for Breast Tumor Detection," Engineering in Medicine and Biology Society (EMBC), 36^{th} Annual International Conference of the IEEE, p. 2873 - 2876, 2014.
4. Tafreshi, A. K., Nasrabadi A. M., Omidvarnia A. H., "Epileptic Seizure Detection Using Empirical Mode Decomposition," IEEE Symposium on Signal Processing and Information Technology (ISSPIT), 2008.
5. Tafreshi, A. K., Nasrabadi A. M., Omidvarnia A. H., "Empirical Mode Decomposition in Epileptic Seizure Prediction," published in proceeding of the IEEE Symposium on Signal Processing and Information Technology (ISSPIT), 2008.
6. Tafreshi, A. K., Nasrabadi A. M., Omidvarnia A. H., "Evaluation of Epileptic Seizure Onset in EEG Signals Using Empirical Mode Decomposition and Correlation Dimension", 15^{th} Iranian Conference on Biomedical Engineering (ICBME), 2008.

GRANTS AND AWARDS

2014: Research Grant and Scholarship: "Development of a Prototype System for Harmonic Motion Microwave Doppler Imaging," 114E036, Cost Action TD1301, The Scientific and Technological Research Council of Turkey (TÜBİTAK).

2012: Research Grant and Scholarship: "Harmonic Motion Microwave Doppler Imaging Method," 112E031, The Scientific and Technological Research Council of Turkey (TÜBİTAK).

2008: The only recipient of full Erasmus Mundus scholarship from Iran in 2008 for the PhD program in Electrical and Electronics Department of Middle East Technical University.

2008: Ranked 2^{nd} among 13 graduate students in Biomedical Engineering Department of Islamic Azad University.

2006: Ranked 2^{nd} among 300 participants in the M.Sc. entrance exam of Islamic Azad Universities of Iran.